Investigating Deep Brain Stimulation as a Tool to Prevent Secondary Neurodegeneration Following Stroke

by

John Welsh

B Eng (Electrical)(Hons) / B Math

2021

Supervised by:

Professor Richard Middleton

&

Professor Frederick Rohan Walker

A thesis submitted in fulfilment of the requirements
for the degree of Doctorate of Philosophy in Electrical Engineering at
The University of Newcastle, Australia.

This research was supported by an Australian Government Research Training Program (RTP) Scholarship

Declaration

I hereby certify that the work embodied in the thesis is my own work, conducted under normal supervision. The thesis contains no material which has been accepted, or is being examined, for the award of any other degree or diploma in any university or other tertiary institution and, to the best of my knowledge and belief, contains no material previously published or written by another person, except where due reference has been made. I give consent to the final version of my thesis being made available worldwide when deposited in the University's Digital Repository, subject to the provisions of the Copyright Act 1968 and any approved embargo.

John Welsh

Abstract

A stroke occurs every nine minutes in Australia [1] and is a leading cause of death and disability worldwide [2]. Approximately fifteen million people around the world suffer from a stroke each year, of which five million die from initial trauma and a further five million suffer from ongoing disability [2].

Not only does it leave patients with permanent damage caused by the initial blocked or ruptured blood vessel, it is also known to cause regions that are connected to the infarction[1] to die over time. This secondary neurodegeneration (SND) may be linked to accelerated cognitive decline, dementia and other neurological disorders [3, 4, 5]. A key contributor to SND is a process called excitotoxicity, where an imbalance of excitatory signalling in regions connected to the lesion can lead to cell death by an array of biochemical pathways. One of the secondary regions susceptible to SND after cortical stroke is the thalamus, which will form the focus of this thesis.

An in-silico model of the thalamocortical network was developed to capture the dynamics of excitatory inputs to the sensory thalamus. The model strongly supports the role of corticothalamic neurons as modulatory inputs and sensory inputs as drivers. We found two key scenarios, whereby stroke can lead to the generation of aberrant signalling in the thalamus: (1) the loss of corticothalamic excitation switches neurons from a tonic mode of firing to bursting and (2) significant over-excitation from spilled extracellular glutamate generates both increased responses to stimulation and spontaneous firing. The latter of these two observations is strongly linked to the hypothesis of excitotoxicity.

In-vivo electrophysiological recordings in an anaesthetised mouse model of stroke, confirms that a cortical lesion impacts activity throughout the thalamocortical network. The loss of cortical activity lead to a decrease in thalamic activity and also a loss of feedback from the cortex in the somatosensory response. The recordings did not find support for the hypothesis of over-excitation or hyperexcitability and did not show evidence of cell loss caused by SND. The somatosensory evoked response in the VPL is the first to be recorded in a mouse model, and the waveform shows

[1] Site of tissue death

similarities to those recorded from other rodent species in the literature. The neuronal sources of each peak in the evoked potential were explored to suggest likely contributions from pre-synaptic, thalamo-reticular and corticothalamic neurons, which was supported in computational simulations.

A new method is proposed to extract spike times and firing rates from electrophysiological recordings. The algorithm constructs a global spike waveform dictionary which is used in conjunction with a sparse optimisation approach to discriminate overlapping spikes in a sliding time window. This proposed method was found to be effective in both real and simulated, low SNR, multi-unit recordings. A simple, signed-refractory policy was shown to significantly improve the performance of a number of conventional spike detection algorithms.

Finally, a method was developed to chronically implant electrodes in the mouse thalamus for freely-moving recording and deep brain stimulation (DBS). A safe and effective set of stimulation parameters was determined to maximally stimulate the thalamocortical pathway. A pilot study of DBS to rescue thalamocortical neurons showed some minor, but not statistically significant, improvements that warrant further investigation with a larger animal cohort.

Contents

List of Figures

List of Tables

Nomenclature

Ca^{2+}	Calcium Ion
Cl^{-}	Chloride Ion
K^{+}	Potassium Ion
Na^{+}	Sodium Ion
Aβ	Amyloid-Beta
AD	Alzheimer's Disease
AMPA	α-amino-3-hydroxy-5-methyl-4-isoxazolepropionic acid
AMPAR	AMPA Receptor
APP	Amyloid Precursor Protein
ATP	Adenosine Triphosphate
BDNF	Brain-derived Neurotrophic Factor
CT	Corticothalamic
CTD	C-Terminal Domain
DBS	Deep Brain Stimulation
EAATs	Excitatory Amino Acid Transporters
ECoG	Electrocorticography
EEG	Electroencephalography
ER	Endoplasmic Reticulum

ET Essential Tremor

GABA Gamma-Aminobutyric acid

HFS High Frequency Stimulation

iGluR Ionotropic Glutamate Receptors

K/X Ketamine/Xylazine Anaesthesia

KA Kainic Acid

KAR Kainic Acid Receptor

LFP Local Field Potential

LTS Low-Threshold Spikes

MCA Middle Cerebral Artery

ML Medial Lemniscus

MRI Magnetic Resonance Imaging

mt Mitochondria

MUA Multi-Unit Activity

NeuN Neuronal Nuclear Antigen

NMDA N-methyl-D-aspartate

NMDAR NMDA Receptor

nNOS neuronal Nitric Oxide Synthase

NO Nitrous Oxide

PD Parkinson's Disease

POm Posterior Medical Complex

PSD-95 Postsynaptic Density Protein 95

PT Photothrombotic

RMS Root Mean Square

SN Substantia Nigra

SND Secondary Neurodegeneration

SSEP Somatosensory Evoked Potentials

SSFL Forelimb representation area of the somatosensory cortex

SSHL Hindlimb representation area of the somatosensory cortex

STN Subthalamic Nucleus

STT Spinothalamic Tract

SUA Single-Unit Activity

TBI Traumatic Brain Injury

TC Thalamocortical

VB Ventrobasal complex of the Thalamus

VGCC Voltage Gated Calcium Channel

VGIC Voltage Gated Ion Channel

VPL Ventral Posteriolateral Nucleus

VPM Ventral Posteriomedial Nucleus

Acknowledgements

First and foremost, I would like to express gratitude to my primary supervisor, Professor Rick Middleton, for his guidance throughout the past 4 years. The time he has dedicated to meetings, intellectual insights, inspiring conversations and technical assistance has heralded progression of this project, and it is has been thoroughly appreciated.

Secondly, I would like to thank my co-supervisor, Professor Rohan Walker, whose support in biomedical areas, supply and funding of lab resources and staff and introduction to the world of stroke and SND have made this project possible.

I would like to thank my colleagues at HMRI who have helped me along the way. Namely Kristy Martin and Marina Ilicic for their roles in performing animal experiments and lab procedures, also Rebecca Hood and Kirby Warren for assisting me with animal care, laboratory work and numerous questions over the years. The lab staff from the EE and ME departments at the university have been of significant help with hardware resources and big thanks also to Ramon Delgado for collaboration on signal processing aspects of the project.

Finally, I would like to thank my family and friends for their support throughout these sometimes stressful years, especially my partner Bridget, parents and siblings. Their support and encouragement has motivated me and allowed me to continue chasing my goals.

Outline of Report

This thesis is organised into 6 chapters:

- **Chapter 1** provides a brief background on stroke, SND, excitotoxicity and DBS.
- **Chapter 2** investigates the stroke-induced thalamocortical network disruption using computational models and compares the results to evidence in the literature.
- **Chapter 3** details results from electrophysiological recordings of thalamic neurons after stroke.
- **Chapter 4** describes a novel spike detection method used to extract unit activity from MUA recordings.
- **Chapter 5** assesses the feasibility of using DBS as a treatment for SND.
- **Chapter 6** provides the conclusion to the thesis and suggestions for future works.

Chapter 1

Background

This chapter provides a brief introduction to the topics of stroke & secondary neurodegeneration. It reviews the current literature to elucidate causes of secondary neurodegeneration and potential treatment interventions with a focus on Deep Brain Stimulation.

1.1 Stroke

A stroke affects one Australian every nine minutes on average [6], and is the second leading cause of death and a major cause of disability worldwide [7]. A stroke occurs when there is either an occlusion (ischaemic stroke) or rupture (haemorrhagic stroke) of a blood vessel within the brain. The most common type of stroke is ischaemic stroke, depicted in Figure 1.1, which affects approximately 80% of sufferers [8]. The main cause of ischaemic stroke and other cardiovascular diseases is atherosclerosis; where fats, cholesterol and other substances accumulate in arteries to form plaques [8]. These plaques can form directly in the brain, or elsewhere and dislodge to later create a blockage in the cerebrovascular network.

The disruption in blood supply results in ischaemia where cells are deprived of oxygen and glucose essential for survival. This triggers cell death within minutes [9] with the amount of damage proportional to the duration of ischaemia [10]. Physical symptoms, such as muscular weakness, paralysis and speech impairment, can present within seconds of stroke and the most severe cases can result in death or permanent neurological deficits [7].

The region comprising the initial, irreversible loss of cells to necrotic death is known as the stroke core. Surrounding the core, is an area of hypo-perfused, yet salvageable tissue known as the ischaemic

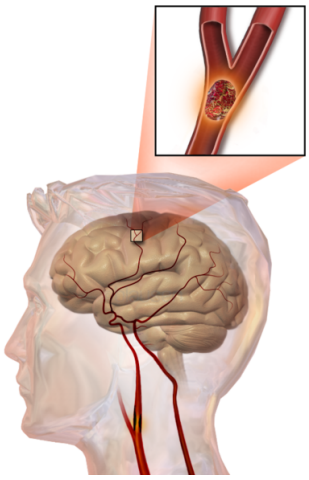

Figure 1.1: Stroke: An occlusion forming in the cerebrovascular network prevents the necessary supply of oxygen and glucose to parts of the brain triggering cell death within minutes (Image taken from [11] © Blausen Medical Communications, Inc.)

penumbra which is susceptible to damage over the following hours to days after the stroke event [12, 13]. Although receiving less research, evidence shows initially intact regions of the brain connected to the primary site of infarction also begin to die in the weeks to months after stroke, in a process referred to as Secondary Neurodegeneration (SND) [14, 15, 16, 17]. This is believed to be linked to the progressive cognitive decline experienced by stroke sufferers [5, 4, 18].

1.2 Secondary Neurodegeneration

Secondary neurodegeneration has been consistently observed in both human and animal subjects following stroke affecting the cerebral cortex [16]. It has been shown to occur in the thalamus [14, 17], substantia nigra [19] and more recently the hippocampus [18]. The pathological changes are notably similar to neurodegenerative diseases such as Alzheimer's Disease (AD), with evidence of neuronal loss, accumulation of the neurotoxic protein amyloid-β (Aβ) and a significant inflammatory response [16]. SND is not specific to stroke and can also result from other stroke-like injuries to the cerebral cortex [20].

Unlike the primary lesion, SND is not due to insufficient blood supply [14]. It is believed to result from a combination of processes including excitotoxicity, retrograde degeneration, inflammation, accumulation of neurotoxic proteins and oxidative damage [14]. Pathological changes in secondary regions develop within days after injury and can progress over the coming weeks, months and years

[14, 16]. This offers a time-window for treatment and intervention.

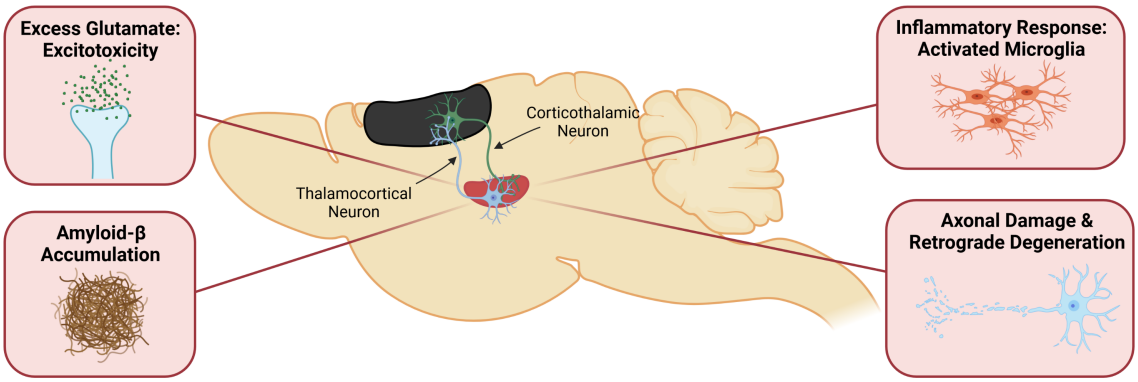

Figure 1.2: One example site of Secondary Neurodegeneration (SND) in the thalamus (red) after cortical infarction (black) in the mouse brain, with reciprocal corticothalamic and thalamocortical connections shown. A number of injurious processes occur at the sites of SND including increased concentrations of glutamate, accumulation of amyloid-β, a significant inflammatory response and axonal damage and retrograde degeneration. (Created with BioRender.com)

A link between the initial and secondary sites of damage is that they are directly connected via neuronal projections (see Figure 1.2), suggesting a means of propagating the injury. Secondary damage in the thalamus is focal to specific nuclei with regions between the infarct and secondary site spared. This signifies that there is no spread through the extracellular space such as the progressive neurotoxicity in the cortical penumbra [21, 22].

The existence of reciprocal connections between the infarct and secondary sites of injury supports the leading hypothesis that damage to neuronal inputs originating from the infarct can lead to an excitatory-inhibitory imbalance in the connected region [20, 23]. It has also been shown that more distant, polysynaptically connected regions can be affected, such as the loss of substantia nigra (SN) neurons following MCAO [19], suggesting there may be a network wide disruption that extends beyond directly connected neurons.

Anterograde degeneration of corticothalamic projections to the thalamus occurs in the first 3-4 days after cortical lesion [24], preceding the loss of thalamic neurons. Significant thalamic loss is evident by the end of the first week [25, 17] and continues for weeks in mice [17] and progressing for longer in humans[26, 27].

1.3 Thalamocortical Network

Of particular interest in this thesis are two regions of the brain - the somatosensory cortex and the somatosensory thalamus, that are the primary regions damaged by stroke and SND respectively. The network of connections between these two regions is of significant importance as it is believed to be what links the degeneration of thalamic neurons to the initial injury in the cortex. This section will describe the connectivity between the two regions, known as the thalamocortical network, and the basic properties of neurons, the fundamental cells in the brain responsible for the transmission and processing of information.

The brain is the principal component of the central nervous system (CNS) and consists of an interconnected network of approximately 100 billion neurons with upwards of 100 trillion synapses in humans [28]. The cerebral cortex is the outermost region of the brain consisting primarily of grey matter and is involved in processing sensory, motor and cognitive functions [28]. The cortex is structured in 6 vertical layers, that are easily identified by different compositions of neuronal sub-types and location of afferent and efferent projections. Layer IV is also known as the granular layer, describing the small-bodied granule cells that compose it, and is the main receiver of subcortical projections. The outermost three layers (I, II and III) are the supragranular layers and primary sources of intrahemispheric and corticocortical connections. Layers V and VI, the infragranular layers, are the main source of projections to subcortical locations.

The somatosensory thalamus is a dense mass of grey matter located deeper in the forebrain below the cerebral cortex. It primarily acts as a relay, with additional gating and modulatory functions, for sensory and motor signals to and from the cerebral cortex but also has a key role in the regulation of arousal and sleep [29, 28]. The thalamus is strongly connected to the cerebral cortex through direct and polysynaptic pathways.

Much of this thesis will focus on the study of rodent brains, which although different in structure to human brains, depicted in Figure 1.3, are available to reproducibly generate a model of SND [17, 30, 23].

The rodent somatosensory thalamus can be delineated into individual nuclei that correspond to sensory processing from different regions of the body. The ventrobasal complex (VB) of the thalamus contains the ventral posterior lateral (VPL) nucleus that receives inputs from the spinal cord, related to the body below the neck e.g. limbs, trunk, tail etc., and the ventral posterior medial (VPM) nucleus that receives inputs from the trigeminal nerve, related to the face and whiskers [32, 33]. The posterior medial complex (POm) of the thalamus is a secondary sensory nucleus that receives inputs from the body and also projects to the cerebral cortex [33]. Other sensory nuclei include the lateral geniculate nucleus, receiving input from the optic tract and output to the visual cortex

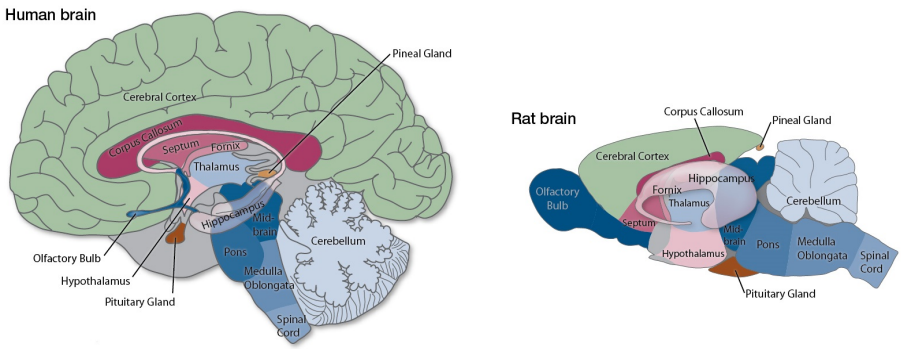

Figure 1.3: A comparison of the human and rodent brain (Not to Scale) shows large differences in the proportions of different brain regions. However the effects of stroke and secondary neurodegeneration are similar between species and use of a rodent model allows for thorough and reproducible investigations into diagnosis and treatment. Image adapted from [31]

and the medial geniculate nucleus, whose input is from the inferior colliculus and projects to the auditory cortex [33].

The VB and POm are afflicted by SND with higher prevalence than other thalamic nuclei due to the corresponding cortical regions being supplied by vessels more prone to stroke i.e. the middle carotid artery (MCA) [34]. The rodent VB has a simpler structure to larger mammals as it is composed almost exclusively of excitatory thalamocortical (TC) neurons, without interneurons [35, 36].

Thalamocortical neurons project to the somatosensory cortex, specifically layer IV but also directly synapse to layer VI corticothalamic neurons [37, 38]. They sprout collaterals that innervate the thalamic reticular nucleus (TRN), a nucleus surrounding the thalamus and composed of inhibitory GABAergic neurons which creates a loop of feedback inhibition. Corticothalamic (CT) neurons from layer VI project to TC neurons and also sends collaterals to the TRN [38]. This forms a tightly coupled thalamocortical network, shown in Figure 1.4 with feedback able to control and modulate sensory processing.

Inputs to the VPL arrive via the medial lemniscal (ML) fibres or spinothalamic tract (STT), which transmit touch and proprioceptive or nociceptive signals respectively [39]. There are also additional cholinergic and noradrenergic inputs from the brainstem that act to modulate the firing properties of TC neurons [33].

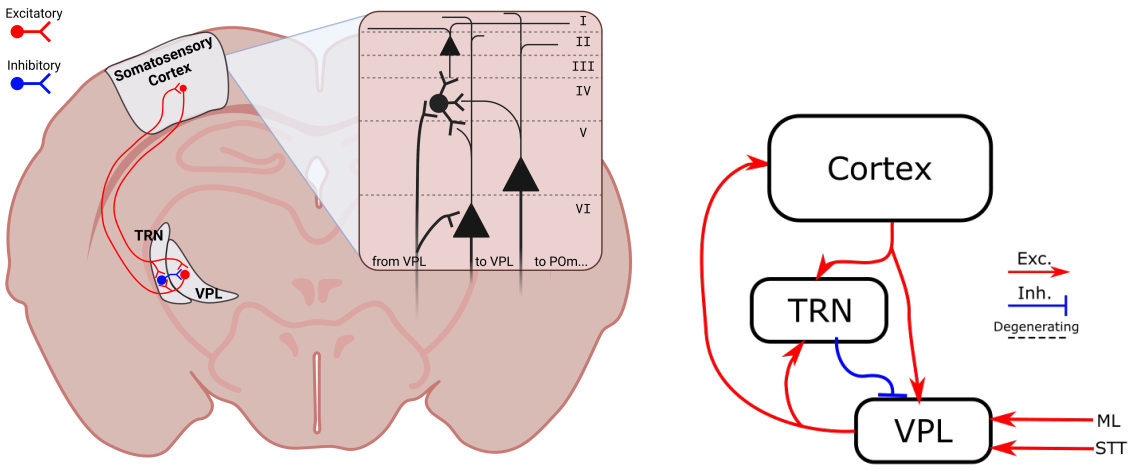

(a) (Created with BioRender.com) **(b)**

Figure 1.4: Neuronal connections between the somatosensory cortex, ventral posterior lateral (VPL) nucleus of the thalamus and thalamic reticular nucleus (TRN) forming the primary, sensory thalamocortical network. (a) Excitatory and inhibitory connections between each region overlaid on a coronal slice of the mouse brain, inset: the 6 layers of the sensory cortex, from the superficial layer I to the deepest layer VI, showing thalamocortical synapses to layer IV and VI neurons and the origin in layer VI of corticothalamic projections. (b) Simplified block diagram of the thalamocortical network including fibres relaying sensory information from the peripheral nervous system: medial lemniscus (ML) and spinothalamic tract (STT). Red arrows indicate excitatory neuronal connections and inhibitory connections are shown as blue.

1.3.1 Neurons

Neurons are excitable cells that transmit information via electrochemical signals and connect in networks to form systems that perform sensory, motor and cognitive functions [28], their general structure is shown in Figure 1.5a.

Neurons communicate by 'firing' and sending an electrical pulse, known as an action potential (see Figure 1.5b), through the axon to connected neurons at junctions of axon terminals and dendrites called synapses [28]. The signal propagates through the synapses either via direct ionic channels or via release and binding of neurotransmitters, where it creates a post-synaptic potential at the soma. Inputs integrating to a depolarisation greater than an action potential threshold will trigger an all-or-nothing action potential at the axon hillock of the post-synaptic neuron [28].

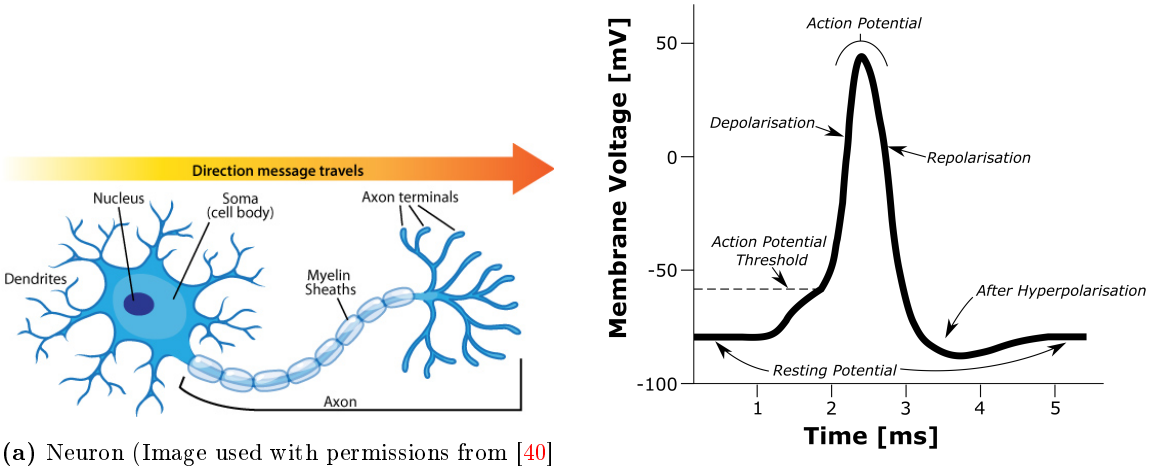

(a) Neuron (Image used with permissions from [40] © Arizona Board of Regents / ASU Ask A Biologist)

(b) Action Potential

Figure 1.5: Key components of a neuron and generation of an action potential: Neurons communicate by generation of an action potential in the somatodendritic structure that travels along the axon to terminals that connect to other neurons. (a) The key structures within a neuron include the dendrites and soma where an action potential is generated, the axon that propagates the action potential and the axon terminals that synapse to dendrites on connected neurons. (b) An action potential is triggered when the membrane voltage of a neuron reaches an action potential threshold causing a brief depolarisation and repolarisation. This is followed by a hyperpolarisation that defines a refractory period where a neuron is less-primed to generate another action potential.

Neurotransmitters bridge the communication gap between neurons. They are released from pre-synaptic terminals upon depolarisation and diffuse to post-synaptic terminals where they bind to specific receptors and allow flow of ions into the neuron [28]. This gating process is also controlled by co-agonist binding, membrane potential and antagonist binding. Glutamate exists as the most abundant excitatory neurotransmitter and Gamma-Aminobutyric acid (GABA) as the most common inhibitory transmitter [28].

Neurons are generally classed as excitatory or inhibitory. Excitatory neurons release neurotransmitters into the synapse that trigger an influx of cations (namely Na^+& Ca^{2+}), creating a positive post-synaptic potential promoting action potential initiation [28]. Inhibitory neurons trigger the influx of anions (Cl^-) or efflux of cations (K^+) creating a negative post-synaptic potential that hyperpolarises the soma potential away from the action potential threshold [28]. This simplified description forms the basis for how neurons communicate.

The initiation and propagation of an action potential is determined by ion flow through the cell

membrane. The flow is modulated by ion channels that act as gates controlled by both membrane potential and ligand binding. In an un-excited state the voltage across the neuronal membrane is held at a negative value known as the 'resting potential' [28]. A combination of ATP-powered ion pumps, exchangers and leakage channels ensure this steady state and healthy intracellular ion concentrations are maintained.

Voltage-gated ion channels (VGICs) play a vital role in the generation and propagation of action potentials along the axon and activate as a function of membrane potential. VGICs exist on the soma, dendrites, axon terminals, along the entirety of unmylenated axons and are concentrated at the nodes of ranvier along mylenated axons [28].

1.4 Excitotoxicity

Excitotoxicity is hypothesised to be a major part of the pathological process contributing to SND [20, 23] and other neurodegenerative diseases. This section explores the two neurotoxic components, Glutamate & Aβ, that when produced in excess, contribute to SND. Other factors contributing to SND will be discussed later in Section 1.6.

1.4.1 Glutamate Toxicity

1.4.1.1 Glutamate

Glutamate is the most abundant excitatory neurotransmitter in the human brain [41]. Its primary function is facilitating communication between synaptically connected neurons. Upon depolarisation, vesicles of glutamate are released from the pre-synaptic terminal diffusing into extracellular space and to the post-synaptic terminal of the synaptically connected neuron [28].

At the post-synaptic terminal glutamate can bind to both ionotropic glutamate receptors (iGluRs) or G-protein coupled metabotropic glutamate receptors (mGluRs) [41]. The activation of iGluRs opens the associated permeable membrane channel allowing the influx of cations, predominately $Na^{+}$and Ca^{2+}, into the receiving neuron producing excitatory post-synaptic potential (EPSP's) that depolarise the neuron and can trigger an action potential [41]. Metabotropic glutamate receptors do not form an ion channel but rather modulate nearby ion channels and intracellular signalling cascades through secondary messengers. The three main iGluRs present in the CNS are the AMPA receptor (AMPAR), NMDA receptor (NMDAR) and kainic acid (KA) receptor (KAR), named after their respective selective agonist molecules [28].

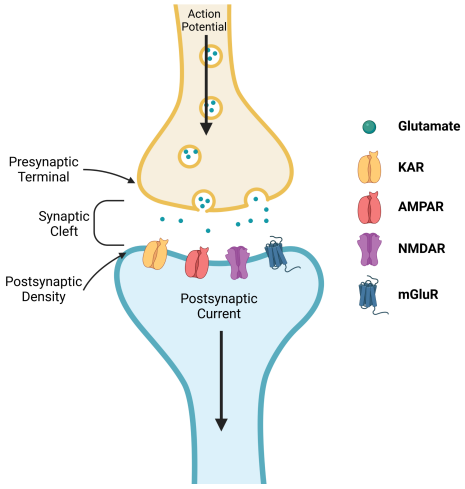

Figure 1.6: Glutamate is released from presynaptic axon terminals into the synaptic cleft. This glutamate diffuses through extracellular space where it binds to ionotropic glutamate receptors, including KAR, AMPAR and NMDAR, and metabotrobic glutamate receptors in dendrites of the post-synaptic neuron. Ionotropic glutamate receptors open a permeable membrane channel through which cations flow creating a post-synaptic current. (Created with BioRender.com)

Glutamate is primarily cleared from the synapse and extracellular space via astrocytic excitatory amino acid transporters (EAATs), converted into glutamine and transported back to the pre-synaptic neuron for glutamate re-synthesis [42]. A small portion of EAATs also exist on pre-synaptic neurons.

The neurotoxic effect of sustained exposure to glutamate has been known for decades [43]. Historically, two modes of glutamate toxicity have been considered. The first, here referred to as 'Acute Toxicity', is neuronal injury and death caused by acute swelling due to a large influx of ions and water during prolonged depolarisation [44, 45]. The second, 'Chronic Toxicity' pathway, is due to Ca^{2+}influx and increased intracellular concentrations triggering apoptotic events [44, 46]. The first is shown to occur only at significantly high glutamate concentrations [44] and therefore only briefly mentioned. The chronic pathway predominates at lower concentrations of glutamate and the effect is gradual [44] and more consistent with the time frame of SND and other neurodegenerative diseases [41].

1.4.1.2 Acute Toxicity

Acute toxicity is commonly associated with stroke or traumatic brain injury (TBI) [47, 22, 41]. Upon structural neuronal injury, hypoxia or glucose deprivation, large amounts of glutamate can be released into extracellular space due to direct damage of the cytoskeleton and vesicles spilling out, or indirectly by depleting energy stores maintaining membrane potentials that control neurotransmitter

release [47, 41].

Excessive amounts of extracellular glutamate results in the sustained activation of iGluRs and rapid influx of Na^+causing depolarisation and secondary influx of $Cl^-$and water [45, 44]. This leads to acute swelling and rupture of the cell membrane [45, 44] which can trigger further damage by releasing additional glutamate.

1.4.1.3 Chronic Ca^{2+}- Dependent Toxicity

Chronic toxicity differs from the acute mode by both time scale and mechanisms of action. Chronic toxicity was first isolated by determining that unlike the acute pathway dependent on $Na^+$and Cl^-influx it depends only on Ca^{2+}[45, 44, 46].

NMDARs are implicated as the primary channel for Ca^{2+}influx leading to excitotoxicity [22]. Repetitive activation of NMDARs and influx of Ca^{2+}can lead to sustained elevations of intracellular Ca^{2+}concentrations. This is well known to have neurotoxic effects [48, 22, 41]. The contribution of other calcium channels, including voltage-gated calcium channels (VGCCs), have been found to be insignificant in most cases [49].

A number of Ca^{2+}induced pathways are implicated in excitotoxicity (reviewed in [47, 50, 22]). Sustained elevations of cytosolic calcium leads to mitochondrial dysfunction and activation of enzymatic pathways of neuronal death [47, 22, 50]. It is additionally associated with increased production of free radicals and oxidative stress known to induce apoptosis [51, 22].

Neurons have a number of mechanisms to control intracellular Ca^{2+}concentrations. An imbalance in these systems can lead to elevated $Ca^{2+}$for a prolonged and potentially toxic period of time. Calcium homeostasis is regulated by a combination of ionic calcium channels, calcium extrusion systems (ATPase pumps and Na^+/Ca^{2+}exchangers) and calcium binding proteins [46].

At resting potential Ca^{2+}ATP-ase pumps are the principle component of Ca^{2+}extrusion. At high Ca^{2+}concentrations Na^+/Ca^{2+}exchangers dominate [46] and are the primary mechanism to reduce the toxic levels present in excitotoxicity [46]. The fact that Ca^{2+}concentrations can not always be kept to healthy levels suggests these mechanisms have limited throughput and saturate at some point. This makes limiting sustained Ca^{2+}influx important to prevent neurotoxic effects.

Contrary to the hypothesis of high-intracellular calcium concentration, it was found that the specific triggering and influx of Ca^{2+}through NMDAR's is a major contributor to neurotoxicity, rather than just increased intracellular Ca^{2+}levels [52]. Loading neurons to similar intracellular Ca^{2+}levels through other channels resulted in only a fraction of the total cell death, indicating that entry pathway is key [52].

Activation of NMDAR's is linked to a number of downstream signalling pathways via proteins bound to their intracellular C-terminal domains (CTD) via scaffolding proteins such as postsynaptic density protein 95 (PSD-95). One such example is the neuronal nitric oxide synthase (nNOS) which is bound to PSD-95 and triggers nitric oxide (NO) production when activated by Ca^{2+}influx through the NMDAR [53, 54]. NO is important for normal physiological functions as an intercellular messenger [54, 55], however has been shown to exhibit neurotoxic effects when produced in excess due to the production of additional reactive oxygen species such as peroxynitrite [56, 54].

A number of other downsignalling pathways have been linked to NMDARs and cell death, including activation of pro-death FOXO, inactivation of pro-survival Akt, shut-off of CREB, inactivation of ERK1/2, activation of calpains that cleave NCX2 and STEP, activation of DAPK1 and many others (see [57, 58, 22, 53, 59]).

1.4.1.4 2B Or Not 2B - is the NR2B subunit the culprit?

There are two competing hypotheses that relate NMDAR activation to excitotoxicity: the sub-unit hypothesis and location hypothesis. Both build from the initial discovery that NMDAR's are specifically linked to excitotoxic cell death and go further to implicate either specific sub-unit compositions of NMDAR's or the cellular location of NMDAR's as the culprit.

Hardingham *et al.* [60] showed that activation of NMDARs located within synapses increased CREB activity and upregulated brain-derived neurotrophic factors (BDNF) - promoting cell survival. Conversely, activation of extra-synaptic NMDAR's shut-off CREB, blocked BDNF expression, caused a loss of mitochondrial membrane potential (MMP) and consequently resulted in cell death [60, 57]. Extrasynaptic NMDARs are activated from glutamate spillover due to high frequency synaptic activity that saturates the glutamate uptake mechanisms within the synaptic cleft [61]. Extrasynaptic NMDARs are also strongly stimulated by increased extracellular glutamate due to neuronal injury, such as in the excitotoxic environment in the acute phase of stroke[22].

NMDARs are heterotetramer structures assembled from combinations of six possible sub-units: GluN1, GluN2A-D and GluN3A-B. They contain a necessary GluN1, as the receptor for co-agonist binding of glycine (or D-Serine), combined with GluN2 & GluN3 subunits, containing the glutamate binding site [62, 63]. The sub-unit compositions change the electrophysiological properties as well as the intracellular signalling pathways associated with the receptor [63, 62]. The most common subunit compositions are a GluN1 dimer with a GluN2A or GluN2B dimer [59], but the composition of subunits varies greatly in different regions of the brain and changes over developmental age [62, 64].

The subunit hypothesis suggests that activation of GluN2B-containing NMDARs leads to excitotoxic cell death whereas activation of GluN2A-containing NMDARs promotes cell survival [65]. Each

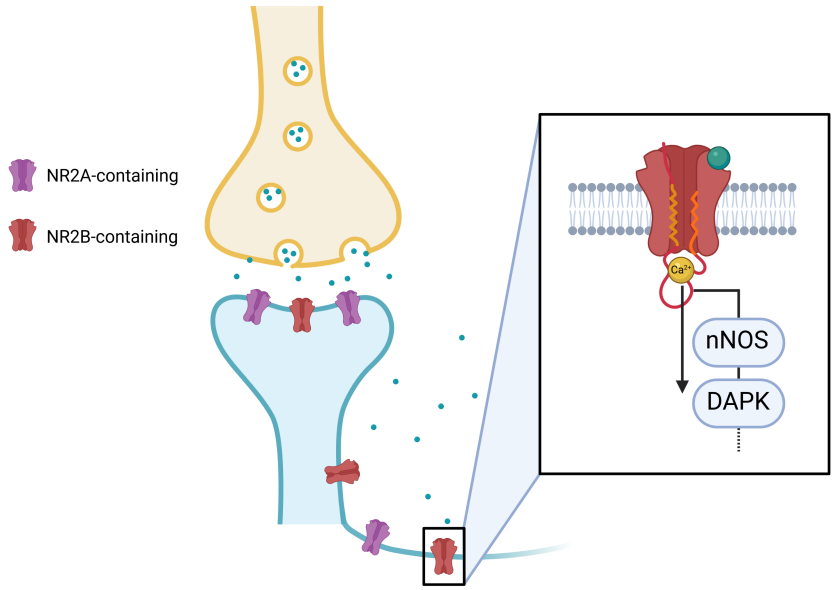

Figure 1.7: Two competing theories of excitotoxicity argue that the location of the receptor outside of the synapse or the presence of the NR2B subunit is the culprit in excitotoxicity. Inset: the toxicity of the NR2B subunit is associated with signalling proteins linked to its intracellular C-terminal domain including nNOS and DAPK among others (Created with BioRender.com).

GluN2 sub-unit expresses an unique intracellular CTD. As mentioned in the previous section these CTD's contain signalling proteins that are preferentially activated by Ca^{2+}flux through the receptor. It is believed the different signalling pathways that are activated on each of the sub-unit CTD's contribute to the either neuroprotective or neurotoxic effect [66].

Liu *et al.* [65] found blocking NR2B-containing receptors prevented apoptosis, but blocking NR2A-containing receptors increased apoptosis in-vitro. Genetic deletion of NR2A had no effect on excitotoxic cell death, but deletion of NR2B significantly decreased apoptosis [65]. There remained a small amount of cell death signifying additional contribution from non-NR2B pathways. The group also showed that NR2B sub-units facilitated excitotoxic cell death, whether at synaptic or extra-synaptic locations [65].

The most compelling evidence for the sub-unit hypothesis is from experiments by Martel *et al.* [66], who genetically replaced the CTD of NR2B subunits with that of NR2A subunits and showed that the cell death at lower glutamate concentrations was significantly reduced. At high glutamate concentrations, however, neurons containing either CTD were equally susceptible to cell death, presumably due to toxicity of intracellular Ca^{2+}dependant pathways.

These two hypotheses are weakly linked, but still disputed, by evidence that GluN2B-containing receptors are primarily found at extrasynaptic sites whereas GluN2A subunits are more prevalent in synaptic receptors [65, 67, 62, 61]. The sub-unit compositions and locations vary greatly with age [64], which may explain some of the contradictory evidence [68, 69].

1.4.2 Amyloid-Beta

The presence of Aβ in regions of SND [16, 14] raises the question as to whether it has a causal relationship to SND, contributes to SND or is a consequence of other processes. Forms of Aβ are known to be neurotoxic [70] and have been implicated as the major cause of neuronal degeneration in Alzheimer's disease [70, 71].

Amyloid-β is a polypeptide derived from the amyloid precursor protein (APP), a transmembrane protein concentrated in the synapses of neurons. It is produced through a particular succession of proteolytic cleavages; first β-secretase of APP followed by γ-secretase [72]. The functions of Aβ have yet to be fully elucidated, but the complete removal of Aβ results in neuron-specific cell death indicating it plays an essential role in normal physiology [71].

The neurotoxicity of Aβ has been known for decades [70]. A complete understanding of the processes involved are unknown but it is believed that oligomerisation of Aβ monomers leads it to have toxic effects, by building up to form insoluble plaques. Recent evidence suggests that the intermediary soluble oligomers may also exhibit toxic properties [73, 16]. The 'Amyloid Cascade' is a leading hypothesis for the sequence of events leading to Aβ-induced neurodegeneration in Alzheimer's disease [74]. It starts with the increased production and accumulation of Aβ that oligomerise and deposit plaques on to synapses. This causes a progressive injury to the neuron via altered ionic homeostasis and oxidative injury as well as an inflammatory response which releases further neurotoxic cytokines. Eventually this leads to widespread neuronal dysfunction and cell death [74].

In Alzheimer's Disease, the increase in Aβ production is believed to be due to genetic mutation, however in the case of SND it is plausible that it can be caused by pathological activity. Aβ levels are managed by Aβ-degrading enzymes (reviewed in [75]) that maintain healthy concentrations. Depending on the exact amino-acid location of cleavage, Aβ is formed into different lengths of residues (36-43 amino acids in length), that are associated with different propensities to oligomerise and therefore varied toxicities. The most common form produced is Aβ(1-40), but Aβ(1-42) is of importance due to its inherent disposition to oligomerise and form neurotoxic plaques [73].

The production of Aβ has been shown to correlate with neuronal activity [72, 76, 77]. NMDAR activation and the subsequent Ca^{2+}influx [78] has been shown to promote β-secretase cleavage over α-cleavage thus leading to increased Aβ levels [78].

If pathological activity develops in the thalamus due to network dysfunction triggered by stroke, it is therefore possible to produce higher levels of Aβ. Further evidence shows the presence of Aβ plaques correlate with high activity regions within the brain [79, 76] and that patients with neurological disorders such as epilepsy, with elevated neuronal activity, are likely to develop Aβ plaques and the onset of Alzheimer's disease at an earlier age [80].

Aβ oligomers have been shown to inhibit synaptic transmission [81]. It is hypothesised Aβ regulates the excitability of a neuron and thus prevents excitotoxicity by providing a negative feedback response [72, 71, 82]. However, higher levels of Aβ production increase the probability of Aβ(1-42) and the formation of neurotoxic plaques and fibrils. It has been suggested that neurons could lose sensitivity to Aβ-induced synaptic depression resulting in a pathogenic state [72].

1.4.2.1 Aβ linked to Glutamate Toxicity

Compounding the problem, are suggestions that Aβ may increase the effects of glutamate toxicity. Studies suggest that synthetic Aβ can leave neurons more susceptible to glutamate toxicity by reducing Ca^{2+}extrusion potential [48] or inducing hyperexcitability [83].

Aβ has been found to modulate ion channels [84, 82], with evidence of un-aggregated Aβ increasing Ca^{2+}influxes and aggregated Aβ decreasing calcium currents [84], possibly reflecting a progression of the pathology. Further studies review links between neuronal hyperactivity, Aβ and the onset of Alzheimer's disease [85, 83].

Finally there is evidence that the accumulation of Aβ can form membrane pores permeable to $Ca^{2+}$and increase calcium influx and intracellular stress [48].

1.4.3 Excitotoxicity and Stroke

Excitotoxicity plays a role in the ischaemic cascade associated with stroke [86, 87, 22] and the progressive cell death expanding into the penumbra [88].

The primary energy source for intracellular processes is ATP, which is produced through cellular respiration and the oxidation of glucose. There are no long-term stores of ATP in the brain, so under ischaemic conditions local ATP is depleted within minutes [87]. Depletion of energy stores results in the failure of ATP-dependent ion pumps and the loss off ionic homeostasis. Glutamate release from neurons is regulated by intracellular calcium signalling and the loss of ionic gradient results in release of neurotransmitter into extracellular space [89]. This triggers excitotoxicity, further loss of calcium homeostasis [90] and spreading toxic conditions into the penumbra. This ionic imbalance is associated with the phenomenon of cortical spreading depression [91].

1.4.4 Excitotoxicity and Neurodegeneration

It is hypothesised that the thalamus develops pathological activity following stroke which drives an excitotoxic insult leading to SND [20, 14]. A comparison can be made to patients that suffer from epilepsy and seizures, where regions of the brain experience sustained periods of hyperactive firing. It has been shown that induced cortical seizures can produce neurodegeneration in neighbouring cortical areas and also the thalamus [92]. Collins *et al.* [92] reviewed a number of other cases where focal epilepsy is found to cause distant lesions and believe it to be caused by excitotoxicity through glutamatergic corticothalamic projections. Further studies have linked epilepsy to neurodegeneration and found relief by blocking NMDAR's [47]. Ross *et al.* [20] demonstrated that the pathology of SND could be replicated by Kainic Acid (KA; an additional mediator of Ca^{2+}excitotoxicity) injection into cortex instead of a stroke, although this slightly delayed the temporal progression.

Glutamate toxicity has been implicated in other neurodegenerative conditions including Alzheimer's disease, amyotrophic lateral sclerosis (ALS), Huntington's disease and Parkinson's disease (PD) [93, 47, 94, 22, 41]. It is suggested that the initial loss of dopaminergic neurons in PD, results in the disinhibition of the subthalamic nucleus (STN) that accelerates the death of neurons in the substantia nigra (SN) via excitotoxicity [95, 96]. Parkinsonian patients show increased glutamate concentrations in blood plasma suggesting there is increased excitatory transmission [96] which has been confirmed specifically in the rodent SN [97]. Vucic *et al.* [98] suggest cortical hyperexcitability mediates pathogenesis of ALS and subsequent excitotoxic neurodegeneration, with similar effects for Alzheimer's and Parkinson's diseases.

1.5 Pathological Activity

Stroke results in death and de-afferentation of local neuronal populations that can have a large impact on the dynamics of brain activity. There exists a fine balance of excitatory and inhibitory influences on each neuron and populations thereof [99]. When neurons die from stroke, balance is lost and disturbances in neuronal activity can propagate through a vast network [100, 101]. Particular alterations in activity, here referred to as pathological activity, are one postulate for the link between stroke and SND that connects the infarction to neurodegeneration in polysynaptic regions.

"Diaschisis" is a term often used to describe the effects of focal lesions on distant brain activity [102, 103], relating the injury to functional deficits and neurological disorders [103, 104]. Previous studies have reported functional deficits and network reorganisation resulting from stroke [99, 105] and the occurrence of pathological activity in the form of epileptic seizures [106, 107, 108].

Interestingly, when focusing on activity within the thalamus, cortical lesions have been found to have varying effects. Nguyen *et al.* [109] reviewed decreased thalamic metabolism and hypo-activity in conjunction with thalamic atrophy. While Paz *et al.* [106] recorded increased activity and bursting behaviour within the VPL. Additionally, it has been well studied that cortical excitability is increased for days to months after stroke [110, 111, 112] .

The particular pathology of thalamic hyperexcitability is of great interest as it may generate excitotoxic processes that contribute to SND. A number of hypotheses can be formed using a network model to explain the generation of this activity:

- De-afferentation of cortical projections to the inhibitory thalamic reticular nucleus, resulting in dis-inhibition of thalamus [113, 106, 114].
- Loss of direct cortical excitation to the thalamus, resulting in hyperpolarisation of the membrane potential and increased bursting propensity [115].
- Increased cortical excitation of the thalamus via hyper-excitable peri-infarct projections [111], due to the loss of cortical interneurons [112], or reduction in GABA-A receptor expression [111].

The often varied effects of stroke on neuronal activity found in the literature is somewhat expected, as exact lesion size, location and inter-patient anatomical variability is critical in the precise network pathology that develops [100, 101, 116]. Further investigation is required to determine the exact effects of stroke on thalamic activity in a reproducible environment and how it correlates with SND.

Exacerbating the acute phase of this problem is the brain's response to stroke; boosting plasticity mechanisms to replace and compensate for damaged connections [28]. This process includes upregulating excitatory NMDA receptors [117] and decreasing inhibitory GABA binding [118] and receptors [111]. This results in localised changes in activity and rewiring of networks to redistribute functions via new pathways sometimes through sub-cortical regions including the thalamus [105, 99, 116]. Additional surviving brain tissue and redundant pathways can be recruited [105].

The generation of pathological activity in the thalamus and possible contributions to excitotoxicity are investigated further in the next chapter.

1.6 Other Contributions to SND

We have so far focused on excitotoxicity, but there exist a number of other factors that may contribute to the progression of SND that are worth mentioning. In particular the roles of other glial cells,

namely microglia and astrocytes, and the insult to the axon terminals of thalamocortical neurons that reside within the stroke core and penumbra.

1.6.1 Microglia

Microglia are the primary immune cells of the CNS. They are constantly surveilling, by extension and retraction of their processes, to detect and clean up damaged neurons, redundant synapses, Aβ plaques and infection [119, 120].

Normally they play a neuroprotective role but have been considered to be involved in the development of SND ([121, 17], reviewed in[122]). Severe microglial activation is present in the thalamus from 3 days after stroke and persists for at least 4 weeks [17]. The intensity of microglial activation strongly correlates with neuronal loss [17], but slightly precedes neuronal death, suggesting a role of inflammation in the progression of SND.

Microglia have been shown to migrate to and contact preferentially with active neurons [123, 120] and are attracted to glutamate induced Ca^{2+}signalling [124], which may be the response to pathological conditions in the thalamus. They have been shown to regulate neuronal activity, prevent hyperexcitability and reduce intracellular Ca^{2+}transients and decay times [120]. Without microglia, and their exertion of anti-excitotoxic effects, excitotoxic damage to the cortical penumbra can increase the infarct size by 60% [123].

The detrimental effects of microglia come from their reactive form, which can trigger from changes in extracellular K^{+}(indicative of ruptured neurons), pro-inflammatory cytokines or cell necrosis factors [125]. Reactive microglia undergo functional and morphological changes including the secretion of cytotoxic and pro-inflammatory molecules that have neurotoxic effects [125, 119, 88]. Therefore there exists a balance of neuroprotective and neurotoxic contributions, that if lost, could see microglia contribute to the pathology of SND.

1.6.2 Astrocytes

Astrocytes are the most abundant glial cell in the CNS, and perform a variety of roles to support neurons. As the predominant source of EAATs, astrocytic uptake of glutamate is crucial in the prevention of excitotoxicity and the maintenance of high SNR in synapses [42]. Astrocytes convert glutamate to glutamine (via glutamate-glutamine cycle), which is then recycled and converted back into glutamate or GABA in presynaptic neurons. In high glutamate concentration environments, astrocytes process additional glutamate by metabolism [126, 127, 128]. Evidence has shown that

after ischaemia the expression of EAATs is downregulated for many days [129] [130], however some contrary evidence exists (reviewed in [88]).

Intense astrogliosis has been observed in regions of SND [30, 16]. Similarly to microglia, reactive astrocytes change morphology and function. In certain forms they release glutamate, upregulate inflammatory signalling and downregulate pro-survival pathways and can contribute to neurodegeneration [131, 132, 133].

1.6.3 Retrograde Degeneration

Many groups have suggested that thalamic neurons undergo retrograde degeneration following cortical stroke due to axonal damage [134, 135, 136, 137] and loss of cortical synapses [137]. This fits the observation that only thalamic nuclei projecting to the damaged area are harmed [137].

Kanomori *et al.* [138] showed retrograde degeneration of retinal ganglia cells occurred after laser injury to their axons. The soma only started degenerating after 3 days and progressed up to 28 days, a very similar timeline to SND. The reason for degeneration was proposed to be the deprivation of growth factors produced at the post-synaptic target. In line with SND, it has been shown that thalamic neurons in specific relay nuclei are more affected than those in non-specific nuclei that also project to spared regions of the cortex [137, 139], perhaps due to them still receiving neurotrophic factors from the preserved synapses.

Glutamate receptors not only exist on dendrites and soma but also exist on axons. Given the toxic glutamate concentrations present in the cortex after stroke, TC axons could be afflicted by direct excitotoxic insult. Hosie *et al.* [140] demonstrated that bath application of glutamate to axon terminals isolated in separate wells from the soma experience excitotoxic injury. However they showed that this damage was isolated to the axon and did not spread back to the soma.

Morales *et al.* [141] showed possible evidence for retrograde excitotoxicity - in which excitotoxic insult via glutamate injection into the striatum resulted in the degeneration of thalamic projections to the area. This was speculated to be due to insult of the axon terminals which would parallel TC axon terminals in the cortex following ischaemic stroke. Similarly, convulsant injected into the S1 and M1 cortices resulted in the degeneration of VPL neurons in the same way as SND, but showed a slightly slower progression [20].

Ross *et. al* [20] reviewed the latency of thalamic degeneration after cortical lesions in different sized mammals, and concluded that larger animals such as cats and monkeys experienced a longer delay before degeneration. If the damage was triggered from signalling imbalance at the soma, it is not clear why such a delay would be present, but would correspond to the time taken for retrograde

degeneration to reach the soma. One possible explanation could be that the signalling imbalance may not arise until complete corticothalamic degeneration, which similarly, would be proportional to axon length [142] and thus longer in larger species.

Iizuka *et al.* [137] and Kataoka *et al.* [134] showed that the terminal degeneration of CT neurons occurred on days 1-3 post-injury. The degeneration of TC neurons begins at this time and progresses to become significant by day 7 [137, 134, 17]. This raises an additional hypothesis that there is an acute excitotoxic insult, outside of pathological network activity, due to the delayed degeneration of CT terminals that releases glutamate into the thalamic extracellular space [143, 20].

Further evidence against a purely retrograde injury is the fact that the TRN and SN can also be affected by SND [143], and these regions do not project to the damaged region of the cortex nor are they supplied by the occluded cerebral artery. Interestingly, the TRN is unaffected by small PT infarcts as the VB complex of thalamus is, but rather degeneration is apparent after MCAO which affects a larger cortical area [143]. The CT projections directly to TRN are known to degenerate and there is also evidence of terminal degeneration in the SN and other trans-callosal locations [134]. This gives further evidence to the theory of delayed glutamate release from degenerating projections.

TRN neurons contain parvalbumin, a calcium binding protein, which has been shown to be protective against excitotoxicity [144]. This may give an additional buffer against small excitotoxic insults from photothrombotic (PT) stroke but still succumbs when there is total de-efferentation due to MCAO.

The particular susceptibility of thalamocortical neurons is likely due to its reciprocal connection with infarct and receiving both axonal injury and excitotoxic insult to the soma. Other regions with projections to the infarct zone or receiving projections from the injured area are often spared [137, 134].

In summary, there a range of plausible mechanisms that could account for the degeneration of thalamocortical neurons outside of the hypothesised development of pathological activity and network dysfunction. The injury to thalamocortical axons from the stroke infarct or through excitotoxicity in the penumbra could alone trigger the retrograde degeneration of thalamocortical neurons along with the deprivation neurotrophic factors from lost thalamocortical synapses. An additional explanation is the acute release of glutamate from degenerating corticothalamic neurons creating a chronic, excitotoxic environment in thalamus thus leading to a delayed cell death.

1.7 Treatments

This section explores successful treatments used to either specifically target SND or more generally to protect against excitotoxicity in other applications. We also explore the current uses and success

of deep brain stimulation (DBS) and alternative stimulation methods.

1.7.1 Treatments for SND

A number of treatments have been shown to reduce the severity of thalamic SND after cortical insult and are summarised in Table 1.1.

It is important to note that most of these treatments were administered in the sub-acute phase of stroke and in some instances reduced the infarct size (e.g [145, 146, 147]). Given that the infarct size is related to the extent of SND it should not be ruled out that these treatments acted at the cortical site and by reducing cortical damage were able to rescue thalamic neurons.

It is also worth noting the timing of these successful treatments, with all but Polentes *et al.* [147] preceding neuronal loss in thalamus. Similar to Xing *et al.* [148], Anttila *et al.* [149] tested the administration of neurotrophic factors but not until 7 days post-stroke and found it did not prevent neuronal loss like in Xing *et al.* [148], however was still effective in promoting functional recovery. The difference in delivery method may also be responsible for different results between the investigations.

Table 1.1: Current treatments used for Secondary Neurodegeneration

Species	Stroke Model	Treatment	Mechanism	Outcome	Author
Mouse	PT	Low-Oxygen Post Conditioning, 11% Oxygen for 8h/day, Days 2-14 post-stroke.	Anti-excitotoxic, Reduced PSD-95 and binding of NR2B.	Reduced Neuronal Loss, Reduced Microglia Activation.	Pietrogrande *et al.* 2019 [23]
Rat	MCAO	B3C - bis(propyl)-cognitin, 0.5,1.0 mg/kg i.p. daily, Days 1-14 post-stroke.	Cathepsin-B inhibitor, (Also an NMDAR antagonist).	Reduced Neuronal Loss, Reduced Gliosis, Reduced Aβ deposits, Improved neurological function.	Zuo *et al.* 2020 [145]
Rat	MCAO	Memantine, 20 mg/kg i.p. daily, Days 1-8 post-stroke.	NMDAR antagonist.	Reduced Neuronal Loss, Reduced Gliosis, Reduced tau deposits, Reduced sensory Decline.	Liang *et al.* 2020 [150]
Mouse	dMCAO	Dihydrocapsaicin (DHC), 8 hrs infusion, Started 3hrs post-stroke.	Pharmacological Hypothermia.	Reduced Neuronal Loss, Reduced Astrogliosis, Improved Neurological Function.	Cao *et al.* 2017 [146]
Rat	MCAO	Netrin-1, 600 ng daily intracerebral infusion, Days 1-8 post-stroke.	Pro-angiogenic	Improved BBB, Improved Neurological Function.	Yu *et al.* 2017 [151]
Rat	MCAO	Ebselen, 30mg/kg daily Gastric Gavage, Days 1-14 post-stroke.	Antioxidant.	Reduced Neuronal Loss, Reduced Gliosis.	Li *et al.* 2015 [152]
Rat	MCAO	Bepridil, 50mg/kg p.o. daily, Days 2-24 post-stroke.	Ca^{2+}Channel Blocker, APP-Cleavage Inhibitor.	Reduced Aβ accumulation, Reduced Ca^{2+}accumulation, Improved Functional Recovery.	Sarajarvi *et al.* 2012 [153]
Mouse	PT	Bepridil, 50mg/kg p.o. daily, Days 2-24 post-stroke.	Ca^{2+}Channel Blocker, APP-Cleavage Inhibitor.	Reduced Aβ accumulation, Reduced Ca^{2+}accumulation.	Lipsanen *et al.* 2013 [154]

Rat	MCAO	DAPT, 50mg/kg p.o., 3 days post-stroke.	Ca^{2+}Channel Blocker, APP-Cleavage Inhibitor.	Reduced Aβ accumulation, Reduced Neuronal Loss, Reduced Gliosis, Improved Sensory Function.	Zhang *et al.* 2011 [155]
Rat	MCAO	3-MA, Intraventricular Injection, 1 day post-stroke.	Autophagy Inhibitor.	Reduced Aβ accumulation, Reduced Neuronal Loss.	Zhang *et al.* 2012 [156]
Rat	MCAO	Cerebrolysin, 5 ml/kg i.p. daily, Days 1-13 post-stroke.	Neurotrophic Factors.	Reduced Aβ accumulation, Reduced Neuronal Loss, Reduced Astrogliosis, Improved Sensory Function.	Xing *et al.* 2014 [148]
Rat	MCAO	Stem Cell Transplant (hiPSC's), 1 week post-stroke.	Trophic Effects Reconstruction.	Reduced Atrophy, Reduced Astrogliosis, Improved Functional Recovery. *__Note__: SND assessed in SNr	Polentes *et al.* 2012 [147]

1.7.2 Treatments for Excitotoxicity

A number of the effective treatment methods in the previous section target the excitotoxic insult to the thalamus during SND. Therefore it is worthy to explore treatment methods used against excitotoxicity in other contexts.

Numerous studies have used NMDAR antagonists *in vitro* to prevent neuronal death [44, 157]. However *in vivo* experiments and clinical trials using NMDAR antagonists have failed and it is speculated to be due to the essential roles of NMDARs (reviewed in [158, 159, 160]). The activation of NMDA receptors is known to play an important role in mediating synaptic plasticity [161] and therefore inhibiting NMDA could have negative consequences for learning, memory and other pro-survival signalling pathways [161, 94, 162, 58].

Memantine is an approved treatment used for excitotoxicity in Alzheimer's disease [163]. It is also an NMDAR antagonist but its success is believed to be due to its low binding affinity (reviewed in [160]). Ifenprodil, a specific NR2B-containing NMDAR antagonist, has also shown some success [164].

A current trend of treatments is to reduce extracellular glutamate concentrations by upregulating EAATs. Lewerenz *et al.* [41] reviewed successful trials for a number of neurodegenerative diseases in particular the prominence in ALS treatment.

Huang *et al.* [165] utilised laser therapy as neuroprotection against excitotoxicity. Cytochrome c oxidase is a mitochondrial transmembrane protein that absorbs photons to increase electron transport in the respiratory chain therefore increasing ATP production and maintaining the mitochondrial membrane potential and preventing a number of the before-mentioned apoptotic pathways.

Almeida *et al.* [166], showed the neuroprotective effects of BDNF against glutamate excitotoxicity.

Goldshmit *et al.* [167] treated mice with blood glutamate scavengers to reduce glutamate concentrations in the cerebrospinal fluid. After spinal cord injury the treated mice showed greater protection to excitotoxicity resulting in reduced cell loss and inflammation as well as promotion of recovery. Blood glutamate scavengers have also successfully been used by Nagy *et al.* [168] to reduce excitotoxicity and thus the infarct size in a PT stroke model.

Rodriguez *et al.* [169] reviewed the use of hormones, including Prolactin and progesterone, to prevent glutamate and KA excitotoxicity in the hippocampus.

A number of genetic knock-out models in animal studies have also shown efficacy, but can not readily be converted to clinical studies. These include disruption of the nNOS-PSD95 binding [170, 171], overexpression of EAATs and Glutamate dehydrogenase [172] and knock-out of tau expression [173].

1.7.3 Deep Brain Stimulation

Deep brain stimulation is a method of delivering an electrical stimulation to targeted areas of the brain via surgically implanted electrodes [174], such as shown in Figure 1.8. Electric stimulation has been used to treat neurological disorders for many years [1] with particular success in recent decades for Parkinson's disease and Essential Tremor. Deep Brain Stimulation has replaced the rather archaic method of surgical lesioning, e.g thalatomies and pallidotomies, [174, 175, 176] as it provides a means of reversibility and adaptability to the patients response.

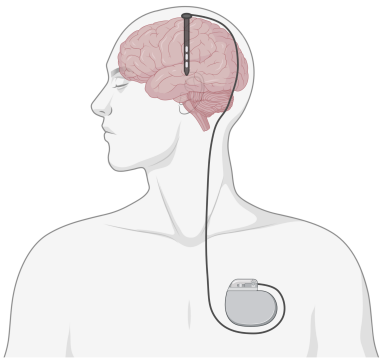

Figure 1.8: Depiction of a DBS probe implanted in the human brain. By delivering electrical impulses to target brain structures neuronal activity in these areas can be modulated to suppress symptoms of neurological disorders (Created with BioRender.com).

Electrodes are implanted using stereotactic procedures into the target region of the brain. The coordinates are individualised using MRI or CT scans to account for inter-patient discrepancies and often inserted in conjunction with microelectrodes to optimise the placement in the region of interest [174, 177]. Further post-operative imaging is used to confirm the location of the probe[177, 174].

1.7.3.1 Current DBS Applications

Recent decades have seen DBS gain popularity as treatment option for a range of neurodegenerative diseases, movement disorders and psychiatric illnesses (reviews in [178, 174, 175, 177, 179]), often when traditional pharmacological treatments prove ineffective. Some examples are listed below:

- Suppressing symptoms of Parkinson's disease and Essential Tremor [180, 176, 181, 182, 183].
- Treatment of Epilepsy [184, 185].

[1] Interestingly dating back over 2 millennia when electric rays were used to 'treat' headaches [174, 175]

- Improve cognitive function and slow the progression in Alzheimer's disease [186, 187, 188].
- Alleviate symptoms of depression [189, 190].
- Treatment of psychological conditions including Schizophrenia [191], Tourette syndrome [192, 193, 194], obsessive compulsive disorder [195] and neuropathic pain [196] .

Of particular interest, DBS has been used in stroke patients to suppress symptoms of post-stroke pain [197] (and reviewed in [198]). In animal studies of stroke DBS has promoted neurogenesis and motor recovery [199, 200] and restored synaptic function and memory [201].

1.7.3.2 Mechanism of Action

Deep Brain Stimulation directly modulates a neuron's membrane potential and therefore the response of voltage-gated ion channels. The resultant ion flux can trigger action potentials within target neurons. Axons have much lower activation thresholds than the soma and are therefore preferentially stimulated by DBS [202] creating both antidromic[2] and orthodromic[3] signals from the stimulated node. The production of an action potential requires a voltage gradient parallel to the axon [202] and activation depends on intrinsic properties of the cell including types of ion channels, diameter and also the orientation and distance between the neuron and probe.

There are a number of theories of how DBS achieves clinical benefits. The primary aim of DBS is to stabilise pathological activity created by damaged neuronal circuits. Pathologies such as Parkinson's disease, where chronic oscillations are generated and sustained in sensorimotor loops, require inhibition, but how this is achieved is still somewhat unknown. High frequency stimulation (HFS - 100+ Hz) has been shown to achieve the best results while low frequency stimulation, especially in the range of the β-Band oscillations synonymous with Parkinson's disease, seems to have an additive affect and increase symptom severity [182, 175].

'Informational Lesioning' is a leading theory of disrupting the transmission of pathological activity. The CNS facilitates a complex communication framework that encodes messages between populations of neurons at characteristic frequencies. This results in a system of local and long range oscillator circuits that are highly dependent on temporal correlation of signals. Information lesioning introduces high frequency, repetitive stimulation to these circuits de-synchronising information flow [203, 204].

In cases such as Parkinson's disease where pathological oscillations occur in the β-frequency range that includes the processing of sensorimotor functions, thus believed to be the link to generate

[2] Propagating towards the soma
[3] Propagating away from the soma (normal direction)

tremor, the oscillations are shifted or entrained to higher frequencies [203, 204, 176] where they are believed to have no undesirable effects.

Antidromic Blockade is a theory by which high-frequency stimulation can preferentially block the transmission of action potentials through slow conducting fibres. Deep Brain Stimulation can evoke action potentials that travel in the reverse direction (i.e. antidromic) that collide with and cancel orthodromic, somatodendritic generated action potentials[205].

Direct inhibition via 'Depolarisation Block' or 'Stimulation Block' is a theory consolidating evidence of decreased firing rates around the site of HFS. It was believed that DBS only had a direct effect in stimulating a neuron to produce an action potential, but possible mechanisms exist to directly inhibit a neuron from firing.

Shin *et al.* [206] suggests that HFS-induced accumulation of extracellular K^+concentrations from repetitive depolarisation create the effects of inhibition. However no evidence was found of inhibition during the application of HFS [206]; perhaps the high extracellular K^+increased the activation threshold that normal excitation levels could not overcome but DBS could. This theory aligns with the slow recovery of firing rates after DBS has ceased [203].

Others suggest that HFS modulates the gating of VGIC's in a way that prevents action potential initiation by inactivating Na^+channels and increasing K^+channel flow [204]. Beurrier *et al.* [207] report that STN HFS creates a blockade of specific VGIC's (persistent $Na^+$and L- and T-type Ca^{2+}), at higher frequencies of 166 Hz with no effect at 100 Hz. Firing was still able to be evoked during this period but the threshold was much greater and the inhibition lasted minutes after stimulation had stopped [207]. Ultra-high frequency stimulation (kHz+) has been used to create ionic channel blocks in peripheral nerve fibres, it is believed a constant activation of K^+channels or constant inactivation of Na^+channels prevent action potential initiation [208].

Indirect Inhibition is a method to inhibit a target area by stimulating at a secondary site. Deep Brain Stimulation can be used to activate populations of GABA-ergic neurons that project to the desired location and produce an inhibitory effect [203, 204].

1.7.3.3 Neuroprotection

There is evidence that DBS can induce a neuroprotective effect. Some suggest this is due to the cessation of pathological activity and in particular the prevention of glutamate excitotoxicity [209, 210, 95] while an alternative hypothesis is the stimulation-evoked increase in neurotrophic factors (BDNF) [211, 212].

Deep Brain Stimulation is currently considered foremost as a symptomatic treatment rather than for long-term prevention of degenerative disease [179]. Some evidence shows HFS of STN can rescue dopaminergic neurons of the SN in animal models induced with Parkinsonian symptoms [209]. However neuroprotective effects in clinical studies have not been concluded or found significant (reviewed in [176, 213, 204]). Instances of increased longevity of DBS patients could be attributed to improved quality of life and living conditions [204].

Lower frequencies of DBS (5-20Hz) could be used to restore healthy levels of activity to inactive regions undergoing neurodegeneration via neuroprotective mechanisms mentioned above. Low frequency stimulation has been applied non-specifically to optical nerves and photoreceptors of eyes undergoing retinis pigmentosa and macular degeneration with promising results [214, 215, 216, 217, 218].

It seems paradoxical to claim that applying DBS to a target region can reduce the effects of excitotoxicity, unless committed to the direct or indirect inhibition hypotheses. Therefore further investigation is needed and target regions carefully assessed for their vulnerability.

1.7.3.4 Side Effects - Surgery

Deep Brain Stimulation requires an invasive procedure but provides an advantage over non-invasive stimulation methods, such as transcranial magnetic and electrical stimulation, to specifically target sub-cortical regions including the thalamus. Implantation of electrodes into the brain risks the possibility of infection or haemorrhaging during insertion or movements of the brain thereafter [174, 176]. Adverse effects can include hematomas, cerebral contusions, neurological deficits and psychiatric conditions [219].

1.7.3.5 Side Effects - Stimulation

Current DBS methods do not have precise spatial control and the generated electric field can propagate to regions adjacent to the target. This 'spillage' can induce harmful symptoms depending on the structures affected. Stimulation can cause both permanent and transient cognitive, psychiatric and functional disorders [176, 177, 174] that can often be managed by stimulation parameter adjustments at the expense of treatment efficacy.

These problems are being addressed in ongoing work on new probe designs and field steering that provides a method for both non-invasive targeting of deep brain structures [220] and optimisation of target coverage to minimise spillage [221, 222].

1.7.4 Closed-Loop DBS

We considered the use of a closed-loop DBS system but did not pursue this direction, for further background information see Appendix A.5.

1.7.5 Alternative Stimulation Methods

Alternate methods of modulating neuronal activity include:

- Optogenetics: Genetically mutating neuron ion channels via viral injection to make them responsive to stimulation or inhibition by particular frequencies of light. Has been utilised in animal models post-stroke to suppress epileptic activity [106], and promote recovery of thalamocortical circuits and motor function [223, 224]
- Transcranial magnetic stimulation: Magnetic coils placed on the scalp used to induce electrical currents within the brain. Has been shown to improve functional recovery and enhance neurogenesis in animal models of stroke [225, 226, 227].
- Transcranial electrical stimulation: Stimulation applied through electrodes placed on the scalp. Has shown to improve stroke recovery in human [228] and animal studies [229, 227].

Both transcranial stimulation methods have had varying success in treatment of stroke patients (see [230, 231, 232, 188, 233, 234, 235]).

Each of the non-invasive methods have some distinct advantages over DBS. Transcranial magnetic and electrical stimulation are a preferred treatment method for a range of clinical treatments due to the non-invasive nature and ease to set up. However they have a limited ability to target subcortical regions such as the thalamus. Optogenetics can provide a direct and controlled inhibition of a target area but increases complexity of setup and is less clinically-adaptable than DBS.

Ultrasound stimulation is a promising new method of non-invasive brain stimulation that offers both high spatial resolution and the ability to target deeper brain regions [236, 237], including specifically the VPL [238]. Transcranial ultrasound stimulation has been used to promote recovery after stroke [239] and used in a closed-loop system to suppress seizures [240, 241].

An additional promising non-pharmacological approach is near infrared radiation (NIR) to trigger neuroprotective pathways. It has been shown to prevent mitochondrial dysfunction linked to apoptosis by rescuing mitochondrial membrane potential and ATP production [242, 243, 244], reduce binding of Aβ to synaptosomes [242], reduce Aβ plaques and tangles [244] and reduce the effects of excitotoxicity [165].

Alternatively, natural stimulation via peripheral sensory pathways would offer the best translation to clinical practice. It is widely known that exercise [245, 246, 247] and sensory interaction with the environment [248] are effective promoters of stroke recovery, due to among factors the activity-dependent increase in neurotrophic factors [249]. This effect could be enhanced by peripheral stimulation devices [250], especially in the context of SND affecting the somatosensory pathway. Of interest it has been shown that visual [251, 252] and audio stimulation [253] reproduce the benefits of direct 40 Hz stimulation in reducing Aβ accumulation, even reaching brain regions outside of the specific sensory path. This may offer a way of translating the benefits of 40Hz stimulation in rodent models of stroke recovery [254] to clinical practice.

1.8 Summary

Secondary neurodegeneration is a clear problem given the prevalence of stroke in the community, which will continue to grow with an ageing population [7]. It warrants additional research to discover causes and develop treatments that prevent further decline of patients and promote functional recovery and quality of life.

A clear, single mechanism of SND has not been elucidated and it is more likely a multi-factorial process resulting from compounding insults. There is an acute glutamate release due to injury of corticothalamic neurons, possible chronic glutamate release due to network imbalance and impaired glutamate clearance all contributing to an excitotoxic environment. Furthermore, injury of TC axons, within the infarct and penumbra, and deprivation of NTFs from their cortical synapses will place additional stress on the neurons as would any cytotoxic factors released with the inflammatory response and the accumulation of Aβ.

The treatment methods used in the current literature have been reviewed, and there is a clear opportunity to investigate the benefits of DBS given its growing success in the treatment of other neurological conditions.

The next chapter will investigate, using computational models, the possible development of pathological activity in the thalamus following stroke and how it may contribute to excitotoxic insult.

Chapter 2

The Effect of Stroke on the Thalamocortical Network

A leading hypothesis for SND is the development of pathological activity in the thalamus as a consequence of stroke. This chapter will explore the possible impacts of stroke on thalamic activity using computational models and compare them to recording results from the literature. Finally, possible links between pathological thalamic activity and excitotoxicity are explored.

2.1 Introduction

The thalamus and cortex are tightly linked with reciprocal direct and indirect connections that play a key role in modulating sensory input. Once thought of as a simple relay station, the complex circuitry in thalamocortical networks allows significant processing of information within the thalamus [29]. In this chapter we focus specifically on the network associated with the sensory transmission that is afflicted by SND after stroke to the sensorimotor cortex. These sensory nuclei are referred to as 'first-order' relays, that receive their primary inputs from the peripheral nervous system and project them to the sensory cortex [255]. Additionally, there exists 'higher-order' relay nuclei whose inputs and outputs are within the cortex and provide control and processing of information flow between cortical regions[255]. Altogether the thalamus has a significant role in sensory processing, cognitive function and behavioural states.

Thalamocortical neurons are known to operate in two distinct modes, consisting of tonic firing or bursting [35, 256, 257]. While the membrane potential is maintained around -60mV, thalamocortical

neurons fire in a tonic mode where there is a close to linear relationship between input signal and output [35]. When TC neurons are hyperpolarised, their T-Type Ca^{2+}channels become de-inactivated and respond to depolarising inputs or re-polarisation with bursts of action potentials [256, 257]. Tonic and bursting modes are respectively associated with awake and sleep states.

A number of in-silico models developed over the years have been used to represent aspects of thalamocortical networks. The scale and detail of these models vary dramatically, from population firing-rate based models and neural mass models [258, 259, 260], to spiking and IFB neuron models [261, 262, 263, 114, 264] to Hodgkin-Huxley style models incorporating individual ionic channels [265, 266, 267] and realistic morphologies with multiple cellular compartments [268, 269, 270, 271, 272, 273].

A small number of works have looked at the effect of a cortical lesion on thalamic activity. In particular, Proske *et al.* [263] and Wijngaarden *et al.* [114] used a hybrid model of spiking neurons with T-Type channels to explore the effects of stroke. They replicated bursting behaviour in the non-specific relay neurons of the thalamus that may be associated with thalamocortical dysrhythmia observed in stroke patients [114]. Interestingly though, the model showed no change in behaviour of specific relay neurons such as those comprising the VPL. Destexhe [270] modelled the impact of corticothalamic projections on activity of thalamic neurons and showed how decortication was able to recreate the desynchronisation of thalamic-generated spindles in a cat.

None of these works have reproduced some of the observed effects of stroke, namely bursting in the VPL to sensory input or increased spontaneous activity. Nor have they related them to a possible excitotoxic insult and the progression of SND. In this chapter we use a minimal HH-style model to incorporate key ion channels capturing the bursting behaviour of TC neurons.

2.2 Thalamocortical Network Model

The thalamocortical network used in this chapter is based on single compartment models of thalamocortical (TC), thalamoreticular (TRN) and corticothalamic (CT) neurons representing the primary somatosensory network. Thalamocortical neurons project to layer IV in the respective region of the somatosensory cortex but also directly synapse to layer VI neurons [37]. The CT neurons represent the projections from layer VI that are reciprocally connected to TC neurons and also project collaterals to the TRN. The TRN neurons only connect to TC neurons. All TC and CT neurons are excitatory, i.e. using glutamate as the neurotransmitter, while TRN neurons are inhibitory and release GABA. The simplified network model is depicted in Figure 2.1, showing the impact of stroke on network connectivity and the progression to SND.

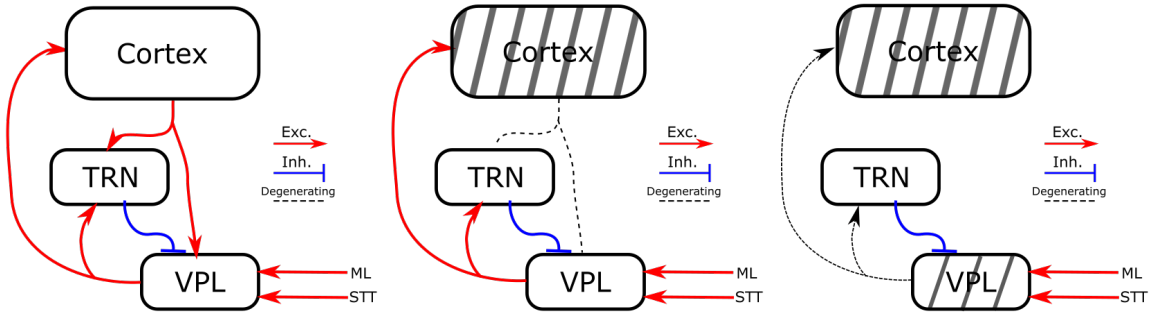

(a) Healthy **(b)** After Stroke **(c)** Progression of SND

Figure 2.1: Simple network diagram showing the effect of stroke on thalamocortical network connections. The immediate effect of stroke is the loss of cortical neurons and degeneration of corticothalamic fibres. In the weeks after stroke, thalamocortical axons experience retrograde degeneration followed by their death.

2.2.1 Model Description

Intrinsic parameters for each population of neurons are taken from previous works that derived them from in-vitro experiments. Synaptic parameters are then fit to reproduce empirical results and behaviours observed both in-vitro and in-vivo. ([274, 115]). The backbone of this model is derived from previous works by Destexhe *et al.* [265, 266] in modelling the thalamocortical network and is detailed below.

The membrane potential, v, of each neuron is described by the equation below:

$$C_m \frac{\mathrm{d}v}{\mathrm{d}t} = -I_L - \sum I_{int} - \sum I_{syn} \tag{2.1}$$

Where C_m is the membrane capacitance, I_L, represents the leakage currents, I_{int} the intrinsic voltage-gated ionic channels and I_{syn} the synaptic receptor currents and which are outlined in the following subsections.

2.2.1.1 Ionic Channels

All neuron types possess a general leak current, I_L, while a specific potassium leak current,I_{K_L}, is also specified for thalamocortical neurons.

$$I_L = g_L(v - V_L) \tag{2.2}$$

$$I_{K_L} = g_{K_L}(v - E_K) \tag{2.3}$$

The inclusion of fast sodium, I_{Na}, and delayed rectifier potassium, I_K, currents recreate the generation of action potentials. These models were derived from hippocampal neurons [275] and modified for the behaviour of thalamocortical neurons [276, 265].

$$I_K = g_K n^4 (v - E_K) \tag{2.4}$$

$$\frac{\mathrm{d}n}{\mathrm{d}t} = \frac{n_\infty - n}{\tau_n} \tag{2.5}$$

$$\alpha_n = \frac{0.032(15 - v^*)}{\exp((15 - v*)/(5)) - 1} \tag{2.6}$$

$$\beta_n = 0.5 \exp\left(\frac{10 - v^*}{40}\right) \tag{2.7}$$

$$\tau_n = \frac{1}{\alpha_n + \beta_n} \tag{2.8}$$

$$n_\infty = \frac{\alpha_n}{\alpha_n + \beta_n} \tag{2.9}$$

$$I_{Na} = g_{Na} m^3 h (v - E_{Na}) \tag{2.10}$$

$$\frac{\mathrm{d}m}{\mathrm{d}t} = \frac{m_\infty - m}{\tau_m} \tag{2.11}$$

$$m_\infty = \frac{\alpha_m}{\alpha_m + \beta_m} \tag{2.12}$$

$$\tau_m = \frac{1}{\alpha_m + \beta_m} \tag{2.13}$$

$$\alpha_m = \frac{0.32(13 - v^*)}{\exp((13 - v^*)/(4)) - 1} \tag{2.14}$$

$$\beta_m = 0.28 \frac{v * -40}{\exp((13 - v^*)/4) - 1} \tag{2.15}$$

$$\frac{\mathrm{d}h}{\mathrm{d}t} = \frac{h_\infty - h}{\tau_h} \tag{2.16}$$

$$h_\infty = \frac{\alpha_h}{\alpha_h + \beta_h} \tag{2.17}$$

$$\tau_h = \frac{1}{\alpha_h + \beta_h} \tag{2.18}$$

$$\alpha_h = 0.128 \exp\left(\frac{17 - v^*}{18}\right) \tag{2.19}$$

$$\beta_h = \frac{4}{1 + \exp((40 - v^*)/5)} \tag{2.20}$$

Where $v*$ represents a shifted voltage for action potential threshold, which is adjusted for each neuronal sub-type and detailed in Table 2.1.

Each neuron possesses a number of additional, unique voltage-gated channels. T-Channels on thalamocortical neurons produce the low-threshold spikes (LTS), they are de-inactivated at hyperpolarised membrane potentials and when repolarised can give rise to bursts of action potentials. The T-Channel current, I_T is defined as below [277]:

$$I_T = g_T m_T^2 h_T (v - E_{Ca}) \tag{2.21}$$

$$\frac{\mathrm{d}m_T}{\mathrm{d}t} = \frac{m_{T_\infty} - m_T}{\tau_{m_T}} \tag{2.22}$$

$$\frac{\mathrm{d}h_T}{\mathrm{d}t} = \frac{h_{T_\infty} - h_T}{\tau_{h_T}} \tag{2.23}$$

$$m_{T_\infty} = \frac{1}{1 + \exp(-(v + 59)/6.2)} \tag{2.24}$$

$$h_{T_\infty} = \frac{1}{1 + \exp((v + 83)/4)} \tag{2.25}$$

$$\tau_{h_T} = \begin{cases} \exp\left(\frac{v+469}{66.6}\right) & v < V_T \\ \exp\left(\frac{v+24}{-10.5}\right) + 28 & v \geq V_T \end{cases} \tag{2.26}$$

$$\tau_{m_T} = \frac{1}{\exp((v + 134)/-16.7) + \exp((v + 18.8)/18.2)} + 0.612 \tag{2.27}$$

Hyperpolarisation-activated cyclic nucleotide (HCN) channels exist on thalamocortical neurons and generate a H-Current, I_h, at hyperpolarised membrane potentials. It is additionally modulated by intracellular calcium concentration to transition to a higher conductance 'open-locked' state O_L, with model described as [265]:

$$I_h = g_h m_h (v - V_h) \tag{2.28}$$

$$m_H = O + 2O_L \tag{2.29}$$

$$s\frac{\mathrm{d}O}{\mathrm{d}t} = \alpha_H C + -(\beta_H + k_{h3})O + k_{h4} O_L \tag{2.30}$$

$$\frac{\mathrm{d}O_L}{\mathrm{d}t} = k_{h3} O + -k_{h4} O_L \tag{2.31}$$

$$\frac{\mathrm{d}P_1}{\mathrm{d}t} = -k_{h2} P_1 + (1 - P_1) k_{h1} \tag{2.32}$$

$$\alpha_H = \frac{H_\infty}{\tau_H} \tag{2.33}$$

$$\beta_H = \frac{1 - H_\infty}{\tau_H} \tag{2.34}$$

$$H_\infty = \frac{1}{1 + \exp((v + 75)/5.5)} \tag{2.35}$$

$$\tau_H = 20 + \frac{1000}{\exp((v + 71.5)/14.2) + \exp(-(v + 89)/11.6)} \tag{2.36}$$

$$k_{h1} = k_{h2} \left(\frac{[Ca]_i}{0.002} \right)^4 \tag{2.37}$$

$$k_{h3} = k_{h4} \frac{P1}{0.01} \tag{2.38}$$

$$(C + O + O_L) = 1 \tag{2.39}$$

A form of T-Channel also exists in reticular neurons whose current, I_{T_s}, also gives ability to generate LTS bursts [268]:

$$I_{T_s} = g_{T_s} m_{T_s}^2 h_{T_s} (v - E_{Ca}) \tag{2.40}$$

$$\frac{\mathrm{d}m_{T_s}}{\mathrm{d}t} = \frac{m_{T_{s\infty}} - m_{T_s}}{\tau_{m_{T_s}}} \tag{2.41}$$

$$\frac{\mathrm{d}h_{T_s}}{\mathrm{d}t} = \frac{h_{T_{s\infty}} - h_{T_s}}{\tau_{h_{T_s}}} \tag{2.42}$$

$$\tau_{m_{T_s}} = 3 + \frac{1}{\exp((v + 134)/-16.7) + \exp((v + 18.8)/18.2)} \tag{2.43}$$

$$\tau_{h_{T_s}} = 85 + \frac{1}{\exp((v + 25)/10) + \exp(-(v + 100)/15)} \tag{2.44}$$

$$m_{T_{s\infty}} = \frac{1}{1 + \exp(-(v + 50)/7.4)} \tag{2.45}$$

$$h_{T_{s\infty}} = \frac{1}{1 + \exp((v + 78)/5)} \tag{2.46}$$

Slow activating M-Channels shape the response of CT Neurons to create modes of repetitive firing and bursting [266]:

$$I_M = g_M m_M (v - E_K) \tag{2.47}$$

$$\frac{\mathrm{d}m_M}{\mathrm{d}t} = \frac{m_{M_\infty} - m_M}{\tau_M} \tag{2.48}$$

$$m_{M_\infty} = \frac{1}{1 + \exp(-(v + 35)/10)} \tag{2.49}$$

$$\tau_M = \frac{\tau_{M_{Max}}}{3.3 \exp((v + 35)/20) + \exp(-(v + 35)/20))} \tag{2.50}$$

The models for I_T, I_{T_s} & I_h were fit from in-vitro experiments performed at $\approx$ 24 °C (T_1). The rates are therefore adjusted for an in-vivo body temperature of 37°C (T_2) using an assumed Q10 factor of 2.5:

$$\phi = Q_{10}{}^{(T_2 - T_1)/10} \tag{2.51}$$

$$\tau_{new} = \tau/\phi \tag{2.52}$$

The parameters of the model are detailed in Table 2.1, note that the leakage conductance and voltage of TC neurons was adjusted to give a resting membrane potential of approximately -70mV in line with recordings from rodents [274, 106] and prevent the generation of spontaneous oscillations.

Table 2.1: Neuron Model Parameters

Parameter	**Unit**	**TC**	**TRN**	**Ctx**	**Source**
Surface Area	μm^2	29×10^3	14.3×10^3	29×10^3	[266]
C	$\mu F/cm^2$	1	1	1	[265, 266]
g_L	mS/cm^2	0.05	0.05	0.1	[265, 266]
V_L	mV	-73	-90	-70	[265, 266]
g_{KL}	mS	4×10^{-6}			[265]
g_{Na}	mS/cm^2	90	200	50	[265, 266]
E_{Na}	mV	50	50	50	[265, 266]
g_K	mS/cm^2	10	20	5	[265, 266]
E_K	mV	-100	-90	-100	[265, 266]
$v*$	mV	$v - 25$	$v - 55$	$v - 63$	[265, 266, 275]
g_T	mS/cm^2	2			[265, 277]
V_T	mV	-80			[265, 277]
g_{T_s}	mS/cm^2		0.8		[265, 268]
g_h	mS/cm^2	0.02			[265]
V_h	mV	-40			[265]
k_{h2}	ms^-1	4×10^-4			[265]
k_{h4}	ms^-1	0.001			[265]
V_h	mV	-40			[265]
g_M	mS/cm^2			0.07	[266]
$\tau_{M_{\text{Max}}}$	ms			1000	[266]

We defined the intra- and extracellular ionic concentrations as given in Table 2.2, and unless specified elsewhere reverse potentials for each ionic species were calculated using Equation 2.53.

Table 2.2: Ion Concentrations of Intracellular and Extracellular Compartments

Ionic Species	Intracellular [mM]	Extracellular [mM]
Na^+	15	145
K^+	140	5
Cl^-	5	110
Ca^{2+}	240×10^{-6}	2
Mg^{2+}	-	2

$$E_x = \frac{-RT}{z_x F} \ln\left(\frac{[x]_i}{[x]_e}\right) \tag{2.53}$$

2.2.1.2 Receptor Models

Five receptor subtypes (AMPAR, NMDAR, KAR, GABAaR and GABAbR) are considered to simulate the synaptic connections between neurons. The following model represents the ligand-dependent transition between closed and open states for AMPAR, NMDAR, KAR and GABAaRs [278], where r_x denote the portion of receptors in the open state.

$$C \underset{\beta(v)}{\overset{\alpha(v)}{\rightleftharpoons}} O \tag{2.54}$$

$$\frac{\mathrm{d}r_x}{\mathrm{d}t} = \alpha_x[T](1 - r_x) - \beta_x r_x \tag{2.55}$$

$$I_x = g_x r_x (v - E_x) \tag{2.56}$$

Where $x \in \{\text{AMPAR, GABAaR, KAR}\}$ and $[T]$ is the neurotransmitter concentration. NMDARs are additionally modulated by an Mg^{2+}block at low membrane voltages and hence combined with the above gating equation, the current is derived by:

$$B_{Mg} = \frac{1}{1 + \exp(-0.062v)([\mathrm{Mg}^+]/3.57)} \tag{2.57}$$

$$I_{\mathrm{NMDAR}} = g_{\mathrm{NMDAR}}\, B_{Mg}\, r_{\mathrm{NMDAR}}\, (v - E_{\mathrm{NMDAR}}) \tag{2.58}$$

Where $[Mg^+]$ is the extracellular magnesium concentration.

A different kinetic model is required for GABAbRs as they are metabotropic receptors. Similarly to above, the receptor is still triggered by GABA to give a portion of activated receptors, r. Instead of directly conducting ion currents, it modulates the conductance of K^+channels via the production

of G-Proteins, whose concentration here is represented by the variable s. We use the model from Destexhe *et al.* [278] described as:

$$\frac{\mathrm{d}r}{\mathrm{d}t} = K_1[GABA](1-r) - K_2 r \tag{2.59}$$

$$\frac{\mathrm{d}s}{\mathrm{d}t} = K_3 r - K_4 s \tag{2.60}$$

$$I_{\mathrm{GABAbR}} = g_{\mathrm{GABAbR}} \frac{s^4}{s^4 + K_d}(V - E_K) \tag{2.61}$$

The opening and closing rates of lemniscal and CT synapses were derived from empirical data presented in [274],and is described in Table 2.3. Note that β_{AMPAR} had to be decreased from 1/5.14, to meet the rise time of non-NMDAR currents, alternatively the time-course of synaptic glutamate could be altered. α_{NMDAR} and α_{KAR} were assumed to be 1/10 and 1/5 of α_{AMPAR}.

Table 2.3: Receptor parameters for excitatory thalamic synapses.

Parameter	Units	ML Value	CT Value
α_{AMPAR}	$\mathrm{mM}^{-1}\mathrm{ms}^{-1}$	1.5	0.11
β_{AMPAR}	ms^{-1}	1/4.07	1/7
α_{NMDAR}	$\mathrm{mM}^{-1}\mathrm{ms}^{-1}$	0.15	0.011
β_{NMDAR}	ms^{-1}	1/45.1	1/104.4
α_{KAR}	$\mathrm{mM}^{-1}\mathrm{ms}^{-1}$	-	0.022
β_{KAR}	ms^{-1}	-	87.9

The receptor parameters for remaining synaptic connections, are detailed in Table 2.4, taken from [278]:

Table 2.4: Receptor parameters for all other synapses.

Parameter	Units	Value
E_{AMPAR}	mV	0
α_{AMPAR}	$\text{mM}^{-1}\text{ms}^{-1}$	0.94
β_{AMPAR}	ms^{-1}	0.18
E_{NMDAR}	mV	0
α_{NMDAR}	$\text{mM}^{-1}\text{ms}^{-1}$	0.11
β_{NMDAR}	ms^{-1}	0.0066
E_{GABAaR}	mV	E_{Cl}
α_{GABAaR}	$\text{mM}^{-1}\text{ms}^{-1}$	10.5
β_{GABAaR}	ms^{-1}	0.16
E_{GABAbR}	mV	E_K
K_1	$\text{mM}^{-1}\text{ms}^{-1}$	0.09
K_2	ms^{-1}	0.0012
K_3	ms^{-1}	0.18
K_4	$\text{mM}^{-1}\text{ms}^{-1}$	0.034
K_d	$\text{mM}^{-1}\text{ms}^{-1}$	100

The concentration of neurotransmitter in the synapse after pre-synaptic firing is modelled as an exponential decay with a maximum concentration set to 1mM, upon presynaptic firing, and decay rate of $\tau = 2$ms as observed by Clements [279].

2.2.1.3 Calcium Dynamics

A simple calcium model, from [280], is used to simulate the concentration of intracellular calcium in a thin shell of 0.1µm depth below the neuronal membrane, with volume $\mathcal{V}_{shell}$, as described in Equation 2.62. A single decay model represents the diffusion of Ca^{2+}into the remaining cytosol and extrusion through pumps and exchangers, with τ_{Ca} set to 5ms. The intracellular Ca^{2+}concentration updates the reverse potential of calcium channels using Equation 2.53.

$$\frac{\mathrm{d}[Ca]_i}{\mathrm{d}t} = \frac{J_{Ca}}{\mathcal{V}_{shell}} + ([Ca]_i(0) - [Ca]_i)/\tau_{Ca} \tag{2.62}$$

Where J_{Ca} is the net calcium flux through calcium-permeable channels:

$$J_{Ca} = \frac{-(I_T + I_{NMDAR})}{z_{Ca}F} \tag{2.63}$$

2.2.1.4 Short-term Synaptic Plasticity

Synapses exhibit time-dependent responses to repetitive stimulation known as short-term synaptic plasticity, that can enhance (synaptic facilitation) or reduce (synaptic depression) the amplitude of successive post-synaptic currents. The primary mechanism behind synaptic facilitation is an increased release of neurotransmitter [281]. This is promoted by rises in pre-synaptic Ca^{2+}levels [282, 283, 281] which can be due to activation of pre-synaptic receptors by neurotransmitter spillover [284]. Synaptic depression can result from the depletion of readily-releasable neurotransmitter vesicles [281], reduction in neurotransmitter release [284] and receptor desensitisation [285].

The presence of short-term synaptic plasticity in excitatory thalamic synapses is evident in the work by Miyata *et al.* [274], where it is shown that corticothalamic synapses exhibit a clear facilitatory response, while lemniscal synapses a depressive response, to trains of stimulation. We use a form of synaptic plasticity model that has been previously described [286, 287]. Two variables are used at each synapse to represent the dynamics of facilitation, F, and depression, D.

The two models mentioned, [286, 287], do not include the dynamics of neurotransmitters. They use a single conductance parameter to describe synaptic transmission, which is scaled by the facilitation and depression variables to determine post-synaptic current. Given the primary mechanisms of synaptic plasticity, mentioned above, involve the pre-synaptic release of glutamate, we instead scale the release of glutamate from pre-synaptic neurons in our model by the plasticity variables. This also takes a conservative approach in estimating excess glutamate release in the context of excitotoxicity.

$$\frac{\mathrm{d}X}{\mathrm{d}t} = \frac{1 - X}{\tau_X} \tag{2.64}$$

$$\text{if (Presynaptic Event)} : \qquad X \to p_X X \tag{2.65}$$

Where $X \in \{F, D\}$. Therefore the concentration of glutamate in the synaptic cleft, $[Glu]$ after a pre-synaptic action potential can be described as:

$$[Glu]_{Syn} = C_{max} F D \exp(-t/\tau_{Glu}) \tag{2.66}$$

The values p and τ were estimated from the excitatory post-synaptic currents in [274] and the values are given in Table 2.5.

Table 2.5: Synaptic plasticity parameters for the thalamus

Parameter	ML Synapse	CT Synapse
p_D	0.6	0.8
τ_D	180 ms	50 ms
p_F	-	2
τ_F	-	70 ms

2.2.1.5 Tuning Thalamic Synapses

Using empirical data from a set of experiments performed by Miyata and Imoto [274] we are able to tune the conductance of the excitatory thalamic synapses, i.e. corticothalamic and medial lemniscal, to match that of ventrobasal thalamocortical neurons specific to mice. It was found that multiple stimulations of corticothalamic fibres at 40Hz were required to reliably elicit an action potential in TC neurons, while stimulation of the ML resulted in a burst to the first input but lack of response to the later pulses at 20 Hz. The CT synapse is composed of both NMDARs, AMPARs and KARs with peak currents through NMDARs twice that of non-NMDARs. Conversely, the ratio of NMDAR current to non-NMDAR current in the ML synapse is roughly half. Using these pieces of information, an estimate of the total conductance at each synapse was made to agree with the in-vitro observations (Figures 2.2,2.3). We assume that action potentials in all cortical projections to the thalamus were simultaneously triggered and thus the conductance of each individual synapse is equal to the total divided by the number of cortical projections to a single TC neuron.

Table 2.6 lists the final excitatory post-synaptic current values compared to [274]:

Table 2.6: Summary of modelled medial lemniscal and corticothalamic synapse properties.

Property	Desired Value	Actual Value
Peak NMDA : non-NMDA ratio (ML)	0.6 ± 0.16	0.55
Peak NMDA : non-NMDA ratio (CT)	1.91 ± 0.31	1.94
non-NMDA rise-time (ML)	0.93 ± 0.25	0.96
non-NMDA rise-time (CT)	1.97 ± 0.61	1.94
AMPA decay constant (ML)	4.07 ± 2.11	4.13
AMPA decay constant (CT)	5.14 ± 1.29	7.00
NMDA rise-time (ML)	-	3.02
NMDA rise-time (CT)	-	3.63
NMDA decay constant (ML)	45.1 ± 4.2	45.1
NMDA decay constant (CT)	104.4 ± 37.8	104.4

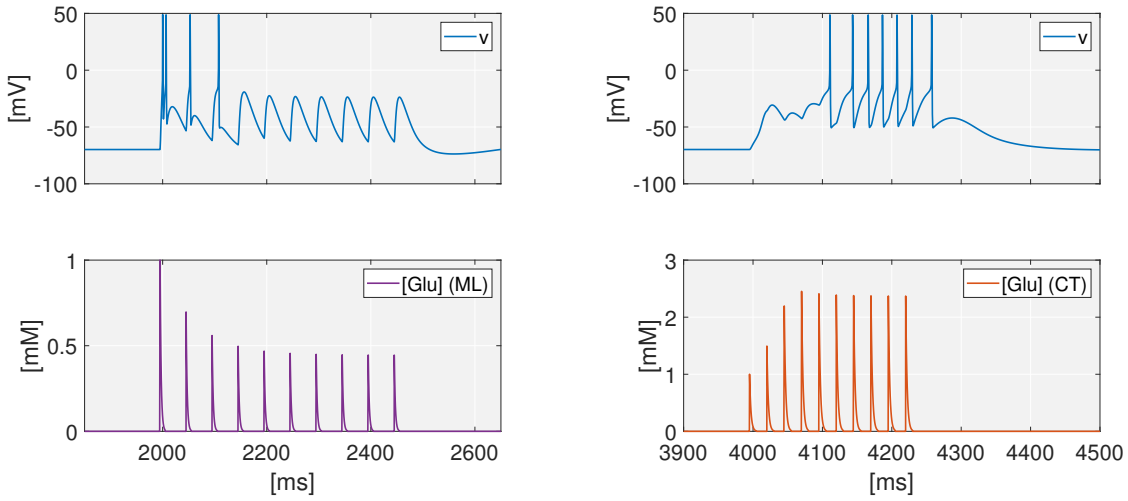

(a) Simulated response of TC neurons to 20Hz stimulation of ML fibres: (top) TC membrane potential, (bottom) glutamate in the ML synapse.

(b) Simulated response of TC neurons to a 40Hz stimulation of CT fibres: (top) TC membrane potential, (bottom) glutamate in the CT synapse.

Figure 2.2: Simulated responses in thalamocortical neurons to ML and CT stimulation. The synaptic conductances were tuned to fit experimental data obtained by Miyata and Imoto [274] at a resting potential of approximately -70 mV. Multiple stimulations of CT fibres at 40Hz were required to begin eliciting action potentials. TC neurons burst to the first ML stimulation but could not follow high frequency input. The introduction of synaptic plasticity shows depression of glutamate release from ML and facilitation from CT fibres.

2.2.1.6 Connectome

The remaining synaptic conductances and transmission delays are modified from those found in the literature. Connectivity and transmission delays are taken from [263] which represents a structure of parallel barrelloids. TC and TRN neurons are reciprocally connected one-to-one in pairs, with eight cortical neurons reciprocally connecting to a single TC/TRN neuron pair as shown in Figure 2.4, with the receptors present at each synapse labelled. We assume the cortical synapse to TRN neurons is equal to that which we tuned for TC neurons. Heterogeneity in the transmission pathway is introduced with the addition of a random zero to two second delay derived from a uniform distribution, $U[0, 2]$, as described in Table 2.7.

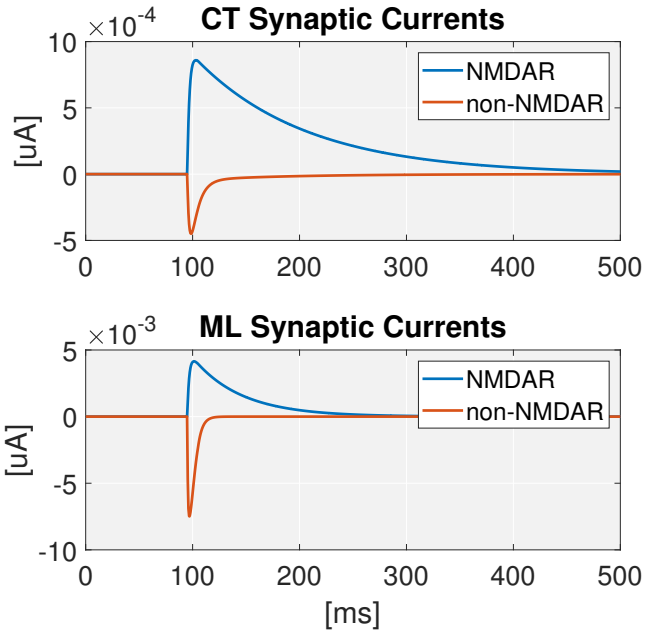

Figure 2.3: Simulated NMDAR and non-NMDAR post-synaptic currents in a TC neuron from a single stimulation of ML and CT fibres at a resting potential of 40mV for NMDAR currents and -90 mV for non-NMDAR currents. The rise and decay times of currents evoked from CT stimulation are significantly slower and the peak NMDA:non-NMDA current ratio significantly larger (1.94 compared to 0.55).

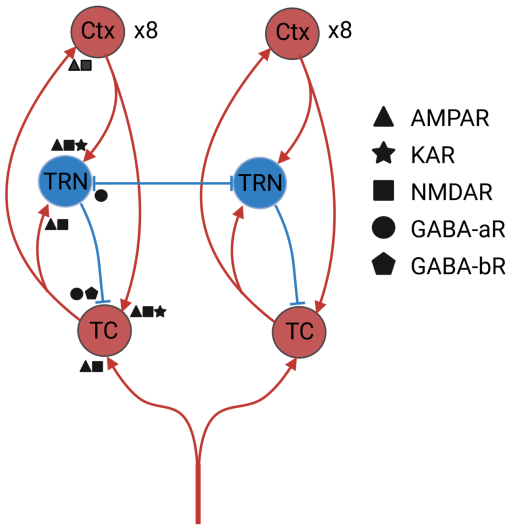

Figure 2.4: Structure of the thalamocortical network model showing the connections between individual neurons and the receptors located in each synapse.

Table 2.7: Network connectivity - Conductances and Delays

Connection	**Type**	**Conductance [µS]**	**Delay [ms]** [263]
ML →TC	AMPAR NMDAR	0.12 0.48	0
TC →TRN	AMPAR NMDAR	0.2 0.05 [265]	$3 + U[0, 2]$
TC →CT	AMPAR NMDAR	0.04 0.01	$7 + U[0, 2]$
TRN →TC	GABAaR GABAbR	0.04 0.04 [265]	$3 + U[0, 2]$
CT →TC	AMPAR KAR NMDAR	0.0372 0.0124 1.116	$7 + U[0, 2]$
CT →TRN	AMPAR NMDAR	0.0372 1.116	$7 + U[0, 2]$
TRN →TRN	GABAaR	0.2 [265]	$1 + U[0, 2]$

2.2.1.7 Cortical Input

Thalamocortical synapses make up only 5-10% of inputs to layer VI cortical neurons [29], therefore we simulate other inputs to the corticothalamic neurons. We use a Poisson distributed spike train of 5-15 Hz (similar to in [266]), with a 1ms refractory period to excite CT neurons. This represents the average firing rate and predominately un-synchronised cortical activity in the awake state.

2.2.1.8 Numerical Simulation

The model was simulated in Matlab (v2018a) with custom scripts. The system of differential equations is solved using either forward Euler's method or Matlab's stiff solver *ode15s* with a maximum time-step $\mathrm{d}t = 0.01$ms.

2.3 Effect of Stroke on Thalamocortical Network

2.3.1 Loss of corticothalamic excitation switches TC neurons from a tonic firing mode to bursting

A common theme in recordings from the thalamus after stroke is the presence of bursting and 'after-discharges' to peripheral stimulation [115, 288]. The typical bursting response of TC and TRN neurons is largely governed by the de-inactivation of T-Type Ca^{2+}channels at hyperpolarised membrane potentials. Upon re-polarisation the T-Channel gives rise to a large inward Ca^{2+}current upon which multiple action potentials are generated.

The corticothalamic neurons originating in layer VI of the cortex have a modulatory influence on the firing mode of VPL neurons [29]. This is reflected in Figures 2.3 and 2.2, showing the slow prolonged time-course of post-synaptic current in the CT synapse. Persistent, sub-threshold stimulation from CT neurons can provide enough depolarisation to prevent significant de-inactivation of T-Type Ca2+ channels of TC neurons. This maintains the neurons in a tonic mode of firing and allows a 'linear' transmission of sensory information.

This phenomena has been recorded by Hirai *et al.* [115] in awake rodents after cortical lesion and is replicated in the basic TC network shown in Figure 2.5. The decrease in membrane potential of TC neurons fits the assumption that corticothalamic projections have a net excitatory effect on TC neurons.

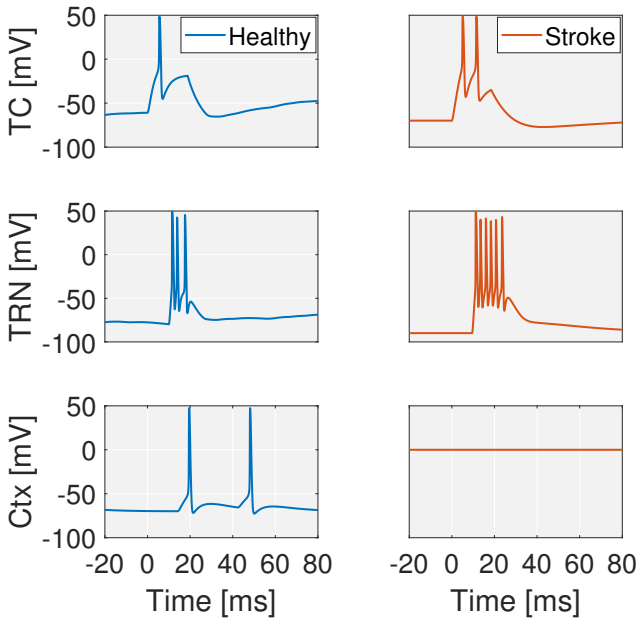

Figure 2.5: Loss of tonic cortical excitation after stroke leads to the development of LTS bursts in TC and TRN neurons in a simulated thalamocortical network (Pre-synaptic cortical firing rate = 10 Hz).

We further explore the conditions in which bursting develops by removing the cortical connections from the network model and replacing them with direct current injections into TC and TRN neurons to simulate the modulatory influence of the cortex. The resulting response of TC and TRN under different levels of excitation is shown in Figure 2.6.

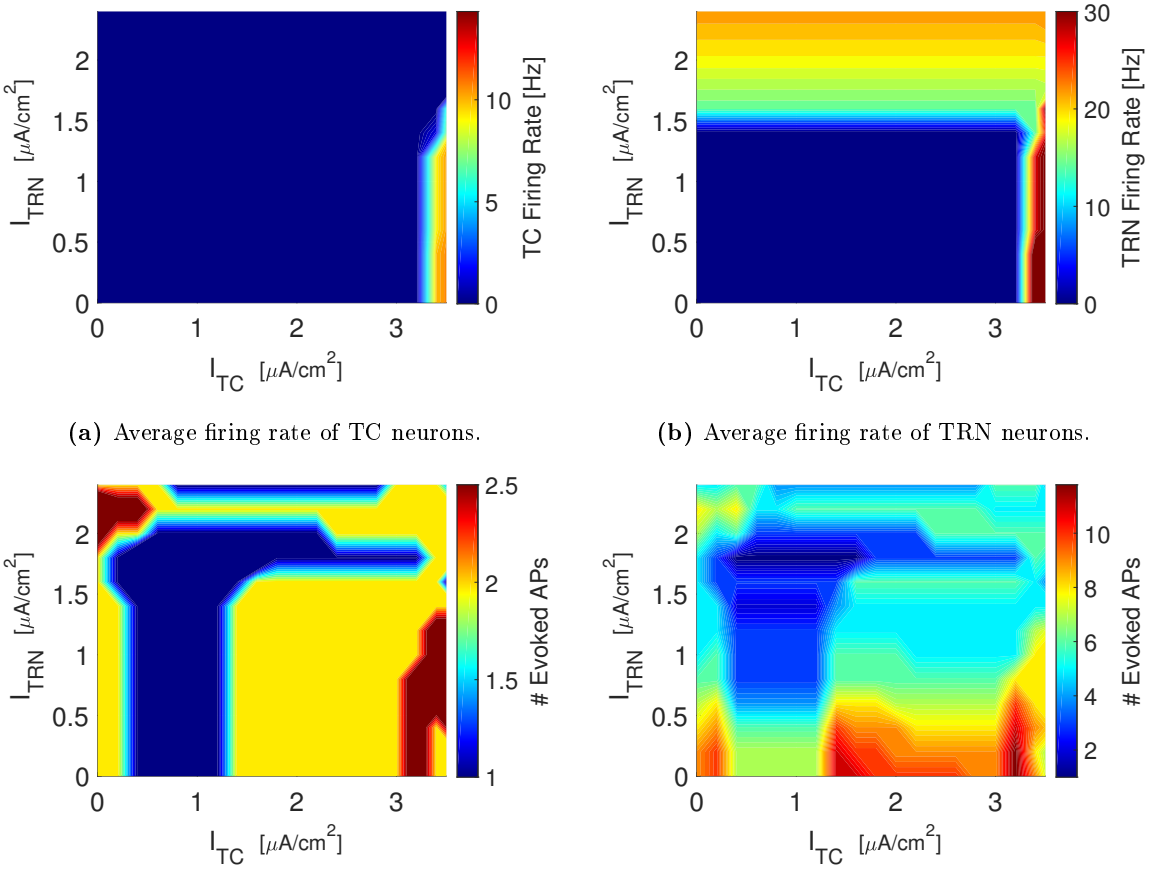

(a) Average firing rate of TC neurons.

(b) Average firing rate of TRN neurons.

(c) Number of APs evoked in TC neurons.

(d) Number of APs evoked in TRN neurons.

Figure 2.6: The number of evoked action potentials to peripheral stimulation and average firing rate of TC and TRN neurons under different levels of excitation. TC neurons can burst to peripheral input while both under-excited or over-excited and operates in tonic mode for moderate values. Extreme response of TC neurons occurs when significantly over excited (bottom-right of (c)) or under-excited due to tonic hyperpolarisation from active TRN neurons (top-left of (c)). TRN neurons were also seen to burst when under-excited (bottom of (d)).

We show an important set of phenomena in Figure 2.6. Firstly, TC neurons are found to burst at both low and high values of injected current, but for moderate values there is a 1-1 spike response, suggestive of the tonic mode of firing. Secondly the bursting response of TRN neurons is also lost as excitation is increased. Extreme responses of TC neurons occur when significantly over excited or when under-excited due to hyperpolarisation from tonic activity of TRN neurons. Figure 2.7 shows that the T-Channel current drives the bursting response of TC neurons at low resting potentials but

are absent at depolarised states. In the latter case, bursting is generated due to increased excitation, depolarising the neuron to being close to the activation voltage for Na^+channels to generate an action potential.

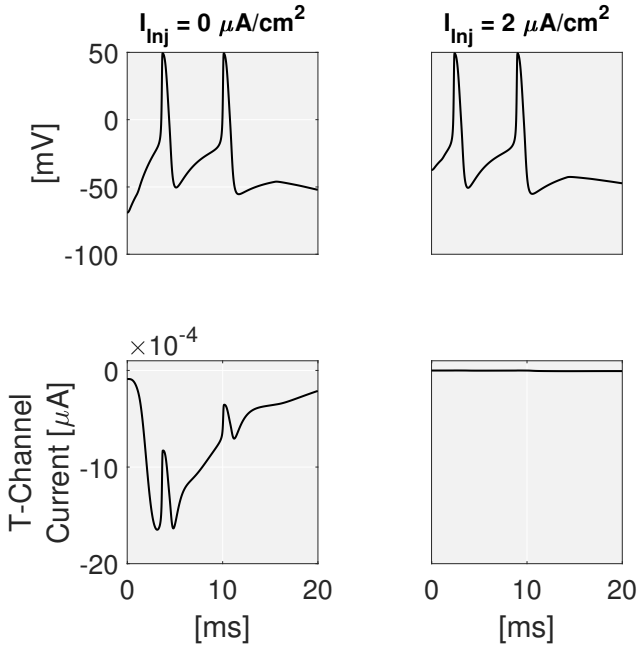

Figure 2.7: T-Channel current drives bursting response at low-resting potentials but not depolarised potentials. With zero injected current and a hyperpolarised membrane potential (left column), a significant T-channel current is evoked, which triggers the bursting response of TC neurons to depolarisation. Contrarily a significantly depolarised TC membrane potential (left column) has no T-channel current but also bursts to depolarisation.

In similar conditions to TC neurons, TRN neurons were found to burst while under-excited. This increase in TRN bursting was also recorded by Hirai *et al.* [115] which resulted in significant hyperpolarisation of TC neurons which rebounded with further LTS spikes. We were able to recreate this effect by increasing the T-Channel conductance by 10%, removing the GABA-bRs and doubling the GABA-aR conductance instead. The result shown in Figure 2.8, shows the development of rebound spikes with a period of approximately 100ms, the same latency as the late discharges observed by Hirai *et al.* [115]. We found that these oscillatory responses between TC and TRN neurons could continue indefinitely and may also explain the observations of after-discharges that have been recorded for up to seconds [288].

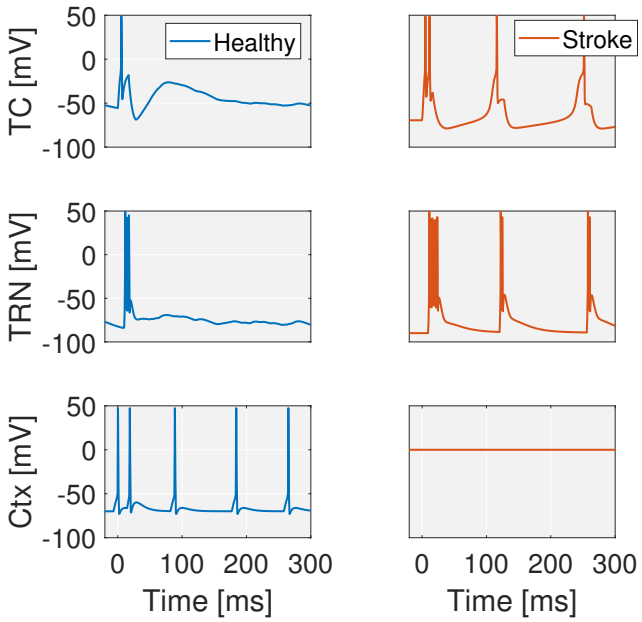

Figure 2.8: The hyperpolarised membrane potential of TC neurons, in the case of stroke, is susceptible to the generation of oscillatory rebound spikes. The hyperpolarised membrane potential causes a burst response to be triggered from ML stimulation, triggering a burst response in TRN neurons which induces significant hyperpolarisation of TC neurons and the generation of rebound spikes.

We further explored the conditions for oscillatory after discharges in the TC-TRN network and observed that although an initial burst response and single rebound spike could be generated under conditions of low or high excitation, the continual late discharges were only present under low excitation, see Figure 2.9.

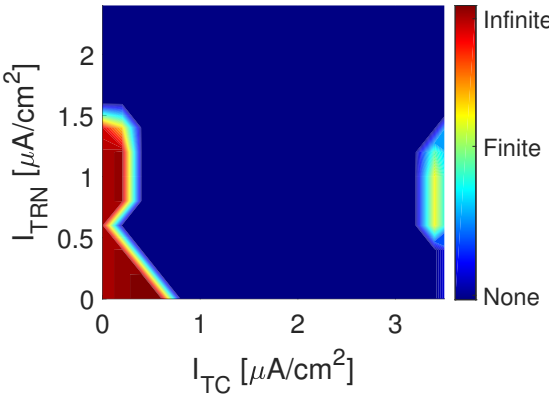

(a) Conditions for late rebound bursts and infinite oscillations.

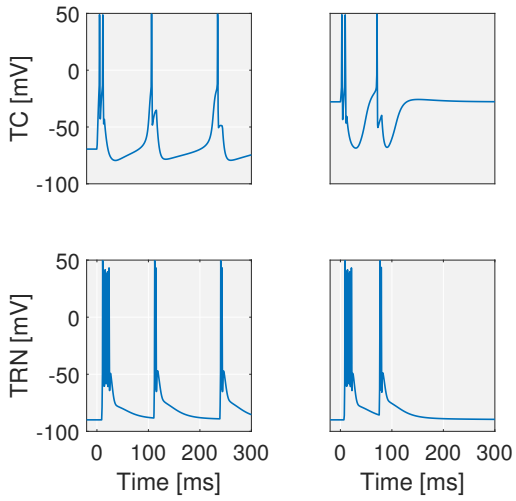

(b) Examples of infinite bursting oscillations in under-excited states (left) and finite rebound bursts when depolarised (right).

Figure 2.9: Oscillatory bursting activity only develops in under excited TC Neurons when the interplay with TRN neurons generates rhythmic rebound spikes.

2.3.2 Release of glutamate from degenerating corticothalamic neurons increases thalamocortical excitation

In the previous section we demonstrated that bursting of TC neurons to peripheral input can occur due to either a loss of excitation or increased excitation. After stroke, from a network based outlook, it is not clear how excitation of TC neurons can increase. The excitatory projections from the cortex are lost and we have found no evidence of increased activity of lemniscal fibres or the peripheral nervous system.

There is, however, evidence suggesting an increased concentration of glutamate in the rat thalamus in the first week after MCAO, which doesn't return to normal until 14 days [20], and this is believed to be released from degenerating corticothalamic neurons [20]. Studies recording the activity of TC neurons after cortical lesion have found both increased firing rates and increased responses to sensory stimulation [289, 288, 290]

An acute release of glutamate from injured corticothalamic neurons directly into the extracellular space surrounding TC neurons would cause hyperexcitability and explain an increase in spontaneous and evoked responses (simulated in Figure 2.10). This would fit both hypotheses of excitotoxic

damage, as the release is in close proximity to NR2B rich corticothalamic synapses but also cause a spillover onto extrasynaptic NMDARs. Note that the inclusion of additional NMDARs to represent those found at extrasynaptic locations would further amplify this effect and reduce the concentration of glutamate required.

An additional source of increased glutamate at corticothalamic synapses may be from hyperexcitable, peri-infarct CT projections [291, 111, 112]. But further details on the exact connectivity between surviving peri-infarct regions and neurons affected by SND is needed.

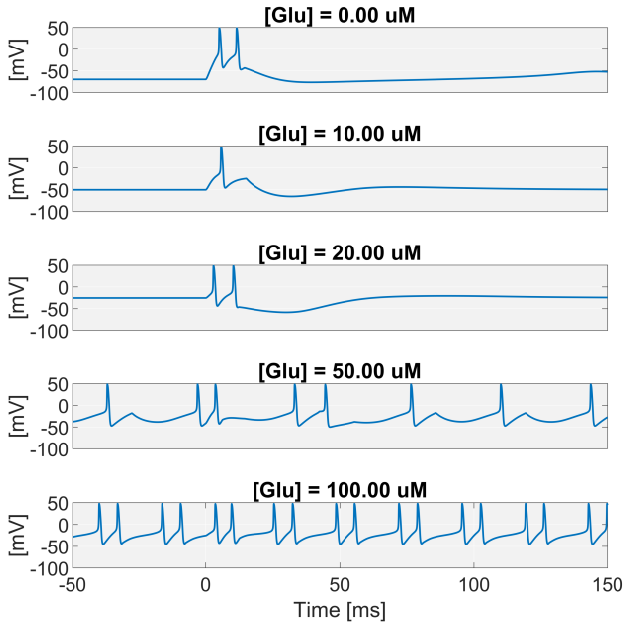

Figure 2.10: Increased extracellular glutamate increases spontaneous firing rate and produces bursting response to sensory input in TC neurons.

2.3.3 Accumulation of intracellular Calcium

Conversely to the first assumption of TC neurons becoming hyperpolarised after loss of cortical excitation, it has been shown in one instance that after stroke, surviving, but injured, thalamocortical neurons had a depolarised resting potential in-vitro [106]. It was determined that the half-activation voltage of HCN channels was shifted by approximately 10mV to a more depolarised value [106]. In the model presented by Paz *et al.* [106] this property accounted for the increased propensity of TC neurons to burst to a hyperpolarising input, and promoted epileptic activity.

The HCN channel is regulated by intracellular calcium concentration, which promotes the transition of open HCN channels into a state of higher conductance (see Equation 2.67). The activation of a regulator $P_0 \rightarrow P_1$ encourages transition to the 'open-locked' state O_L and thus shifting the half activation voltage (Figure 2.11). Interestingly, this may align with injury associated with excitotoxicity and an increased intracellular calcium concentration.

$$C \underset{\beta(v)}{\overset{\alpha(v)}{\rightleftharpoons}} O \tag{2.67}$$

$$P_0 + 2\mathrm{Ca}^{2+} \underset{k_2}{\overset{k_1}{\rightleftharpoons}} P_1 \tag{2.68}$$

$$O + P_1 \underset{k_3}{\overset{k_4}{\rightleftharpoons}} O_L \tag{2.69}$$

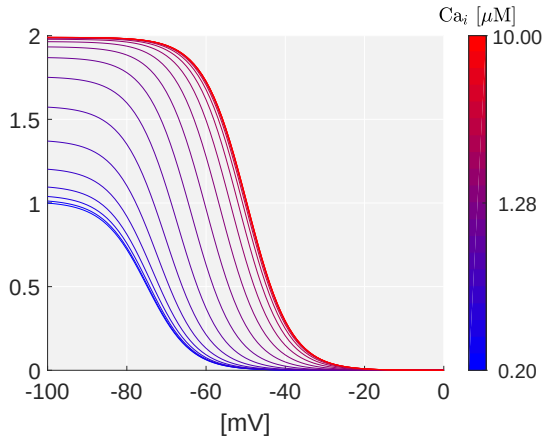

Figure 2.11: HCN activation dependence on intracellular Calcium concentration: with increasing intracellular Ca^{2+}concentration the half activation voltage is shifted to a more depolarised value. This is due to the transition to a higher conductance state as described in Equation 2.67

We explored a possible link between these phenomena and whether the progression of excitotoxicity and intracellular Ca^{2+}accumulation could increase excitability of TC neurons and reproduce bursting responses. By varying the basal intracellular calcium concentration from 200nM to 10µM we observed the opposite effect. The depolarising shift in resting-state potential prevented the de-inactivation of T-type channels and in fact reduced the propensity to burst to excitatory and inhibitory inputs, seen in Figure 2.12. However due to the contribution of intracellular Ca^{2+}in depolarising the resting membrane potential, there was a decrease in the extracellular glutamate concentration required to generate an excitatory burst response.

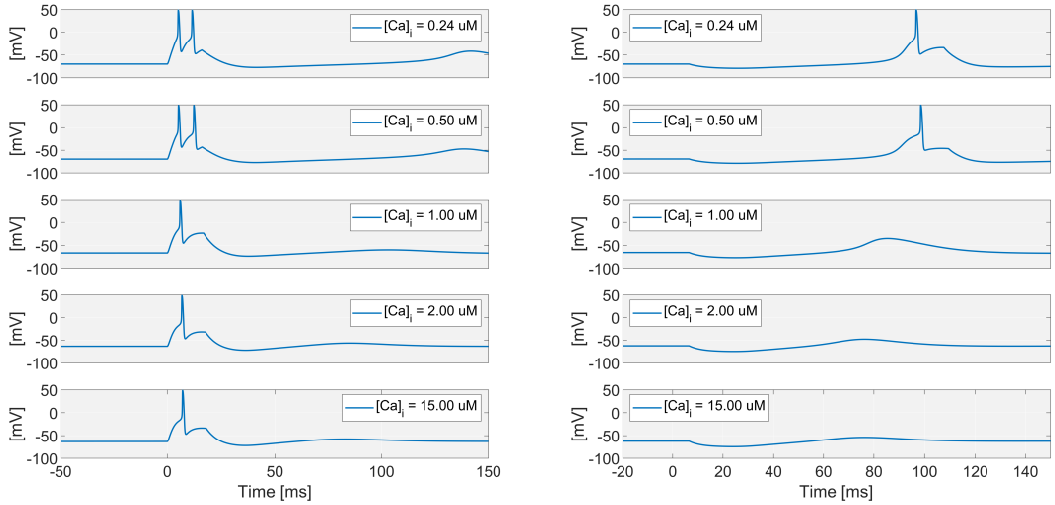

(a) Response to excitatory peripheral input.

(b) Response to inhibitory TRN burst.

Figure 2.12: Increased intracellular calcium concentration shifts the HCN-channel half-activation voltage and depolarises thalamocortical neurons resting potential. This depolarisation reduces the propensity to burst to peripheral input and generate rebound low-threshold spikes from inhibitory input.

It should be noted that the model for I_h presented in [106] uses a significantly different half-activation voltage and time-constant. Both the H- and T-Channels contribute to the rebound LTS. Our model uses a half-activation voltage of -75mV compared to their -105 and -95 mV for healthy and injury models. This means that a significantly greater hyperpolarisation is required to activate the H-channel, which for them was easier to reach in the injury model.

2.4 Simulated Evoked Potentials

We have simulated a number of observations and possible outcomes for stroke-induced pathological activity in the thalamocortical network. Given the plan to verify this activity in-vivo by recording from implanted electrodes, we can simulate the voltage trace expected to be recorded in extracellular space. The major contributors to the Local Field Potential (LFP) are the slow, post-synaptic currents which can be related to the extracellular voltage given the formula below [292]:

$$V_X = \frac{R_e}{4\pi} \sum_i \frac{I_{syn_i}}{r_i} \tag{2.70}$$

Where R_e is the extracellular resistivity (230 Ωcm), I_{syn_i} is the total synaptic current from compartment i and r_i is the radial distance of each compartment to the location of the recording electrode. The voltage trace is then low-pass filtered using a 4^{th}-order, zero-phase, Butterworth filter with cut-off frequency $f_c = 150$Hz to reflect the bandwidth typical of the recorded LFP signals. Note that we scaled the contribution of currents at corticothalamic synapses by a factor of five, to simulate the increased current that would be generated in distal dendrites [270].

The evoked potential generated by simulating an input volley of excitatory transmitter onto TC neurons reflects that acquired from stimulation of peripheral sensory neurons which polysynaptically project to the VPL. In clinical applications this is known as a Somatosensory Evoked Potential (SSEP) and will be discussed in further detail in Chapter 3.

First we simulate the SSEP evoked in a network consisting of five TC and TRN neuron pairs each connected to eight excitatory layer VI neurons. We assume a recording electrode is located in the VB thalamus and therefore randomly distribute the five TC neurons at radial distances in $U[0, 150]$ µm. The evoked waveform shown in Figure 2.13 shows three key peaks: (1) an initial negative depolarisation triggered by excitatory post-synaptic currents in the medial lemniscal synapse (2) a slight positive peak generated by inhibitory currents from GABA-ergic TRN neurons and (3) a later negative peak generated by excitatory corticothalamic feedback. Interestingly, we notice a second smaller negative peak following the first that is due to the momentary decrease in synaptic current as the action potential is generated. This simulated waveform agrees with evoked responses recorded by others [293, 294, 295].

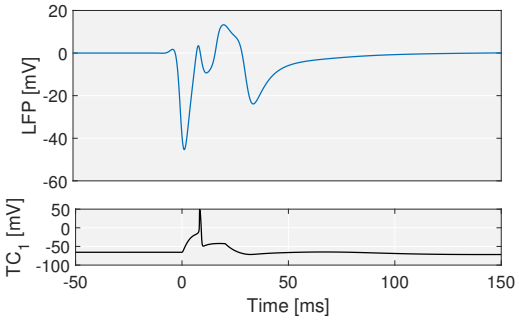

(a) Simulated thalamic SSEP waveform (top) and membrane potential of a single TC neuron (bottom)

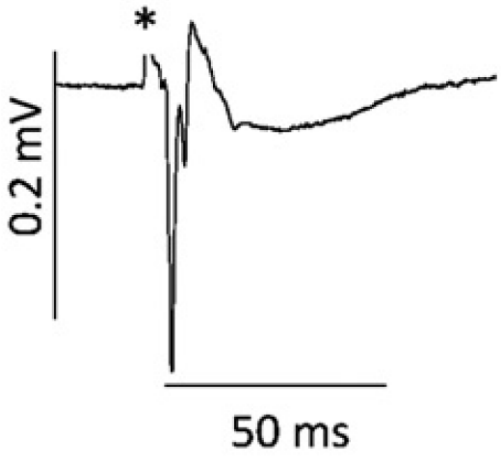

(b) Thalamic SSEP Recorded by Alonso-Calvino *et al.* [293] with Cortical Feedback (Licensed under the CC BY-NC-ND 4.0)

Figure 2.13: A simulated thalamic SSEP waveform shows three key peaks: (1) an initial negative depolarisation triggered by excitatory post-synaptic currents in the medial lemniscal synapse (2) a slight positive peak generated by inhibitory currents from GABA-ergic TRN neurons and (3) a later negative peak generated by excitatory corticothalamic feedback.

By simulating the effects of stroke and retrograde degeneration, we can predict the changes in the thalamic SSEP waveform. Stroke caused the loss of corticothalamic synaptic currents generating the late negative peak in the waveform (Figure 2.14a). Retrograde degeneration can be simulated by removal of TC axons and therefore synaptic connections to the TRN. With progressive retrograde degeneration of TC fibres, the TRN is no longer activated and therefore the slight positive peak (occurring at $\approx$ 20ms) after initial depolarisation is lost (Figure 2.14b). Note that the momentary small positive peak at 10 ms results from the TC neuron action potential and is due to the reversal of synaptic currents when the membrane voltage exceeds the reverse potential for the excitatory receptors.

Given the hypothesis of hyperexcitability, we assess the LFP signature under the bursting conditions mentioned above. From normal, depolarised and hyperpolarised resting potentials the same lemniscal glutamate input is applied to our model TC neurons. It can be seen in Figure 2.15 that a slight increase in amplitude is evident in under-excited neurons, and this is due to the enhanced synaptic current resulting from an increased voltage difference to the reverse potential of the excitatory receptors. The amplitude difference however, does not linearly reflect the doubling of action potentials

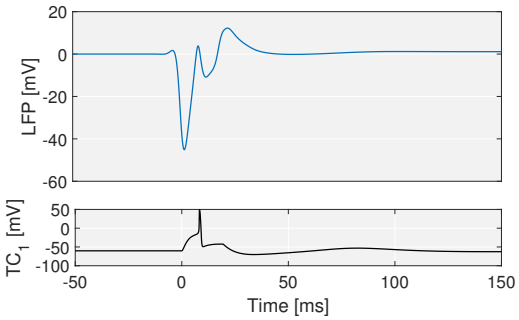

(a) Simulated thalamic SSEP waveform (top) and membrane potential of a single TC neuron (bottom) after stroke.

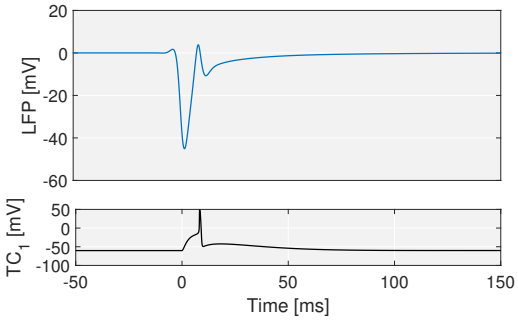

(b) Simulated thalamic SSEP waveform (top) and membrane potential of a single TC neuron (bottom) after retrograde degeneration of TC axons.

Figure 2.14: Simulated thalamic SSEP waveforms after stroke and retrograde degeneration of TC axons. Stroke causes the loss of the late latency negative potential from corticothalamic feedback. The progressive retrograde degeneration of TC axons prevents the activation of the TRN and thus the positive peak associated with inhibitory feedback is lost.

generated. Interestingly, we observe that in the over-excited state that the amplitude of the evoked LFP response has in fact decreased, even with multiple action potentials generated. Conversely to the under-excited state, less synaptic current is generated in this case.

2.5 Discussion

We have put together an in-silico model able to describe the effects of stroke on thalamic activity recorded by other groups. A common phenomena recorded in TC neurons is the increased response to sensory input and bursting. The cortex provides an excitatory influence that can control the resting membrane potential of TC neurons and thus directly influence the mode of firing. Through loss of excitation, TC neurons were found to burst to peripheral input and combined with feedback from TRN neurons, can generate oscillatory bursting between nuclei, similar to that involved in the generation of sleep spindles and epilepsy.

An alternate explanation, and one that would fit the hypothesis of excitotoxicity, is increased extracellular concentrations of glutamate. This glutamate was able to reproduce bursting to peripheral input and also increased spontaneous firing rates, however could not explain the generation of oscillatory bursting and spindle-like LTS bursts described one day after cortical lesion [115]. This may be reflective of the timeline after stroke; in the acute time-frame following cortical injury TC

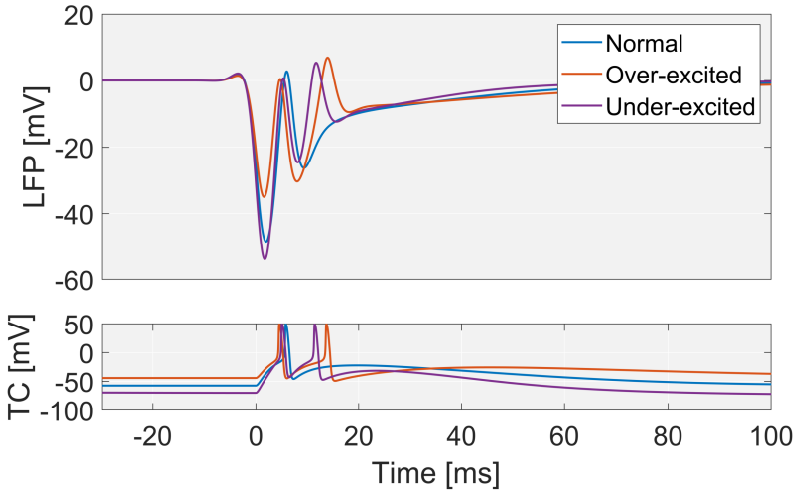

Figure 2.15: Differences in the generated LFP waveforms between tonic responses to stimuli and bursting responses at over-excited and under-excited states.

neurons are under-excited but later when glutamate is released from degenerating CT projections become over-excited.

The generation of rebound spikes and oscillatory discharges were dependent on the inhibitory post-synaptic currents induced by TRN neurons. While we were able to accurately recreate the excitatory currents based on empirical data, we used models of the inhibitory synapses from the literature which were derived from hippocampal neurons [278]. The overall predictions of this model would be greatly improved with experimental data specific to TRN projections to the mouse thalamus.

While it is more commonly believed that the alteration in thalamic activity after stroke is caused by a network dysfunction, due to the loss of polysynaptic cortical inputs, a number of observations could also be explained by changes to the individual neuronal properties. It is known that a number of adaptive processes are triggered in the cortex following stroke that are believed to increase excitability to promote plasticity and functional recovery [296, 297], including the downregulation of GABAaRs and upregulation of NMDARs [111].

2.5.1 Hyperexcitability - are there benefits?

So far we have considered hyperexcitability as an injurious behaviour due to possible links with excitotoxicity. However, instances of hyperexcitability in the peri-infarct area of the cortex are

believed to be crucial in the process of spontaneous recovery after stroke. Works by Carmichael *et al.* [297, 298, 299] suggest cortical hyperexcitability promotes activity-dependent plasticity, long-term potentiation of synapses and growth cone formation. Fujioka *et al.* [291] suggest hyperexcitability is associated with the rewiring of receptive fields in the cortex that promotes functional recovery. Thus increased activity in certain situations may be beneficial, but balance is essential and either state of over-excitation or under-excitation for a prolonged period of time can be detrimental.

2.5.2 Excitotoxicity

We developed a network model to replicate the development of pathological activity in the thalamus to predict what may generate an excitotoxic insult. There are two glutamatergic inputs to the rodent sensory thalamus: CT projections or ML/STT pathways. There has been no evidence that peripheral input through the ML or STT is altered by stroke and the small portion of NMDARs, and in particular absence of NR2B-containing NMDARs [274], suggests an excitotoxic insult is unlikely to be generated at these synapses. Alternatively, corticothalamic synapses contain a larger portion of NMDARs with approximately 10% of post-synaptic NMDAR current being through NR2B-containing receptors [274]. This suggests a possible excitotoxic insult if any hyperexcitable, peri-infarct CT neurons remain intact. However we conclude that the most likely source of excitotoxicity is through extracellular spillage of glutamate from degenerating CT neurons. This not only over-stimulates the NMDAR-rich CT receptors, but diffusion into extracellular space activates extrasynaptic NMDARs, which under both hypotheses mentioned in Section 1.4.1.4, are agreed to be linked to excitotoxicity.

It should be noted that Miyata and Imoto [274] performed their experiments into synaptic receptor composition in juvenile mice at 12 - 17 post-natal days, and it is known that sub-units change with age [62]. Only minor changes in receptor composition occur after this stage in development [64], but in considering NR2B composition the values given by Miyata and Imoto should be considered as the upper limit.

2.5.3 Regulation of membrane potential and the pathology of bursting

The increased prevalence of bursting and oscillations within the thalamocortical network after stroke has been said to resemble that during sleep, with the presence of spindle-like activity [115]. In this chapter we have considered the role of corticothalamic neurons in providing a modulatory depolarisation of thalamocortical neurons to operate in the tonic mode of firing. Outside of the ML/STT, TRN and CT connections, mentioned in this chapter, approximately 30% of synapses arrive from other regions including the brainstem [29]. These afferents use neurotransmitters such

as noradrenaline, serotonin, acetlycholine and histamine. Noradrenaline and acetlycholine release in the thalamus increases with state of alertness [300, 301], which has been shown to depolarise thalamocortical neurons and promote the transition from bursting to tonic mode [302, 303]. One mechanism for this is by modulation of K^+leakage channel conductance through activation of metabotropic receptors, which has been modelled for TRN neurons in [304]. We used a fixed value of $g_{KL} = 3$nS, as used in [265], which creates a slight depolarisation that prevents the spontaneous generation of spindles.

Not only does the array of neurotransmitters from brainstem projections have a direct excitatory effect, but they also modulate the efficacy of corticothalamic and lemniscal synapses [305, 306]. Therefore it would be beneficial to model the effects of these additional neurotransmitters and explore if it is possible for TC neurons to become hyperpolarised enough after stroke to generate bursting activity.

While bursting of thalamocortical neurons is most commonly associated with states of sleep, it is also strongly linked to the processing of pain signals in an awake state [307, 308]. Considering a common sequela of stroke is the development of post-stroke pain [309, 310] in an estimate of 10-20% of patients [311], it is possible that altered thalamic activity may lead to aberrant pain processing contributing to these disorders, similar to thalamic hyperexcitability leading to central pain syndrome after STT lesions [312].

2.5.4 Potential use of DBS

There are two main phenomena here that can explain the development of pathological activity in the thalamus after stroke. From Figure 2.5 we can see that the increased spontaneous firing rate can be quenched by increasing the excitation of TRN neurons (i.e. top right of each plot). Thus a low level chronic stimulation of the TRN may prove beneficial in reducing metabolic stress associated with the generation of action potentials and potential symptoms associated with thalamocortical bursting in an over-excited state. How DBS may interact with intracellular Ca^{2+}dynamics and post-synaptic currents through NMDARs that are linked to excitotoxicity remains to be investigated.

Given the alternative assumption of an under-excited state, a chronic sub threshold stimulation of thalamocortical neurons could depolarise them enough to prevent bursting behaviour that may be linked to neurological disorders such as the development of post-stroke pain.

2.6 Summary

This chapter has utilised a computational model of the thalamocortical network to explore the possible impacts of stroke on thalamic activity. We have shown that two scenarios are able to reproduce the main phenomena from experimental results in the literature. Firstly, the loss of cortical excitation can result in a decreased membrane potential of thalamic neurons which results in the de-inactivation of T-Type calcium channels and a bursting response to peripheral input. Secondly, an increase in extracellular glutamate due to spillage from degenerating corticothalamic neurons may generate both an increased spontaneous firing rate and evoked responses and is the most likely contributor to excitotoxicity and SND.

In the following chapter we will explore the changes in thalamic activity in a mouse model of stroke using electrophysiological recordings.

Chapter 3

Probing the Thalamocortical Network After Stroke

To elucidate network dysfunction following stroke and map the electrophysiological changes of thalamic neurons, we have recorded brain activity from a mouse model of photothrombotic stroke through surgically implanted micro-electrodes. The aim is to identify changes in activity of the thalamocortical network and how they may contribute to the pathology of SND.

3.1 Introduction

Investigations of neural activity have been carried out for decades, in humanity's pursuit to understand the functioning of our brains. From the 18^{th} century when Luigi Galvani discovered the link between neural transmission and electricity, to the late 19^{th} century when Richard Caton made the first recordings from a living brain with a galvanometer [313] and in 1924 when Hans Berger performed the first electroencephalogram (EEG) recording on a human patient [314].

Neural communication is governed by electrochemical signalling that can be recorded with the use of electrodes. The preferred recording method, in most clinical situations, is via EEG, where electrodes are placed on the scalp. Increased resolution and target specificity can be obtained from more invasive methods such as electrocorticography (ECoG), when electrodes are placed on the cortical surface, or from depth-implanted electrodes which penetrate into the brain (shown in Figure 3.1). The risk and resources associated with the latter reserve them for patients with severe and drug-refractory illnesses. ECoG has use in localising zones of seizure generation [315] and depth electrodes are

finding increasing use, often in conjunction with DBS, for conditions such as Parkinson's disease, epilepsy, schizophrenia and many more [316].

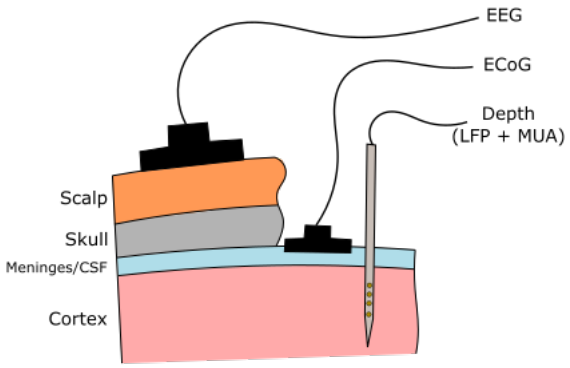

Figure 3.1: Different types of electrode configurations can be used at varying invasive levels: EEG (electroencephalogram) electrodes are placed on the scalp, ECoG (electrocorticography) electrodes on the cortical surface and depth electrodes implanted into deeper structures.

Electrodes implanted into the brain record minute changes in extracellular potentials that reflect the summation of neuronal activity in the neighbourhood of the probe. The recorded potentials are a mix of high frequency 'spikes' generated by the fast ionic currents responsible for action potential generation and propagation and low frequency content reflecting slower ionic processes and synaptic currents [317]. These signal bandwidths are often split with different sets of data analytics applied to each.

High frequency portions of the signal (>250Hz) are referred to as Single-Unit Activity (SUA) when action potentials from a single neuron are isolated, or more commonly Multi-Unit Activity (MUA) when multiple neurons are recorded simultaneously. The resolution of these traces is determined by the density of neurons in the region of interest but also the properties and positioning of the electrode. The electrodes must be in close proximity (<100µm) to the neuron(s) of interest and require a fine-tipped, often high-impedance contact to isolate single neurons.

Activity in the lower frequency bands (<250Hz) is referred to as the Local Field Potential (LFP) and contain activity of neurons within a much wider radius of the electrode. Others have estimated the spatial resolution of LFPs to be approximately 250µm [318]. However this depends entirely on the size and orientation of the electric field generated from the ionic channels to the position of the electrode. In some cases, such as the large pyramidal neurons within the hippocampus, their LFP contribution can dominate the signal recorded within 1000's of micrometers [319, 320, 317].

3.1.1 Somatosensory Evoked Potentials

Somatosensory Evoked Potentials (SSEPs) are a useful tool to evaluate the condition of the sensory pathway within the CNS, and is commonly used to assess the severity of stroke and predict functional recovery in patients [321, 322].

The VPL and somatosensory cortex are key relay and processing hubs for sensory input. They are activated through polysynaptic connections originating from mechano-, thermo-, chemo- and noci-ceptors that exist in abundance throughout the body, and transduce sensory stimuli into an electrical signal [39]. Noxious stimuli arrive at the VPL via the spinothalamic tract, whereas typical touch and proprioceptive signals are relayed through the medial lemniscal pathway. Further information on the somatosensory pathway is given in Appendix A.2.

Thus, by stimulating the nerve fibres in the peripheral nervous system, we can trigger activation of neurons in our regions of interest (VPL & SS Cortex), and assess how they respond to a controlled input. Mechanical, chemical or temperature stimulation can be used to target a specific sensory channel. In this thesis we elicit evoked potentials via electrical stimulation of all nerve fibres in the mouse fore- and hind-paws.

3.2 Previous Work

In the following two sections we summarise previous works in the literature that have recorded from the cortex and thalamus in healthy and stroke subjects, with a focus on somatosensory evoked potentials.

3.2.1 Cortical Recordings

Both cortical and thalamic activity reflects the state of arousal in the subject, and when alert, displays 'high' frequency low-amplitude activity that is largely de-synchronised across neuronal populations. During increasing stages of sleep and drowsiness, large amplitude, slow rhythms develop (with the exception of REM). The undulations in these slow waves reflect the up and down states of the cortex that are controlled by thalamic activity [323] and can be seen in the example traces of an anaesthetised mouse in Figure 3.2.

Cortical SSEPs in healthy subjects recorded via ECoG or EEG exhibit a waveform with three distinct peaks: P1, N1 & P2, shown in Figure 3.3. The peaks are notated based on their polarity and latency from stimulation (N = negative, P = positive), but it should be noted that recording with implanted

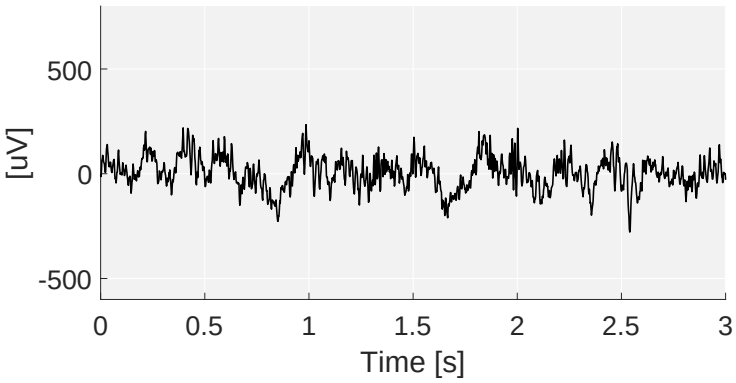

(a) Awake - small amplitude, high frequency activity.

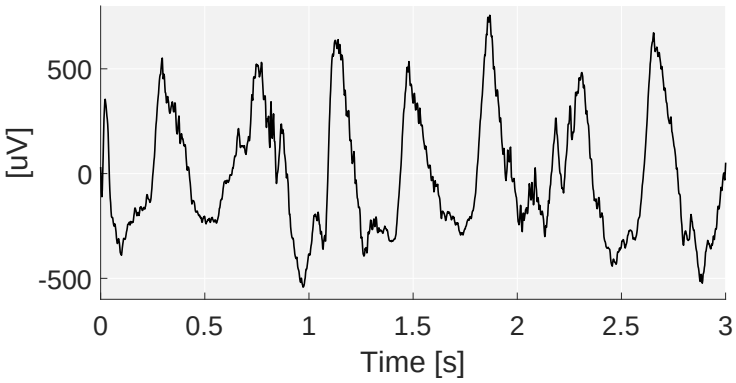

(b) Under Ketamine (Stage III-3) - large amplitude slow wave activity.

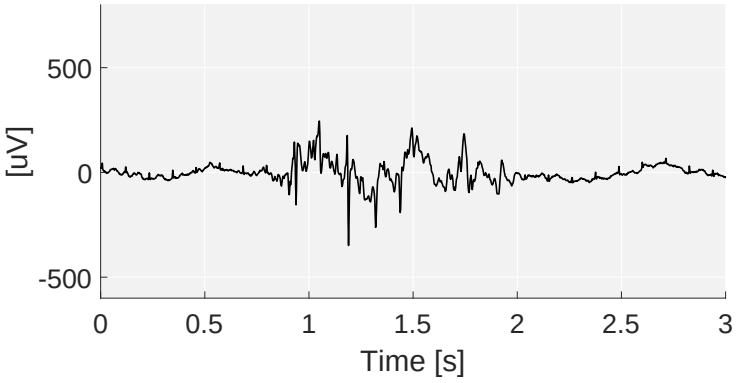

(c) Under Isoflurane (1.5%) - infrequent bursts of activity.

Figure 3.2: Example ECoG recordings from the somatosensory cortex of a mouse under different types of anaesthesia.

electrodes at different layers of the cortex alters the shape [324]. Latencies can vary between subjects and significantly between species, therefore we only denote the peaks with numbers based on the order of occurrence e.g. P1 & P2 represent the first and second positive peak in the waveform.

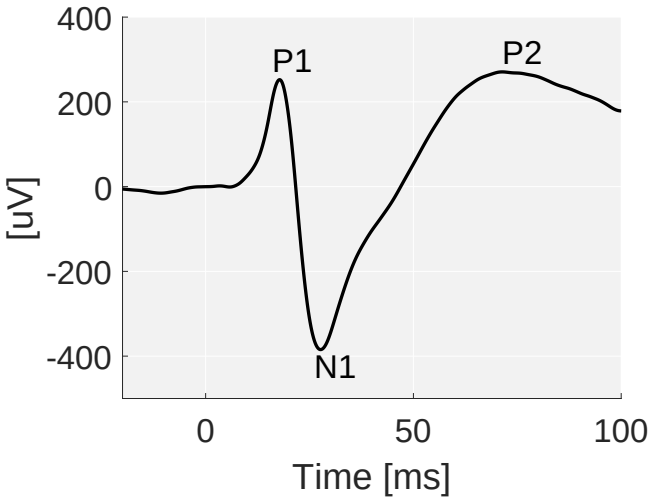

Figure 3.3: An example cortical SSEP waveform recorded from forelimb region of the mouse cortex (SSFL) by ECoG electrodes. Each of the prominent positive and negative peaks are marked (P1, N1, P2).

3.2.1.1 After Stroke

It is well established that cortical infarcts cause the attenuation or abolition of sensory evoked potentials due to neuronal loss in that region [325]. Furthermore cortical SSEPs can be used to estimate the extent of damage and make predictions on the potential for functional recovery [326, 321, 322]. Coyer *et al.* [327] showed that cortical components of the SSEP were abolished just minutes after MCAO with the onset of neuronal dysfunction but was able to recover if reperfused in time, otherwise a permanent deficit resulted.

Stroke has also been found to enhance evoked responses in the contralateral hemisphere [325]. Iwayama *et al.* [328] found that silencing S1 increased the response amplitude in the opposite S1 to contralateral paw stimulation and postulated interhemispheric inhibition via the corpus callosum for this effect. Mohajerani *et al.* [105] showed that mini-strokes enhanced the sensory response in the unaffected hemisphere to both contra- and ipsilateral stimulation, and showed that the effect persisted in acallosal mice suggesting the mechanism is through a subcortical pathway rather than transcallosal dis-inhibition. The peri-infarct region within the cortex also shows signs of

hyperexcitability [291, 111, 112].

3.2.2 Thalamic Recordings

A common consensus in the literature is that evoked SSEP waveform in the thalamus consists of three distinct components, described as: (1) an initial positive (or biphasic) wave indicative of activity in the fibre tracts terminating in the thalamus, (2) a prominent negative peak associated with post-synaptic currents in VB neurons and (3) later latency responses due to feedback from TRN and CT projections [329, 330, 331, 332, 333, 302, 295, 293].

We have summarised the latencies of evoked potentials in the VB thalamus from a number of previous studies, given in Table A.2. The depolarisation of VB neurons to forepaw stimulation, indicated by unit activity or LFP peaks, occurs at a latency of approximately 5-8ms, with hindpaw responses later at 8-11ms. The aforementioned investigations were performed in rats or larger mammals and to date we have not found any evoked LFP responses in a mouse model. Only one study by Miyata *et al.* [334], recorded changes in spiking activity in the minutes to hours after noxious stimuli from formalin injection into the paw of mice, but not evoked waveform is described.

3.2.2.1 After Stroke or Cortical Damage

A change in thalamic activity after stroke is of significant importance to determine whether pathological activity develops that may lead to an excitotoxic insult associated with SND. Recording from the thalamus after stroke has received limited attention, but there has been a number of studies where other modes of cortical injury or suppression have been used (e.g. lesions, ablations, silencing etc.). These works, summarised in Table 3.1, show a variety of changes in the thalamus recorded mostly immediately, but up to weeks after stroke. Although observations are mixed, there are a number of descriptions of increased responses and activity that may be related to hyper-excitability and excitotoxicity.

Table 3.1: Previous recordings from the thalamus after cortical stroke (or model of suppression)

Species	Cortical Injury	Recording Type	Time (Post-Stroke)	Observations
Rat	Ablation	SUA	Immediately	High-frequency discharges.
			<1.5 hrs	Decreased activity, normal evoked responses.
			1.5 - 6 hrs	Increased spontaneous activity and evoked responses.
Cat	Carotid Artery Occlusion	LFP	Immediate	Increased response. Return to normal after reperfusion.
Rat	De-cortication	SUA	Immediate	Increased response and after-discharges
Rat	Silencing (Lidocaine)	LFP & MUA	Immediate	No change in evoked responses to low-frequency stimuli. Decreased response to high-frequency stimuli.
Rat	MCAO	SUA	1-14 Days	No change in evoked responses to low-frequency stimuli. Decreased response to high-frequency stimuli. Less responsive neurons found at 14 days post-stroke.
Rat	Lesion	SUA	1 Day	Increased unit responses at early latencies (10-20ms) Increased unit responses at late latencies (50-100ms). Increased prevalence of burst firing. No change in mean firing rates.
Cat	Silencing (Cooling)	LFP	Immediate	Increased evoked response.
Rat	PT-Stroke	In-vitro	1 week	Increased excitability.
		In-vivo	>1 week	Seizure activity.
Rat	Lesion	LFP	Days 1-3	Loss of late latency response (cortical feedback) No loss of initial depolarisation.
Rat	Silencing (TTX)	LFP	Immediate	Loss of late latency response (cortical feedback) No loss of initial depolarisation.
Rat	Silencing (Cooling or Mg^{2+})	SUA	Immediate	No difference in VPM response. Transient increase then depression of POm response.

3.3 Experimental Procedures

3.3.1 Animals

For the following animal studies, we use C57BL/6J mice, obtained from the Animal Services Unit at the University of Newcastle. All experiments were approved by the University of Newcastle Animal Care and Ethics Committee and conducted in accordance with the New South Wales Animals Research Act (1985) and the Australian Code of Practice for the use of animals for scientific purposes.

Before intervention animals were housed up to five per cage and individually after, in a temperature and humidity controlled room with a reverse light/dark cycle. All recordings and behavioural analysis was performed in the dark phase. Animals were given standard laboratory chow and ad lib access to water.

3.3.2 Stroke Induction

Strokes were induced via a photothrombotic procedure known to reproduce focal lesions in the SS cortex [340, 341, 121, 17, 30, 23]. Mice were anaesthetised through constant inhalation of 2% Isoflurane and positioned in a stereotactic frame, with body temperature maintained by a regulated heat mat. Mice were injected intraperitoneally with a diluted Rose Bengal (RB; Sigma, USA) solution (0.2ml at 10mg/ml) and a surgical incision was made to expose the skull. A cold light source with 5mm aperture was centred at the desired stereotactic coordinates over the SS cortex [AP = 0, ML = 2.2] and lowered to the skull. Eight minutes after RB injection the light was switched on for 15 minutes to induce thrombosis. After which the surgical incision is closed and the mouse is allowed to recover. Mice were excluded if they did not show signs of stroke when brains were collected.

3.3.3 Anaesthesia

For electrode implantation surgeries and throughout recordings mice were anaesthetised with Ketamine and Xylazine (K/X). An initial dosage of Ketamine 100mg/kg and Xylazine 10mg/kg was used and bolus injections of 1/3 of the original dose was given upon return of the paw withdrawal reflex. During recordings, mice were maintained at stage III-3 of anaesthetic depth, as is common in electrophysiological experiments [36, 342, 323]. Stage III-3 is a surgical depth of anaesthesia and synonymous with slow wave rhythmic LFP recorded from the SS cortex [36].

3.3.4 Electrode Surgery

Animals were anaesthetised with K/X and body temperature maintained at 37°C via a regulated heat mat. The mouse's skull is surgically exposed and burr holes drilled at the desired coordinates with reference to definable sutures on the mouse skull (see Figure 3.4). Electrodes were inserted into our two regions of interest, the VPL and SS cortex, using a stereotactic arm at a rate of approximately 0.2mm/s to minimise additional trauma.

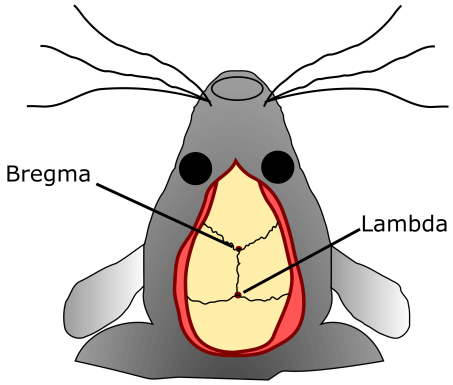

Figure 3.4: Locations of Bregma and Lamdba on the mouse skull at the points of intersection of skull sutures. These two points are used as references for stereotactic coordinates to align electrodes with the target region of the brain.

The location of the VPL, was determined from stereotactic coordinates using Paxinos and Franklin's mouse atlas [343], shown in Figure 3.5. Through initial exploration we determined the optimal location for recording thalamocortical neurons to be at [-1.7 AP, 1.8 ML,-3.4 DV] [1]. This is in agreement with the location of thalamocortical neurons determined by retrograde tracer injection into the SS cortex [223], and the regions affected by SND [30, 121, 17, 23].

Similarly, coordinates for cortical recordings in the SSHL and SSFL were determined to be [-0.9, 1.4, -] and [0, 2, -] respectively, unless stated otherwise. For depth recordings in the cortex, electrodes were lowered 0.5mm from the surface into layer IV corresponding to the termination of thalamocortical neurons.

[1] Stereotactic Coordinates are given as referenced to bregma [Anterior-Posterior, Medial-Lateral, Dorsal-Ventral] in mm

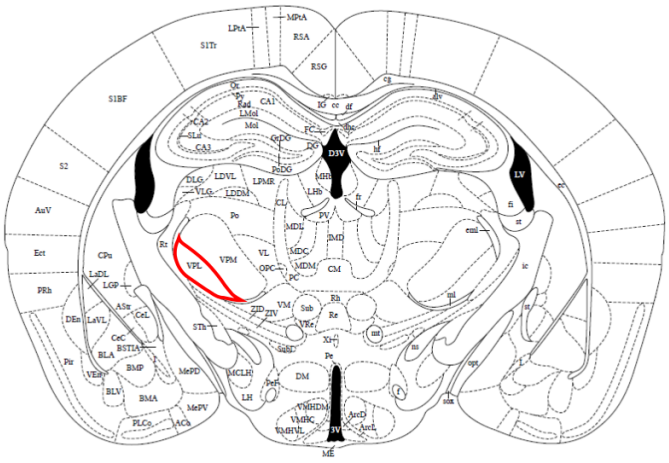

Figure 3.5: Paxinos & Franklin Atlas marked with the location of the VPL in a coronal slice of the adult C57BL/J6 mouse [343].

3.3.5 Recording Setup

Recordings were conducted within a grounded Faraday cage. Electrodes were connected to an isolated *Animal BioAmp* (FE136 or FE234, ADInstruments) via a shielded cable. The signal was amplified and digitised at 20kHz using *PowerLab 4/35* (PL3504, ADInstruments) with a bandwidth of [1-5000 Hz]. The signal was recorded in *LabChart* (Version 8.1.11, ADInstruments) and exported for offline analysis in *MATLAB* (R2018a, Mathworks) using custom scripts.

A *Stimulus Isolator* (FE180, ADInstruments) was used for peripheral stimulation, to trigger SSEPs. The stimulator was connected to needle electrodes (MLA1203, ADInstruments) that were subcutaneously inserted into the hind- and fore-paw of the mouse, with cathode positioned proximal to the mouses body. Stimulus pulses were delivered in sets of 100 trials at a frequency of 1.1-1.8 Hz and a pulse width of 0.5ms. Unless mentioned otherwise a suprathreshold current amplitude of 5-10mA was used to recruit all nerve fibres, both ML and STT pathways [293]), which elicited small twitches in the digits of the stimulated paw.

3.3.6 Histology

Animals were euthanised via lethal injection of sodium pentobarbital (Lethabarb, Virbac, Australia). They were transcardially perfused with saline followed by 4% PFA. Brains were extracted and sectioned at 60µm on a freezing microtome (-20 deg; Leica, Aus). Sections were stained for NeuN, mounted on slides and imaged at 40x magnification. NeuN is a neuron-specific nuclear protein, that can be immunohistochemically detected and is commonly used to detect the presence of and count healthy neuronal cells [344, 345].

3.4 Data Analysis

For data analysis, raw signals were split into two components - LFP and MUA. The LFP signal was extracted using a 4^{th}-order, low-pass Butterworth filter, with f_c=250Hz. Similarly, MUA was extracted using a 4^{th}-order, high-pass Butterworth filter with f_c=250Hz.

3.4.1 Spike Detection

Spike detection was performed on MUA signals using methods described in Chapter 4. We extracted spike times to estimate firing rates of spontaneous activity, and assess spike counts in SSEPs.

3.4.2 Spectral Estimation

Spectral estimation was performed using Welch's method [346] on LFP signals from spontaneous recordings. We used 5 second hamming windows with 50% overlap. Where frequency bands are mentioned we used definitions of Delta, Theta, Alpha, Beta & Gamma defined in Appendix A.1. Power values in each band were calculated by integrating the power spectral density function within the defined frequency range.

3.4.3 Spontaneous Signal Power

The power of spontaneous activity was quantified by taking the RMS value of spontaneous LFP signals.

3.4.4 SSEP Quantification

Somatosensory evoked potentials were recorded in sets of 100 trials and waveforms averaged across a period from 100ms pre- to 100ms post-stimulus. Stimulus artefacts were removed by applying a linear interpolation from 0.5ms pre-stimulation to 2ms post-stimulation waveform. For LFP measures the stimulus artefact was removed after averaging the raw waveforms and before applying the low-pass filter. For MUA signals the stimulus artefact was removed immediately after applying the high-pass filter.

We quantified SSEP responses using three different methods:

1. **SSEP Amplitude** was calculated as the difference of peak values of the averaged LFP waveforms.
2. **SSEP RMS** was calculated as the RMS value of the LFP waveform post stimulation minus pre stimulation.
3. **SSEP Spike Count** was calculated as the average number of spikes post stimulation minus pre stimulation. (Note: 2ms bins are used when displaying post-stimulation spike histograms)

3.4.5 Histological Analysis

Secondary neurodegeneration was quantified by counting NeuN+ cells in the contra- and ipsilateral VPL. Automated NeuN counts were performed in ImageJ (*v1.53e* [347]), as described below:

1. Convert image converted to 8-bit black and white.
2. Apply binary threshold to separate NeuN material from background.
3. Separate clustered cells by segmentation.
4. Count the number of neurons using particle analysis.

Each step in this process is visualised in Figure 3.6.

In most cases the automatic threshold value (determined using IsoData [348]) was sufficient. However in some instances large amounts of background staining were included and therefore the threshold was manually adjusted. Note that the threshold was set based on the contralateral (unaffected) side, so both images from the contra- and ipsi-lateral hemispheres of the same subject used the same threshold.

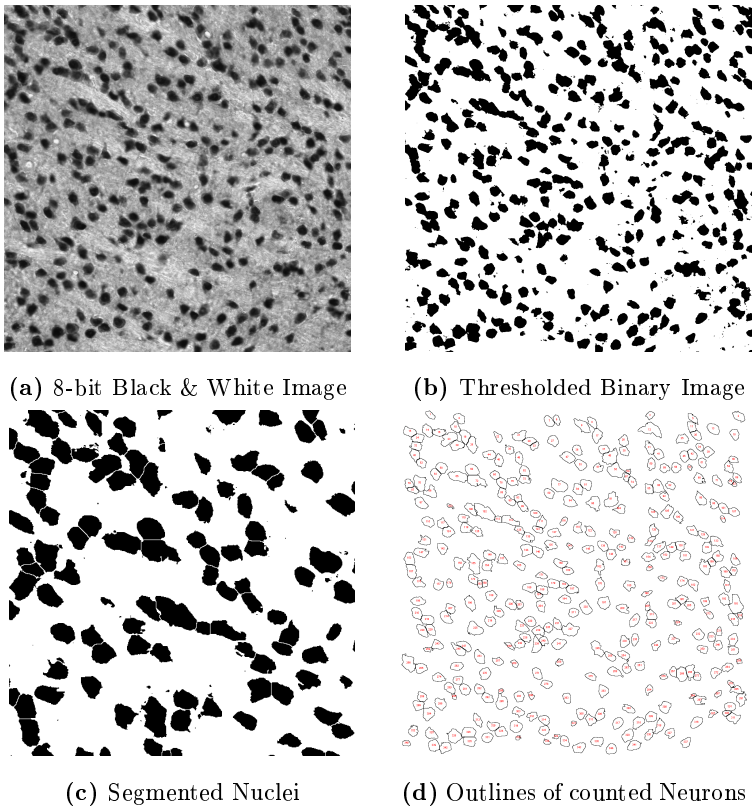

(a) 8-bit Black & White Image **(b)** Thresholded Binary Image

(c) Segmented Nuclei **(d)** Outlines of counted Neurons

Figure 3.6: Steps for automated counting of NeuN+ cells in ImageJ: (a) the image is cropped to the ROI and converted to black & white, (2) a binary threshold is applied to separate the dark regions comprising of neurons from the background, (3) overlapping nuclei are segmented and (4) each segmented neuron is counted.

NeuN cell counts of the thalamus were formulated by taking the ratio of NeuN+ cells in the ipsilateral (affected) hemisphere to the number in the contralateral hemisphere i.e:

$$\%NeuN = \frac{\#NeuN+_{Ipsi}}{\#NeuN+_{Contra}} \tag{3.1}$$

3.4.6 Statistical Tests

We used the Mann-Whitney U test or one-way ANOVA followed by Tukey-Kramer multiple comparison post-hoc test all implemented in Matlab. Levels of statistical significance are depicted as: *=$p<0.05$, **=$p<0.01$, ***=$p<0.001$.

3.5 Study 1 - Thalamic and Cortical Recordings after Stroke

The first study aimed to assess the change in thalamic activity in the weeks following stroke and correlate them with the progression of SND.

3.5.1 Methods

A total of 46 male C56BL/6 mice (aged 9-17 weeks), were divided into seven groups, corresponding to the number of days post stroke procedure that recordings were performed [Day 0 - Naive (n=7), Day 7 - Sham/Stroke (n=6/7), Day 14 - Sham/Stroke (n=7/6), Day 28 - Sham/Stroke (n=7/7)].

Stainless steel monopolar electrodes (PlasticsOne - Part# MS303/3-AIU) were stripped at the end to expose 0.3mm of conductor. The electrode was inserted sequentially into the somatosensory cortex (SSHL) [-0.9, -1.4, -0.5] followed by the VPL [-1.7, -1.8, -3.4]. A reference screw was placed over the olfactory bulb. The ideal positioning of the electrodes is shown in Figure 3.7, superimposed on the Paxinos Mouse Brain Atlas [343].

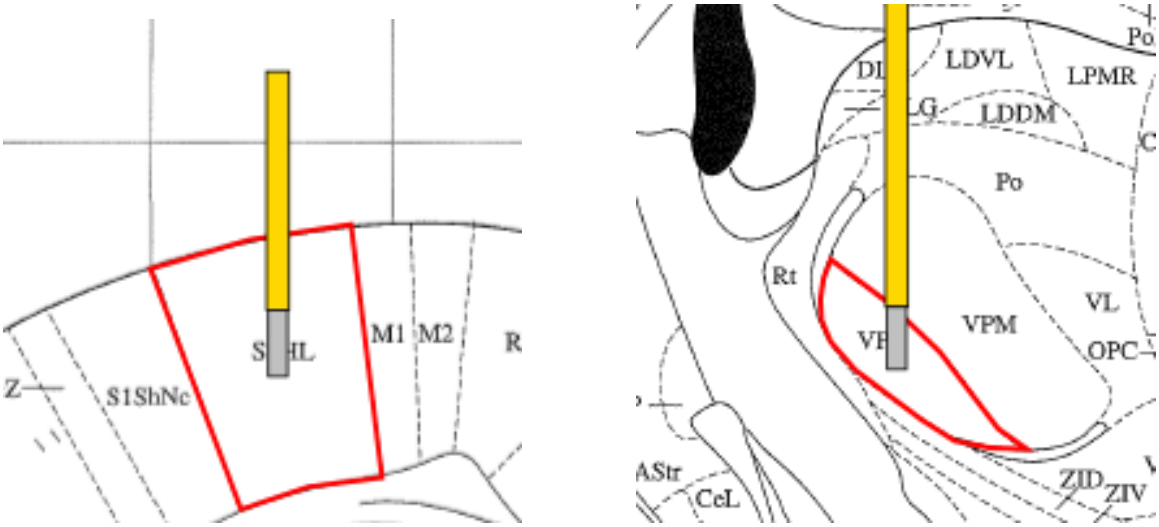

(a) Cortical Electrode Placement **(b)** Thalamic Electrode Placement

Figure 3.7: Ideal electrode placements within target regions of the (a) Cortex (SSHL) and (b) Thalamus (VPL) of a mouse brain. The grey tips are the exposed contact of the electrode (≈0.3mm in height) and the yellow segment is the polymide insulation.

Evoked potentials to stimulation of both the hind-paw and fore-paw, contralateral to the hemisphere of the brain affected by stroke, were recorded in the cortex and thalamus. In the cortex, three sets of

SSEP trials to each paw were obtained. In the thalamus, six sets of SSEPs were recorded from each paw, but due to the lack of consistent finding of the hind-paw response, only those of the fore-paw are used. Between each set of SSEPs, 3 minutes of spontaneous activity was recorded.

3.5.2 Results

Stroke abolished the SSEPs in the affected cortex to both contralateral forelimb and hindlimb stimulation (Figures 3.8,3.9).

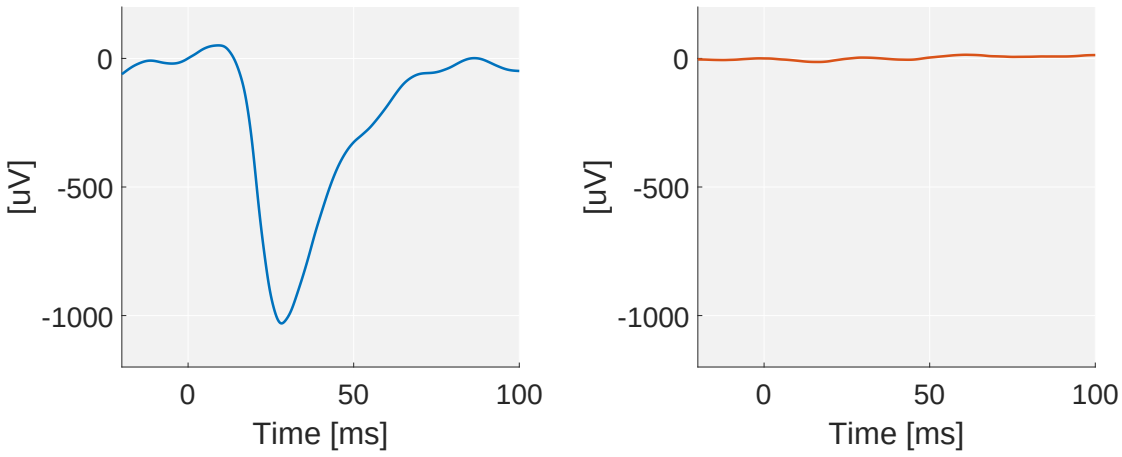

(a) Sham Day 28

(b) Stroke Day 28

Figure 3.8: An example cortical SSEP waveform evoked from hind-paw stimulation at 28-days post-surgery in a (a) sham mouse and (b) stroke mouse. The evoked waveform is completely abolished in the stroke mouse.

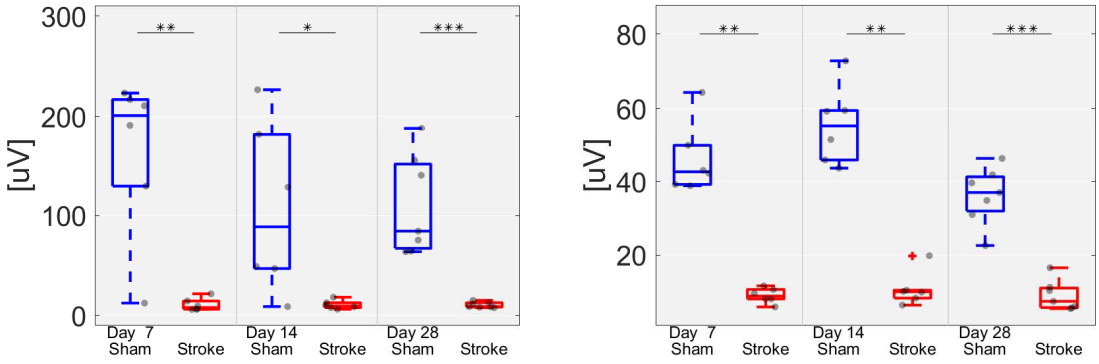

(a) Cortical HL SSEP RMS

(b) Cortical FL SSEP RMS

Figure 3.9: Comparison of the cortical SSEP power (RMS) between stroke (red) and sham (blue) mice at 7, 14 and 28 days post-surgery. The stroke mice have significantly lower SSEP power to both hindlimb stimulation (a) and forelimb stimulation (b) compared to sham mice at all three time-points.

The total power of thalamic SSEPs in stroke-affected mice compared to sham-treated mice was decreased at all three time-points after surgery (7, 14 and 28 days), as shown in Figures 3.10.

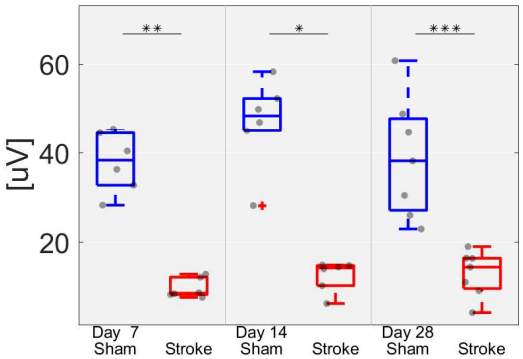

Figure 3.10: The forelimb-evoked thalamic SSEP power is significantly reduced in stroke mice (red) compared to sham mice (blue) at all three time-points post surgery (7, 14 and 28 days).

There was a clear difference in the shape of the thalamic SSEP waveforms between stroke and sham groups - with a noticeable loss of response at latencies greater than 15ms post stimulation, as shown

in Figure 3.11b.

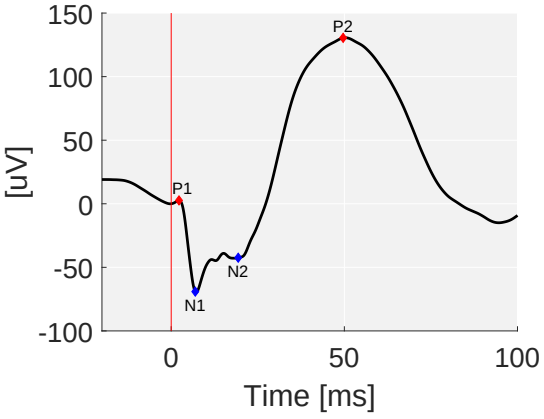

(a) Healthy Thalamic SSEP

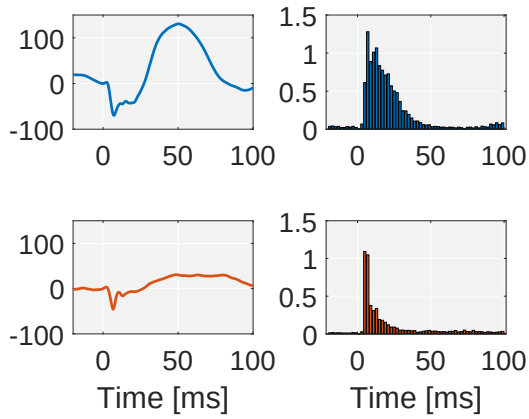

(b) Sham (Blue) Vs Stroke (Red) Thalamic SSEP Waveforms and Spike Histogram.

Figure 3.11: Example thalamic SSEPs from mice 7 days after stroke, showing a characteristic loss of LFP amplitude and unit spikes in the late-latency portion (> 20ms) of the response. The N2 and P2 peaks are mostly lost in the stroke mice (b, lower left) as well as spike counts at latencies later than 20ms post-stimulation (b, lower right).

Separating the waveform into early and late latency components ('Early' Amplitude = P1-N1 and 'Late' Amplitude = P2-N2, depicted in Figure 3.11a) we showed that it was entirely in the late latency range that stroke affected the waveform (Figure 3.12).

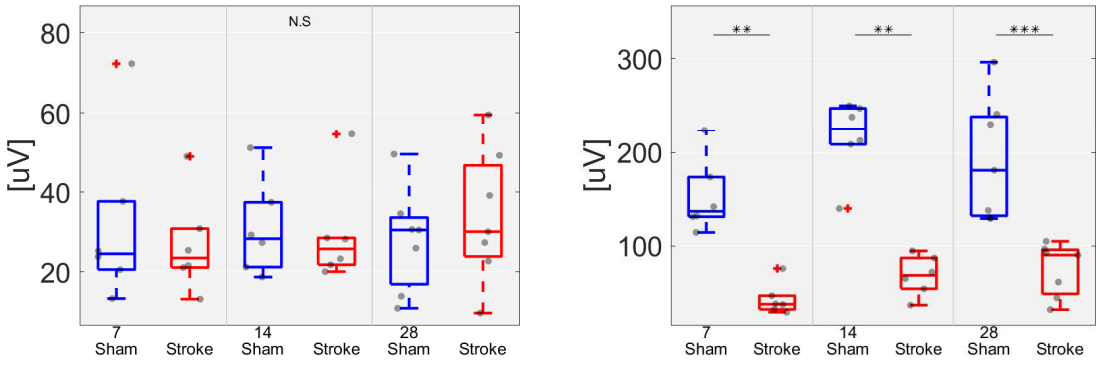

(a) Amplitude of early thalamic SSEP peaks (P1 - N1) **(b)** Amplitude of late thalamic SSEP peaks(P2 - N2)

Figure 3.12: A comparison of early and late latency SSEP peak amplitudes shows that the early SSEP waveform (left) is unchanged between stroke (red) and sham (blue) mice, but the late SSEP waveform (right) is significantly reduced in stroke mice at all time-points post-surgery.

We compared the average RMS of spontaneous recordings from the cortex and thalamus for each group of mice, to compare overall neural activity. As shown in Figure 3.13, slight reductions in the stroke groups can be seen but no significant difference between stroke and sham groups was found.

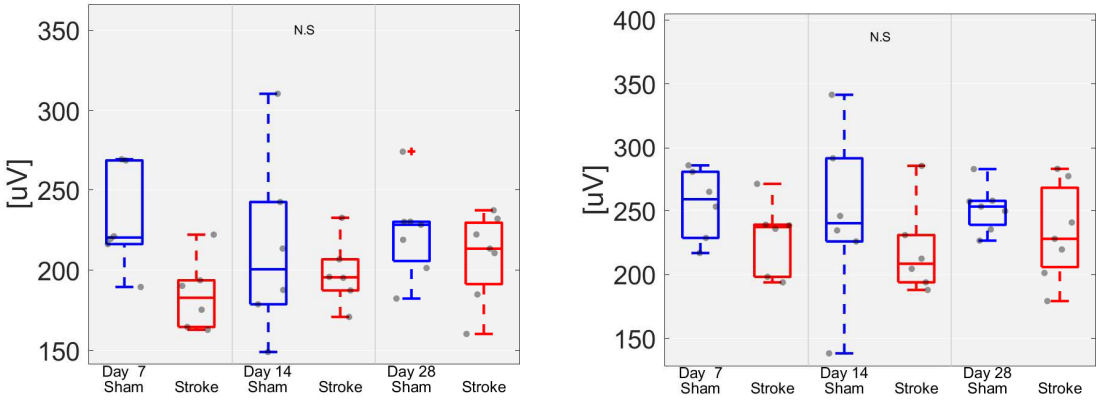

(a) Spontaneous Cortical LFP RMS **(b)** Spontaneous Thalamic LFP RMS

Figure 3.13: A comparison of spontaneous LFP activity quantified by the RMS power in the (a) cortex and (b) thalamus after stroke. No statistically significant differences are noted.

3.5.2.1 Histology

Stroke significantly reduced the number of NeuN+ cells in the thalamus at 28 days post-stroke ($p<0.01$) (Figure 3.14a).

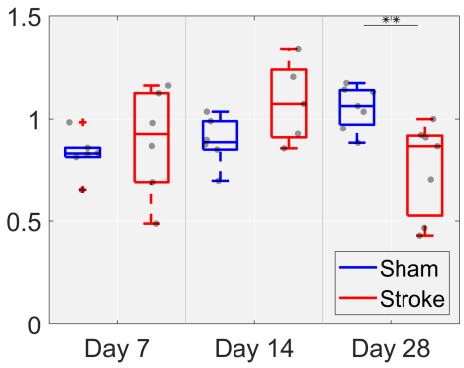

(a) NeuN+ cell count comparison between stroke and sham animals

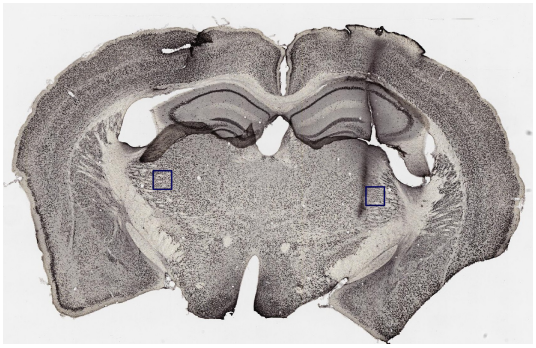

(b) Example of electrode track preventing correct placement of ROIs (blue squares) for processing NeuN counts.

Figure 3.14: There is a significantly reduced number of NeuN-positive cells in the thalamus of stroke mice (red) compared to sham mice (blue) by 28-days post-stroke.

3.5.3 Discussion

A clear change in the thalamic SSEP waveform was noticeable after stroke Figure 3.11. By splitting the response into two components: early latency response (<15ms) and late-latency response (>15ms), we found no evidence that the early response was altered by stroke (Figure 3.12). From previous studies [294, 293, 302], the depolarisation of thalamic neurons to peripheral stimulation occurred in this early latency period and generated a prominent negative peak comparable to our 'N1' (also see review in Appendix A.3) and there existed a feedback component in the late latency window. The origin of these peaks was also supported in the simulation studies in Section 2.4. By making this distinction between initial thalamic activation and feedback we could come to the conclusion that there was no change in thalamic activity and stroke only removed the corticothalamic feedback path, in agreement with a purely cortical injury.

Others have shown there is significant degeneration of thalamocortical neurons from 7 days after stroke [17], and we showed a significant loss of NeuN+ cells at 28 days (Figure 3.14a). There was added difficulty in assessing NeuN+ cell counts due to the presence of an electrode track directly in or adjacent to the VPL, see Figure 3.14b. This often meant taking the closest available brain slice

without significant electrode damage which may have affected the results and the lack of significance at days 7 and 14. However at no time-point was there a significant loss in the negative peak believed to represent the depolarisation of thalamocortical neurons.

One explanation is the early latency response represents a pre-synaptic potential that persists due to intact ML and STT fibres. Following cortical ablation, it is found that the contribution from thalamocortical fibres to the cortical SSEP still persists [332], so in a similar manner a presynaptic contribution from ML and STT fibres to the thalamus may persist. This would contradict with what other groups have previously reported, indicating that the depolarisation of thalamic neurons elicits the negative peak (N1) in the thalamic SSEP waveform [302, 293, 329]. It is important to note that the difference in rodent species may alter the SSEP waveform and the previous mentioned studies are all recorded from adult rats.

We confirmed that choice of reference location had no impact on the thalamic SSEP recorded (see Appendix B.4). We also confirmed the early response in the SSEP is not volume-conducted from the brainstem, by determining the evoked response there occurs 2-3ms earlier (Appendix B.2).

The evoked potentials recorded in the VB complex of a rat by Andersen *et al.* [332] are very similar to the SSEP waveforms we have recorded in the mouse VPL. They describe an initial positive-negative diphasic waveform as the discharges from medial lemniscal fibres and the negative peak as the synaptic activation of the thalamic neurons. They too recorded a later, large positive peak with duration of approximately 100ms, that is seen to oscillate a number of times (comparable to our recordings see Appendix B.3). However after cortical ablation the large positive waves persisted, so was determined to be generated in purely thalamic circuitry. Given that TC excitability was significantly attenuated during the P-wave it is believed to be generated by post-synaptic inhibition from TRN neurons and hence our results would indicate a loss of influence from the TRN. This could be explained by decreased excitability of TRN neurons [113] or the degeneration of TC collaterals activating the TRN. We showed support for the origin of the prolonged P-wave from TRN inhibitory currents in simulated models too (Appendix B.6, Figure B.8).

Additionally, we sought to explain the source of the N2 peak in the thalamic SSEP that we have not found a consensus for in the literature. We assessed the possibility that the N2 peak is of cortical origin and volume-conducted to the thalamus, which would explain the loss after stroke. By comparing the latencies of the N1 peak in layer IV of the cortex and N2 peak in the thalamus we noted a strong correlation ($r=0.58$, $p=0.012$), data is shown in Figure 3.15. The thalamic N2 peak always preceded the cortical N1 peak with an average delay of 4.9ms, suggesting they are not of the same source. It doesn't however rule out the possibility of origins in deeper cortical layers, as the TC neurons also excite layer VI neurons. The difference between unit responses to sensory input in layers IV and VI in the rat was only 1ms [115], however it may differ in a mouse model and under

different anaesthesia. It also doesn't rule out the source being corticothalamic feedback from layer VI.

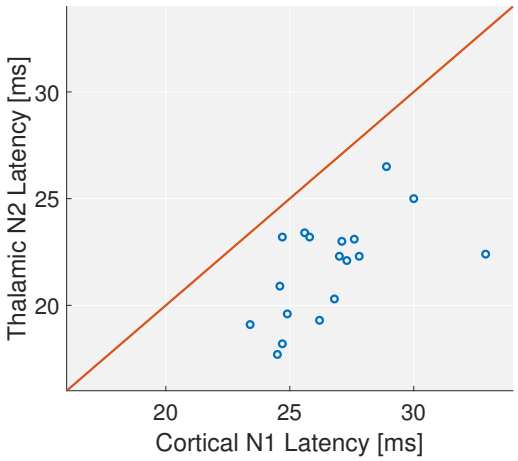

Figure 3.15: The latency of the thalamic SSEP N2 peak was consistently earlier than the cortical SSEP N1 peak (red line = 1:1). A correlation of r=0.58 with p=0.012 was found and the average delay from thalamic N2 peak to cortical N1 peak was 4.9ms. This evidence suggests that the peaks are not of the same source and the secondary activation of thalamic neurons precedes that of layer IV cortical neurons.

Anderson *et al.* [338] recorded a second negative potential that occurred approximately 6ms after the depolarisation of VPM neurons to whisker stimulation. By applying tetrotodoxin (TTX), a sodium channel blocker that inhibits action potential generation, to the cortex they found no change in the amplitude of the early negative peak but almost a complete loss of the secondary peak and thus concluded it was of cortical origin. This does not rule out the possibility of a volume-conducted waveform from the cortex but the presence of unit activity in our recordings does suggest local origins.

We also propose that there may be significant contribution to the LFP waveform from the TRN, which in mice, is only 100's of µm from the recording location in the VPL. We simulated this possibility, shown in Appendix B.6 (Figure B.9) and were able to reproduce a second negative peak that occurred at the correct latency. Interestingly, it been proposed that unit spikes from TRN axons may also be recorded from electrodes in the VB thalamus of rats [349]. Together, this hypothesis would also explain the loss of both N2 and P2 peaks in the thalamic SSEP waveform by 7 days post-stroke and also the loss of unit spikes in this later-latency period.

It was surprising to find that although cortical SSEPs were completely abolished as expected

(Figures 3.9), we detected no change in spontaneous activity from the cortex and similarly in the thalamus (Figure 3.13). The small size of the mouse brain and use of LFPs may contribute to this phenomena. Neighbouring cortical and hippocampal neurons are known to produce large amplitude LFP signatures [320, 319] that may dominate the recorded signal in the affected area [350], thus loss of a small population of neurons may not appear significant. Furthermore the somatodendritic geometry of TC neurons is spherically symmetrical with very small dipoles and therefore creates a closed-field and only small LFP amplitude [317]. The use of averaged SSEPs and a controlled input delivered asynchronously to background activity helps to cancel activity not generated in the somatosensory pathway.

3.6 Study 2 - Local Changes in Thalamocortical Activity

A significant limitation from the previous study is the potential contamination from non-local neuronal activity. Here we change the recording configuration and utilise a bipolar electrode (a.k.a. stereotrode) to apply spatial filtering and reduce the impact of volume conduction [319]. While the benefit of this configuration is improved spatial resolution, we now have the added complexity of unknown electrode orientation w.r.t. to the neuronal sources. Therefore, as is seen in later figures, there are no longer the identifiable positive-negative peaks (e.g. P1, N1).

Additionally, we improved the procedure for surgical implantation of the electrodes. Upon inspection of retrieved brain slices from the previous study we noticed some deviation from the ideal position in the VPL. Some deviation is to be expected due to inter-animal variability, but minimising the final displacement is important to reduce variation in LFP amplitude from the source and be close enough to consistently record unit activity. We therefore optimised the location in the dorsal-ventral axis by recording from all depths below 3mm in increments of 200µm and using those with the largest thalamic response to stimulation.

3.6.1 Methods

A total of 21 mice, were divided into 6 groups, Naïve (n=5), Stroke Day 1 (n=4), Stroke Day 3 (n=4), Stroke Day 7 (n=5).

A twisted pair of stainless steel electrodes (Plastics One, MS333/3-B/SPC) was inserted into the SSFL [-0.4, 2, -0.5] and VPL [-1.7, 1.8, 3.4], see electrode placements in Figure 3.16. A common reference screw was placed over the Olfactory Bulb.

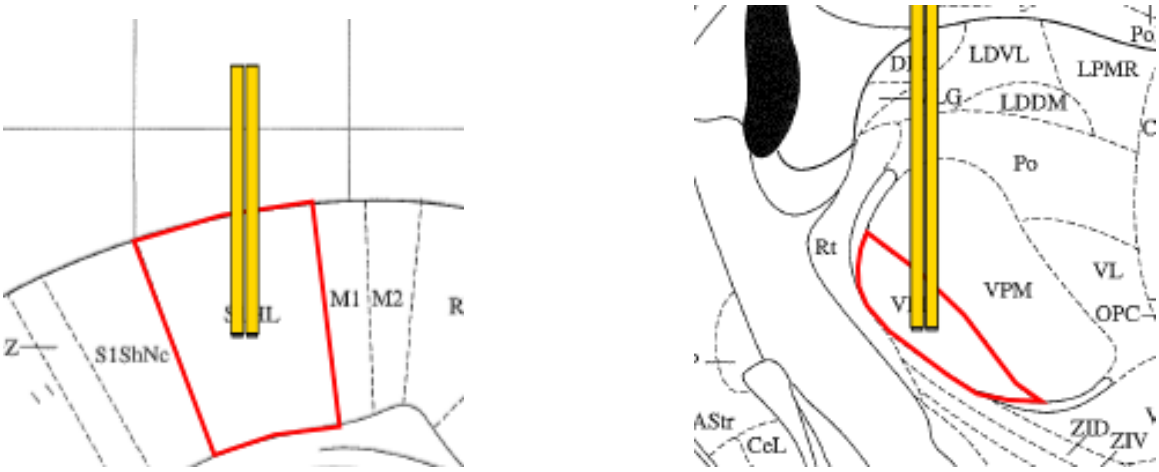

(a) Cortical Electrode Placement

(b) Thalamic Electrode Placement

Figure 3.16: Ideal stereotrode electrode placements within target regions of the (a) Cortex (SSFL) and (b) Thalamus (VPL) of the mice brain.

3.6.2 Results

We found an immediate loss of spontaneous cortical activity after stroke (Figures 3.17a, 3.18a) and a similar decrease in spontaneous thalamic activity (Figures 3.17b, 3.18b).

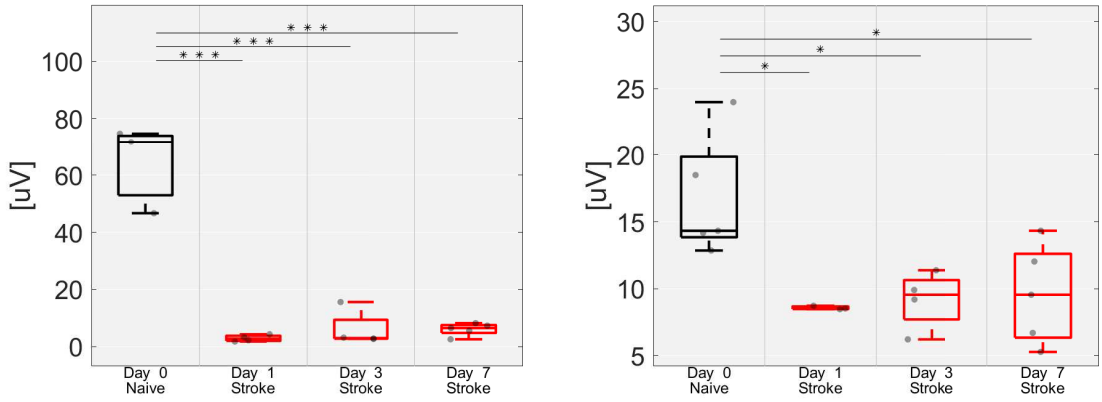

(a) Cortical LFP RMS **(b)** Thalamic LFP RMS

Figure 3.17: There is a significant loss of spontaneous (a) cortical and (b) thalamic LFP activity after stroke (red) compared to naïve (black) mice when recording with a bipolar electrode configuration.

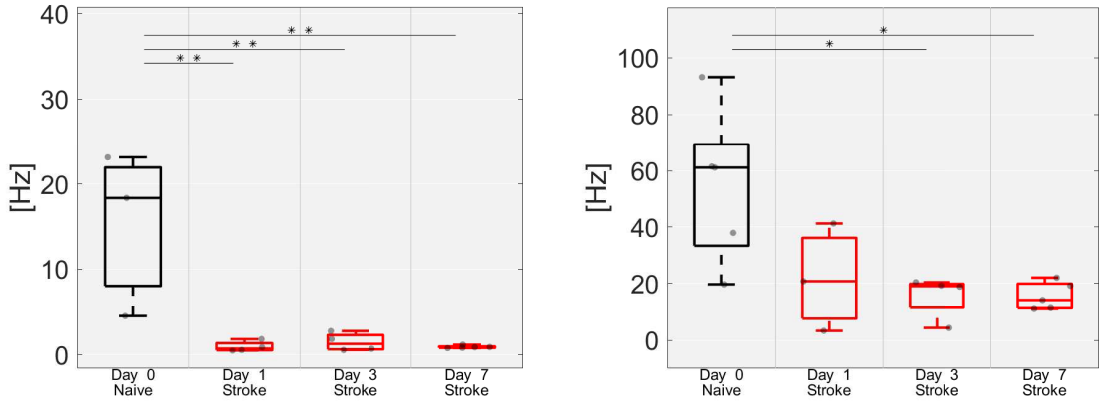

(a) Cortical Firing Rate **(b)** Thalamic Firing Rate

Figure 3.18: There is a significant loss of spontaneous (a) cortical and (b) thalamic unit activity after stroke (red) compared to naïve (black) mice.

Again we confirmed the abolition of cortical SSEP (Figure 3.19a) and also found that the thalamic SSEP had decreased by day 7 (Figure 3.19b).

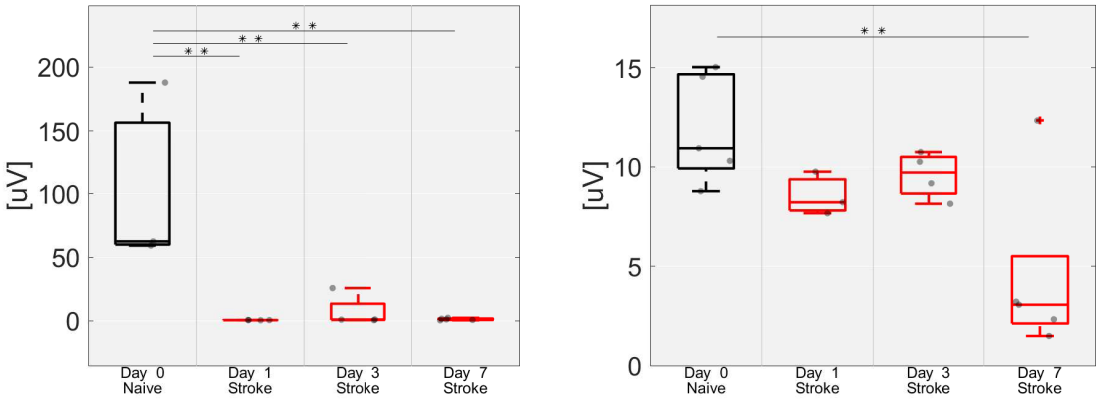

(a) Cortical SSEP LFP RMS

(b) Thalamic SSEP LFP RMS

Figure 3.19: A comparison of cortical and thalamic SSEP's recorded using a bipolar electrode configuration shows an immediate loss of cortical SSEP power and a delayed loss of thalamic SSEP power in stroke mice (red) compared to naïve mice.

3.6.3 Discussion

The use of differential recording between twisted electrode pairs was effective in isolating local neuronal activity. This allowed us to detect the loss of spontaneous activity in the cortex due to stroke (Figures 3.17a, 3.18a) as well as reconfirm the loss of cortical SSEP (Figure 3.19a).

We found a significant decrease in spontaneous thalamic activity in all stroke time-points (Figures 3.17b, 3.18b) but the thalamic SSEP did not decrease until day 7 (Figure 3.19b) which corresponds to the onset of SND and loss of thalamic neurons [17]. Combining this result with the observation of lost thalamic SSEP from days 7-28 in the previous section, we observe that thalamic SSEP decreases in the same timeline as neuronal degeneration.

The immediate loss of spontaneous activity in the ipsilateral thalamus agrees with hypometabolism recorded by Kataoka *et al.* on the first day after MCAO [134] and reflects a loss of excitatory cortical input to the region.

We further inspected the thalamic SSEP waveform and noticed a similar trend in early and late latency responses (Figure 3.20) to the previous section. However, we know that the cortex is functionally silent at day 3 (Figures 3.17a, 3.18a) and has no response to stimulation (Figure 3.19a) and can therefore rule out contribution from corticothalamic feedback. Given the use of a bipolar

recording configuration, we also dismiss the possibility of volume conducted potentials. One explanation is that the thalamic response to stimulation is lost at the onset of SND between days 3 & 7 and the remaining potential is of pre-synaptic origin. However this would disagree with other electrophysiology experiments [293, 294].

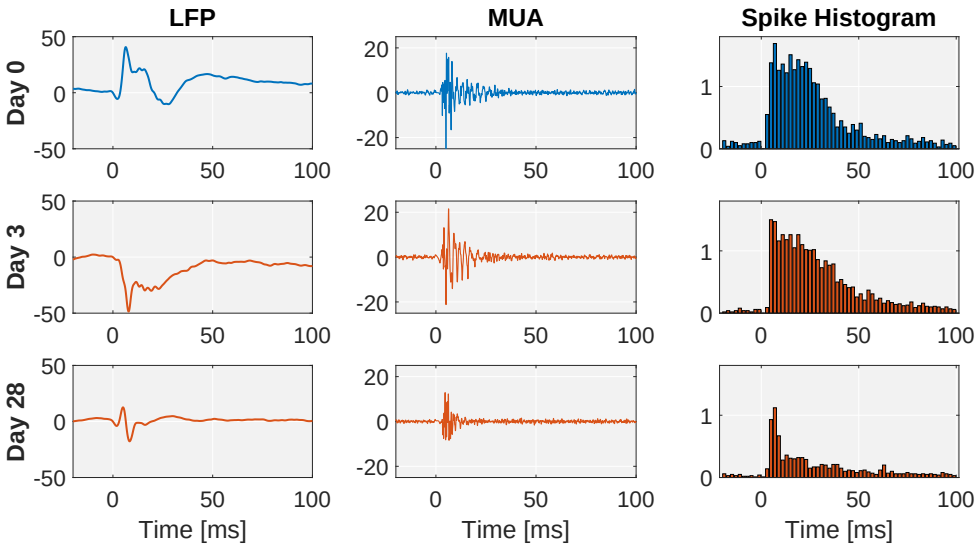

Figure 3.20: A clear difference in Thalamic SSEP Waveforms between Naïve (Blue) and Stroke (Red) mice by 28 days post-stroke.

An alternate explanation is derived from the origin of the late-latency components from TRN depolarisation or feedback, as mentioned in the previous section and described in [332]. Retrograde degeneration of TC neurons is in the early stages at day 3 and significant by day 7, which effectively disconnects the TC neurons from the TRN and thus would abolish the contributions from the TRN to the LFP signal. There is some chance that TC soma and the synapse with ML fibres remain intact, as NeuN can be reduced in pathological conditions such as ischaemia without the loss of cell body [351]. This could suggest that depolarisation of degenerating/damaged thalamic neurons persists and is recorded through day 28, but there is no transmission by TC neurons to the TRN.

3.7 Overall Discussion

3.7.1 Deconstructing the Thalamic SSEP waveform

A large amount of ambiguity surrounds the sources of extracellular potentials present in SSEPs recorded from the VPL. The SSEP recorded in the thalamus may contain: (1) volume-conducted potentials from nuclei in the somatosensory pathway preceding the thalamus (i.e. cuneate nucleus), (2) pre-synaptic activity from afferent fibres to the thalamus, (3) post-synaptic depolarisation of thalamocortical neurons, (4) volume-conducted potentials from regions proceeding the thalamus in the somatosensory pathway (i.e. TRN, SS cortex) and (5) feedback containing both pre- and post-synaptic activity to the thalamus from reciprocally connected regions (i.e. TRN and SS Cortex) [330].

We identified the post-synaptic depolarisation of thalamocortical neurons as the primary signal of interest and, like many other groups [293, 295] (also see Appendix A.3), attributed this to the large negative peak (previously denoted as N1) occurring at a latency of 6-8ms following electrical stimulation of the forepaw. Our results suggested no change in this early component of the SSEP waveform, depicted again in Figure 3.21, in the weeks following stroke when there is believed to be significant loss of thalamocortical neurons.

We did observe a significant loss of activity occurring at latencies later than 15ms post-stimulation - however this may only reflect the known loss of corticothalamic activity or contributions of the TRN. The loss of TRN activity would explain retrograde degeneration of TC neurons in the early stages of SND, but the persistence of the N1 peak does not suggest TC neurons are dying. Another source of the early negative potential in the SSEP could be from the POm, a secondary sensory nuclei of the thalamus, that is activated by peripheral stimulation at a similar latency to the VPL [352]. However the POm is also known to be afflicted by SND in a similar manner to the VPL [17], and therefore we would also expect the loss of any contribution to the LFP.

We further break down the early component of the thalamic SSEP in Figure 3.22 into what we interpret as the pre- and post-synaptic potentials. We had previously recorded the evoked response in the brain-stem which we found to occur at approximately 4ms (Appendix B.2) and thus attribute the activity of medial lemniscal fibres to the small biphasic wave occurring at 3-5ms, that is also associated with initial sharp peak(s) in the MUA trace. Following the pre-synaptic potential is the post-synaptic potential of thalamocortical neurons at a latency of 6-8ms consisting of a larger negative peak in the LFP signal and simultaneous unit activity.

One explanation for our results is that the remaining negative potential in the thalamic SSEP after stroke is purely pre-synaptic. We can not rule this out, but in agreement with other studies suggest

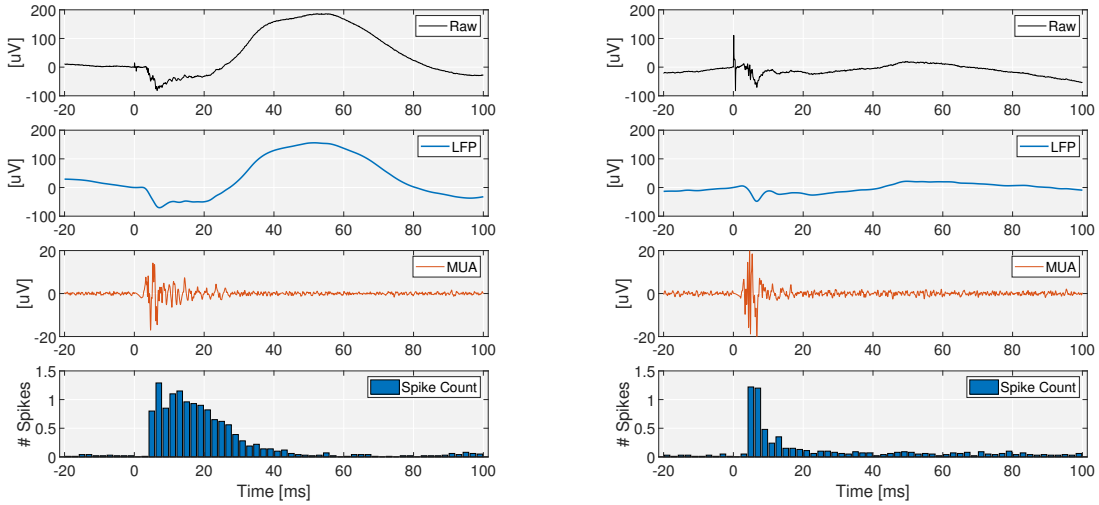

(a) Sham Mouse **(b)** Stroke Mouse

Figure 3.21: A comparison of thalamic SSEP waveforms recorded from (a) sham and (b) stroke mice shows the loss of SSEP at latencies greater than 15 ms. (top) Raw LFP signal, (2nd row) LFP-filtered signal, (3rd row) MUA filtered signal and (4th row) spike counts.

the negative potential occurring 6-8ms after fore-limb sensory stimulation is the depolarisation of thalamocortical neurons.

3.7.2 Lack of Evidence Supporting Hyperexcitability

We have shown the loss of cortical activity, both spontaneous and evoked potentials from day 1 post-stroke (Figures 3.17a , 3.19a & 3.9). We have also shown spontaneous thalamic activity to have decreased from day 3 post-stroke (Figure 3.17b & 3.18b) and the decrease in parts of the evoked potentials starting from day 7 (Figure 3.19b) in alignment with the onset of SND.

However, we have not captured any signs of hyperexcitability that may be linked with an excitotoxic insult to thalamic neurons. One possible explanation is the influence of anaesthesia masking hyperexcitability, another is that aberrant neuronal activity only occurs in the immediate hours following injury [288]. These limitations along with others are explored in the following subsections.

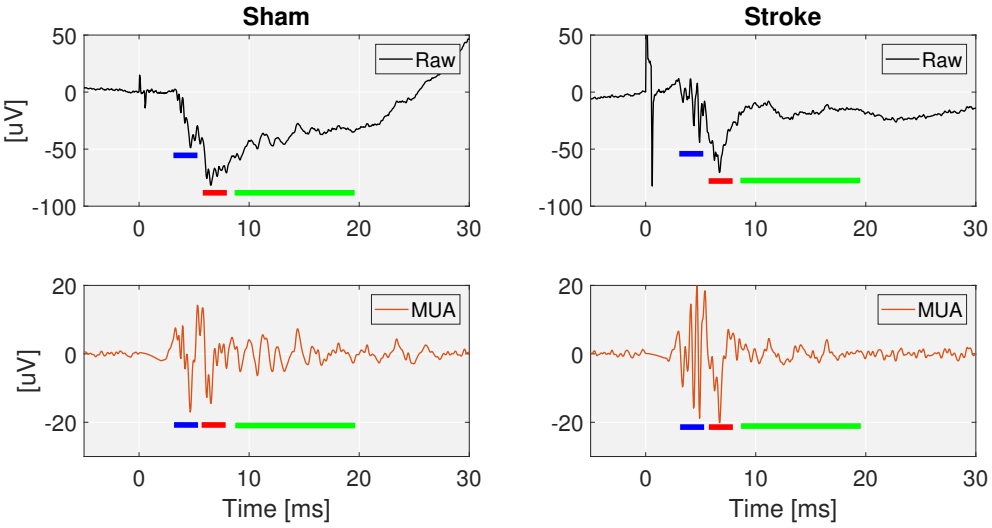

Figure 3.22: Decomposition of the early components of the thalamic SSEP waveform in a sham and stroke mouse. The very early component (blue line) occurs at 3-5 ms post-stimulation and likely represents the pre-synaptic potentials from medial lemniscal fibres. The next early component (red line) is a negative peak occurring at a latency of 6-8 ms post-stimulation and likely represents the depolarisation of thalamocortical neurons. Following these two early peaks are possible contributions from TRN and corticothalamic feedback that is mostly abolished in stroke mice.

3.7.2.1 Effect of Anaesthesia

Anaesthesia is necessary to place the animal in a comfortable and safe state during surgery (inducing unconsciousness, amnesia, analgesia and immobility [353]). Although the complete set of mechanisms have not been elucidated it is believed to be a combination of a general inhibition of neurons and a disruption of coherent activity [354]. At a molecular level anaesthetics are known to modulate or agonise/antagonise ligand-gated ion channels and inactivate voltage gated ion channels [354] thereby inhibiting neural activity and cognitive functions of specific brain networks [353, 355]. Of note, Lobb *et al.* found that the choice of anaesthetic on thalamic recordings had a more significant effect on neuronal activity than the underlying pathology being investigated [356].

We reflect on the use of Ketamine/Xylazine as an appropriate anaesthesia for electrophysiological experiments. While cortical and thalamic activity is still present under K/X, as opposed to the abolishment of cortical potentials under other anaesthesias such as Isoflurane (see Appendix B.5), it is not without significant effect on activity within these regions. Of note we have found evidence in the literature that K/X suppresses activation of layer VI cortical neurons to sensory input [115]. This is a very significant finding as these layer VI CT neurons project to the VPL and provide

feedback and modulation. Therefore it is likely that this suppression via K/X mimics the effects of stroke in removing CT influence over the thalamus. Hence any 'hyperexcitability' generated by the loss of CT feedback caused by stroke could be present in the intact network under K/X anaesthesia.

As was explored in Chapter 2, via computational models, the loss of excitatory CT input can switch neurons in the thalamus from a tonic to bursting firing mode, which is supported in recordings from a model of cortical lesion in the rat [115]. Given the functional disconnection of the cortex back to the thalamus under K/X, it is likely that TC neurons also switch to a burst mode. This would mean hyperexcitability, as defined by bursting to sensory input, exists in both sham and stroke mice.

Further evidence to support the presence of thalamic bursting under K/X is the large 'P2' wave in thalamic FL SSEPs recorded from sham mice (Figure 3.11a) and the presence of oscillatory waves in the late-latency component of the waveform (see Appendix B.3). These were hypothesised by Andersen *et al.* [332] to be the hyperpolarisation currents induced by TRN feedback to TC neurons, and we support this claim with simulated results in Appendix B.6. Given that TC neurons burst to sensory input, this would trigger bursts in TRN neurons (also explored in Chapter 2) and therefore large hyperpolarisation currents back to TC neurons that we recorded under K/X. Hyperpolarisation of TC neurons de-inactivates the T-Type Ca2+ channels triggering bursting upon repolarisation, which triggers bursting of TRN neurons thus creating these oscillations.

Urethane does not exert a significant effect on layer VI CT neurons [357] and may explain the lack of distinct positive wave and oscillatory behaviour others have recorded in thalamic SSEPs [293, 329], and also the presence of a distinct corticothalamic feedback wave in their recordings.

A burst-response by TC neurons fits the evidence of hyperexcitability that others have recorded in the thalamus after stroke (or cortical lesion/suppression). Unit recordings show direct evidence of bursting and after-discharges [115, 289, 288] and it is thought that bursting drives the increased amplitude of SSEP waveforms recorded by others [337, 290].

Alternatively, Anderson *et al.* [338] proposes that K/X anaesthesia triggers hyperactivity in both the thalamus and cortex, at least in the gamma band, but reduces evoked gamma-band activity in sensory evoked potentials. This is another mechanism by which K/X could mask hyperexcitability.

The other indication of excitotoxicity was hypothesised to be an increased excitation via extracellular glutamate released from degenerating corticothalamic neurons and the triggering of extra-synaptic NMDARs. Given that the primary mechanism of K/X anaesthesia is as an NMDAR antagonist [358, 359], this effect may be masked. This point also explains the indication that Ketamine suppresses excitotoxic cell death after stroke or TBI [360, 361].

3.7.2.2 Time-point of recordings

A possibility is that recordings made from day 1 post-stroke have missed the period of hyperexcitability that would align with an acute release of glutamate from CT neurons lost in the infarct. As described by Ross *et al.* [288], there are significant changes in excitability immediately after cortical ablation that abnormally fluctuated for several hours following.

3.7.2.3 Signal Quantification

Finally, we reflect on whether our methods for quantification are suited to predict hyperexcitability. The previous works, described in Section 3.2.2.1, measured changes in thalamic activity by comparing firing rates and amplitudes or spike/unit counts of SSEPs, all of which we have investigated. Studies assessing hyper-excitability specifically in the ventrobasal thalamus in the context of Spinal Cord Injury (SCI) have used the same [362, 312, 363, 293, 364].

From our simulated SSEP studies, we showed that increased activity of thalamic neurons (i.e. action potentials generated in response to stimuli), did not necessarily correlate with the amplitude of the LFP waveform (Figure 2.5), but instead represents the magnitude of post-synaptic currents. Post-synaptic currents reflect a combination of pre-synaptic neuronal activity (i.e. time-course of glutamate in the synapse) and resting membrane potential of the post-synaptic neuron. In most cases, increased post-synaptic currents would generate increased activity of the post-synaptic neuron, but the state of the neuron also needs to be accounted for. Therefore if pre-synaptic activity of ML or STT fibres hasn't changed, which we don't expect after stroke, there may not be an increase in the amplitude of the LFP potential.

Unit-activity on the other hand would give a direct measurement of the activity of thalamic neurons. Given the relatively large electrodes we have used (125µm diameter), a large number of neurons are sampled simultaneously, resulting in a significant number of overlapping spikes which can often appear as a single spike in MUA traces. Therefore, an increased number of synchronised thalamic action potentials to medial lemniscal input may only appear, and be detected as, a single spike event. The issue of spike detection in MUA recordings and our proposed methods are detailed in the following chapter.

3.7.3 No evidence for the loss of evoked Thalamic Potentials

With some uncertainty surrounding the origins of each component of the thalamic SSEP waveform, we question the possible scenarios in which the N1 peak is in fact the depolarisation of TC neurons

that others have described [293, 294, 302], and why it may persist through the progression of SND when thalamocortical neurons are believed to be lost. Three possible scenarios are considered: an insignificant loss of TC neurons, counteracting effects of cell loss and hyperexcitability and a possible bias in recording methods.

3.7.3.1 Insignificant Cell Death

Loss of TC neurons after PT stroke in rodent models is commonly assessed by counts of NeuN+ or Nissl stained neurons in preserved brain slices. These two stains bind specifically to neuronal nuclear antigens or Nissl bodies respectively that are exclusively found in neurons. Estimates from previous studies suggest an approximate 30% reduction in NeuN or Nissl-positive cell counts at 28 days post-stroke [150, 149, 365, 122]. This however may underestimate the actual loss of neurons, due to the shape of window used to extract ROIs that often includes spared regions in neighbouring nuclei.

Given a predicted effect size of 30% for the decrease in thalamic evoked potential (assuming the number of responsive neurons is proportional to the amplitude), Type 1 error rate of 0.05(α), power of 80% ($\beta = 0.2$) and standard deviation up to 20%, we had the statistical power to find significance in our Study1 results given we used n=7 for each group.

NeuN has been used for decades as a neuron-specific marker in neuroscience [345, 344], but there has been questions over its ability to accurately indicate neuronal loss [351]. In particular it has been shown that neurons lose expression or immunoreactivity of NeuN after metabolic stress or axotomy [351, 366], both of which are believed to affect TC neurons after stroke. These neurons may be injured, and depleted of the NeuN protein but maintain cellular integrity [351] and can replenish NeuN in the following days and weeks [366]. Similar evidence has been found with the expression of Nissl bodies after axotomy [367].

Interestingly, Kluge *et al.* [17] found that the area of NeuN+ cell loss in the ipsilateral thalamus although peaking at day 28 post-stroke was no longer significant by day 56, suggesting a mechanism for repopulation of mature neurons [17]. There may be a possibility that TC neurons lose NeuN expression but survive and replenish stores in days 28-56 when the pathological environment has settled and in this case NeuN may overestimate the level of neuronal loss. However it is also readily explainable by neurogenesis, which has been found to occur in the peri-infarct cortex and hippocampus following stroke [368, 369].

3.7.3.2 Counter-effects of Cell Loss and Hyperexcitability

Two of the hypotheses investigated in this chapter were that of thalamic hyperexcitability followed by progressive thalamic cell death. Since no conclusive evidence was found either way it could be possible that a smaller number of hyperexcitable neurons compensate for those lost which evens out the loss of response. As found by Paz *et al.* , surviving thalamocortical neurons after PT stroke were injured and become hyperexcitable [106].

3.7.3.3 Recording Procedure

Although the first set of recordings were taken from fixed electrode coordinates, all others since have 'optimised' the electrode position to that where the greatest response to stimulation is found. If a subset of surviving neurons are clustered together around the electrode this may give the appearance of normal activity, even if other adjacent populations of neurons are lost.

3.8 Summary

This chapter has detailed our investigation into the electrophysiological changes in cortical and thalamic populations of neurons after stroke. We confirmed immediate abolition of cortical activity and we have shown decreased spontaneous activity in the thalamus from the first day post-stroke. Thalamic neurons were found to still respond normally to peripheral stimulation in the first week but were altered at the same time as the onset of SND. This is the first time that spontaneous and evoked responses in the thalamus have been recorded in a mouse model of PT stroke and the first to relate it to SND. Further work is required to isolate the exact neuronal sources of activity present in thalamic SSEPs so definitive conclusions can be made.

Chapter 4

Spike Detection from MUA Recordings

This chapter introduces a new method of neuronal spike detection to discriminate overlapping spikes in multi-unit recordings. Improvement in spike detection allows researchers to obtain a better understanding of neural coding and receptive fields, take more accurate measures of firing rates and apply these findings to the diagnosis and treatment of medical conditions.

4.1 Introduction

The detection of neuronal spikes in extracellular recordings is a key tool in understanding and quantifying neuronal function. This helps researchers gain an understanding of cognitive function and the ability to discriminate between healthy and pathological medical conditions. Recordings of Multi-Unit Activity (MUA) contain voltage spikes generated by action potentials from a multitude of neurons in close vicinity to the probe. Neural probes used for recording simultaneous MUA and Local Field Potentials (LFP), with greater electrode contact size, allow effective recordings of population-wide dynamics but at the expense of the discrimination of individual spikes. Neurons in local populations often fire synchronously [370], which combined with a greater number of simultaneously recorded neurons, gives a high probability that two spiking events will overlap. This overlap can cause the spike waveforms to cancel out or merge together giving the appearance as one event, which conventional spike detection algorithms struggle to discriminate. Without the accurate discrimination of overlapping spikes, firing rates will be underestimated and there will be a loss of

information crucial to studies of neural coding. A typical MUA recording from a microwire electrode is shown in Fig 4.1.

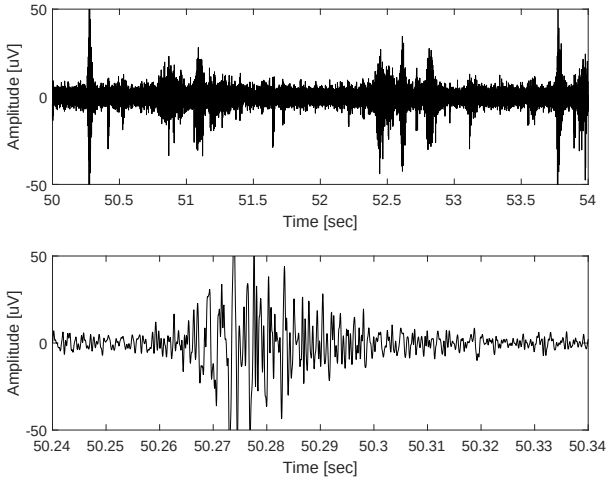

Figure 4.1: Example MUA recording depicting densely overlapping spikes.

Spike detection is most commonly performed using an amplitude threshold. A threshold is set manually or as a function of statistical measures of the signal [371], and discriminates spikes as occurring at each threshold crossing. This method performs well in signals having high Signal-to-Noise Ratio (SNR), however fails in low SNR environments and is complicated by the presence of overlapping spikes in how to effectively resolve multiple adjacent threshold crossings.

Non-linear energy transforms have been shown to improve performance in low SNR environments [372, 373, 374], but lack resolution in overlapping spikes. This is largely due to the windowing effect of the energy operator, that smooths the output of two closely overlapping spikes into a single peak (see Fig 4.6).

Methods implementing template matching [375, 376, 377, 378, 379] seek an optimal set of filters, either using entire spike waveforms or a reduced set of features, to distinguish spikes from the rest of the signal. Matched filters provide the optimal level of detection in low SNR environments in the presence of white Gaussian noise [380]. Without prior knowledge of the spike waveforms, additional methods are required to build the set of filters and therefore the performance highly depends on how well these spike waveforms approximate the real extracellular spikes.

The above methods are effective in discriminating spikes with sufficient temporal separation, but suffer when multiple spikes exist in close proximity. To overcome the specific problem of overlapping waveforms several methods have been proposed [381, 382, 383, 377, 384, 385, 378, 386]. The simplest

is to subtract the detected spike waveforms (based on the template matching approach) from the signal and re-analyse the residue, however inaccuracies in the spike model produce additional noise and transient spikes in the residue [387].

Other methods compare a library of overlapping templates to every detection of a possible spike. Accounting for all time separations and differences in amplitudes is computationally expensive and infeasible in on-line processing. Methods have been proposed to reduce the computational burden by shrinking the template dictionary and/or by using greedy algorithms [381, 382, 388, 384, 385, 378].

These algorithms utilise individual templates for single units and their performance is tested in very simplified models of MUA data where single units are readily discriminated. In denser MUA data (often with more than 10 units) single units are not readily separated, therefore only generalised spike waveforms can be used. This additionally requires for the amplitude of each spike waveform to be solved, and forgoes probabilistic approaches able to benefit from prior spike train information from each unit [382, 384, 385, 378].

Here we present an algorithm to detect and resolve overlapping spike waveforms in a two step procedure. The first step detects and discriminates spike waveforms that are likely to describe the MUA signal and obtains their corresponding time-shift. The second step of the proposed method focuses on resolving overlapping spike waveforms. Both steps rely on recent developments in sparse optimisation techniques to allow fast algorithm execution. Finally we introduce a novel refractory period policy to improve the performance of standard spike detection algorithms in the presence of overlapping spikes.

4.2 Methods

This section describes a novel two step procedure for spike detection and resolution of overlapping spike waveforms. To compute the amplitude and time-shifts of overlapping spikes, methods based on sparse optimisation [383, 59] have shown promising results. Such methods are guaranteed to resolve overlapping spikes under suitable conditions [389, 390] expressed in terms of the mutual coherence of the dictionary of spike waveforms, $\{\mathbf{w}_i\}_{i=1}^n$, and that is given by:

$$\mu = \max_{i \neq j} \frac{\mathbf{w}_i^T \mathbf{w}_j}{\|\mathbf{w}_i\| \|\mathbf{w}_j\|} \tag{4.1}$$

The mutual coherence measures the ability of a spike waveform dictionary to resolve overlapping spikes and it has been used in the development of algorithms such as the Continuous Basis Pursuit (CBP) method to resolve overlapping spikes [383]. To take into account that the overlapping spikes

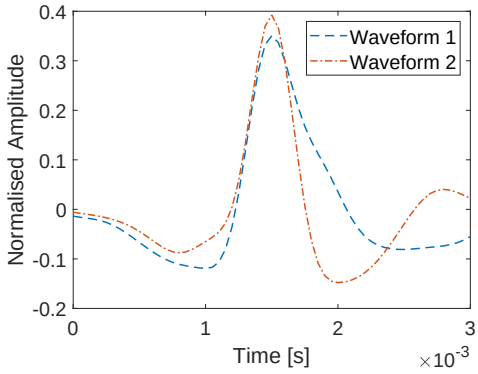

(a) Original waveform dictionary.

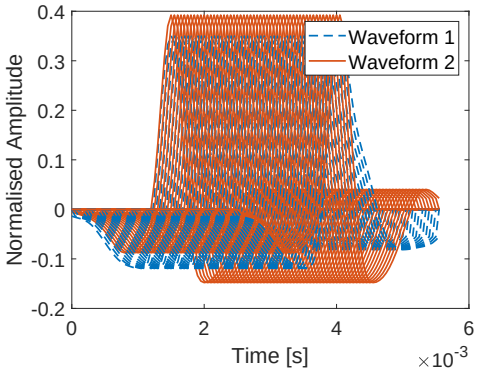

(b) Extended waveform dictionary.

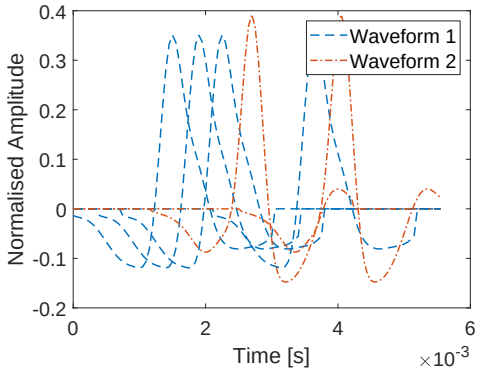

(c) Global waveform dictionary.

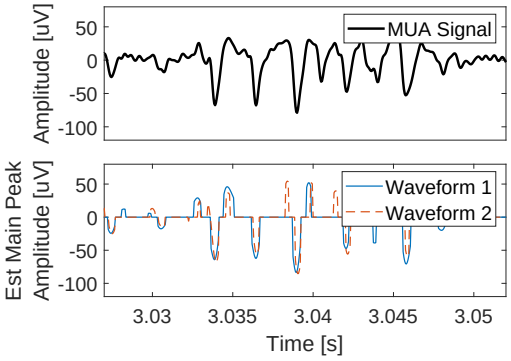

(d) Main peak amplitudes assigned to each waveform.

Figure 4.2: First stage of the proposed method. Figures 4.2a-4.2c show the steps taken to construct the global waveform dictionary. Figure 4.2c illustrates the outcome of the first stage of the proposed method.

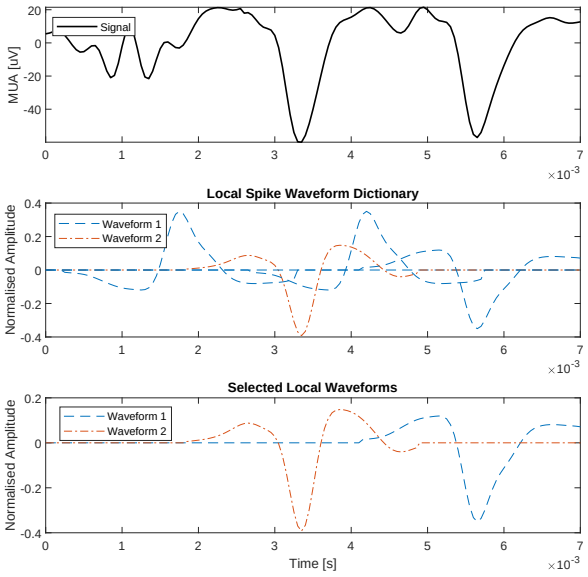

Figure 4.3: Illustration of a local waveform dictionary (middle) that can resolve overlapping spikes in the MUA signal (top).

may be shifted in time, Ekanadham *et al.* [383] extended the original dictionary of spike waveforms shapes with regularly spaced time-shifted spike waveforms. The time-shifted waveforms should be separated enough to ensure that the sparse optimisation algorithm can resolve the overlapping spikes. This approach helps to avoid testing for all possible waveforms and time-shift combinations which grow exponentially with the number of overlapping spikes to be considered [383]. The method is applied over batches of data and it performs well in practice, but it may suffer from inconsistencies at the points close to the data batch borders. Additionally, the method used by Ekanadham *et al.* [383] considers an extended waveform dictionary that may include spike waveforms which are slightly misaligned with respect to the generating data.

We propose to resolve the amplitude and time shifts of the overlapping spikes in a two step procedure. The first step uses a global waveform dictionary that is applied over the whole data set to discriminate between candidate waveform shapes and to find their respective time-shifts. To this end, a sparse optimisation problem is solved for each data sample with the peak location, peak magnitude and spike waveform of the dominant spike being recorded. This first step uses a global waveform dictionary in which the spike waveforms are mostly misaligned between them. This means that when analysis is performed on the current sample, the method is not testing if the peak of the spike is located at the current sample, but if there is a spike in the neighbourhood of the current sample that is consistent

with a waveform from the global dictionary. The sparse optimisation computation results in a spike being selected as the dominant spike, forcing neighbouring spikes to compete to be selected.

The second step of the proposed procedure uses the outcome from the first step containing the spike waveforms and time-shifts of the spike candidates. This information is then used to construct a (local) waveform dictionary of time-shifted spike waveforms that may better describe the measured signal at a local level. This local waveform dictionary is used in a sparse optimisation problem to resolve overlapping spikes by selecting a subset of spikes from the spike candidates and estimating their amplitude. The local dictionary only considers a few samples at a time and this may deteriorate the ability of the algorithm to resolve spikes located at the end of the considered window. To overcome this issue, we propose to only accept the first occurring spike estimated within the time window. Thus, the sliding window provides a preview of the data that may help to resolve overlapping spikes at the beginning of the current time window and help to mitigate the adverse effects introduced by overlapping spikes that are partially contained within the sliding window.

The rest of this section provides details on each component of the proposed algorithm.

4.2.1 Construction of the global spike waveform dictionary

First, a spike waveform dictionary is obtained from an initial set of spikes discriminated by a conventional amplitude threshold. The waveforms are extracted and grouped into clusters via a standard k-means procedure, and the centroids of each used as the initial spike waveform dictionary with the main peaks of each waveform aligned (Figure 4.2a).

An extended waveform dictionary is then constructed from time shifted copies of each spike waveform in the initial dictionary (Figure 4.2b). Next, the extended waveform dictionary is reduced to form a dictionary with a mutual coherence less than a prescribed value that ensures the resolution of overlapping spike under suitable assumptions. Here, the value of $\mu \leq \mu_{max} = 1/k$ is used where k is the maximum number of overlapping spikes to be considered, see [390] for further details.

The threshold in the mutual coherence is based on the result provided in Herzet *et al.* [390] that guarantees the greedy sparse optimisation algorithm resolves the sum of k dictionary elements if:

$$\mu < \min\left\{\frac{1}{k}, \frac{1}{2(k-1)\alpha + 1}\right\}, with\ \frac{1}{2} \leq \alpha \leq 1 \tag{4.2}$$

where α is the decay rate of the coefficients of the true sparse solution. This result is based on the analysis of a worst-case scenario, and less conservative thresholds have been proven for the average case (see [391]). Here we assume that $\alpha = 1/2$.

The global spike waveform dictionary is constructed by an iterative algorithm that at each iteration selects a pair of time-shifted waveforms from the extended waveform dictionary having the largest cross-correlation. Between the two selected time-shifted spike waveforms, the time-shifted waveform corresponding to the waveform having more time shifted copies is discarded from the extended waveform dictionary. The iterations are repeated until the resulting dictionary satisfies the mutual coherence upper limit.

Notice that the main peaks of the waveforms in the resulting global spike waveform dictionary are, in general, not aligned with each other (Figure 4.2c).

4.2.2 Selection of the dominant peaks

Once the global spike waveform dictionary has been computed, this is used to solve a sparse optimisation problem over a sliding window. The sparse optimisation solution is used to determine the possible location and corresponding waveform of the candidate spikes (Figure 4.2d).

The sparse optimisation problem to be solved is given by

$$\min_{\mathbf{x}\in\mathbb{R}} \quad \|\mathbf{y}_{t-m:t-1} - \mathbf{W}\mathbf{x}\|_2^2 \tag{4.3}$$

$$\text{subject to} \quad \|\mathbf{x}\|_0 \leq k \tag{4.4}$$

where $\mathbf{W} \in \mathbb{R}^{m\times n}$ is the global spike waveform dictionary, $\mathbf{y}_{t-m:t-1} \in \mathbb{R}^m$ is the vector of measured samples for the current time window. The solution of (4.3) is given by $\mathbf{x}(t) \in \mathbb{R}^n$ and it contains at most k non-zero elements. Computing the optimal solution of (4.3) is computationally expensive due to the combinatorial nature of the problem. However, an approximate solution of (4.3) can be obtained using greedy algorithms such as Orthogonal Matching Pursuit (OMP) [392] and Orthogonal Least Squares (OLS) [393]. Since (4.3) is solved over a sliding window, the number of sparse optimisations during this stage of the proposed procedure is equal to the number of measured samples to be analysed. Thus, efficient implementations of OMP and OLS are needed such as the ones described in [394, 395].

To determine the waveform of the candidate spike and its corresponding time-shift, the first dictionary element selected by a greedy algorithm computing $\mathbf{x}(t)$ is selected as the dominant spike waveform within the current time window. Next, the time-shift and amplitude of the main peak is recorded as well as its corresponding spike waveform index. Because the main peaks in waveform dictionary $\mathbf{W}$ are not aligned with each other, nearby spikes mutually exclude each other to be selected as the dominant spike within the sliding window. This may help to reduce the incidence of false positive detections in low-SNR scenarios.

If a peak location is selected more than once as the dominant peak, the resulting peak magnitude is the average over the peak magnitudes at that location.

The sliding window approach we implement is different from the approach considered by other methods based on sparse optimisation. For example, Ekanadham *et al.* [383] solved the sparse optimisation problem over contiguous non-overlapping data blocks.

4.2.3 Construction of the local waveform dictionary

The previous step provides time-shifted spike waveform candidates that approximate the measured samples over the current time window much better than the global waveform dictionary. At each sample for which at least one main peak value has been computed, the waveform having the largest peak magnitude is assigned to that sample. Next, contiguous samples having the same waveform and the same main peak sign are grouped together and the sample within the group having the largest main peak is selected as a candidate for inclusion in the local waveform dictionary. Long groups are split to consider the possibility of overlapping spikes with the same waveform. Once all the time-shifted waveform candidates within the current time window have been included, a local waveform dictionary is obtained by computing a regression matrix having mutual coherence satisfying $\mu < \mu_{max}$. This is done by using an iterative procedure like the one used to construct the global spike waveform dictionary. However, for the local waveform dictionary the decision of which waveform is discarded from the dictionary is not based on the number of copies of the waveform amplitude, but is based on the amplitude of the main peak. See Figure 4.3 for example of the local dictionary.

Remark 1. *The condition $\mu < \mu_{max}$ ensures that spike waveforms which are similar to each other and/or too close to each other are not included in the local waveform dictionary because they are indistinguishable from each other and cannot be distinguished by the proposed method. Thus, the construction of waveform dictionaries with reduced mutual coherence is an important element of the proposed method.*

4.2.4 Moving horizon spike resolution

Next the local waveform dictionary is used to resolve potential overlapping spikes using a sparse optimisation problem. A sparse optimisation problem similar to (4.3) is solved using a local waveform dictionary $\mathbf{W}(t)$. Each of the spikes estimated by the local sparse optimisation problem is then compared against a given spike magnitude threshold. If more than one spike is larger than the threshold, then only the first occurring spike is included in the estimated signal. The next local

sparse optimisation problem only considers candidate spikes that are located after the peak of the recently considered spike. This means that the next local sparse optimisation problem may consider a part of the data that has been already considered in the previous iteration.

Remark 2. *When the spike waveforms are consistent over several experiments, the proposed method can be implemented online using a moving window for each stage of the proposed approach.*

4.2.5 Resolving Overlapping Spikes in Conventional Methods

Conventional spike detection methods can detect spike events but fail to effectively discriminate multiple overlapping spikes, as seen in Figure 4.4. A refractory period is often implemented to avoid double detection caused by threshold crossings from multiple peaks of a single waveform [396]. This is done by setting a period (typically 1ms) in which only one spike can be detected. The approach works well in single unit recordings or in MUA with low number of units, as the biophysical mechanisms for action potential generation limit the time in which successive action potentials may be produced. A direct trade-off exists between setting a refractory period duration to prevent double detection and the difference in spike times of overlapping spikes that can be resolved.

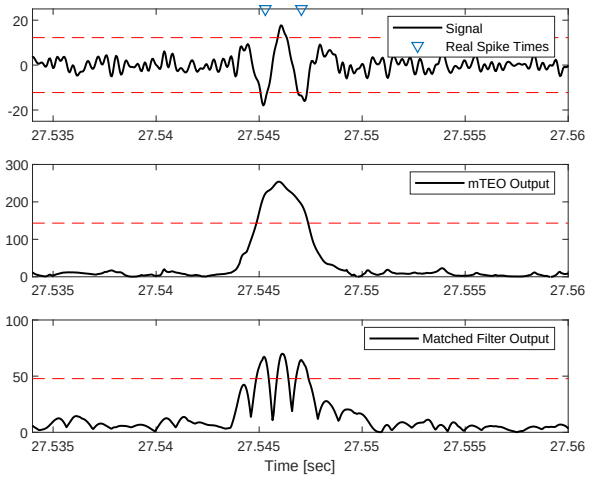

Figure 4.4: Limitations of conventional detection methods on two overlapping spikes: Amplitude Threshold (top) - 3 threshold crossings are present for only 2 real spikes with the largest being neither of the real spike peaks. mTEO (middle) - only a single peak in the output. Matched Filter (bottom) - 3 adjacent peaks result from the convolution of known waveforms (that include both positive and negative peak values).

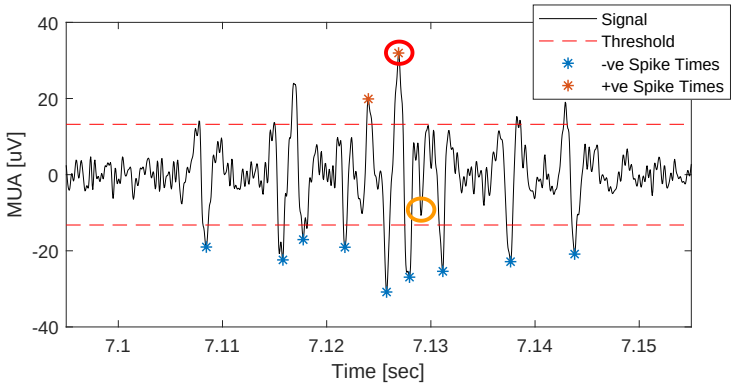

Figure 4.5: Separating detection of positive and negative spike peaks in the amplitude threshold method. (False Positive circled red, False Negative circled orange).

We propose a simple amendment that can improve the performance of amplitude threshold detection by introducing a signed dependent refractory period policy. A single action potential can produce multiple peaks above a given threshold, most commonly a single large peak with smaller, adjacent, opposite-polarity peaks. By allowing a smaller refractory period for threshold crossings of the same polarity it is unlikely to detect the same spike twice, but allows detection of overlaps up to this degree. A normal (1-1.5ms) refractory period can be used for adjacent crossings of opposite polarity. Simply put, negative threshold crossings are considered first using a short refractory period (0.5ms) followed by any missed positive polarity spikes that are $\geq$ 1ms away from existing spikes (See Figure 4.5).

By using only a single-signed threshold for detecting spikes, the number of double detections and therefore false positives is reduced. However, extracellular action potential waveforms vary due to neuronal geometry and distance and orientation to the electrode and unless both positive and negative thresholds are used, spikes lacking a large peak of that polarity will not be detected.

A similar adjustment can be applied to the mTEO algorithm. The shortfall with the conventional method is the output over two overlapping spikes can produce a single local peak. See in Figure 4.6a how taking all local maxima above the threshold can provide better resolution of overlaps, however only up to a certain degree until a single local peak results from two spikes. By splitting the signal into positive and negative components and applying the mTEO algorithm, the improved SNR is maintained but with additional distinction of adjacent peaks. Alternatively, the window size or resolution can be reduced for the original implementation to give detail of adjacent peaks, but this loses information on polarity. The same refractory policy as above can be applied to the new mTEO output by taking all output peaks from one polarity combined with those of the other polarity greater than 1ms away.

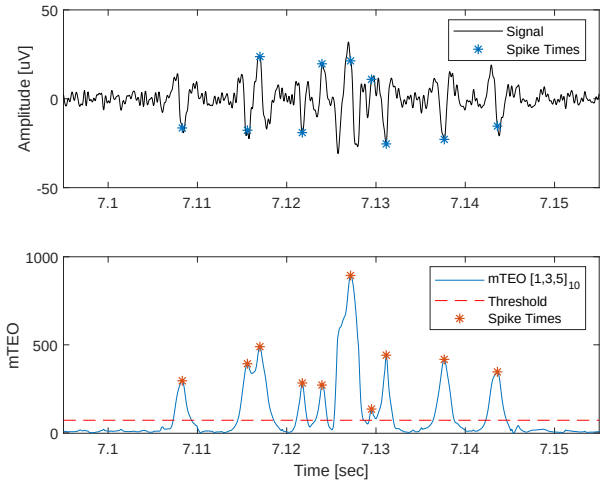

(a) Original mTEO with local maxima detection.

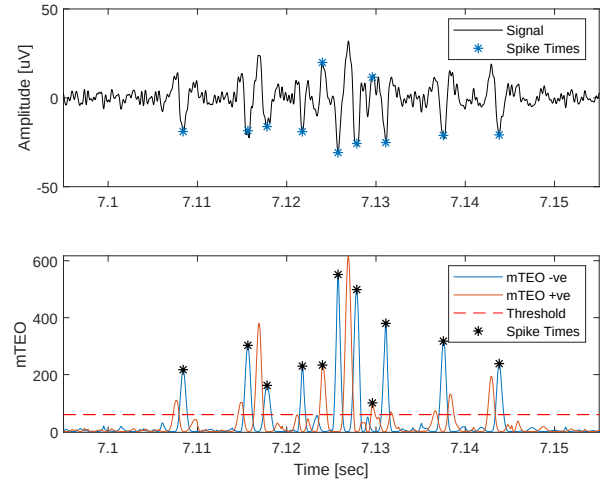

(b) Modified mTEO with split positive/negative detection.

Figure 4.6: Performance of the modified mTEO algorithms on overlapping spikes.

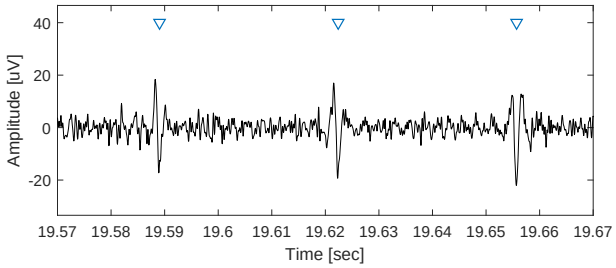

(a) Signal 1: Uniformly Spaced Spikes.

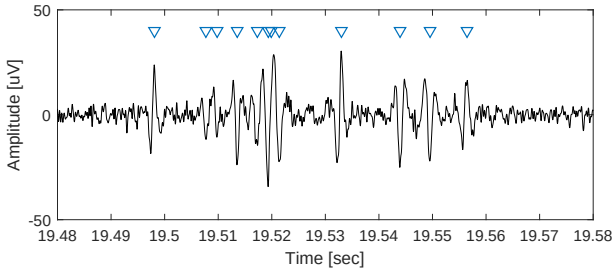

(b) Signal 2: Overlapping Spikes.

Figure 4.7: Preview of simulated recordings (spike times indicated by arrows).

4.3 Results

4.3.1 Establishing a Ground Truth

To illustrate the performance of the proposed method a simulated signal with known spike times is constructed using a database of recorded spike waveforms to form a ground truth (from [397, 398]).

A small number of simulated neurons (approximately 20) are assigned a unique spike waveform, amplitude for a desired SNR and a firing rate ($U \sim [0.5, 4.5]$ Hz). Spike trains are generated with Poisson distributed Inter-Spike Intervals (ISIs) and a renewal process equal to a refractory period of 1ms [399]. To replicate the level of overlap typical in MUA recordings, both a correlation in the spike times (representing the synchronous firing of neurons in a local population) and bursting (short periods of repetitive firing common in certain neuronal types) were added. Synchronous firing is implemented by creating the Poisson distributed spike trains by sampling from correlated uniform distributions [400]. The spike trains from each neuron are then shifted in time by a value sampled from the normal distribution ($\mu = 0$, $\sigma = 50$ms) to prevent them all occurring at the same time point and creating an overlapping sequence of spikes. Bursting is incorporated using a Poisson distribution ($\mu = 1$) to give the number of spikes to occur at each spike event generated by the

previous spike train, with inter-spike interval sampled from a Poisson distribution from 1 to 4ms [399]. Any adjacent spike times within 0.5ms are removed to establish a practical test for the spike detection algorithms and prevent complete cancellation of waveforms.

Noise is added to the generated signal as a combination of white Gaussian (external/electrical) noise and biological noise consisting of tiny (1uV) spike waveforms added at each sample of the signal, which reasonably replicates frequency content and point distributions of noise from real recordings [398]. The signal is then filtered to a typical MUA bandwidth using a zero-phase, 4th order, Butterworth, band-pass filter with corner frequencies of 0.25 and 5 kHz.

Two test signals are generated:

1. Uniformly-spaced spikes (no overlap)
2. Correlated spike trains (significant overlap)

Example traces from these signals are shown in Figure 4.7.

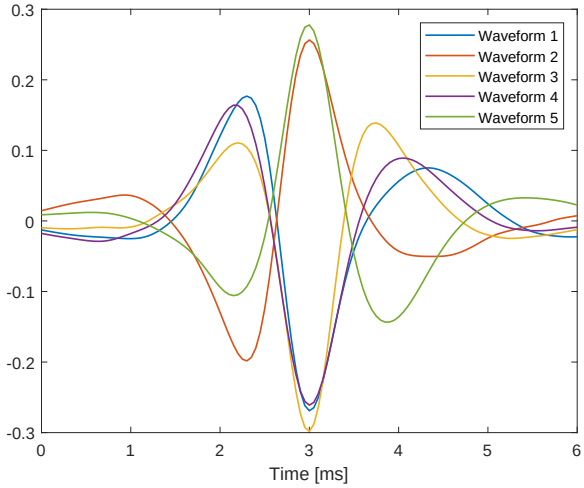

Figure 4.8: Example set of spike waveforms used in the simulated signals.

4.3.2 Comparison with existing methods

The performance of each algorithm is evaluated using Receiver Operating Characteristic (ROC) curves, using a varied threshold, to establish the percentage of correct detections as a function of the False Positive Rate (FP Rate).

The performance of the proposed method is compared against three other commonly used algorithms:

1. **Amplitude** Thresholding: Simplest and most widely used method in the literature.
2. **mTEO**: Most popular and best performing energy-based spike detection method [373]. Here the equivalent resolutions of k = {1,3,5} samples at 10kHz are used.
3. **Matched Filter**: A set of known matched filters applied to set an upper limit for template/filter based algorithms.

In these results a generous matching threshold is used - a spike time must be $\leq$ 1ms from the largest peak of the true spike waveform when inserted into the signal. If a single spike time is designated between overlapping spikes (as seen in the middle of two spikes in Figure 4.4), it is not considered a false positive, however only the closest real spike is classified as detected.

The following sections show the performance of the proposed method on simulated data, where it achieves a perfect 100% detection rate with zero false positives given non-overlapping spikes and shows enhanced performance on overlapping spikes against conventional methods. The new refractory policy also shows improvements in detection rates against conventional polices when it comes to overlapping spikes.

4.3.3 Amplitude Thresholding

A refractory period ensures that only a single spike, with the maximum amplitude, in the given time window is detected.

Figure 4.9 shows the results of varying this time window. With uniformly spaced spikes (33ms ISI), the longer refractory period obviously performs best. However this limits the detection rate for overlapping spikes. The novel refractory policy (*Amplitude**, light blue line) provides the best trade-off between detection rate and false positives.

The novel refractory policy has the benefits of a single-signed threshold in reducing double detections, but by also considering peaks of the opposite polarity improves the detection potential. See in Figure 4.10 how this improves detection rate against a single-signed policy with little effect on false positives. This effect is enhanced in low SNR environments, see later in Figure 4.17.

4.3.4 mTEO

The novel refractory policy is implemented on the modified mTEO algorithm and compared against the proposed method and conventional mTEO methods. Conventional mTEO and with local maxima detection also achieve perfect results on the well spaced spike signal, but the detection of overlapping

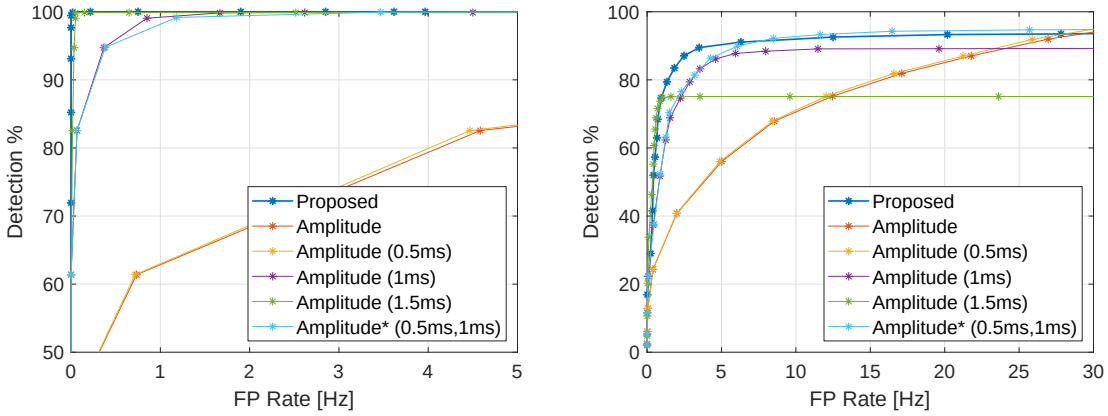

(a) Uniform Spaced Spikes.

(b) Overlapping Spikes.

Figure 4.9: Performance of the proposed method against conventional amplitude thresholding and new refractory policies.

spikes is limited. A high true:false positive ratio is achieved but they are ineffective in resolving the remaining overlapping spikes. The modified $mTEO^*$ method does not suffer the same limitations and can resolve additional overlapping spikes with no great expense of false positives, see Figure 4.11.

4.3.5 Matched Filters

Given a sufficient refractory period applied to the matched filter output it can achieve a perfect result in the case of well separated spikes. However applying this same refractory period to a signal with overlapping spikes, directly limits the detection potential. As seen in Figure 4.12 a large refractory period ensures a high true:false positive ratio but the number of spikes that can be detected is severely limited.

4.3.6 Performance in Low SNR

The performance of the proposed method and refractory policies are now assessed under a low SNR environment, herein the SNR is calculated (similar to in [373]) by:

$$SNR = \sqrt{\frac{E[S_{peak}]^2}{E[N^2]}} \tag{4.5}$$

Where S_{peak} is the distribution of peak values as they appear in the test signal without noise and N is the pure noise signal.

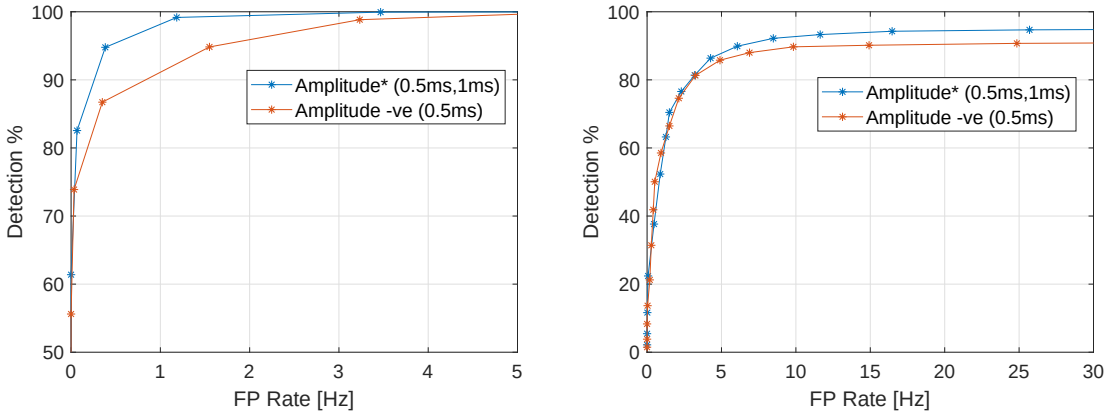

(a) Uniform Spaced Spikes.

(b) Overlapping Spikes.

Figure 4.10: Comparison of the new refractory policy and a single (negative) polarity policy.

Two new signals are generated by adding further white, Gaussian noise to the simulated signals from above. Table 4.1 gives the resultant SNR's for all signals used, and examples of the new traces are shown in Figure 4.13.

	SNR	
Signal	Normal	w/ Added Noise
Uniform	8.43	3.15
Correlated	9.57	3.58

Table 4.1: Simulated Signal SNR's

The following Figs. 4.14, 4.15 & 4.16 show the performance of the proposed method and conventional refractory policies in a low SNR environment. An additional result, denoted *Proposed**, shows the performance of the proposed algorithm given that the spike shapes are learnt from the previous high SNR signal. This shows the potential performance if spike shapes can be better learnt in low SNR environments, and how it significantly outperforms the other methods. Matched filters provide the best performance given well-spaced spikes, closely followed by the proposed method. Given overlapping spikes the proposed method is on par with the best of the conventional methods and the improved refractory policies. Considering that, especially in low SNR environments, the perfect matched filters are unobtainable, the proposed method is still the best option.

Figure 4.17 re-iterates that, in low SNR environments, only considering a single-signed threshold, forgoes detection of a considerable number of spikes without a significant peak in that direction.

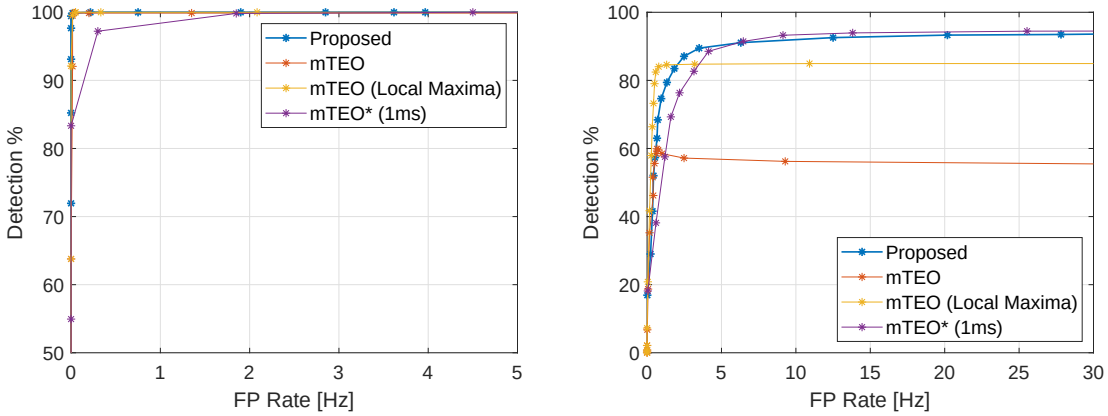

(a) Uniform Spaced Spikes.

(b) Overlapping Spikes.

Figure 4.11: Performance of the proposed method against the conventional mTEO and new refractory policy.

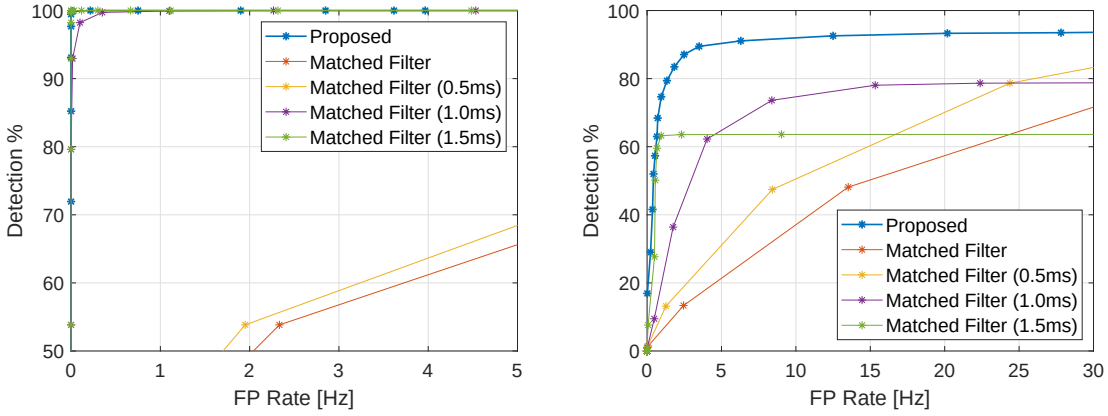

(a) Uniform Spaced Spikes.

(b) Overlapping Spikes.

Figure 4.12: Performance of the proposed method against conventional matched filter with refractory periods.

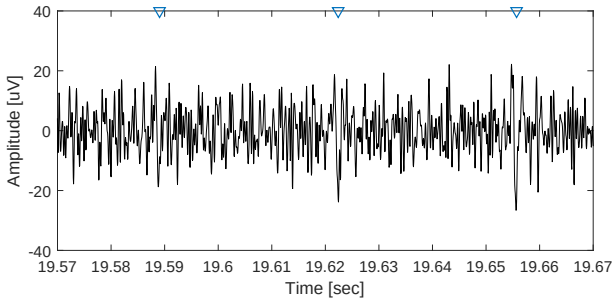

(a) Uniformly Spaced Spikes.

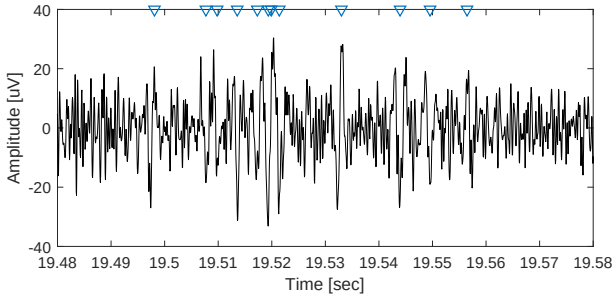

(b) Overlapping Spikes.

Figure 4.13: Preview of simulated recordings with low SNR.

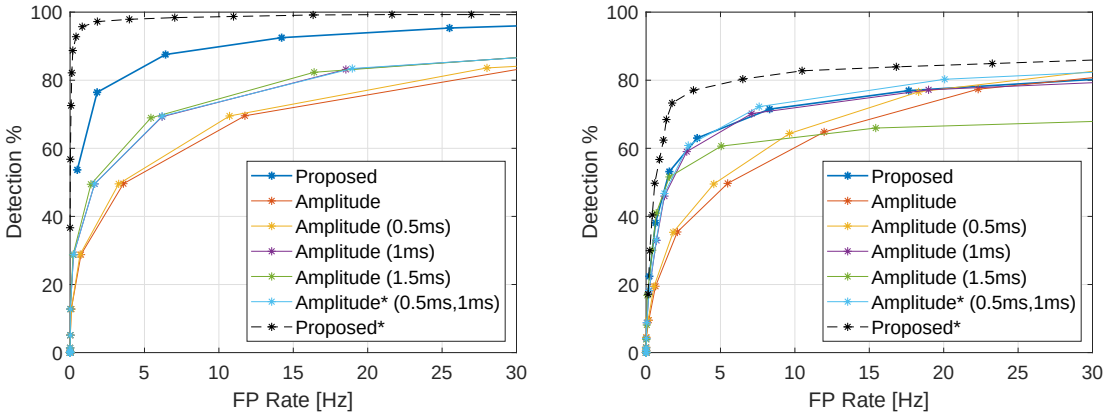

(a) Uniformly Spaced Spikes.

(b) Overlapping Spikes.

Figure 4.14: Amplitude threshold performance in low SNR signals.

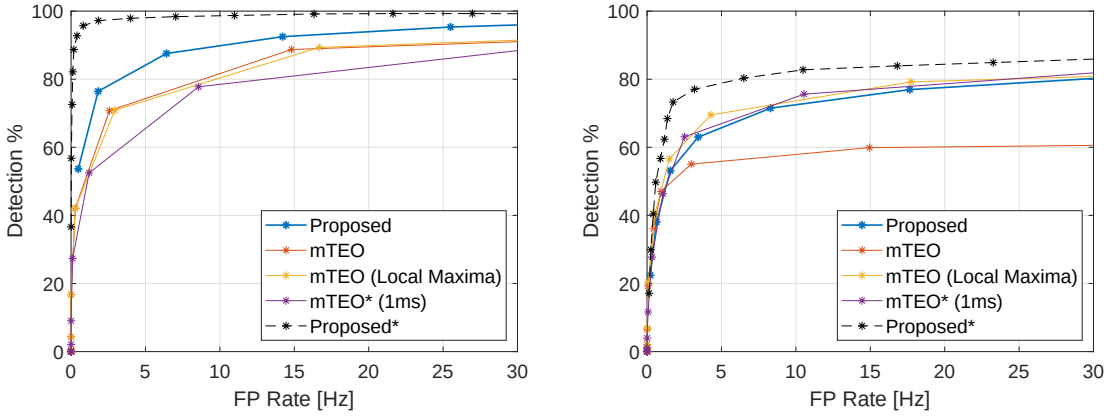

(a) Uniformly Spaced Spikes. **(b)** Overlapping Spikes.

Figure 4.15: Performance of mTEO algorithms in low SNR signals.

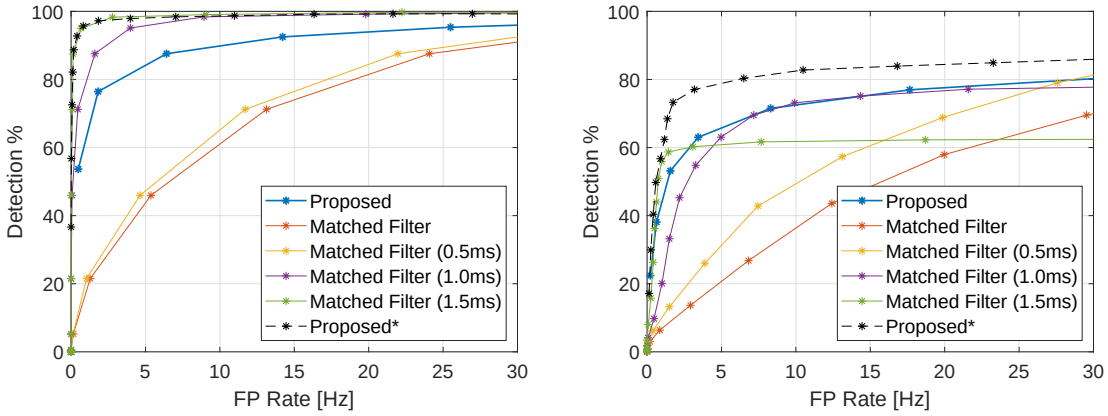

(a) Uniformly Spaced Spikes. **(b)** Overlapping Spikes.

Figure 4.16: Performance of matched filter algorithms in low SNR signals.

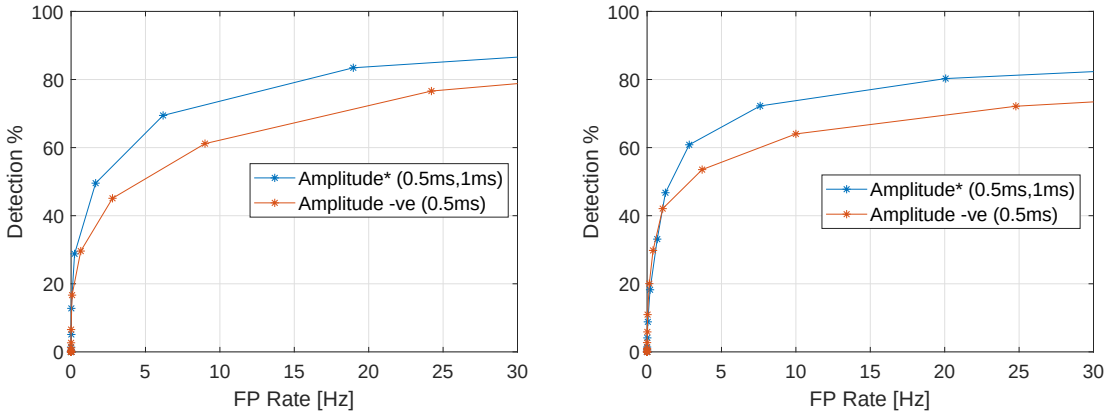

(a) Uniform Spaced Spikes.

(b) Overlapping Spikes.

Figure 4.17: Comparison of the new refractory policy and a single polarity policy in low SNR recordings.

4.3.7 Real Data

The performance of the proposed method on real data is shown in Figure 4.18, alongside simulated data, where the estimated signal is reconstructed. The autocorrelation of the residual in the simulated signal well-approximates the known residual, Figure 4.19b, and a similar trend is evident from the residual of the real signal, Figure 4.19a.

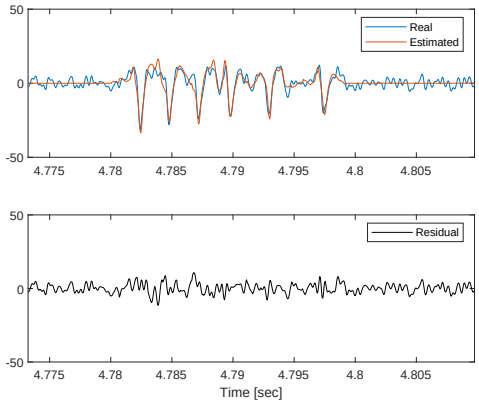

(a) Real Signal.

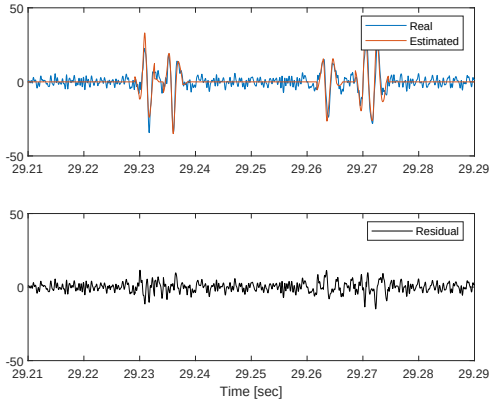

(b) Simulated Signal.

Figure 4.18: Estimation of real and simulated signals by the proposed method and the resultant residuals.

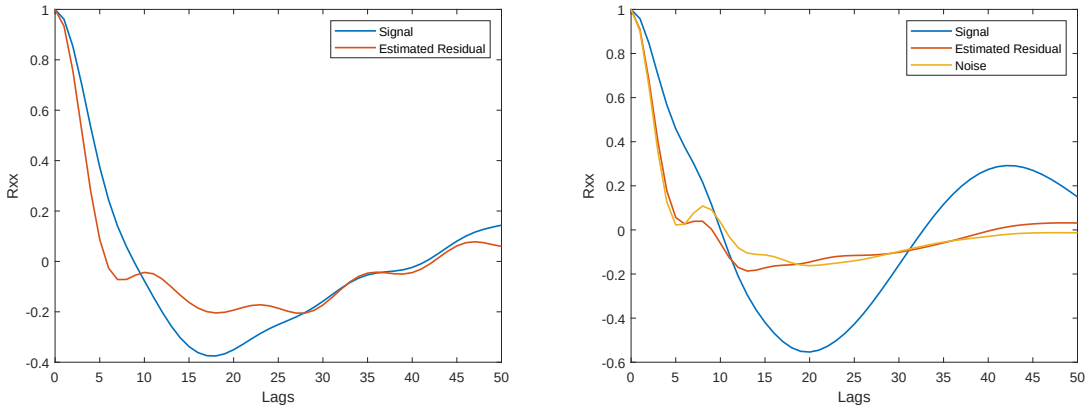

(a) Real Signal.

(b) Simulated Signal

Figure 4.19: Autocorrelation of residuals from the proposed method applied to real and simulated datasets.

4.4 Discussion

The spike detection algorithm outlined in this chapter provides a novel way of extracting spike times and resolving overlapping spikes in MUA recordings. As shown here, the methods are able to outperform conventional techniques and potentially improve current neurological diagnostics and treatments.

As mentioned in Section 4.2, this algorithm can be implemented in real-time and provide online spike detection, provided a preliminary recording period or prior data are available to learn the spike waveforms. This allows use in real-time neural control systems for treatment, such as for epilepsy and Parkinson's Disease [401, 402], or brain-computer-interfaces.

The benefit of using microwire electrodes or others with relatively large contact sizes (100+ µm in diameter) is the ability to sample an entire sub-population of neurons at once. Action potential waveforms are believed to be recorded up to 140 µm from the electrode [403]. This allows a population-wide recording from a single electrode. Alternatively, arrays of smaller electrodes can be used to sample single or a small number of neurons, in which spike detection can be performed more effectively, and combined to give a population wide measure. This however incurs higher costs for electrodes and amplifiers while requiring accurate spike sorting to ensure spikes from single neurons are not counted multiple times on adjacent channels [404].

Nevertheless, there is widespread use of microwire electrodes for population-wide recordings with dense, overlapping multi-unit activity. To quantify the neuronal activity present it is necessary to extract spike times from these signals. Therefore this work presents a new algorithm effective in discriminating spikes from this type of signal.

The algorithm can be readily implemented in spike-sorting applications [371, 377, 378], where spike times of individual neurons are extracted in the study of neural coding, receptive fields or for individual unit firing rates. Given a set of initially detected single unit templates, the algorithm well describes the limit of overlap that is possible to detect based on the mutual coherence of the spike waveform templates.

The novel refractory period policy described has shown to increase the detection rate of conventional methods in signals with highly overlapping spikes. By implementing the signed-policy and considering only one polarity in the window of considerable overlap between waveforms, multiple distinct spikes can be discriminated without double detections of opposite polarity peaks. Including an opposite polarity check at a longer refractory period ensures that spike waveforms without a considerable peak in the first direction can still be detected, which is especially important in low SNR cases where only a single peak is evident. We used a short refractory period for the negative polarity as most spike

waveforms recorded on single ended probes consist of a large negative peak. As mentioned in the previous section, the exact spike waveform largely depends on the neuronal and electrode geometries as well the relative locations and orientations, see [317] for an example of how the waveform produced in extracellular space varies with location around the neuron. With prior knowledge of the type of neurons being recorded and expected spike waveforms or some supervision, the refractory policy can be set to favour a particular polarity. With differential recordings, such as with stereotrodes, and assuming similar arrangements of neurons at each electrode site, the favoured polarity is arbitrary.

4.5 Summary

This chapter has introduced a new method of spike detection effective in resolving overlapping spikes. It has also introduced a new refractory period policy that can be used with conventional spike detection algorithms to improve their performance in the presence of overlapping spikes. Either of these methods can be used to improve the detection of spike times in dense MUA recordings with many overlapping waveforms.

Chapter 5

Deep Brain Stimulation

This chapter outlines the investigation into DBS as a treatment method for SND. A pilot study of DBS as a potential therapy to limit SND in a mouse model of PT stroke is conducted. This limited study did not show any significant improvements, likely due to the low number of animals used. However it did determine an effective set of stimulation parameters, a safe DBS protocol and uncovered areas worth further investigation.

5.1 Introduction

Deep Brain Stimulation is used for a wide variety of neurological disorders, but here we investigate its use in preventing SND in the VPL after stroke. Given our results in previous chapters we propose two potential treatment strategies using DBS: (1) prevent the effects of excitotoxicity and (2) promote recovery and pro-survival signalling. Applications for each of these strategies are explored below before determining the latter option provides a greater chance of effectiveness.

5.1.1 Anti-excitotoxicity

One option is to suppress the excitotoxic insult that is believed to be a major contributor to SND. We determined the most likely source of excitotoxicity is the spillage of glutamate from degenerating corticothalamic axons into the extracellular space in the thalamus. Unlike the proposed use of DBS to reduce excitotoxic stress on the substantia nigra in PD [210, 405, 406, 407], we can not suppress the activity of presynaptic neurons to reduce glutamate release. Glutamate is already in abundance in the VPL and we offer no mechanism by which DBS can promote glutamate clearance.

It has been proposed that GABA may attenuate excitotoxicity [408], and reduce stroke damage (Reviewed in [409]). Given the reduced excitability of TRN neurons after cortical stroke [113], boosting the excitability back to normal levels may prove beneficial in increasing GABA-ergic inhibition of TC neurons. TRN stimulation has been used as a treatment for a number of neurological conditions [410, 411, 412]. Given that TRN plays a key role in sensory processing and arousal care must be taken [413, 414], but a sub-threshold stimulation protocol may work [415].

Clarkson *et al.* [416] found that blocking GABAaRs in the early phase after stroke increased infarct size but inhibiting GABAaRs in the weeks following stroke promoted recovery. This suggests the benefit of a two-phase treatment regime, where reduced excitation is crucial in the acute phase to suppress excitotoxic damage, but increased excitation is necessary in post-acute phase to promote recovery. The prolonged time-course of SND doesn't have distinct time-points, but the return of normal glutamate levels in the thalamus in the second week following stroke [20] may indicate a time to switch treatments from suppressing damage to promoting recovery.

The earliest time-point that DBS electrodes can be implanted in our PT stroke model of the mouse is at 3-days post-stroke. Allowing an additional 3-4 days recovery means that a substantial portion of this beneficial time-window for GABA has passed. For this reason and the added complexity of insertion of electrodes into the TRN, we decided to target the recovery phase.

5.1.2 DBS for Neuroprotection & Recovery

The most promising application of DBS in the context of SND is providing neuroprotection, recovery and rehabilitation via the stimulation of pro-survival signalling pathways in thalamocortical neurons. It has been shown that chronic electrical stimulation of neurons promotes the expression of neurotrophic factors [212, 417, 418]. This has been used to improve rehabilitation from spinal cord injury [417], promotes survival and function of retinal cells from neurodegenerative disorders [215, 419, 217] or axotomy [216] and accelerate regeneration of motor axons [212, 420]

In the context of stroke recovery in animal models, chronic stimulation of thalamocortical pathways has been shown to improve motor recovery. This has been achieved via indirect stimulation of the lateral cerebellar nucleus [199, 224] or direct TC stimulation via optogenetics [223]. It may seem counter-intuitive to further stimulate a neuronal population believed to be experiencing excitotoxic injury but promoting normal function and boosting pro-survival signalling pathways may outweigh the potential negative impacts of further metabolic stress due to stimulation.

5.2 Thalamocortical Stimulation

This section details the preliminary investigation into the stimulation of the thalamocortical pathway in a mouse model. We used 8 naïve mice to determine safe and effective parameters and protocols, guided by an extensive literature review into DBS applications in rodents (See Appendix A.4).

Electrode placement in the VPL was performed using the same procedure as in Chapter 3 and verified by the presence of a thalamic SSEP. For stimulation, a twisted-pair bipolar electrode ensures that a localised electric field is created within the target structure, and limits spillage into neighbouring nuclei. An ECoG screw was placed over SSFL for simultaneous cortical recordings.

Stimulation was performed using the same *Stimulus Isolator* (FE180, ADInstruments) from Chapter 3. We injected a current-controlled, monopolar, square pulse with varying amplitude, pulse-width and frequency as described in the following sections.

5.2.1 TC-Evoked Waveforms

Stimulation of the target thalamocortical neurons was verified by recording the evoked response from the cortex using an ECoG screw placed over SSFL, see diagram in Figure 5.1. The waveform should match that of an SSEP but at a reduced latency. We recorded a set of distinct waveforms evoked from thalamic stimulation that are shown in Figure 5.2.

There are two characteristic waveform shapes evoked from thalamocortical stimulation. Notably, those in Figure 5.2 (a) and (b) show a main TC evoked potential occurring approximately 10 ms before the forelimb evoked cortical response. The waveforms in (c) and (d) consist of a small early response and the main response occurring only 3-4ms before the forelimb evoked response. These differences likely reflect the location of the stimulating electrode. A typical thalamic response to fore-limb stimulation occurs at approximately 6-8 ms which is followed by the positive peak of the cortical SSEP at approximately 18 ms. In (a) and (b) the evoked response from stimulating the thalamus occurs approximately 10ms prior to the fore-limb evoked response, which is readily explained by the stimulation of either the TC soma or axon fibres (shown as points (1) and (4) in 5.3 below), skipping the latency of peripheral transmission to the thalamus. Note that axons are preferentially stimulated ([202, 421]) and therefore the most likely scenario. In Figures (c) and (d) the main response occurs only 4 ms prior to the forelimb evoked response, which is exactly the delay from the forelimb to the cuneate nucleus in the brain stem where medial lemniscal fibres are activated. Therefore the likely explanation is ML or STT fibres are primarily triggered (stimulation point (3) in the below figure) and the small, initial response could be antidromic activation of CT fibres(point (2)).

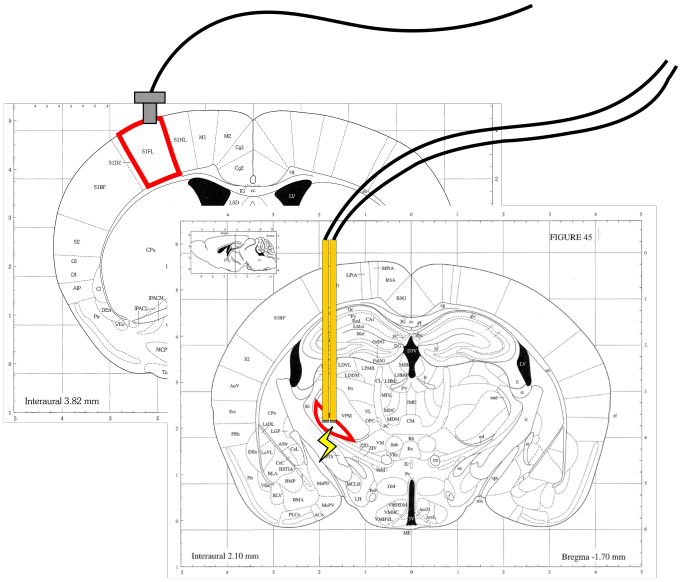

Figure 5.1: Stimulation of the thalamocortical pathway by an implanted electrode in the VPL is assessed by recording the evoked potentials from the somatosensory cortex via ECoG.

5.2.2 Parameter Selection

We varied the stimulation current, pulse width and sign to determine the best set of parameters. Increasing both current and pulse-width was found to increase the evoked response in the cortex and decrease the onset latency (Figures 5.4,5.5). Changing the polarity was found to have little effect (Figure 5.6).

5.2.3 DBS Frequency

We tested the effect of DBS applied to the VPL by simultaneously recording from the SSFL cortex via ECoG in 3 naïve mice. A 30 second window was used to determine baseline ECoG activity, followed by 10-30 seconds of stimulation at frequencies ranging between 1 and 100 Hz. The power of the cortical LFP signal during stimulation was normalised to the baseline value and is shown in Figure 5.7.

It was shown that increasing frequency increased LFP power in the cortex to a maximum at 5Hz, before decreasing to a minimum, and hints of suppression, at 100 Hz. This aligns with a consensus in the literature that high frequency stimulation (100 Hz+) leads to neural inhibition, while low frequency stimulation can enhance neural activity. Alternatively, TC neurons may be activated at

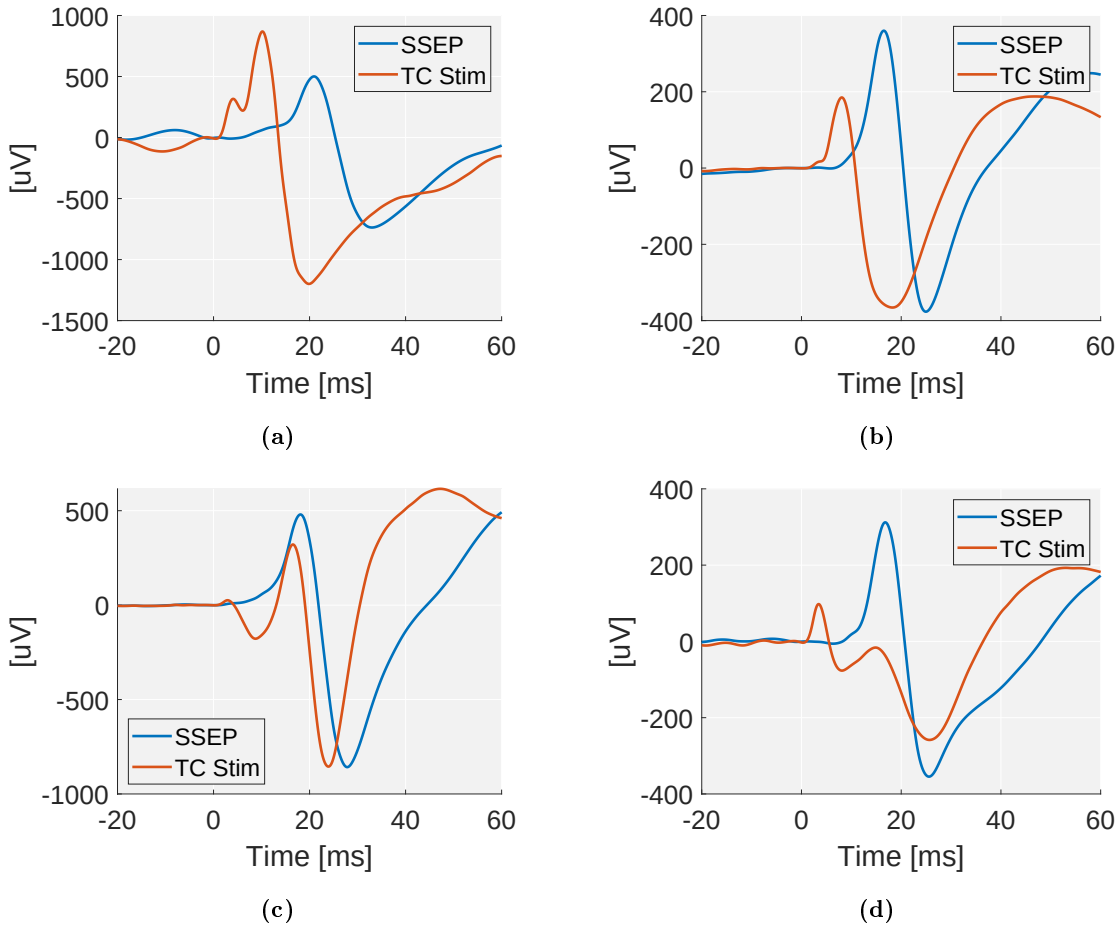

Figure 5.2: Evoked potentials in the cortex of four different naïve mice from forelimb stimulation (SSEP) vs direct thalamocortical stimulation (TC Stim). A similar waveform is evoked in both cases but at an earlier latency when directly stimulating the thalamus.

high frequencies but thalamocortical synapses experience synaptic depression.

Hence, to optimise maximal stimulation of the thalamocortical pathway and limit total current injection, a DBS frequency of 5Hz was chosen. This result gives support to the use of and possible benefits of a 5Hz stimulation frequency used in other studies [223].

5.2.4 Safety

We confirmed that stimulation of up to 500µA, 200 µs at 5Hz for 1 hour caused no visible signs of damage in Cresyl Violet stained brain slices from the thalamus.

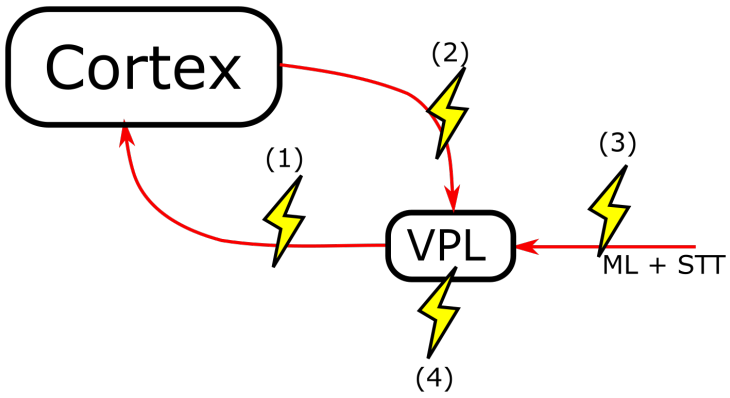

Figure 5.3: Electrode position determines which components in the somatosensory pathway are activated and the resulting evoked potential in the cortex. (1) = thalamocortical axons, (2) corticothalamic axons, (3) = medial lemniscal fibres or spinothalamic tract, (4) = thalamocortical cell bodies.

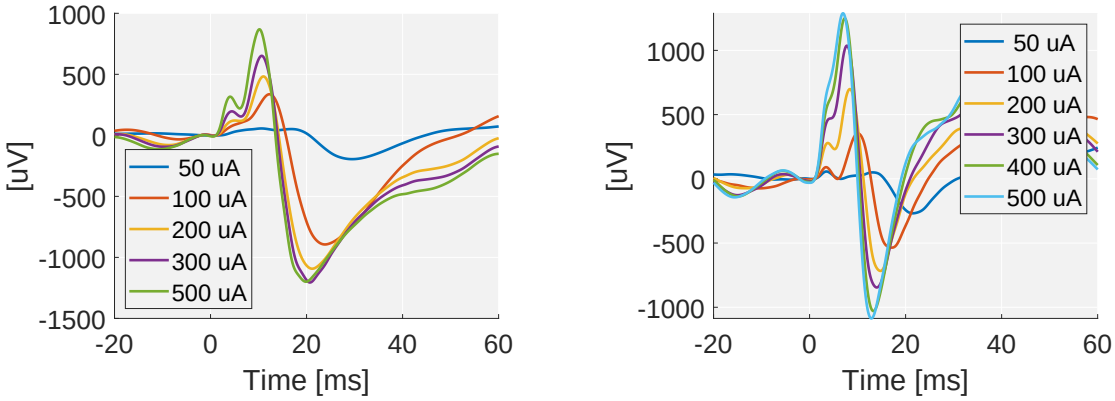

Figure 5.4: Increasing stimulation intensity increased the amplitude and decreased the latency of the evoked waveforms in the cortex (Using a pulse width of 200 µs).

A stimulation protocol of 200µA, 100 µs at 5Hz was also well tolerated in all but one naïve mouse, in which the stimulation amplitude was reduced to accommodate. Throughout all conscious stimulation and recording sessions, mice were constantly monitored for any signs of adverse reactions.

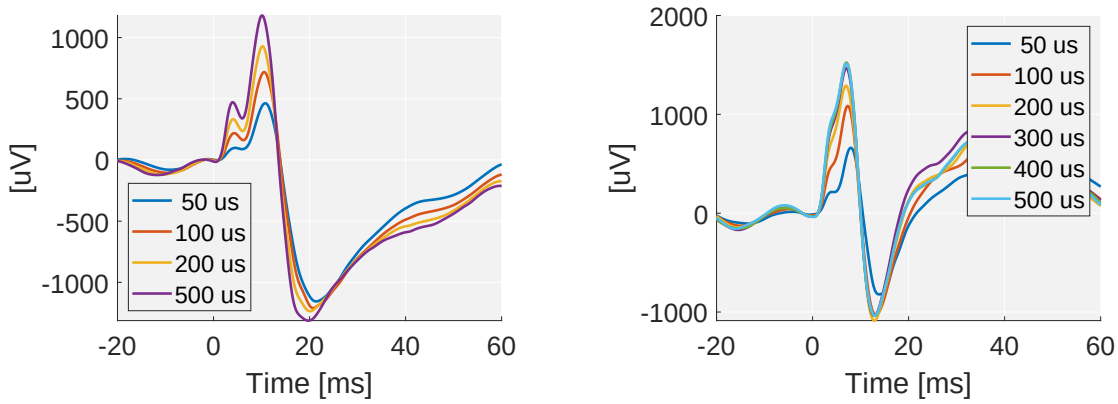

Figure 5.5: Increasing stimulation pulse width increased the amplitude and slightly decreased the latency of the evoked waveform in the cortex (Current = 500µA).

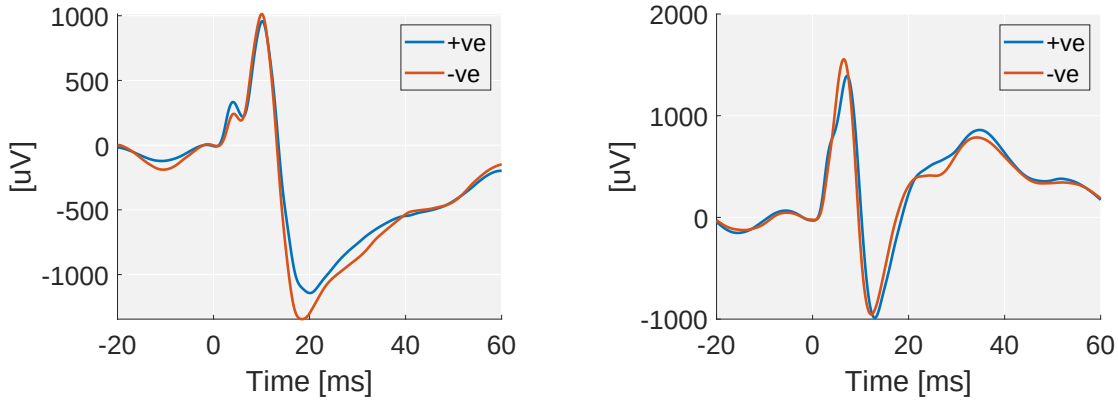

Figure 5.6: Reversing the stimulation polarity had no effect on the evoked waveform in the cortex.

5.3 DBS Pilot Study

A pilot study was undertaken to assess the benefit of chronic stimulation to the thalamocortical pathway following stroke, in hopes to preserve TC neurons and promote recovery in the cortex. Similar approaches of stimulating the thalamocortical pathway via optogenetics have been previously used to promote recovery from stroke [223, 224], however neither group studied the impact on SND. A total of seven mice were divided into two groups: Stroke + DBS (n=4) & Stroke + No DBS (n=3).

Stroke was induced on day 0 and mice were given 3 days to recover before electrodes were implanted. The following week after stroke (days 7-11), mice were treated with chronic DBS for 1 hour daily.

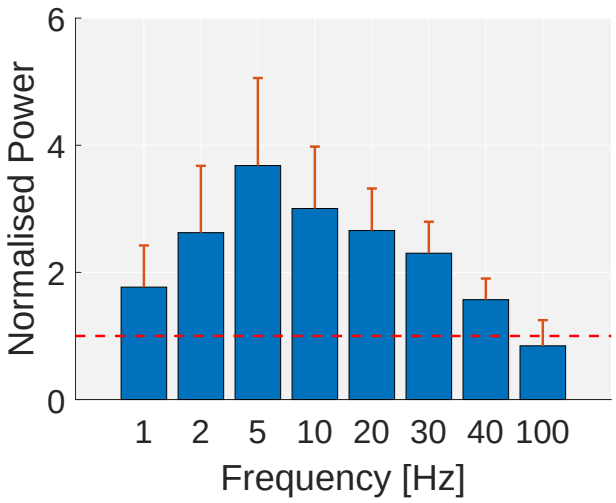

Figure 5.7: Cortical LFP power was observed to increase with thalamic DBS frequency to a maximum at 5Hz before dropping to a minimum at 100Hz suggesting possible depression.

On day 14 we performed a final recording before mice were sacrificed and there brains collected for histological analysis. Behavioural tests were conducted on days 0, 3, 7 and 14 before each major procedure, this schedule is depicted in Figure 5.8.

Both stroke and electrode procedures were performed as per previously described (Section 3.3), however the electrode implantation surgery was performed under Isoflurane (1-2%) for quicker and easier recovery from anaesthesia. We used a twisted, bipolar electrode (PlasticsOne - E363/3-2TW) in the thalamus, bilateral ECoG screw electrodes (PlasticsOne - E363/96/2.4/SPC) over each SSFL region of the cortex and a reference ECoG screw over the cerebellum. To accommodate for chronic and awake recordings, electrodes were inserted into a six-channel pedestal (PlasticsOne MS363), before being implanted into the mouse. Cyanoacrylate was used to seal burr holes around the electrodes, dental cement (Jet Tooth Shade Acrylic Powder A1 & Jet Acrylic Liquid) to secure the entire electrode apparatus in place and VetBond tissue adhesive to close any remaining open incisions.

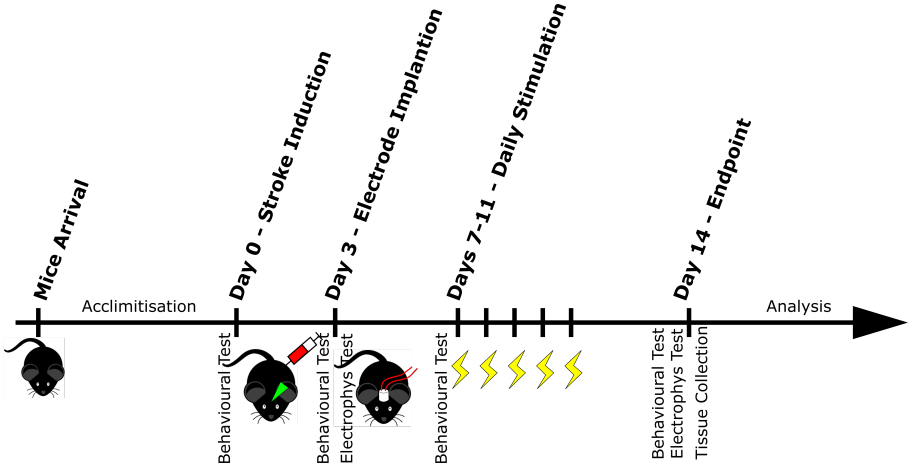

Figure 5.8: Pilot Study Outline

5.3.1 DBS Setup

A multi-channel commutator (PlasticsOne *SL6C*), held by a retort stand, allowed mice to freely move during recording and DBS. This setup is shown in Figure 5.9. Both the stimulator and recording amplifier were connected via a shielded cable to one side of the commutator and the other side connected to the implanted pedestal with a spring-covered cable. Prior to each DBS session mice were acclimatised to the recording chamber for at least 30 minutes. Mice were briefly anaesthetised with Isoflurane to allow safe connection and disconnection of the recording cable to the electrode pedestal. All recording and stimulation sessions were performed during the dark cycle, with lights dimmed and external noise minimised.

(a) Naive mouse with chronically implanted thalamic and cortical electrodes (situated inside the white pedestal headpiece).

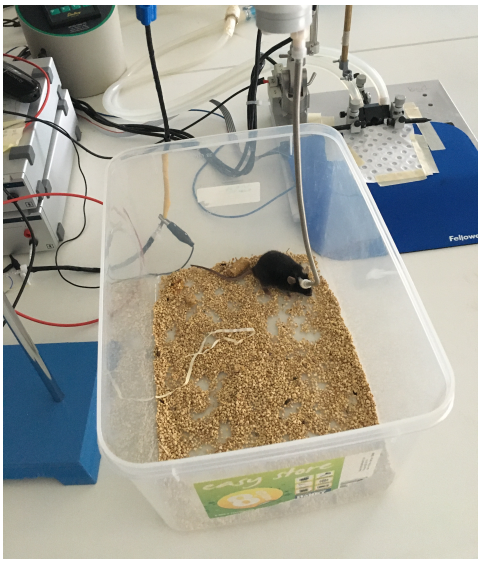

(b) Freely moving mouse with implanted electrodes connected to recording and stimulation devices via a commutator.

Figure 5.9: Example of the DBS setup for freely moving mice.

5.3.2 Results

5.3.2.1 Functional Recovery

The cylinder test was used to assess the functional recovery of mice, by evaluating the forelimb preference used for support when rearing up to a wall [422]. Briefly, mice are placed within a small cylinder in which they naturally explore by placing their fore-paws on the walls. Impairment from stroke leads to the preferential use of the non-affected limbs. An asymmetry score is determined by the difference in number of limb placements on the cylinder wall during full rears which is normalised out of the 20 first touches and described in Equation 5.1:

$$\text{Assymetry} = \frac{\#_{left-touches} - \#_{right-touches}}{20} \tag{5.1}$$

We observe a trend towards asymmetry on days 7 and 14 in both groups, but there was no significant

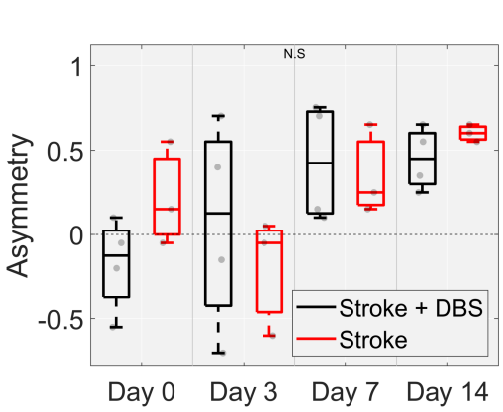

(a) Asymmetry scores at all time-points.

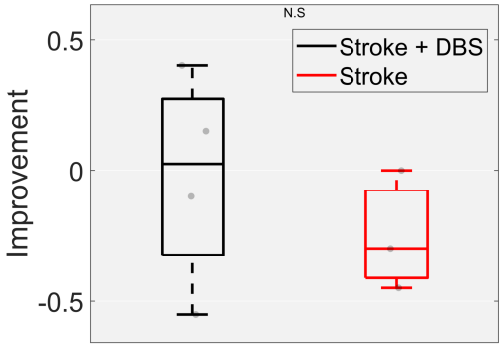

(b) Change in asymmetry from pre- to post-DBS treatment (positive = improvement)

Figure 5.10: No significant improvement on functional recovery was observed in DBS treated mice, as determined by the cylinder test.

difference between DBS and no DBS at any time point (Figure 5.10). The lack of significant difference is not unexpected due to the low sample size.

5.3.2.2 Histology

The ratio of NeuN+ cells in the ipsilateral to contralateral thalamus to stroke was assessed but no statistical significance was found, see Figure 5.11. A small loss in NeuN+ cells in stroke mice compared to naive can be seen but given a significant outlier in the DBS group and such low numbers, no conclusion can be made. Similarly to the previous chapter, Figure 3.14b, the presence of an electrode tract in the vicinity of the thalamus impeded the extraction of suitable ROIs.

5.3.2.3 Electrophysiology

We did not find that DBS had a significant effect on evoked potentials in the affected hemisphere (Figure 5.12) nor on the evoked potential in the cortex from thalamocortical stimulation(Figure 5.13.

Little change was noted in the power of spontaneous, awake activity from the thalamus and affected cortex (Figure 5.14) nor on the power of the evoked potential in the cortex to TC stimulation. Overall these results are lacking significant statistical power due to the low number of animals used and high variability in some of the recorded signals.

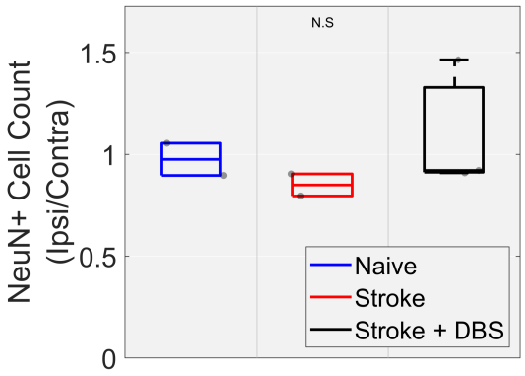

Figure 5.11: No significant rescue of NeuN+ cells in the thalamus of mice after DBS treatment was found.

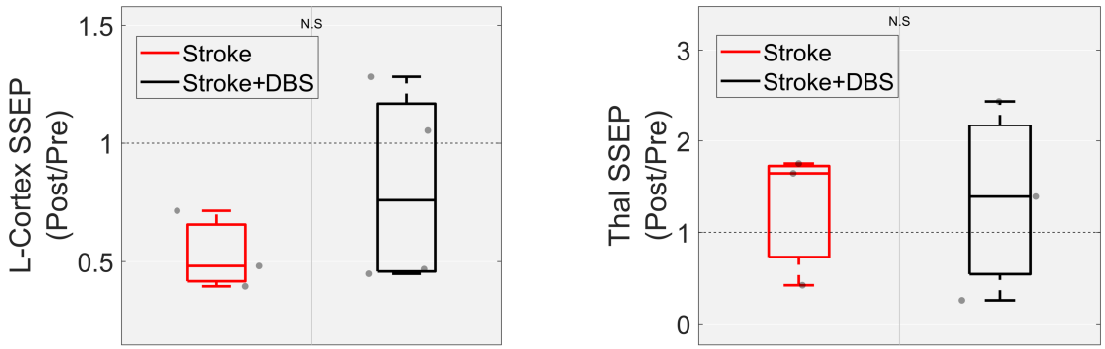

(a) Change in residual cortical SSEP power.

(b) Change in thalamic SSEP power.

Figure 5.12: No significant effect of DBS was found on the evoked potentials recorded from the cortex and thalamus in the stroke-affected hemisphere.

5.4 Effect of an Encapsulation Layer on DBS Efficacy

It is a well known phenomenon that an encapsulation layer forms around implanted electrodes due to the inflammatory response of the body, and this can affect stimulation and recording quality [423]. The encapsulation by extracellular matrix proteins and infiltration of microglia can increase the impedance of the electrode-brain interface [424], as well as corrosion of the electrodes in the electrolytic environment of the brain [424]. Computational models have shown the impact of the encapsulation on the propagation of DBS waveforms through the brain [425].

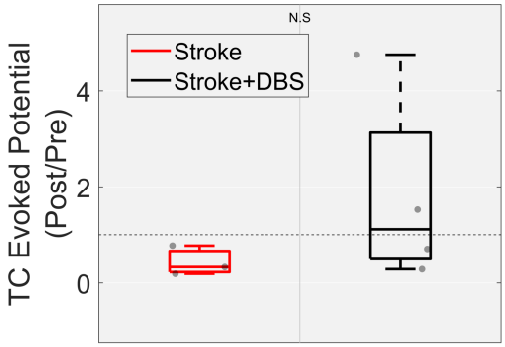

Figure 5.13: No significant effect of DBS was found on the power of the evoked potential from stimulation of the affected thalamocortical pathway.

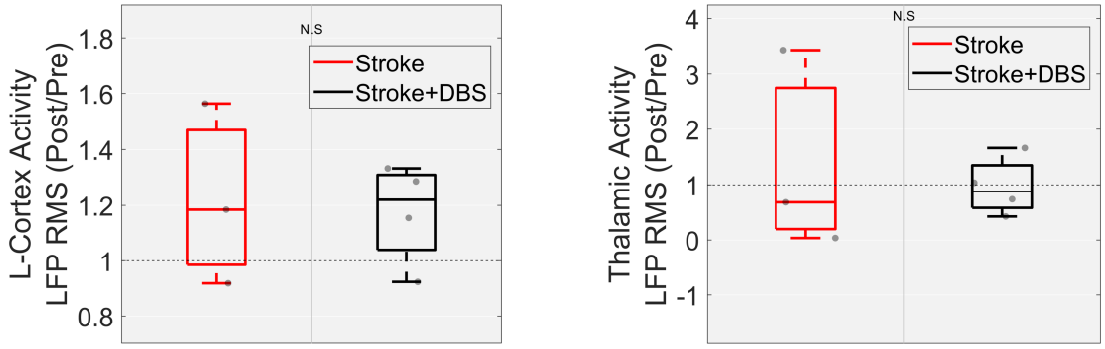

(a) Change in spontaneous cortical LFP power.

(b) Change in spontaneous thalamic LFP power.

Figure 5.14: No significant effect of DBS was found on the spontaneous LFP power recorded from the cortex and thalamus of the stroke-affected hemisphere.

We observed a slight trend of an increasing stimulus artefact amplitude between each day of treatment (Figures 5.15a & 5.16) and a very prominent increase during the one hour stimulation sessions (Figure 5.15b). Given the use of a current-controlled DBS waveform, it is likely that increased impedance in the electrode-brain interface leads to a larger extracellular voltage that we record from the ECoG electrode over the somatosensory cortex. It is important to mention that given a the 100 µs stimulation pulse and a sampling frequency of 20kHz it is likely that the stimulus artefact was under-sampled and therefore may not reflect the maximal amplitude.

A gradual increase in impedance over time is readily explained by the formation of an encapsulation

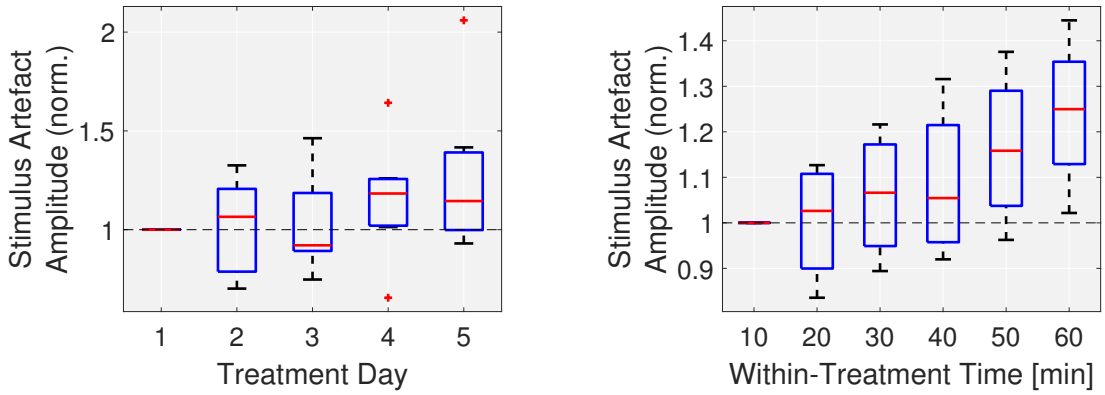

Figure 5.15: The amplitude of the stimulation artefact was found to increase (a) over days between stimulation and (b) within the stimulation session. This can be due to the formation of an encapsulation layer, inflammatory response and corrosion.

layer and corrosion of the electrode [423], but the significant increase during the one hour stimulation periods was of particular interest. It has been shown that transcranial stimulation significantly activates both microglia and astrocytes [426], which may be triggered by the increase in extracellular K^+concentrations from repeated depolarisation of neurons [427]. It is possible that during the stimulation sessions an increased inflammatory response was triggered which increased the electrode-brain interface impedance and thus the stimulation voltage.

While current-controlled stimulation is the preferred method to limit tissue damage, it is the voltage gradient across neurons that triggers the generation of action potentials [202]. Given the stimulation voltage can increase within session it is therefore crucial to monitor to prevent over-activation or spillage to neighbouring regions. It was observed in one naïve mouse and one stroke mouse that within a stimulation session and between sessions the mice began to show reactions to the stimulation current amplitude that was previously well tolerated. There was a clear correlation between the evoked response in the cortex of the naïve mouse to the stimulation artefact, see Figure 5.16.

The stroke mouse initially only tolerated a lower than average stimulation current of 50 µA, but began to show some signs of reaction by the third day of treatment. Figure 5.17 shows that an increase in stimulation artefact amplitude over time crossed a potential maximal tolerability threshold (dotted black line) at this time-point[1]. Note the maximum tolerable stimulation intensity is individual to

[1]The orange dots representing a 'possible reaction' are erring on the side of caution and determining abnormal behaviour indicative of an adverse reaction was purely subjective. With safety and ethical considerations in mind the stimulation was not continued at this intensity.

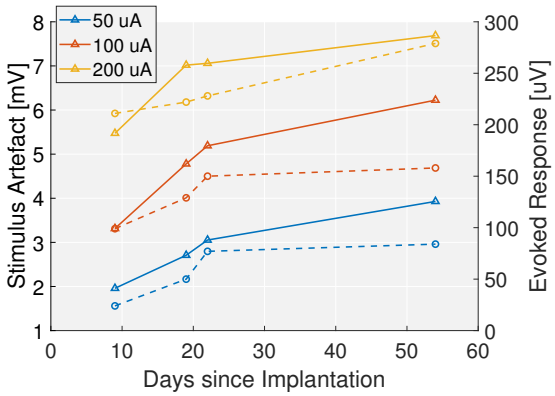

Figure 5.16: A strong correlation exists between the amplitude of the stimulus artefact and the amplitude of the evoked response at fixed stimulation currents across multiple days after electrode implantation.

each mouse and will vary based on the exact electrode location. The stimulation of the sensory thalamus is a delicate task as stimulation may elicit sensations of touch or pain which could pose discomfort to the subject.

5.5 Discussion

The investigation into the use of chronic DBS to promote recovery in a mouse model of PT stroke elucidated some possible improvements (observed in Figures 5.11,5.12,5.13), but no statistical significance was found. There were a number of limitations to this study that and are summarised below:

1. The low numbers of animals did not provide enough statistical power to detect the potential benefits of DBS.

2. Thalamic electrode placement is crucial in both stimulating and recording from the thalamocortical neurons of interest. In only three out of seven mice did we detect substantial unit activity in the SSEPs that would indicate the probe is in an optimal location.

3. The small size of a mouse brain and relatively large electrodes limited the ability to record from multiple cortical regions to investigate recovery and rewiring in peri-infarct areas. This could be remedied by using a rat model or obtaining a micro-ECoG grid. Alternatively, Tennant *et al.* [223] demonstrated the effectiveness of optical imaging, but this would require a transparent electrode and cement configuration to be explored.

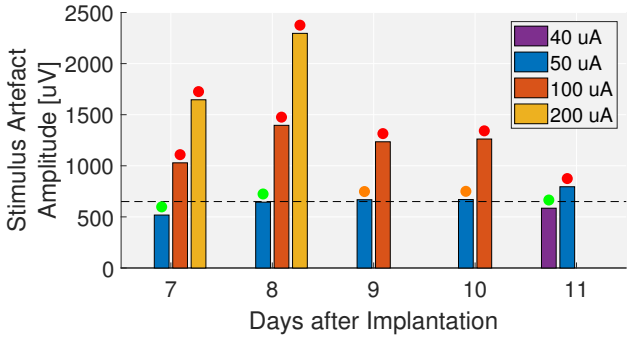

Figure 5.17: An increasing stimulation artefact amplitude over time correlates with the mouse's reaction to previously tolerated stimulation currents. Green dot = well tolerated, Orange dot = possible reaction[1], Red dot = noticeable reaction. The dotted black line represents an individualised upper limit on the maximal stimulation intensity.

4. In two mice, the stimulation amplitude had to be reduced to less than 50 µA by the end of the treatment period. This is likely to have decreased the DBS efficacy and may have limited the potential benefits.

5. The increase in stimulation voltage over time was likely linked to inflammation and the formation of an encapsulation layer. While we showed this affected the tolerance of mice to stimulation it is also possible that the increased inflammatory response could contribute to the pathology of SND.

6. Large electrode tracts were evident in brain slices containing the thalamus, signifying a portion of damage due to implantation. The benefits of stimulation versus injury due to electrode insertion remains to be investigated. Alternatively, non-invasive methods described in Section 1.7.5 could be explored but they forgo the direct recording of thalamic neurons.

7. The implantation of electrodes prior to the stroke procedure would confirm effective stimulation of the thalamocortical pathway given the electrode position. Although some form of evoked potential to thalamic stimulation was recorded from our stroke mice it is not clear which regions were being stimulated due to the lack of a healthy cortical response. If the desired pathway is unable to be stimulated then those animals should be ruled out of the DBS study.

5.6 Summary

This chapter has outlined the initial investigation into the use of deep brain stimulation to promote stroke recovery and protect against secondary neurodegeneration. Some slight improvements were observed, though not statistically significant, that warrant further investigation with a larger cohort of animals. We developed a method for chronic implantation of a thalamic electrode and bilateral cortical ECoGs in a mouse model of PT stroke. We determined safe and effective parameters for stimulation of the thalamocortical pathway and investigated a number of issues and limitations that will be a useful resource in future studies.

Chapter 6

Conclusions

This chapter summarises the contributions made in this thesis and plans for future work.

6.1 Summary of Contributions

Chapter 1

A significant literature review into the contributing factors to SND after stroke has described the likely contribution of excitotoxicity to its progression. Deep Brain Stimulation was elucidated to be of potential benefit to reduce an excitotoxic insult based on network pathology or promote the recovery of thalamocortical neurons by activity-dependent up-regulation of pro-survival pathways.

Chapter 2

Based on previous in-silico models of the thalamocortical network, a significant improvement was made to the dynamics of synaptic inputs to thalamocortical neurons. The introduction of synaptic plasticity and tuning of receptor parameters were vital in reproducing electrophysiological results from the literature. This clarified the key role of corticothalamic neurons in modulating the membrane potential and therefore firing mode of thalamocortical neurons. It was shown that pathological activity in the thalamus after stroke can occur by two distinct mechanisms. The loss of cortical excitation switches neurons to a bursting mode or the accumulation of extracellular glutamate reproduces both an increased evoked response and spontaneous activity that would reflect an excitotoxic insult.

Chapter 3

Using in-vivo electrophysiological recordings we obtained the first, to our knowledge, recordings of

sensory evoked potentials from the VPL of a mouse. We found significant loss in the late latency SSEP response and showed a loss of spontaneous thalamic activity after stroke in an anaesthetised mouse. Our results did not find support for the hypothesis of pathological network signalling after stroke nor did they find a loss of initial thalamic depolarisation to sensory input that would be expected with SND, thus raising questions over the extent of neuronal damage.

Chapter 4

Previous works have considered spike detection and sorting in recordings where unit activity is sparse and temporally isolated. When using larger electrodes, a greater number of neurons are simultaneously recorded leading to a high prevalence of overlapping spikes. With a mixture of recorded and artificially generated multi-unit activity data, we built and tested an algorithm using a sparse optimisation approach to discriminate overlapping spikes. Additionally we showed that a signed, refractory policy was able to improve the performance of existing spike detection algorithms.

Chapter 5

We developed a method for chronic electrode implantation for thalamic recording and stimulation in an awake and freely moving mouse model of PT stroke. Based on a pilot study of chronic DBS as a therapy for SND there were some minor, but not statistically significant, improvements that warrant investigation with a larger cohort of animals. We determined safe and effective set of stimulation parameters and an optimal frequency of 5Hz to maximise stimulation of the thalamocortical pathway. We observed variations in DBS efficacy over time that were managed by adjustments to stimulation parameters.

6.2 Future Works

The results of this thesis suggest several areas of further work that we explore here.

6.2.1 Experimental Work

Single-Unit Recordings: The procurement of fine-tipped electrodes would allow the isolation of activity from single neurons in the thalamus. Firstly, this would remove much of the ambiguity arising from unknown neuronal source contributions in the LFP signal. Secondly, extracting spike times and inter-spike intervals would allow a thorough exploration of bursting activity within the thalamus.

The electrodes utilised in this thesis were 125µm in diameter which is significantly above the threshold for what is typically referred to as 'macro' electrodes (25µm), severely limiting their use for the study of unit-activity. While we developed an algorithm that improved the performance of spike detection in such signals in Chapter 4, there is limitations on what level of accuracy can be obtained.

In-vitro evoked potentials: In-vitro recording from brain slices could lead to further understanding of the local field potentials in the thalamus. A multi-electrode array, with spatially distributed recording contacts, can be used for current-source density analysis to determine the location of neuronal populations responsible for each peak in the evoked potentials. The brain slice would have to be prepared to keep intact the somatosensory network connections between VPL, TRN and SSFL while also preserving the medial lemniscal fibres.

Direct Glutamate Measurements: Excess glutamate in the thalamus is believed to be the major contributor to SND through excitotoxic processes. Ross *et al.* [20] predicted increased glutamate concentration in the thalamus up to 14 days after stroke based on levels of glutamate decarboxylase (enzyme that converts Glutamate to GABA) in the terminals of TRN neurons. While this may serve as a guideline for increased glutamate, direct measurements using microdialysis or glutamate sensing probes [428] would quantify the levels of glutamate and obtain a timeline predictive of when excitotoxic damage is likely to occur. This would further elucidate the likely extent of excitotoxicity and ascertain the crucial timing of treatment regimes.

Further DBS experiments: As mentioned in Chapter 5, increasing the cohort size for the DBS study would give a better idea of the potential benefits of the DBS treatment. Along the lines of neuroprotection and recovery, it would be useful to directly measure the hypothesised DBS-induced increase in neurotrophic factors either with microdialysis or through histology [418] to confirm the mechanism and that the stimulation parameters are optimal. Additionally, we proposed the

application of DBS to the TRN as an alternative method to protect against SND by increasing GABA concentrations to mildly inhibit TC neurons.

6.2.2 Multi-compartment cellular models:

The use of multi-compartment cellular models more accurately captures the dynamics of neuronal firing. In particular the distribution of specific voltage-gated ionic channels and the location of synapses from afferent connections varies between the soma and proximal and distal dendrites. While we have compressed these down to reproduce electrophysiological behaviour in a single-compartment model there is likely dynamics that are not accurately represented.

Additionally, we only considered a minimal HH style model of a thalamocortical neuron with necessary channels to replicate bursting behaviour. TC neurons contain an abundance of other ionic channels, including: persistent Na^+channel (NaP), high-voltage activated L-Type Ca^{2+}channel (CaL), slow inactivating K^+channel (K2), rapidly inactivating K^+channel (A), calcium-activated K^+channels (C, SK) and more (see [280, 277]). In particular, the properties and conductances of Ca^{2+}-modulated K^+channels may significantly alter the response of injured TC neurons if undergoing excitotoxic-related degeneration. Finally, although it is believed that VGCC's such as the L-type Ca^{2+}channel, are only a small contributor to excitotoxic intracellular Ca^{2+}accumulation [49] it would be an important inclusion into models assessing Ca^{2+}-dependent excitotoxicity. .

6.2.3 Model of excitotoxic insults

By extending the neuronal network model to include mechanisms of excitotoxicity, the timing, extent and treatment of SND could be further explored. Works by Muddapu *et al.* [405, 406] have introduced a number of biochemical pathways for cell damage related to excitotoxicity and integrated a cell death function, associated with rises of mitochondrial and endoplasmic reticulum intracellular Ca^{2+}concentrations, to model the progressive excitotoxic death of substantia nigra neurons in Parkinson's disease. A similar approach would benefit the investigation of SND by exploring the extent of injury from intracellular Ca^{2+}dynamics versus those linked to NMDAR .

6.2.3.1 Intracellular Calcium

The intracellular calcium dynamics can be considered using a three-compartment model consisting of the cytosol (cyt), mitochondria (mt) and endoplasmic reticulum (ER). Cytosolic $Ca^{2+}$is regulated by ATP-ase pumps, Na/Ca exchanger and calcium buffers described in [429] and detailed below.

ATPase Pump:

$$I_{pmca} = K_{pc}\left[k_{1,pc}\mathcal{P}(E^*_{1,pc})y_{pc} - k_{2,pc}\mathcal{P}(E^*_{2,pc})(1-y_{pc})\right] \tag{6.1}$$

Where:

$$\begin{aligned}
\frac{\mathrm{d}y_{pc}}{\mathrm{d}t} &= \beta_{pc}(1-y_{pc}) - \alpha_{pc}y_{pc} \\
\beta_{pc} &= k_{2,pc}\mathcal{P}(E^*_{2,pc}) + k_{4,pc}\mathcal{P}(E_{2,pc}) \\
\alpha_{pc} &= k_{1,pc}\mathcal{P}(E^*_{1,pc}) + k_{3,pc}\mathcal{P}(E_{1,pc}) \\
\mathcal{P}(E^*_{1,pc}) &= \left[1 + \frac{K_{pc,i}}{[Ca]_i}\right]^{-1} \qquad \mathcal{P}(E_{1,pc}) = 1 - \mathcal{P}(E^*_{1,pc}) \\
\mathcal{P}(E^*_{2,pc}) &= \left[1 + \frac{K_{pc,e}}{[Ca]_e}\right]^{-1} \qquad \mathcal{P}(E_{2,pc}) = 1 - \mathcal{P}(E^*_{2,pc}) \\
k_{1,pc} &= \left[1 + \frac{0.1}{[ATP]}\right]^{-1} \\
K_{pc,i} &= \left[\frac{180 - 6.4}{1 + [CaCam]/(5\times10^{-5})}\right] \times 10^{-5} \\
K_{pc} &= \kappa_{pmca}\left[\frac{10.56 \times [CaCam]}{[CaCam] + 5\times10^{-5}} + 1.2\right]
\end{aligned}$$

The sodium-calcium exchanger is an antiporter that transports Ca^{2+}out of the neuron, while bringing in one Na^{+}.

$$I_{NaCax} = \kappa_{NaCax}\frac{\exp(\delta_{xm}\frac{EF}{RT})[Na]_i^3[Ca]_e - \exp((\delta_{xm}-1)\frac{EF}{RT})[Na]_e^3[Ca]_i}{(1+\mathcal{D}([Na]_i^3[Ca]_e + [Na]_e^3[Ca]_i))(1+\frac{[Ca]_i}{0.0069})} \tag{6.2}$$

From these we can calculate the total calcium flux:

$$J_{pmca} = \frac{-1}{z_{Ca}\mathcal{V}_{cyt}F}I_{pmca} \tag{6.3}$$

$$J_{NaCax} = \frac{-1}{z_{Ca}\mathcal{V}_{cyt}F}I_{NaCax} \tag{6.4}$$

$$J_{Ca} = \frac{-1}{z_{Ca}\mathcal{V}_{cyt}F}I_{Ca} \tag{6.5}$$

Where I_{Ca} is the net calcium flux through calcium permeable voltage-gated channels and glutamate receptors. The two known calcium permeable VGIC's are the T-Type channel we previously modelled and the high-voltage activated L-type Ca^{2+}channel. For synaptic channels, NMDAR and KAR are highly Ca^{2+}permeable while we suggest that the AMPARs present in the thalamus are not, or contribute insignificantly. The presence of the GluR2 subunit in AMPARs makes them impermeable

to Ca^{2+}[430], and as this is highly abundant in the VB thalamus of rats [431, 432] they can likely be left out.

Two calcium buffering proteins, Calbindin and Calmodulin exist within the cytosol. These buffers are important to model as they reduce the transient rise in intracellular calcium concentration that without the inclusion of buffers may appear to trigger excitotoxic pathways. Their concentrations and calcium-bound states are described as:

Calbindin (Calb):

$$J_{Calb} = k_{calb,b}[Ca]_i[Calb] - k_{calb,d}[CaCalb] \tag{6.6}$$

$$[Calb]_{total} = [Calb] + [CaCalb] \tag{6.7}$$

$$\frac{\mathrm{d}[Calb]}{\mathrm{d}t} = -J_{calb} \tag{6.8}$$

Calmodulin (Cam):

$$J_{cam} = \alpha_{cam}[Cam] - \beta_{cam}[CaCam] \tag{6.9}$$

$$[Cam]_{total} = [Cam] + [CaCam] \tag{6.10}$$

$$\frac{\mathrm{d}[Cam]}{\mathrm{d}t} = -J_{cam} \tag{6.11}$$

$$\alpha_{cam} = K^{cb}_{cam}K^{nb}_{cam}\left[\frac{1}{K^{cb}_{cam} + k^{nd}_{cam}} + \frac{1}{K^{nb}_{cam} + k^{cd}_{cam}}\right] \tag{6.12}$$

$$\beta_{cam} = k^{cd}_{cam}k^{nd}_{cam}\left[\frac{1}{K^{cb}_{cam} + k^{nd}_{cam}} + \frac{1}{K^{nb}_{cam} + k^{cd}_{cam}}\right] \tag{6.13}$$

$$K^{cb}_{cam} = k^{cb}_{cam}[Ca]^2_i \tag{6.14}$$

$$K^{nb}_{cam} = k^{nb}_{cam}[Ca]^2_i \tag{6.15}$$

6.2.3.2 Mitochondria & Endoplasmic Reticulum

The mitochondria and ER form internal stores of calcium within the neuron and the loss of calcium homeostasis here are known to trigger apoptotic pathways as a major contributor to excitotoxicity. The following dynamics were detailed in [433].

The calcium dynamics of the mitochondria are maintained via uptake through the mitochondrial calcium uniporter (mcu) and efflux through the mitochondrial Ca^{2+}/Na^{+}exchanger (out), described by:

$$J_{mcu_{mt}} = k_{mcu_{mt}}\frac{[Ca]^8_i}{K^8_{mcu_{mt}} + [Ca]^8_i} \tag{6.16}$$

$$J_{out_{mt}} = k_{out_{mt}}[Ca]_{mt}\frac{[Ca]^2_i}{K^2_{out_{mt}} + [Ca]^2_i} \tag{6.17}$$

And the change in mitochondrial Ca^{2+}:

$$\frac{\mathrm{d}[Ca]_{mt}}{\mathrm{d}t} = \frac{\beta_{mt}}{\rho_{mt}}(J_{mcu_{mt}} - J_{out_{mt}}) \tag{6.18}$$

Where β_{mt} is the ratio of free to total Ca^{2+}concentration and ρ_{mt} is the volume ratio between mitochondria and cytosol.

ER Ca^{2+}dynamics include an ATP-ase pump into the ER (serca), calcium-induced calcium release (cicr) and a leak channel:

$$J_{serca_{ER}} = k_{serca}[Ca]_i[ATP] \tag{6.19}$$

$$J_{cicr_{ER}} = k_{cicr}\frac{[Ca]_i^2}{K_{cicr}^2 + [Ca]_i^2}([Ca]_{ER} - [Ca]_i) \tag{6.20}$$

$$J_{leak_{ER}} = k_{leak_{ER}}([Ca]_{ER} - [Ca]_i) \tag{6.21}$$

Therefore the change in ER calcium concentration:

$$\frac{\mathrm{d}[Ca]_{ER}}{\mathrm{d}t} = \frac{\beta_{ER}}{\rho_{ER}}(J_{serca_{ER}} - J_{cicr_{ER}} - J_{leak_{ER}}) \tag{6.22}$$

By modelling the intracellular calcium dynamics and using the excitotoxic thresholds of mitochondrial and ER Ca^{2+}concentrations proposed in [406], prediction of the required levels of excitation from different sources, i.e. peri-infarct CT projections, ML inputs and extracellular glutamate, could elucidate the likely contributors to SND.

6.2.3.3 Glutamate modelling and NMDARs

The alternate hypotheses of excitotoxic insult and what we believe to be the most likely contributor to SND, is the stimulation of extrasynaptic NMDARs.The density of extrasynaptic NMDARs on thalamocortical neurons remains unknown as well as the glutamate uptake and recycling rates, making it difficult to model this issue. Estimates at the percentage of extrasynaptic NMDARs in the hippocampus of 37% may be a good place to start [434].

Glutamate uptake from extracellular space is driven by EAAT's whose concentration is primarily on astrocytes in the form of EAAT1-2, but also exist on pre-synaptic neurons as EAAT3-5 [42]. Astrocytes account for approximately 90% of glutamate uptake [88] and thus the density of EAATs and uptake mechanism, including any saturation in the process, will determine the time-course of glutamate persisting in the vicinity of TC neurons after stroke.

Other major contributions to extracellular glutamate originate from astrocytes, through both a glutamate/cystine exchanger (at very low rates of 1-10µM/s) [435, 436] and through Ca^{2+}-dependent

exocytosis which can be triggered by synaptic glutamate concentrations [437, 438]. Some models have been developed for these processes [439, 440, 441]. Given that astrocytic-released glutamate enhances activation of extrasynaptic NMDARs during ischaemia which increases the extent of brain damage [442], it seems an important aspect to include.

6.2.3.4 An NR2B-related Excitotoxic function

The computational models of excitotoxicity in the literature base excitotoxic cell death on firing rates [405, 443, 444], intracellular calcium accumulation [406], or more recently the specific sub-cellular biochemical pathways [445]. The data presented by Martel *et al.* [69] relates both intracellular Ca^{2+}concentrations and NMDAR (and NR2B-specific) currents to the amount of cell loss in-vitro. This could be used to devise a function of cell death based on NMDAR currents versus Ca^{2+}accumulation to separate the two insults.

6.2.3.5 DBS

Finally the possible benefits of DBS to prevent excitotoxicity could be explored in the model. Does high-frequency 'inhibitory' DBS of the thalamus prevent Ca^{2+}accumulation or modulate NMDAR activation? Does tonic, subthreshold stimulation of the TRN have any impact on Ca^{2+}accumulation or NMDAR currents?

References

[1] Stroke Foundation Australia, "Facts and figures about stroke," 2017. Available at https://strokefoundation.org.au [Accessed 30/04/2018].

[2] World Health Organisation, "The atlas of heart disease and stroke," 2004. Available at http://www.who.int/cardiovascular_diseases/resources/atlas/en/.

[3] World Health Organisation, "Neurological disorders," 2006.

[4] J.-H. Sun, L. Tan, and J.-T. Yu, "Post-stroke cognitive impairment: epidemiology, mechanisms and management," *Annals of translational medicine*, vol. 2, no. 8, 2014.

[5] D. A. Levine, A. T. Galecki, K. M. Langa, F. W. Unverzagt, M. U. Kabeto, B. Giordani, and V. G. Wadley, "Trajectory of cognitive decline after incident stroke," *Jama*, vol. 314, no. 1, pp. 41–51, 2015.

[6] D. A. Economics, "The economic impact of stroke in australia," *Melbourne: NSF*, 2013.

[7] M. Katan and A. Luft, "Global burden of stroke," in *Seminars in neurology*, vol. 38, pp. 208–211, Georg Thieme Verlag.

[8] S. Bennett, A. Broadbent, and J. Woodall, *Cardiovascular disease mortality: Trends at different ages*. Australian Institute of Health and Welfare, 2010.

[9] T. H. Murphy, P. Li, K. Betts, and R. Liu, "Two-photon imaging of stroke onset in vivo reveals that nmda-receptor independent ischemic depolarization is the major cause of rapid reversible damage to dendrites and spines," *Journal of Neuroscience*, vol. 28, no. 7, pp. 1756–1772, 2008.

[10] J. L. Saver, "Time is brain - quantified," *Stroke*, vol. 37, no. 1, pp. 263–266, 2006.

[11] Blausen Medical Communications, Inc., "Stroke," 2013. Available at https://commons.wikimedia.org/wiki/File:Blausen_0836_Stroke.png [Accessed 30/05/2018].

[12] G. Marchal, V. Beaudouin, P. Rioux, V. de la Sayette, F. Le Doze, F. Viader, J. M. Derlon, and J. C. Baron, "Prolonged persistence of substantial volumes of potentially viable brain tissue after stroke: a correlative pet-ct study with voxel-based data analysis," *Stroke*, vol. 27, no. 4, pp. 599–606, 1996.

[13] K. Saita, M. Chen, N. J. Spratt, M. J. Porritt, G. T. Liberatore, S. J. Read, C. R. Levi, G. A. Donnan, U. Ackermann, H. J. Tochon-Danguy, *et al.*, "Imaging the ischemic penumbra with 18f-fluoromisonidazole in a rat model of ischemic stroke," *Stroke*, vol. 35, no. 4, pp. 975–980, 2004.

[14] J. Zhang, Y. Zhang, S. Xing, Z. Liang, and J. Zeng, "Secondary neurodegeneration in remote regions after focal cerebral infarction," *Stroke*, vol. 43, no. 6, pp. 1700–1705, 2012.

[15] R. R. Lima, L. N. Santana, R. M. Fernandes, E. M. Nascimento, A. C. A. Oliveira, L. M. Fernandes, E. M. N. d. Santos, P. A. N. Tavares, I. R. d. Santos, A. Gimarães-Santos, *et al.*, "Neurodegeneration and glial response after acute striatal stroke: Histological basis for neuroprotective studies," *Oxidative Medicine and Cellular Longevity*, vol. 2016, 2016.

[16] L. K. Ong, F. R. Walker, and M. Nilsson, "Is stroke a neurodegenerative condition? a critical review of secondary neurodegeneration and amyloid-beta accumulation after stroke," *AIMS MEDICAL SCIENCE*, vol. 4, no. 1, pp. 1–16, 2017.

[17] M. G. Kluge, M. Abdolhoseini, K. Zalewska, L. K. Ong, S. J. Johnson, M. Nilsson, and F. R. Walker, "Spatiotemporal analysis of impaired microglia process movement at sites of secondary neurodegeneration post-stroke," *Journal of Cerebral Blood Flow & Metabolism*, vol. 39, no. 12, pp. 2456–2470, 2019.

[18] S. Sanchez-Bezanilla, R. J. Hood, L. E. Collins-Praino, R. J. Turner, F. R. Walker, M. Nilsson, and L. K. Ong, "More than motor impairment: A spatiotemporal analysis of cognitive impairment and associated neuropathological changes following cortical photothrombotic stroke," p. 0271678X211005877.

[19] J. Hosp, K. Greiner, L. M. Arellano, F. Roth, F. Löffler, J. Reis, and B. Fritsch, "Progressive secondary exo-focal dopaminergic neurodegeneration occurs in not directly connected midbrain nuclei after pure motor-cortical stroke," *Experimental neurology*, vol. 327, p. 113211, 2020.

[20] D. Ross and F. Ebner, "Thalamic retrograde degeneration following cortical injury: an excitotoxic process?," *Neuroscience*, vol. 35, no. 3, pp. 525–550, 1990.

[21] J. C. Zbesko, T.-V. V. Nguyen, T. Yang, J. B. Frye, O. Hussain, M. Hayes, A. Chung, W. A. Day, K. Stepanovic, M. Krumberger, *et al.*, "Glial scars are permeable to the neurotoxic environment of chronic stroke infarcts," *Neurobiology of disease*, 2018.

[22] T. W. Lai, S. Zhang, and Y. T. Wang, "Excitotoxicity and stroke: identifying novel targets for neuroprotection," *Progress in neurobiology*, vol. 115, pp. 157–188, 2014.

[23] G. Pietrogrande, K. Zalewska, Z. Zhao, M. Abdolhoseini, W. Z. Chow, S. Sanchez-Bezanilla, L. K. Ong, S. J. Johnson, M. Nilsson, and F. R. Walker, "Low oxygen post conditioning prevents thalamic secondary neuronal loss caused by excitotoxicity after cortical stroke," *Scientific reports*, vol. 9, no. 1, pp. 1–9, 2019.

[24] E. Jones and T. P. S. Powell, "An electron microscopic study of the mode of termination of cortico-thalamic fibres within the sensory relay nuclei of the thalamus," *Proceedings of the Royal Society of London. Series B. Biological Sciences*, vol. 172, no. 1027, pp. 173–185, 1969.

[25] E. Jones and T. Powell, "The projection of the somatic sensory cortex upon the thalamus in the cat," *Brain research*, vol. 10, no. 3, pp. 369–391, 1968.

[26] A. Brodtmann, M. S. Khlif, N. Egorova, M. Veldsman, L. J. Bird, and E. Werden, "Dynamic regional brain atrophy rates in the first year after ischemic stroke," *Stroke*, vol. 51, no. 9, pp. e183–e192, 2020.

[27] A. Tamura, Y. Tahira, H. Nagashima, T. Kirino, O. Gotoh, S. Hojo, and K. Sano, "Thalamic atrophy following cerebral infarction in the territory of the middle cerebral artery.," *Stroke*, vol. 22, no. 5, pp. 615–618, 1991.

[28] D. Purves, G. Augustine, W. Hall, A. LaMantia, and L. White, *Neuroscience*. Sinauer, 2012.

[29] S. M. Sherman and R. Guillery, "The role of the thalamus in the flow of information to the cortex," *Philosophical Transactions of the Royal Society of London. Series B: Biological Sciences*, vol. 357, no. 1428, pp. 1695–1708, 2002.

[30] K. Zalewska, G. Pietrogrande, L. K. Ong, M. Abdolhoseini, M. Kluge, S. J. Johnson, F. R. Walker, and M. Nilsson, "Sustained administration of corticosterone at stress-like levels after stroke suppressed glial reactivity at sites of thalamic secondary neurodegeneration," *Brain, behavior, and immunity*, vol. 69, pp. 210–222, 2018.

[31] Genetic Science Learning Center, "Animal models for addiction research," 2013. Available at http://learn.genetics.utah.edu/content/addiction/mice/ [Accessed 30/04/2018].

[32] J. T. Francis, S. Xu, and J. K. Chapin, "Proprioceptive and cutaneous representations in the rat ventral posterolateral thalamus," *Journal of neurophysiology*, vol. 99, no. 5, pp. 2291–2304, 2008.

[33] S. M. Sherman and R. Guillery, "Functional organization of thalamocortical relays," *Journal of neurophysiology*, vol. 76, no. 3, pp. 1367–1395, 1996.

[34] T. E. Nogles and M. A. Galuska, "Middle cerebral artery stroke," *StatPearls [Internet]*, 2020.

[35] H. Jahnsen and R. Llinás, "Electrophysiological properties of guinea-pig thalamic neurones: an in vitro study.," *The Journal of physiology*, vol. 349, no. 1, pp. 205–226, 1984.

[36] J. Aguilar, M. Morales-Botello, and G. Foffani, "Tactile responses of hindpaw, forepaw and whisker neurons in the thalamic ventrobasal complex of anesthetized rats," *European Journal of Neuroscience*, vol. 27, no. 2, pp. 378–387, 2008.

[37] C. M. Constantinople and R. M. Bruno, "Deep cortical layers are activated directly by thalamus," *Science*, vol. 340, no. 6140, pp. 1591–1594, 2013.

[38] C. O'Reilly, E. Iavarone, J. Yi, and S. L. Hill, "Rodent somatosensory thalamocortical circuitry: neurons, synapses, and connectivity," *Neuroscience & Biobehavioral Reviews*, 2021.

[39] K. Barrett, S. Boitano, S. Barman, and H. Brooks, "Somatosensory neurotransmission: touch, pain, and temperature," *Ganongs Review of Medical Physiology. 24th ed. New York: McGraw-Hill*, 2012.

[40] B. Szymik, "Neuron anatomy," 2011. Available at https://askabiologist.asu.edu/neuron-anatomy [Accessed 30/4/2018].

[41] J. Lewerenz and P. Maher, "Chronic glutamate toxicity in neurodegenerative diseases, what is the evidence," *Frontiers in neuroscience*, vol. 9, p. 469, 2015.

[42] N. C. Danbolt, "Glutamate uptake," *Progress in neurobiology*, vol. 65, no. 1, pp. 1–105, 2001.

[43] D. Lucas and J. Newhouse, "The toxic effect of sodium l-glutamate on the inner layers of the retina," *AMA archives of ophthalmology*, vol. 58, no. 2, pp. 193–201, 1957.

[44] D. W. Choi, "Ionic dependence of glutamate neurotoxicity," *Journal of Neuroscience*, vol. 7, no. 2, pp. 369–379, 1987.

[45] J. W. Olney, M. T. Price, L. Samson, and J. Labruyere, "The role of specific ions in glutamate neurotoxicity," *Neuroscience letters*, vol. 65, no. 1, pp. 65–71, 1986.

[46] M. Mattson, P. Guthrie, and S. B. Kater, "A role for na+-dependent ca2+ extrusion in protection against neuronal excitotoxicity.," *The FASEB journal*, vol. 3, no. 13, pp. 2519–2526, 1989.

[47] D. W. Choi, "Glutamate neurotoxicity and diseases of the nervous system," *Neuron*, vol. 1, no. 8, pp. 623–634, 1988.

[48] M. P. Mattson, B. Cheng, D. Davis, K. Bryant, I. Lieberburg, and R. E. Rydel, "beta-amyloid peptides destabilize calcium homeostasis and render human cortical neurons vulnerable to excitotoxicity," *Journal of Neuroscience*, vol. 12, no. 2, pp. 376–389, 1992.

[49] R. I. Stanika, I. Villanueva, G. Kazanina, S. B. Andrews, and N. B. Pivovarova, "Comparative impact of voltage-gated calcium channels and nmda receptors on mitochondria-mediated neuronal injury," *Journal of Neuroscience*, vol. 32, no. 19, pp. 6642–6650, 2012.

[50] X.-M. Zhang and J. Zhu, "Kainic acid-induced neurotoxicity: targeting glial responses and glia-derived cytokines," *Current Neuropharmacology*, vol. 9, no. 2, pp. 388–398, 2011.

[51] D. Schubert and D. Piasecki, "Oxidative glutamate toxicity can be a component of the excitotoxicity cascade," *Journal of Neuroscience*, vol. 21, no. 19, pp. 7455–7462, 2001.

[52] R. Sattler, M. P. Charlton, M. Hafner, and M. Tymianski, "Distinct influx pathways, not calcium load, determine neuronal vulnerability to calcium neurotoxicity," *Journal of neurochemistry*, vol. 71, no. 6, pp. 2349–2364, 1998.

[53] M. Arundine and M. Tymianski, "Molecular mechanisms of calcium-dependent neurodegeneration in excitotoxicity," *Cell calcium*, vol. 34, no. 4-5, pp. 325–337, 2003.

[54] V. Calabrese, C. Mancuso, M. Calvani, E. Rizzarelli, D. A. Butterfield, and A. M. G. Stella, "Nitric oxide in the central nervous system: neuroprotection versus neurotoxicity," *Nature Reviews Neuroscience*, vol. 8, no. 10, pp. 766–775, 2007.

[55] H. Prast and A. Philippu, "Nitric oxide as modulator of neuronal function," *Progress in neurobiology*, vol. 64, no. 1, pp. 51–68, 2001.

[56] R. Sattler, Z. Xiong, W.-Y. Lu, M. Hafner, J. F. MacDonald, and M. Tymianski, "Specific coupling of nmda receptor activation to nitric oxide neurotoxicity by psd-95 protein," *Science*, vol. 284, no. 5421, pp. 1845–1848, 1999.

[57] G. E. Hardingham and H. Bading, "Synaptic versus extrasynaptic nmda receptor signalling: implications for neurodegenerative disorders," *Nature Reviews Neuroscience*, vol. 11, no. 10, pp. 682–696, 2010.

[58] T. W. Lai, W.-C. Shyu, and Y. T. Wang, "Stroke intervention pathways: Nmda receptors and beyond," *Trends in molecular medicine*, vol. 17, no. 5, pp. 266–275, 2011.

[59] Q. J. Wu and M. Tymianski, "Targeting nmda receptors in stroke: new hope in neuroprotection," *Molecular brain*, vol. 11, no. 1, pp. 1–14, 2018.

[60] G. E. Hardingham, Y. Fukunaga, and H. Bading, "Extrasynaptic nmdars oppose synaptic nmdars by triggering creb shut-off and cell death pathways," *Nature neuroscience*, vol. 5, no. 5, pp. 405–414, 2002.

[61] C. M. Gladding and L. A. Raymond, "Mechanisms underlying nmda receptor synaptic/extrasynaptic distribution and function," *Molecular and Cellular Neuroscience*, vol. 48, no. 4, pp. 308–320, 2011.

[62] P. Paoletti, C. Bellone, and Q. Zhou, "Nmda receptor subunit diversity: impact on receptor properties, synaptic plasticity and disease," *Nature Reviews Neuroscience*, vol. 14, no. 6, pp. 383–400, 2013.

[63] S. F. Traynelis, L. P. Wollmuth, C. J. McBain, F. S. Menniti, K. M. Vance, K. K. Ogden, K. B. Hansen, H. Yuan, S. J. Myers, and R. Dingledine, "Glutamate receptor ion channels: structure, regulation, and function," *Pharmacological reviews*, vol. 62, no. 3, pp. 405–496, 2010.

[64] X.-B. Liu, K. D. Murray, and E. G. Jones, "Switching of nmda receptor 2a and 2b subunits at thalamic and cortical synapses during early postnatal development," *Journal of Neuroscience*, vol. 24, no. 40, pp. 8885–8895, 2004.

[65] Y. Liu, T. P. Wong, M. Aarts, A. Rooyakkers, L. Liu, T. W. Lai, D. C. Wu, J. Lu, M. Tymianski, A. M. Craig, *et al.*, "Nmda receptor subunits have differential roles in mediating excitotoxic neuronal death both in vitro and in vivo," *Journal of Neuroscience*, vol. 27, no. 11, pp. 2846–2857, 2007.

[66] M.-A. Martel, T. J. Ryan, K. F. Bell, J. H. Fowler, A. McMahon, B. Al-Mubarak, N. H. Komiyama, K. Horsburgh, P. C. Kind, S. G. Grant, *et al.*, "The subtype of glun2 c-terminal domain determines the response to excitotoxic insults," *Neuron*, vol. 74, no. 3, pp. 543–556, 2012.

[67] T. Papouin and S. H. Oliet, "Organization, control and function of extrasynaptic nmda receptors," *Philosophical Transactions of the Royal Society B: Biological Sciences*, vol. 369, no. 1654, p. 20130601, 2014.

[68] J. von Engelhardt, I. Coserea, V. Pawlak, E. C. Fuchs, G. Köhr, P. H. Seeburg, and H. Monyer, "Excitotoxicity in vitro by nr2a-and nr2b-containing nmda receptors," *Neuropharmacology*, vol. 53, no. 1, pp. 10–17, 2007.

[69] M.-A. Martel, D. J. Wyllie, and G. E. Hardingham, "In developing hippocampal neurons, nr2b-containing n-methyl-d-aspartate receptors (nmdars) can mediate signaling to neuronal survival and synaptic potentiation, as well as neuronal death," *Neuroscience*, vol. 158, no. 1, pp. 334–343, 2009.

[70] B. A. Yankner, L. R. Dawes, S. Fisher, L. Villa-Komaroff, M. L. Oster-Granite, and R. L. Neve, "Neurotoxicity of a fragment of the amyloid precursor associated with alzheimer's disease," *Science*, vol. 245, no. 4916, pp. 417–420, 1989.

[71] H. A. Pearson and C. Peers, "Physiological roles for amyloid β peptides," *The Journal of physiology*, vol. 575, no. 1, pp. 5–10, 2006.

[72] F. Kamenetz, T. Tomita, H. Hsieh, G. Seabrook, D. Borchelt, T. Iwatsubo, S. Sisodia, and R. Malinow, "App processing and synaptic function," *Neuron*, vol. 37, no. 6, pp. 925–937, 2003.

[73] C. Haass and D. J. Selkoe, "Soluble protein oligomers in neurodegeneration: lessons from the alzheimer's amyloid β-peptide," *Nature reviews Molecular cell biology*, vol. 8, no. 2, pp. 101–112, 2007.

[74] J. Hardy and D. J. Selkoe, "The amyloid hypothesis of alzheimer's disease: progress and problems on the road to therapeutics," *science*, vol. 297, no. 5580, pp. 353–356, 2002.

[75] A. J. Turner, L. Fisk, and N. N. Nalivaeva, "Targeting amyloid-degrading enzymes as therapeutic strategies in neurodegeneration," *Annals of the New York Academy of Sciences*, vol. 1035, no. 1, pp. 1–20, 2004.

[76] J. R. Cirrito, K. A. Yamada, M. B. Finn, R. S. Sloviter, K. R. Bales, P. C. May, D. D. Schoepp, S. M. Paul, S. Mennerick, and D. M. Holtzman, "Synaptic activity regulates interstitial fluid amyloid-β levels in vivo," *Neuron*, vol. 48, no. 6, pp. 913–922, 2005.

[77] W. J. Jagust and E. C. Mormino, "Lifespan brain activity, β-amyloid, and alzheimer's disease," *Trends in cognitive sciences*, vol. 15, no. 11, pp. 520–526, 2011.

[78] S. Lesné, C. Ali, C. Gabriel, N. Croci, E. T. MacKenzie, C. G. Glabe, M. Plotkine, C. Marchand-Verrecchia, D. Vivien, and A. Buisson, "Nmda receptor activation inhibits α-secretase and promotes neuronal amyloid-β production," *Journal of Neuroscience*, vol. 25, no. 41, pp. 9367–9377, 2005.

[79] R. L. Buckner, A. Z. Snyder, B. J. Shannon, G. LaRossa, R. Sachs, A. F. Fotenos, Y. I. Sheline, W. E. Klunk, C. A. Mathis, J. C. Morris, *et al.*, "Molecular, structural, and functional characterization of alzheimer's disease: evidence for a relationship between default activity, amyloid, and memory," *Journal of Neuroscience*, vol. 25, no. 34, pp. 7709–7717, 2005.

[80] I. R. Mackenzie and L. A. Miller, "Senile plaques in temporal lobe epilepsy," *Acta neuropathologica*, vol. 87, no. 5, pp. 504–510, 1994.

[81] D. M. Walsh, I. Klyubin, J. V. Fadeeva, W. K. Cullen, R. Anwyl, M. S. Wolfe, M. J. Rowan, and D. J. Selkoe, "Naturally secreted oligomers of amyloid β protein potently inhibit hippocampal long-term potentiation in vivo," *Nature*, vol. 416, no. 6880, p. 535, 2002.

[82] C. Priller, T. Bauer, G. Mitteregger, B. Krebs, H. A. Kretzschmar, and J. Herms, "Synapse formation and function is modulated by the amyloid precursor protein," *Journal of Neuroscience*, vol. 26, no. 27, pp. 7212–7221, 2006.

[83] S.-Q. Ren, W. Yao, J.-Z. Yan, C. Jin, J.-J. Yin, J. Yuan, S. Yu, and Z. Cheng, "Amyloid β causes excitation/inhibition imbalance through dopamine receptor 1-dependent disruption of fast-spiking gabaergic input in anterior cingulate cortex," *Scientific reports*, vol. 8, no. 1, p. 302, 2018.

[84] M. Ramsden, Z. Henderson, and H. A. Pearson, "Modulation of ca2+ channel currents in primary cultures of rat cortical neurones by amyloid β protein (1–40) is dependent on solubility status," *Brain research*, vol. 956, no. 2, pp. 254–261, 2002.

[85] T. Nuriel, S. L. Angulo, U. Khan, A. Ashok, Q. Chen, H. Y. Figueroa, S. Emrani, L. Liu, M. Herman, G. Barrett, *et al.*, "Neuronal hyperactivity due to loss of inhibitory tone in apoe4 mice lacking alzheimers disease like pathology," *Nature communications*, vol. 8, no. 1, p. 1464, 2017.

[86] P. Lipton, "Ischemic cell death in brain neurons," *Physiological reviews*, vol. 79, no. 4, pp. 1431–1568, 1999.

[87] K. P. Doyle, R. P. Simon, and M. P. Stenzel-Poore, "Mechanisms of ischemic brain damage," *Neuropharmacology*, vol. 55, no. 3, pp. 310–318, 2008.

[88] D. Belov Kirdajova, J. Kriska, J. Tureckova, and M. Anderova, "Ischemia-triggered glutamate excitotoxicity from the perspective of glial cells," *Frontiers in cellular neuroscience*, vol. 14, p. 51, 2020.

[89] B. Puig, S. Brenna, and T. Magnus, "Molecular communication of a dying neuron in stroke," *International journal of molecular sciences*, vol. 19, no. 9, p. 2834, 2018.

[90] A. N. Nelson, M. S. Calhoun, A. M. Thomas, J. L. Tavares, D. M. Ferretti, G. M. Dillon, and Y. Mandelblat-Cerf, "Temporal progression of excitotoxic calcium following distal middle cerebral artery occlusion in freely moving mice," *Frontiers in Cellular Neuroscience*, vol. 14, 2020.

[91] J. P. Dreier, "The role of spreading depression, spreading depolarization and spreading ischemia in neurological disease," *Nature medicine*, vol. 17, no. 4, pp. 439–447, 2011.

[92] R. C. Collins and J. W. Olney, "Focal cortical seizures cause distant thalamic lesions," *Science*, vol. 218, no. 4568, pp. 177–179, 1982.

[93] W. F. Maragos, J. T. Greenamyre, J. B. Penney Jr, and A. B. Young, "Glutamate dysfunction in alzheimer's disease: an hypothesis," *Trends in Neurosciences*, vol. 10, no. 2, pp. 65–68, 1987.

[94] J. T. Greenamyre and A. B. Young, "Excitatory amino acids and alzheimer's disease," *Neurobiology of aging*, vol. 10, no. 5, pp. 593–602, 1989.

[95] M. Rodriguez, J. Obeso, and C. W. Olanow, "Subthalamic nucleus-mediated excitotoxicity in parkinson's disease: a target for neuroprotection," *Annals of neurology*, vol. 44, no. S1, 1998.

[96] L. Iovino, M. Tremblay, and L. Civiero, "Glutamate-induced excitotoxicity in parkinson's disease: The role of glial cells," *Journal of pharmacological sciences*, 2020.

[97] G. Meredith, S. Totterdell, M. Beales, and C. Meshul, "Impaired glutamate homeostasis and programmed cell death in a chronic mptp mouse model of parkinson's disease," *Experimental neurology*, vol. 219, no. 1, pp. 334–340, 2009.

[98] S. Vucic and M. C. Kiernan, "Transcranial magnetic stimulation for the assessment of neurodegenerative disease," *Neurotherapeutics*, vol. 14, no. 1, pp. 91–106, 2017.

[99] C. Grefkes and G. R. Fink, "Reorganization of cerebral networks after stroke: new insights from neuroimaging with connectivity approaches," *Brain*, vol. 134, no. 5, pp. 1264–1276, 2011.

[100] C. J. Honey and O. Sporns, "Dynamical consequences of lesions in cortical networks," *Human brain mapping*, vol. 29, no. 7, pp. 802–809, 2008.

[101] J. Alstott, M. Breakspear, P. Hagmann, L. Cammoun, and O. Sporns, "Modeling the impact of lesions in the human brain," *PLoS computational biology*, vol. 5, no. 6, p. e1000408, 2009.

[102] C. von Monakow, *Die Lokalisation im Grosshirn und der Abbau der Funktion durch kortikale Herde*. JF Bergmann, 1914.

[103] E. Carrera and G. Tononi, "Diaschisis: past, present, future," *Brain*, p. awu101, 2014.

[104] A. Baldassarre, L. E. Ramsey, J. S. Siegel, G. L. Shulman, and M. Corbetta, "Brain connectivity and neurological disorders after stroke," *Current Opinion in Neurology*, vol. 29, no. 6, pp. 706–713, 2016.

[105] M. H. Mohajerani, K. Aminoltejari, and T. H. Murphy, "Targeted mini-strokes produce changes in interhemispheric sensory signal processing that are indicative of disinhibition within minutes," *Proceedings of the National Academy of Sciences*, vol. 108, no. 22, pp. E183–E191, 2011.

[106] J. T. Paz, T. J. Davidson, E. S. Frechette, B. Delord, I. Parada, K. Peng, K. Deisseroth, and J. R. Huguenard, "Closed-loop optogenetic control of thalamus as a tool for interrupting seizures after cortical injury," *Nature neuroscience*, vol. 16, no. 1, pp. 64–70, 2013.

[107] K. M. Kelly, A. Kharlamov, T. M. Hentosz, E. A. Kharlamova, J. M. Williamson, E. H. Bertram III, J. Kapur, and D. M. Armstrong, "Photothrombotic brain infarction results in seizure activity in aging fischer 344 and sprague dawley rats," *Epilepsy research*, vol. 47, no. 3, pp. 189–203, 2001.

[108] E. Kharlamov, P. Jukkola, K. Schmitt, and K. Kelly, "Electrobehavioral characteristics of epileptic rats following photothrombotic brain infarction," *Epilepsy research*, vol. 56, no. 2-3, pp. 185–203, 2003.

[109] D. K. Nguyen and M. Botez, "Diaschisis and neurobehavior," *Canadian journal of neurological sciences*, vol. 25, no. 1, pp. 5–12, 1998.

[110] R. Domann, G. Hagemann, M. Kraemer, H.-J. Freund, and O. Witte, "Electrophysiological changes in the surrounding brain tissue of photochemically induced cortical infarcts in the rat," *Neuroscience letters*, vol. 155, no. 1, pp. 69–72, 1993.

[111] K. Schiene, C. Bruehl, K. Zilles, M. Qu, G. Hagemann, M. Kraemer, and O. W. Witte, "Neuronal hyperexcitability and reduction of gabaa-receptor expression in the surround of cerebral photothrombosis," *Journal of Cerebral Blood Flow & Metabolism*, vol. 16, no. 5, pp. 906–914, 1996.

[112] I. Buchkremer-Ratzmann and O. W. Witte, "Extended brain disinhibition following small photothrombotic lesions in rat frontal cortex," *Neuroreport*, vol. 8, no. 2, pp. 519–522, 1997.

[113] J. T. Paz, C. A. Christian, I. Parada, D. A. Prince, and J. R. Huguenard, "Focal cortical infarcts alter intrinsic excitability and synaptic excitation in the reticular thalamic nucleus," *Journal of Neuroscience*, vol. 30, no. 15, pp. 5465–5479, 2010.

[114] J. B. Van Wijngaarden, R. Zucca, S. Finnigan, and P. F. Verschure, "The impact of cortical lesions on thalamo-cortical network dynamics after acute ischaemic stroke: a combined experimental and theoretical study," *PLoS computational biology*, vol. 12, no. 8, p. e1005048, 2016.

[115] D. Hirai, K. C. Nakamura, K.-i. Shibata, T. Tanaka, H. Hioki, T. Kaneko, and T. Furuta, "Shaping somatosensory responses in awake rats: cortical modulation of thalamic neurons," *Brain Structure and Function*, vol. 223, no. 2, pp. 851–872, 2018.

[116] C. Grefkes and G. R. Fink, "Connectivity-based approaches in stroke and recovery of function," *The Lancet Neurology*, vol. 13, no. 2, pp. 206–216, 2014.

[117] M. Que, K. Schiene, O. W. Witte, and K. Zilles, "Widespread up-regulation of n-methyl-d-aspartate receptors after focal photothrombotic lesion in rat brain," *Neuroscience letters*, vol. 273, no. 2, pp. 77–80, 1999.

[118] M. Qü, I. Buchkremer-Ratzmann, K. Schiene, M. Schroeter, O. W. Witte, and K. Zilles, "Bihemispheric reduction of gabaa receptor binding following focal cortical photothrombotic lesions in the rat brain," *Brain research*, vol. 813, no. 2, pp. 374–380, 1998.

[119] H. Wake, A. J. Moorhouse, and J. Nabekura, "Functions of microglia in the central nervous system-beyond the immune response," *Neuron glia biology*, vol. 7, no. 1, p. 47, 2011.

[120] M. Merlini, V. A. Rafalski, K. Ma, K.-Y. Kim, E. A. Bushong, P. E. R. Coronado, Z. Yan, A. S. Mendiola, E. G. Sozmen, J. K. Ryu, *et al.*, "Microglial g i-dependent dynamics regulate brain network hyperexcitability," *Nature Neuroscience*, vol. 24, no. 1, pp. 19–23, 2021.

[121] M. G. Kluge, L. Kracht, M. Abdolhoseini, L. K. Ong, S. J. Johnson, M. Nilsson, and F. R. Walker, "Impaired microglia process dynamics post-stroke are specific to sites of secondary neurodegeneration," *Glia*, vol. 65, no. 12, pp. 1885–1899, 2017.

[122] K. A. Jones, I. Zouikr, M. Patience, A. N. Clarkson, J. Isgaard, S. J. Johnson, N. Spratt, M. Nilsson, and F. R. Walker, "Chronic stress exacerbates neuronal loss associated with secondary neurodegeneration and suppresses microglial-like cells following focal motor cortex ischemia in the mouse," *Brain, behavior, and immunity*, vol. 48, pp. 57–67, 2015.

[123] G. Szalay, B. Martinecz, N. Lénárt, Z. Környei, B. Orsolits, L. Judák, E. Császár, R. Fekete, B. L. West, G. Katona, *et al.*, "Microglia protect against brain injury and their selective elimination dysregulates neuronal network activity after stroke," *Nature communications*, vol. 7, no. 1, pp. 1–13, 2016.

[124] D. Sieger, C. Moritz, T. Ziegenhals, S. Prykhozhij, and F. Peri, "Long-range ca2+ waves transmit brain-damage signals to microglia," *Developmental cell*, vol. 22, no. 6, pp. 1138–1148, 2012.

[125] A. Bessis, C. Béchade, D. Bernard, and A. Roumier, "Microglial control of neuronal death and synaptic properties," *Glia*, vol. 55, no. 3, pp. 233–238, 2007.

[126] U. Sonnewald, N. Westergaard, and A. Schousboe, "Glutamate transport and metabolism in astrocytes," *Glia*, vol. 21, no. 1, pp. 56–63, 1997.

[127] L. Hertz and D. L. Rothman, "Glutamine-glutamate cycle flux is similar in cultured astrocytes and brain and both glutamate production and oxidation are mainly catalyzed by aspartate aminotransferase," *Biology*, vol. 6, no. 1, p. 17, 2017.

[128] S. Mahmoud, M. Gharagozloo, C. Simard, and D. Gris, "Astrocytes maintain glutamate homeostasis in the cns by controlling the balance between glutamate uptake and release," *Cells*, vol. 8, no. 2, p. 184, 2019.

[129] C.-T. Wu, L.-L. Wen, C.-S. Wong, S.-Y. Tsai, S.-M. Chan, C.-C. Yeh, C. O. Borel, and C.-H. Cherng, "Temporal changes in glutamate, glutamate transporters, basilar arteries wall thickness, and neuronal variability in an experimental rat model of subarachnoid hemorrhage," *Anesthesia & Analgesia*, vol. 112, no. 3, pp. 666–673, 2011.

[130] W. Krzyżanowska, B. Pomierny, M. Filip, and J. Pera, "Glutamate transporters in brain ischemia: to modulate or not?," *Acta Pharmacologica Sinica*, vol. 35, no. 4, pp. 444–462, 2014.

[131] D. Rossi and A. Volterra, "Astrocytic dysfunction: insights on the role in neurodegeneration," *Brain research bulletin*, vol. 80, no. 4-5, pp. 224–232, 2009.

[132] S. A. Liddelow, K. A. Guttenplan, L. E. Clarke, F. C. Bennett, C. J. Bohlen, L. Schirmer, M. L. Bennett, A. E. Münch, W.-S. Chung, T. C. Peterson, *et al.*, "Neurotoxic reactive astrocytes are induced by activated microglia," *Nature*, vol. 541, no. 7638, pp. 481–487, 2017.

[133] K. Li, J. Li, J. Zheng, and S. Qin, "Reactive astrocytes in neurodegenerative diseases," *Aging and disease*, vol. 10, no. 3, p. 664, 2019.

[134] K. Kataoka, T. Hayakawa, K. Yamada, T. Mushiroi, R. Kuroda, and H. Mogami, "Neuronal network disturbance after focal ischemia in rats.," *Stroke*, vol. 20, no. 9, pp. 1226–1235, 1989.

[135] W. Fujie, T. Kirino, N. Tomukai, T. Iwasawa, and A. Tamura, "Progressive shrinkage of the thalamus following middle cerebral artery occlusion in rats.," *Stroke*, vol. 21, no. 10, pp. 1485–1488, 1990.

[136] J. Baron, "Mapping anterograde and retrograde degeneration after stroke," *Journal of Neurology, Neurosurgery & Psychiatry*, vol. 76, no. 2, pp. 159–160, 2005.

[137] H. Iizuka, K. Sakatani, and W. Young, "Neural damage in the rat thalamus after cortical infarcts.," *Stroke*, vol. 21, no. 5, pp. 790–794, 1990.

[138] A. Kanamori, M.-M. Catrinescu, J. M. Belisle, S. Costantino, and L. A. Levin, "Retrograde and wallerian axonal degeneration occur synchronously after retinal ganglion cell axotomy," *The American journal of pathology*, vol. 181, no. 1, pp. 62–73, 2012.

[139] B. S. Nashold, J. Hanbery, and J. Olszewski, "Observations on the diffuse thalamic projections," *Electroencephalography and clinical neurophysiology*, vol. 7, no. 4, pp. 609–620, 1955.

[140] K. A. Hosie, A. E. King, C. A. Blizzard, J. C. Vickers, and T. C. Dickson, "Chronic excitotoxin-induced axon degeneration in a compartmented neuronal culture model," *ASN neuro*, vol. 4, no. 1, p. AN20110031, 2012.

[141] I. Morales, M. Sabate, and M. Rodriguez, "Striatal glutamate induces retrograde excitotoxicity and neuronal degeneration of intralaminar thalamic nuclei: their potential relevance for p arkinson's disease," *European Journal of Neuroscience*, vol. 38, no. 1, pp. 2172–2182, 2013.

[142] A. J. Canty, J. S. Jackson, L. Huang, A. Trabalza, C. Bass, G. Little, M. Tortora, S. Khan, and V. De Paola, "In vivo imaging of injured cortical axons reveals a rapid onset form of wallerian degeneration," *BMC biology*, vol. 18, no. 1, pp. 1–17, 2020.

[143] M. Dihné, C. Grommes, M. Lutzenburg, O. W. Witte, and F. Block, "Different mechanisms of secondary neuronal damage in thalamic nuclei after focal cerebral ischemia in rats," *Stroke*, vol. 33, no. 12, pp. 3006–3011, 2002.

[144] L. Van Den Bosch, B. Schwaller, V. Vleminckx, B. Meijers, S. Stork, T. Ruehlicke, E. Van Houtte, H. Klaassen, M. Celio, L. Missiaen, *et al.*, "Protective effect of parvalbumin on excitotoxic motor neuron death," *Experimental neurology*, vol. 174, no. 2, pp. 150–161, 2002.

[145] X. Zuo, S. Hu, Y. Tang, L. Zhan, W. Sun, J. Zheng, Y. Han, and E. Xu, "Attenuation of secondary damage and aβ deposits in the ipsilateral thalamus of dmcao rats through reduction of cathepsin b by bis (propyl)-cognitin, a multifunctional dimer," *Neuropharmacology*, vol. 162, p. 107786, 2020.

[146] Z. Cao, A. Balasubramanian, S. E. Pedersen, J. Romero, R. G. Pautler, and S. P. Marrelli, "Trpv1-mediated pharmacological hypothermia promotes improved functional recovery following ischemic stroke," *Scientific reports*, vol. 7, no. 1, pp. 1–11, 2017.

[147] J. Polentes, P. Jendelova, M. Cailleret, H. Braun, N. Romanyuk, P. Tropel, M. Brenot, V. Itier, C. Seminatore, K. Baldauf, *et al.*, "Human induced pluripotent stem cells improve stroke outcome and reduce secondary degeneration in the recipient brain," *Cell transplantation*, vol. 21, no. 12, pp. 2587–2602, 2012.

[148] S. Xing, J. Zhang, C. Dang, G. Liu, Y. Zhang, J. Li, Y. Fan, Z. Pei, and J. Zeng, "Cerebrolysin reduces amyloid-β deposits, apoptosis and autophagy in the thalamus and improves functional recovery after cortical infarction," *Journal of the neurological sciences*, vol. 337, no. 1-2, pp. 104–111, 2014.

[149] J. E. Anttila, S. Pöyhönen, and M. Airavaara, "Secondary pathology of the thalamus after focal cortical stroke in rats is not associated with thermal or mechanical hypersensitivity and is not alleviated by intra-thalamic post-stroke delivery of recombinant cdnf or manf," *Cell transplantation*, vol. 28, no. 4, pp. 425–438, 2019.

[150] Y.-B. Liang, Y.-Q. Guo, P.-P. Song, Y.-H. Zhu, P.-Z. Zhu, R.-R. Liu, J.-M. Xu, and Y.-S. Zhang, "Memantine ameliorates tau protein deposition and secondary damage in the ipsilateral thalamus and sensory decline following focal cortical infarction in rats," *Neuroscience Letters*, vol. 731, p. 135091, 2020.

[151] J. Yu, C. Li, Q. Ding, J. Que, K. Liu, H. Wang, and S. Liao, "Netrin-1 ameliorates blood-brain barrier impairment secondary to ischemic stroke via the activation of pi3k pathway," *Frontiers in neuroscience*, vol. 11, p. 700, 2017.

[152] Y. Li, J. Zhang, L. Chen, S. Xing, J. Li, Y. Zhang, C. Li, Z. Pei, and J. Zeng, "Ebselen reduces autophagic activation and cell death in the ipsilateral thalamus following focal cerebral infarction," *Neuroscience letters*, vol. 600, pp. 206–212, 2015.

[153] T. Sarajärvi, A. Lipsanen, P. Mäkinen, S. Peräniemi, H. Soininen, A. Haapasalo, J. Jolkkonen, and M. Hiltunen, "Bepridil decreases a β and calcium levels in the thalamus after middle cerebral artery occlusion in rats," *Journal of cellular and molecular medicine*, vol. 16, no. 11, pp. 2754–2767, 2012.

[154] A. Lipsanen, S. Flunkert, K. Kuptsova, M. Hiltunen, M. Windisch, B. Hutter-Paier, and J. Jolkkonen, "Non-selective calcium channel blocker bepridil decreases secondary pathology in mice after photothrombotic cortical lesion," *PLoS One*, vol. 8, no. 3, p. e60235, 2013.

[155] Y. Zhang, S. Xing, J. Zhang, J. Li, C. Li, Z. Pei, and J. Zeng, "Reduction of β-amyloid deposits by γ-secretase inhibitor is associated with the attenuation of secondary damage in the ipsilateral thalamus and sensory functional improvement after focal cortical infarction in

hypertensive rats," *Journal of Cerebral Blood Flow & Metabolism*, vol. 31, no. 2, pp. 572–579, 2011.

[156] J. Zhang, Y. Zhang, J. Li, S. Xing, C. Li, Y. Li, C. Dang, Y. Fan, J. Yu, Z. Pei, *et al.*, "Autophagosomes accumulation is associated with β-amyloid deposits and secondary damage in the thalamus after focal cortical infarction in hypertensive rats," *Journal of neurochemistry*, vol. 120, no. 4, pp. 564–573, 2012.

[157] M. P. Mattson, B. Rychlik, J. S. You, and J. E. Sisken, "Sensitivity of cultured human embryonic cerebral cortical neurons to excitatory amino acid-induced calcium influx and neurotoxicity," *Brain research*, vol. 542, no. 1, pp. 97–106, 1991.

[158] C. Ikonomidou and L. Turski, "Why did nmda receptor antagonists fail clinical trials for stroke and traumatic brain injury?," *The Lancet Neurology*, vol. 1, no. 6, pp. 383–386, 2002.

[159] K. W. Muir, "Glutamate-based therapeutic approaches: clinical trials with nmda antagonists," *Current opinion in pharmacology*, vol. 6, no. 1, pp. 53–60, 2006.

[160] A. Lau and M. Tymianski, "Glutamate receptors, neurotoxicity and neurodegeneration," *Pflügers Archiv-European Journal of Physiology*, vol. 460, no. 2, pp. 525–542, 2010.

[161] E. Miyamoto, "Molecular mechanism of neuronal plasticity: induction and maintenance of long-term potentiation in the hippocampus," *Journal of pharmacological sciences*, vol. 100, no. 5, pp. 433–442, 2006.

[162] J. Gécz, "Glutamate receptors and learning and memory," *Nature genetics*, vol. 42, no. 11, p. 925, 2010.

[163] J. L. Molinuevo, A. Lladó, and L. Rami, "Memantine: targeting glutamate excitotoxicity in alzheimer's disease and other dementias," *American Journal of Alzheimer's Disease & Other Dementias®*, vol. 20, no. 2, pp. 77–85, 2005.

[164] J.-y. Sun, S.-j. Zhao, H.-b. Wang, Y.-j. Hou, Q.-j. Mi, M.-f. Yang, H. Yuan, Q.-b. Ni, B.-l. Sun, and Z.-y. Zhang, "Ifenprodil improves long-term neurologic deficits through antagonizing glutamate-induced excitotoxicity after experimental subarachnoid hemorrhage," *Translational Stroke Research*, pp. 1–14, 2021.

[165] Y.-Y. Huang, K. Nagata, C. E. Tedford, *et al.*, "Low-level laser therapy (810 nm) protects primary cortical neurons against excitotoxicity in vitro," *Journal of biophotonics*, vol. 7, no. 8, pp. 656–664, 2014.

[166] R. Almeida, B. Manadas, C. Melo, J. Gomes, C. Mendes, M. Graos, R. Carvalho, A. Carvalho, and C. Duarte, "Neuroprotection by bdnf against glutamate-induced apoptotic cell death is mediated by erk and pi3-kinase pathways," *Cell Death & Differentiation*, vol. 12, no. 10, pp. 1329–1343, 2005.

[167] Y. Goldshmit, E. Banyas, N. Bens, A. Yakovchuk, and A. Ruban, "Blood glutamate scavengers and exercises as an effective neuroprotective treatment in mice with spinal cord injury," *Journal of Neurosurgery: Spine*, vol. 33, no. 5, pp. 692–704, 2020.

[168] D. Nagy, M. Marosi, Z. Kis, T. Farkas, G. Rakos, L. Vecsei, V. I. Teichberg, and J. Toldi, "Oxaloacetate decreases the infarct size and attenuates the reduction in evoked responses after photothrombotic focal ischemia in the rat cortex," *Cellular and molecular neurobiology*, vol. 29, no. 6, pp. 827–835, 2009.

[169] V. Rodriguez-Chavez, J. Moran, G. Molina-Salinas, W. Z. Ruiz, M. Rodriguez, O. Picazo, and M. Cerbon, "Participation of glutamatergic ionotropic receptors in excitotoxicity: the neuroprotective role of prolactin," *Neuroscience*, 2021.

[170] M. Aarts, Y. Liu, L. Liu, S. Besshoh, M. Arundine, J. W. Gurd, Y.-T. Wang, M. W. Salter, and M. Tymianski, "Treatment of ischemic brain damage by perturbing nmda receptor-psd-95 protein interactions," *Science*, vol. 298, no. 5594, pp. 846–850, 2002.

[171] W. Qu, N.-K. Liu, X. Wu, Y. Wang, Y. Xia, Y. Sun, Y. Lai, R. Li, A. Shekhar, and X.-M. Xu, "Disrupting nnos–psd95 interaction improves neurological and cognitive recoveries after traumatic brain injury," *Cerebral Cortex*, vol. 30, no. 7, pp. 3859–3871, 2020.

[172] M. J. Glat, N. Stefanova, G. K. Wenning, and D. Offen, "Genes to treat excitotoxicity ameliorate the symptoms of the disease in mice models of multiple system atrophy," *Journal of Neural Transmission*, vol. 127, no. 2, pp. 205–212, 2020.

[173] M. Bi, A. Gladbach, J. van Eersel, A. Ittner, M. Przybyla, A. van Hummel, S. W. Chua, J. van der Hoven, W. S. Lee, J. Müller, *et al.*, "Tau exacerbates excitotoxic brain damage in an animal model of stroke," *Nature communications*, vol. 8, no. 1, pp. 1–15, 2017.

[174] D. Tarsy, J. L. Vitek, P. Starr, and M. Okun, *Deep brain stimulation in neurological and psychiatric disorders*. Springer Science & Business Media, 2008.

[175] V. A. Sironi, "Origin and evolution of deep brain stimulation," *Frontiers in Integrative Neuroscience*, vol. 5, p. 42, 2011.

[176] A. L. Benabid, "Deep brain stimulation for parkinsons disease," *Current opinion in neurobiology*, vol. 13, no. 6, pp. 696–706, 2003.

[177] S. Miocinovic, S. Somayajula, S. Chitnis, and J. Vitek, "History, applications, and mechanisms of deep brain stimulation," *JAMA Neurology*, vol. 70, no. 2, pp. 163–171, 2013.

[178] J. S. Perlmutter and J. W. Mink, "Deep brain stimulation," *Annu. Rev. Neurosci.*, vol. 29, pp. 229–257, 2006.

[179] V. A. Coenen, F. Amtage, J. Volkmann, and T. E. Schläpfer, "Deep brain stimulation in neurological and psychiatric disorders.," *Deutsches Arzteblatt international*, vol. 112, no. 31-32, pp. 519–526, 2015.

[180] J.A. Obeso et al., "Deep-brain stimulation of the subthalamic nucleus or the pars interna of the globus pallidus in parkinson's disease," *N Engl J Med*, vol. 2001, no. 345, pp. 956–963, 2001.

[181] S. Rehncrona, B. Johnels, H. Widner, A.-L. Törnqvist, M. Hariz, and O. Sydow, "Long-term efficacy of thalamic deep brain stimulation for tremor: Double-blind assessments," *Movement disorders*, vol. 18, no. 2, pp. 163–170, 2003.

[182] P. Blomstedt, U. Sandvik, and S. Tisch, "Deep brain stimulation in the posterior subthalamic area in the treatment of essential tremor," *Movement Disorders*, vol. 25, no. 10, pp. 1350–1356, 2010.

[183] C. De Hemptinne, N. C. Swann, J. L. Ostrem, E. S. Ryapolova-Webb, M. San Luciano, N. B. Galifianakis, and P. A. Starr, "Therapeutic deep brain stimulation reduces cortical phase-amplitude coupling in parkinson's disease," *Nature neuroscience*, vol. 18, no. 5, pp. 779–786, 2015.

[184] R. Fisher, V. Salanova, T. Witt, R. Worth, T. Henry, R. Gross, K. Oommen, I. Osorio, J. Nazzaro, D. Labar, *et al.*, "Electrical stimulation of the anterior nucleus of thalamus for treatment of refractory epilepsy," *Epilepsia*, vol. 51, no. 5, pp. 899–908, 2010.

[185] G. K. Bergey, M. J. Morrell, E. M. Mizrahi, A. Goldman, D. King-Stephens, D. Nair, S. Srinivasan, B. Jobst, R. E. Gross, D. C. Shields, *et al.*, "Long-term treatment with responsive brain stimulation in adults with refractory partial seizures," *Neurology*, vol. 84, no. 8, pp. 810–817, 2015.

[186] A. W. Laxton, D. F. Tang-Wai, M. P. McAndrews, D. Zumsteg, R. Wennberg, R. Keren, J. Wherrett, G. Naglie, C. Hamani, G. S. Smith, *et al.*, "A phase i trial of deep brain stimulation of memory circuits in alzheimer's disease," *Annals of neurology*, vol. 68, no. 4, pp. 521–534, 2010.

[187] K. Hardenacke, E. Shubina, C. Bührle, A. Zapf, D. Lenartz, J. Klosterkötter, V. Visser-Vandewalle, and J. Kuhn, "Deep brain stimulation as a tool for improving cognitive functioning in alzheimers dementia: A systematic review," *Frontiers in Psychiatry*, vol. 4, p. 159, 2013.

[188] N. Hansen, "Brain stimulation for combating alzheimers disease," *Frontiers in Neurology*, vol. 5, p. 80, 2014.

[189] T. E. Schlaepfer, M. X. Cohen, C. Frick, M. Kosel, D. Brodesser, N. Axmacher, A. Y. Joe, M. Kreft, D. Lenartz, and V. Sturm, "Deep brain stimulation to reward circuitry alleviates anhedonia in refractory major depression," *Neuropsychopharmacology*, vol. 33, no. 2, pp. 368–377, 2008.

[190] B. H. Bewernick, S. Kayser, V. Sturm, and T. E. Schlaepfer, "Long-term effects of nucleus accumbens deep brain stimulation in treatment-resistant depression: evidence for sustained efficacy," *Neuropsychopharmacology*, vol. 37, no. 9, pp. 1975–1985, 2012.

[191] J. Kuhn, M. Bodatsch, V. Sturm, D. Lenartz, J. Klosterkötter, P. Uhlhaas, C. Winter, and T. Gründler, "Deep brain stimulation in schizophrenia," *Fortschritte der Neurologie-Psychiatrie*, vol. 79, no. 11, pp. 632–641, 2011.

[192] V. Vandewalle, C. van der Linden, H. Groenewegen, and J. Caemaert, "Stereotactic treatment of gilles de la tourette syndrome by high frequency stimulation of thalamus," *The Lancet*, vol. 353, no. 9154, p. 724, 1999.

[193] A. Viswanathan, J. Jimenez-Shahed, J. F. B. Carvallo, and J. Jankovic, "Deep brain stimulation for tourette syndrome: target selection," *Stereotactic and functional neurosurgery*, vol. 90, no. 4, pp. 213–224, 2012.

[194] L. Almeida, D. Martinez-Ramirez, P. J. Rossi, Z. Peng, A. Gunduz, and M. S. Okun, "Chasing tics in the human brain: development of open, scheduled and closed loop responsive approaches to deep brain stimulation for tourette syndrome," *Journal of clinical neurology*, vol. 11, no. 2, pp. 122–131, 2015.

[195] B. Aouizerate, E. Cuny, C. Martin-Guehl, D. Guehl, H. Amieva, A. Benazzouz, C. Fabrigoule, M. Allard, A. Rougier, B. Bioulac, *et al.*, "Deep brain stimulation of the ventral caudate nucleus in the treatment of obsessive compulsive disorder and major depression," *Journal of neurosurgery*, vol. 101, no. 4, pp. 682–686, 2004.

[196] S. F. Lempka, D. A. Malone, B. Hu, K. B. Baker, A. Wyant, J. G. Ozinga, E. B. Plow, M. Pandya, C. S. Kubu, P. J. Ford, *et al.*, "Randomized clinical trial of deep brain stimulation for poststroke pain," *Annals of neurology*, vol. 81, no. 5, pp. 653–663, 2017.

[197] M. Hirato, T. Miyagishima, T. Gouda, A. Takahashi, and Y. Yoshimoto, "Electrical thalamic stimulation in the anterior part of the ventral posterolateral nucleus for the treatment of patients with central poststroke pain," *Neuromodulation: Technology at the Neural Interface*, vol. 24, no. 2, pp. 361–372, 2021.

[198] K. Hosomi, B. Seymour, and Y. Saitoh, "Modulating the pain network-neurostimulation for central poststroke pain," *Nature Reviews Neurology*, vol. 11, no. 5, p. 290, 2015.

[199] Z. Wu, F. Sun, Z. Li, M. Liu, X. Tian, D. Guo, P. Wei, Y. Shan, T. Liu, M. Guo, *et al.*, "Electrical stimulation of the lateral cerebellar nucleus promotes neurogenesis in rats after motor cortical ischemia," *Scientific reports*, vol. 10, no. 1, pp. 1–14, 2020.

[200] S.-K. K.-C. Sims, A. Rizzo, K. Howard, A. Farrand, H. Boger, and D. L. Adkins, "Comparative enhancement of motor function and bdnf expression following different brain stimulation approaches in an animal model of ischemic stroke," *Neurorehabilitation and neural repair*, vol. 34, no. 10, pp. 925–935, 2020.

[201] E. Gondard, L. Teves, L. Wang, C. McKinnon, C. Hamani, S. K. Kalia, P. L. Carlen, M. Tymianski, and A. M. Lozano, "Deep brain stimulation rescues memory and synaptic activity in a rat model of global ischemia," *Journal of Neuroscience*, vol. 39, no. 13, pp. 2430–2440, 2019.

[202] J. B. Ranck Jr, "Which elements are excited in electrical stimulation of mammalian central nervous system: a review," *Brain research*, vol. 98, no. 3, pp. 417–440, 1975.

[203] S. Chiken and A. Nambu, "Mechanism of deep brain stimulation: inhibition, excitation, or disruption?," *The Neuroscientist*, vol. 22, no. 3, pp. 313–322, 2016.

[204] T. M. Herrington, J. J. Cheng, and E. N. Eskandar, "Mechanisms of deep brain stimulation," *Journal of Neurophysiology*, vol. 115, no. 1, pp. 19–38, 2015.

[205] M. R. García, B. A. Pearlmutter, P. E. Wellstead, and R. H. Middleton, "A slow axon antidromic blockade hypothesis for tremor reduction via deep brain stimulation," *PloS one*, vol. 8, no. 9, p. e73456, 2013.

[206] D. Shin, M. Samoilova, M. Cotic, L. Zhang, J. Brotchie, and P. Carlen, "High frequency stimulation or elevated k+ depresses neuronal activity in the rat entopeduncular nucleus," *Neuroscience*, vol. 149, no. 1, pp. 68–86, 2007.

[207] C. Beurrier, B. Bioulac, J. Audin, and C. Hammond, "High-frequency stimulation produces a transient blockade of voltage-gated currents in subthalamic neurons," *Journal of neurophysiology*, vol. 85, no. 4, pp. 1351–1356, 2001.

[208] X. Zhang, J. R. Roppolo, W. C. De Groat, and C. Tai, "Mechanism of nerve conduction block induced by high-frequency biphasic electrical currents," *IEEE Transactions on Biomedical Engineering*, vol. 53, no. 12, pp. 2445–2454, 2006.

[209] Y. Temel, V. Visser-Vandewalle, S. Kaplan, R. Kozan, M. A. Daemen, A. Blokland, C. Schmitz, and H. W. Steinbusch, "Protection of nigral cell death by bilateral subthalamic nucleus stimulation," *Brain research*, vol. 1120, no. 1, pp. 100–105, 2006.

[210] B. A. Wallace, K. Ashkan, C. E. Heise, K. D. Foote, N. Torres, J. Mitrofanis, and A.-L. Benabid, "Survival of midbrain dopaminergic cells after lesion or deep brain stimulation of the subthalamic nucleus in mptp-treated monkeys," *Brain*, vol. 130, no. 8, pp. 2129–2145, 2007.

[211] A. L. Spieles-Engemann, K. Steece-Collier, M. M. Behbehani, T. J. Collier, S. L. Wohlgenant, C. J. Kemp, A. Cole-Strauss, N. D. Levine, S. E. Gombash, V. B. Thompson, *et al.*, "Subthalamic nucleus stimulation increases brain derived neurotrophic factor in the nigrostriatal system and primary motor cortex," *Journal of Parkinson's disease*, vol. 1, no. 1, pp. 123–136, 2011.

[212] A. A. Al-Majed, T. M. Brushart, and T. Gordon, "Electrical stimulation accelerates and increases expression of bdnf and trkb mrna in regenerating rat femoral motoneurons," *European Journal of Neuroscience*, vol. 12, no. 12, pp. 4381–4390, 2000.

[213] C. Hammond, R. Ammari, B. Bioulac, and L. Garcia, "Latest view on the mechanism of action of deep brain stimulation," *Movement disorders*, vol. 23, no. 15, pp. 2111–2121, 2008.

[214] A. Y. Chow, V. Y. Chow, K. H. Packo, J. S. Pollack, G. A. Peyman, and R. Schuchard, "The artificial silicon retina microchip for the treatment of visionloss from retinitis pigmentosa," *Archives of ophthalmology*, vol. 122, no. 4, pp. 460–469, 2004.

[215] T. Morimoto, T. Fujikado, J.-S. Choi, H. Kanda, T. Miyoshi, Y. Fukuda, and Y. Tano, "Transcorneal electrical stimulation promotes the survival of photoreceptors and preserves retinal function in royal college of surgeons rats," *Investigative ophthalmology & visual science*, vol. 48, no. 10, pp. 4725–4732, 2007.

[216] T. Morimoto, T. Miyoshi, H. Sawai, and T. Fujikado, "Optimal parameters of transcorneal electrical stimulation (tes) to be neuroprotective of axotomized rgcs in adult rats," *Experimental eye research*, vol. 90, no. 2, pp. 285–291, 2010.

[217] A. M. Hanif, M. K. Kim, J. G. Thomas, V. T. Ciavatta, M. Chrenek, J. R. Hetling, and M. T. Pardue, "Whole-eye electrical stimulation therapy preserves visual function and structure in p23h-1 rats," *Experimental eye research*, vol. 149, pp. 75–83, 2016.

[218] A. Schatz, J. Pach, M. Gosheva, L. Naycheva, G. Willmann, B. Wilhelm, T. Peters, K. U. Bartz-Schmidt, E. Zrenner, A. Messias, *et al.*, "Transcorneal electrical stimulation for patients with retinitis pigmentosa: a prospective, randomized, sham-controlled follow-up study over 1 year," *Investigative ophthalmology & visual science*, vol. 58, no. 1, pp. 257–269, 2017.

[219] E. Lagrange, P. Krack, E. Moro, C. Ardouin, N. Van Blercom, S. Chabardes, A.-L. Benabid, and P. Pollak, "Bilateral subthalamic nucleus stimulation improves health-related quality of life in pd," *Neurology*, vol. 59, no. 12, pp. 1976–1978, 2002.

[220] N. Grossman, D. Bono, N. Dedic, S. B. Kodandaramaiah, A. Rudenko, H.-J. Suk, A. M. Cassara, E. Neufeld, N. Kuster, L.-H. Tsai, *et al.*, "Noninvasive deep brain stimulation via temporally interfering electric fields," *Cell*, vol. 169, no. 6, pp. 1029–1041, 2017.

[221] R. Cubo, M. Åström, and A. Medvedev, "Target coverage and selectivity in field steering brain stimulation," in *Engineering in Medicine and Biology Society (EMBC), 2014 36th Annual International Conference of the IEEE*, pp. 522–525, IEEE, 2014.

[222] R. Cubo, M. Åström, and A. Medvedev, "Electric field modeling and spatial control in deep brain stimulation," in *Decision and Control (CDC), 2015 IEEE 54th Annual Conference on*, pp. 3846–3851, IEEE, 2015.

[223] K. A. Tennant, S. L. Taylor, E. R. White, and C. E. Brown, "Optogenetic rewiring of thalamocortical circuits to restore function in the stroke injured brain," *Nature Communications*, vol. 8, no. 1, pp. 1–14, 2017.

[224] A. M. Shah, S. Ishizaka, M. Y. Cheng, E. H. Wang, A. R. Bautista, S. Levy, D. Smerin, G. Sun, and G. K. Steinberg, "Optogenetic neuronal stimulation of the lateral cerebellar nucleus promotes persistent functional recovery after stroke," *Scientific reports*, vol. 7, no. 1, pp. 1–11, 2017.

[225] J. Luo, H. Zheng, L. Zhang, Q. Zhang, L. Li, Z. Pei, and X. Hu, "High-frequency repetitive transcranial magnetic stimulation (rtms) improves functional recovery by enhancing neurogenesis and activating bdnf/trkb signaling in ischemic rats," *International Journal of Molecular Sciences*, vol. 18, no. 2, p. 455, 2017.

[226] H. Li, J. Shang, C. Zhang, R. Lu, J. Chen, and X. Zhou, "Repetitive transcranial magnetic stimulation alleviates neurological deficits after cerebral ischemia through interaction between

rack1 and bdnf exon iv by the phosphorylation-dependent factor mecp2," *Neurotherapeutics*, pp. 1–13, 2020.

[227] J. Boonzaier, G. A. van Tilborg, S. F. Neggers, and R. M. Dijkhuizen, "Noninvasive brain stimulation to enhance functional recovery after stroke: studies in animal models," *Neurorehabilitation and neural repair*, vol. 32, no. 11, pp. 927–940, 2018.

[228] N. Bolognini, C. Russo, M. Souza Carneiro, A. Nicotra, E. Olgiati, V. Spandri, E. Agostoni, A. Salmaggi, and G. Vallar, "Bi-hemispheric transcranial direct current stimulation for upper-limb hemiparesis in acute stroke: a randomized, double-blind, sham-controlled trial," *European Journal of Neurology*, vol. 27, no. 12, pp. 2473–2482, 2020.

[229] A. G. Schjetnan, D. C. Gidyk, G. A. Metz, and A. Luczak, "Anodal transcranial direct current stimulation with monopolar pulses improves limb use after stroke by enhancing inter-hemispheric coherence," *Acta Neurobiol Exp*, vol. 79, no. 3, pp. 290–301, 2019.

[230] W.-S. Kim, B. S. Kwon, H. G. Seo, J. Park, and N.-J. Paik, "Low-frequency repetitive transcranial magnetic stimulation over contralesional motor cortex for motor recovery in subacute ischemic stroke: A randomized sham-controlled trial," *Neurorehabilitation and Neural Repair*, vol. 34, no. 9, pp. 856–867, 2020.

[231] C. Grefkes and G. R. Fink, "Disruption of motor network connectivity post-stroke and its noninvasive neuromodulation," *Current opinion in neurology*, vol. 25, no. 6, pp. 670–675, 2012.

[232] M. Ameli, C. Grefkes, F. Kemper, F. P. Riegg, A. K. Rehme, H. Karbe, G. R. Fink, and D. A. Nowak, "Differential effects of high-frequency repetitive transcranial magnetic stimulation over ipsilesional primary motor cortex in cortical and subcortical middle cerebral artery stroke," *Annals of Neurology: Official Journal of the American Neurological Association and the Child Neurology Society*, vol. 66, no. 3, pp. 298–309, 2009.

[233] B. O. Adeyemo, M. Simis, D. Macea, and F. Fregni, "Systematic review of parameters of stimulation, clinical trial design characteristics, and motor outcomes in non-invasive brain stimulation in stroke," *Frontiers in psychiatry*, vol. 3, p. 88, 2012.

[234] N. Takeuchi and S.-I. Izumi, "Noninvasive brain stimulation for motor recovery after stroke: mechanisms and future views," *Stroke research and treatment*, vol. 2012, 2012.

[235] E. Raffin and H. R. Siebner, "Transcranial brain stimulation to promote functional recovery after stroke," *Current Opinion in Neurology*, vol. 27, no. 1, p. 54, 2014.

[236] D. Folloni, L. Verhagen, R. B. Mars, E. Fouragnan, C. Constans, J.-F. Aubry, M. F. Rushworth, and J. Sallet, "Manipulation of subcortical and deep cortical activity in the primate brain using transcranial focused ultrasound stimulation," *Neuron*, vol. 101, no. 6, pp. 1109–1116, 2019.

[237] A. Fomenko, C. Neudorfer, R. F. Dallapiazza, S. K. Kalia, and A. M. Lozano, "Low-intensity ultrasound neuromodulation: An overview of mechanisms and emerging human applications," *Brain stimulation*, vol. 11, no. 6, pp. 1209–1217, 2018.

[238] R. F. Dallapiazza, K. F. Timbie, S. Holmberg, J. Gatesman, M. B. Lopes, R. J. Price, G. W. Miller, and W. J. Elias, "Noninvasive neuromodulation and thalamic mapping with low-intensity focused ultrasound," *Journal of neurosurgery*, vol. 128, no. 3, pp. 875–884, 2017.

[239] H. Baek, A. Sariev, S. Lee, S.-Y. Dong, S. Royer, and H. Kim, "Deep cerebellar low-intensity focused ultrasound stimulation restores interhemispheric balance after ischemic stroke in mice," *IEEE Transactions on Neural Systems and Rehabilitation Engineering*, vol. 28, no. 9, pp. 2073–2079, 2020.

[240] H. Yang, Y. Yuan, X. Wang, and X. Li, "Closed-loop transcranial ultrasound stimulation for real-time non-invasive neuromodulation in vivo," *Frontiers in Neuroscience*, vol. 14, 2020.

[241] X. Li, H. Yang, J. Yan, X. Wang, X. Li, and Y. Yuan, "Low-intensity pulsed ultrasound stimulation modulates the nonlinear dynamics of local field potentials in temporal lobe epilepsy," *Frontiers in neuroscience*, vol. 13, p. 287, 2019.

[242] M. M. Comerota, B. Krishnan, and G. Taglialatela, "Near infrared light decreases synaptic vulnerability to amyloid beta oligomers," *Scientific Reports*, vol. 7, no. 1, p. 15012, 2017.

[243] Z. Yu, N. Liu, J. Zhao, Y. Li, T. J. McCarthy, C. E. Tedford, E. H. Lo, and X. Wang, "Near infrared radiation rescues mitochondrial dysfunction in cortical neurons after oxygen-glucose deprivation," *Metabolic brain disease*, vol. 30, no. 2, pp. 491–496, 2015.

[244] S. Purushothuman, D. M. Johnstone, C. Nandasena, J. Mitrofanis, and J. Stone, "Photobiomodulation with near infrared light mitigates alzheimers disease–related pathology in cerebral cortex–evidence from two transgenic mouse models," *Alzheimer's research & therapy*, vol. 6, no. 1, p. 2, 2014.

[245] D. H. Saunders, C. A. Greig, and G. E. Mead, "Physical activity and exercise after stroke: review of multiple meaningful benefits," *Stroke*, vol. 45, no. 12, pp. 3742–3747, 2014.

[246] K. Potempa, L. T. Braun, T. Tinknell, and J. Popovich, "Benefits of aerobic exercise after stroke," *Sports Medicine*, vol. 21, no. 5, pp. 337–346, 1996.

[247] D. Zhang, Y. Lu, X. Zhao, Q. Zhang, and L. Li, "Aerobic exercise attenuates neurodegeneration and promotes functional recovery–why it matters for neurorehabilitation & neural repair," *Neurochemistry International*, p. 104862, 2020.

[248] J. Hakon, M. J. Quattromani, C. Sjölund, G. Tomasevic, L. Carey, J.-M. Lee, K. Ruscher, T. Wieloch, and A. Q. Bauer, "Multisensory stimulation improves functional recovery and resting-state functional connectivity in the mouse brain after stroke," *NeuroImage: Clinical*, vol. 17, pp. 717–730, 2018.

[249] A. Berretta, Y.-C. Tzeng, and A. N. Clarkson, "Post-stroke recovery: the role of activity-dependent release of brain-derived neurotrophic factor," *Expert Review of Neurotherapeutics*, vol. 14, no. 11, pp. 1335–1344, 2014.

[250] A. A. Khan, S. K. Ranjha, M. U. Akram, S. G. Khawaja, and A. Shaukat, "Neurotransmission cognitive theory: A novel approach for non-invasive brain stimulation using mechanical vibrations for the rehabilitation of neurological patients," *Medical Hypotheses*, vol. 143, p. 110078, 2020.

[251] H. F. Iaccarino, A. C. Singer, A. J. Martorell, A. Rudenko, F. Gao, T. Z. Gillingham, H. Mathys, J. Seo, O. Kritskiy, F. Abdurrob, *et al.*, "Gamma frequency entrainment attenuates amyloid load and modifies microglia," *Nature*, vol. 540, no. 7632, pp. 230–235, 2016.

[252] A. C. Singer, A. J. Martorell, J. M. Douglas, F. Abdurrob, M. K. Attokaren, J. Tipton, H. Mathys, C. Adaikkan, and L.-H. Tsai, "Noninvasive 40-hz light flicker to recruit microglia and reduce amyloid beta load," *Nature protocols*, vol. 13, no. 8, pp. 1850–1868, 2018.

[253] A. J. Martorell, A. L. Paulson, H.-J. Suk, F. Abdurrob, G. T. Drummond, W. Guan, J. Z. Young, D. N.-W. Kim, O. Kritskiy, S. J. Barker, *et al.*, "Multisensory gamma stimulation ameliorates alzheimer's-associated pathology and improves cognition," *Cell*, vol. 177, no. 2, pp. 256–271, 2019.

[254] M. Balbi, D. Xiao, M. J. Vega, H. Hu, M. P. Vanni, L.-P. Bernier, J. LeDue, B. MacVicar, and T. H. Murphy, "Gamma frequency activation of inhibitory neurons in the acute phase after stroke attenuates vascular and behavioral dysfunction," *Cell Reports*, vol. 34, no. 5, p. 108696, 2021.

[255] S. M. Sherman, "Thalamus plays a central role in ongoing cortical functioning," *Nature neuroscience*, vol. 19, no. 4, pp. 533–541, 2016.

[256] H. Jahnsen and R. Llinás, "Ionic basis for the electro-responsiveness and oscillatory properties of guinea-pig thalamic neurones in vitro.," *The Journal of physiology*, vol. 349, no. 1, pp. 227–247, 1984.

[257] S. M. Sherman, "Tonic and burst firing: dual modes of thalamocortical relay," *Trends in neurosciences*, vol. 24, no. 2, pp. 122–126, 2001.

[258] H. R. Wilson and J. D. Cowan, "A mathematical theory of the functional dynamics of cortical and thalamic nervous tissue," *Kybernetik*, vol. 13, no. 2, pp. 55–80, 1973.

[259] F. Cona, M. Lacanna, and M. Ursino, "A thalamo-cortical neural mass model for the simulation of brain rhythms during sleep," *Journal of Computational Neuroscience*, vol. 37, no. 1, pp. 125–148, 2014.

[260] Y. Ge, Y. Cao, G. Yi, C. Han, Y. Qin, J. Wang, and Y. Che, "Robust closed-loop control of spike-and-wave discharges in a thalamocortical computational model of absence epilepsy," *Scientific reports*, vol. 9, no. 1, pp. 1–16, 2019.

[261] E. M. Izhikevich, "Simple model of spiking neurons," *IEEE Transactions on neural networks*, vol. 14, no. 6, pp. 1569–1572, 2003.

[262] G. D. Smith, C. L. Cox, S. M. Sherman, and J. Rinzel, "Fourier analysis of sinusoidally driven thalamocortical relay neurons and a minimal integrate-and-fire-or-burst model," *Journal of neurophysiology*, vol. 83, no. 1, pp. 588–610, 2000.

[263] J. Henning Proske, D. Jeanmonod, and P. F. Verschure, "A computational model of thalamocortical dysrhythmia," *European Journal of Neuroscience*, vol. 33, no. 7, pp. 1281–1290, 2011.

[264] M. Saponati, J. Garcia-Ojalvo, E. Cataldo, and A. Mazzoni, "Integrate-and-fire network model of activity propagation from thalamus to cortex," *Biosystems*, vol. 183, p. 103978, 2019.

[265] A. Destexhe, T. Bal, D. A. McCormick, and T. J. Sejnowski, "Ionic mechanisms underlying synchronized oscillations and propagating waves in a model of ferret thalamic slices," *Journal of neurophysiology*, vol. 76, no. 3, pp. 2049–2070, 1996.

[266] A. Destexhe, D. Contreras, and M. Steriade, "Mechanisms underlying the synchronizing action of corticothalamic feedback through inhibition of thalamic relay cells," *Journal of neurophysiology*, vol. 79, no. 2, pp. 999–1016, 1998.

[267] T. Bal, D. Debay, and A. Destexhe, "Cortical feedback controls the frequency and synchrony of oscillations in the visual thalamus," *Journal of Neuroscience*, vol. 20, no. 19, pp. 7478–7488, 2000.

[268] A. Destexhe, D. Contreras, M. Steriade, T. J. Sejnowski, and J. R. Huguenard, "In vivo, in vitro, and computational analysis of dendritic calcium currents in thalamic reticular neurons," *Journal of Neuroscience*, vol. 16, no. 1, pp. 169–185, 1996.

[269] A. Destexhe, M. Neubig, D. Ulrich, and J. Huguenard, "Dendritic low-threshold calcium currents in thalamic relay cells," *Journal of Neuroscience*, vol. 18, no. 10, pp. 3574–3588, 1998.

[270] A. Destexhe, "Modelling corticothalamic feedback and the gating of the thalamus by the cerebral cortex," *Journal of Physiology-Paris*, vol. 94, no. 5-6, pp. 391–410, 2000.

[271] R. D. Traub, D. Contreras, M. O. Cunningham, H. Murray, F. E. LeBeau, A. Roopun, A. Bibbig, W. B. Wilent, M. J. Higley, and M. A. Whittington, "Single-column thalamocortical network model exhibiting gamma oscillations, sleep spindles, and epileptogenic bursts," *Journal of neurophysiology*, vol. 93, no. 4, pp. 2194–2232, 2005.

[272] C. C. McIntyre, W. M. Grill, D. L. Sherman, and N. V. Thakor, "Cellular effects of deep brain stimulation: model-based analysis of activation and inhibition," *Journal of neurophysiology*, vol. 91, no. 4, pp. 1457–1469, 2004.

[273] E. Iavarone, J. Yi, Y. Shi, B.-J. Zandt, C. O'reilly, W. Van Geit, C. Rössert, H. Markram, and S. L. Hill, "Experimentally-constrained biophysical models of tonic and burst firing modes in thalamocortical neurons," *PLoS computational biology*, vol. 15, no. 5, p. e1006753, 2019.

[274] M. Miyata and K. Imoto, "Different composition of glutamate receptors in corticothalamic and lemniscal synaptic responses and their roles in the firing responses of ventrobasal thalamic neurons in juvenile mice," *The Journal of physiology*, vol. 575, no. 1, pp. 161–174, 2006.

[275] R. D. Traub, R. K. Wong, R. Miles, and H. Michelson, "A model of a ca3 hippocampal pyramidal neuron incorporating voltage-clamp data on intrinsic conductances," *Journal of neurophysiology*, vol. 66, no. 2, pp. 635–650, 1991.

[276] A. Destexhe, A. Babloyantz, and T. J. Sejnowski, "Ionic mechanisms for intrinsic slow oscillations in thalamic relay neurons," *Biophysical journal*, vol. 65, no. 4, pp. 1538–1552, 1993.

[277] J. R. Huguenard and D. A. McCormick, "Simulation of the currents involved in rhythmic oscillations in thalamic relay neurons," *Journal of neurophysiology*, vol. 68, no. 4, pp. 1373–1383, 1992.

[278] A. Destexhe, Z. F. Mainen, and T. J. Sejnowski, "Kinetic models of synaptic transmission," *Methods in neuronal modeling*, vol. 2, pp. 1–25, 1998.

[279] J. Clements, "Transmitter timecourse in the synaptic cleft: its role in central synaptic function," *Trends in neurosciences*, vol. 19, no. 5, pp. 163–171, 1996.

[280] D. A. McCormick and J. R. Huguenard, "A model of the electrophysiological properties of thalamocortical relay neurons," *Journal of neurophysiology*, vol. 68, no. 4, pp. 1384–1400, 1992.

[281] S. L. Jackman and W. G. Regehr, "The mechanisms and functions of synaptic facilitation," *Neuron*, vol. 94, no. 3, pp. 447–464, 2017.

[282] W. G. Regehr, K. R. Delaney, and D. W. Tank, "The role of presynaptic calcium in short-term enhancement at the hippocampal mossy fiber synapse," *Journal of Neuroscience*, vol. 14, no. 2, pp. 523–537, 1994.

[283] L. He, L. Xue, J. Xu, B. D. McNeil, L. Bai, E. Melicoff, R. Adachi, and L.-G. Wu, "Compound vesicle fusion increases quantal size and potentiates synaptic transmission," *Nature*, vol. 459, no. 7243, pp. 93–97, 2009.

[284] T. Manninen, A. Saudargiene, and M.-L. Linne, "Astrocyte-mediated spike-timing-dependent long-term depression modulates synaptic properties in the developing cortex," *PLoS computational biology*, vol. 16, no. 11, p. e1008360, 2020.

[285] B. M. Kampa, J. Clements, P. Jonas, and G. J. Stuart, "Kinetics of mg2+ unblock of nmda receptors: implications for spike-timing dependent synaptic plasticity," *The Journal of physiology*, vol. 556, no. 2, pp. 337–345, 2004.

[286] J. A. Varela, K. Sen, J. Gibson, J. Fost, L. Abbott, and S. B. Nelson, "A quantitative description of short-term plasticity at excitatory synapses in layer 2/3 of rat primary visual cortex," *Journal of Neuroscience*, vol. 17, no. 20, pp. 7926–7940, 1997.

[287] E. M. Izhikevich and G. M. Edelman, "Large-scale model of mammalian thalamocortical systems," *Proceedings of the national academy of sciences*, vol. 105, no. 9, pp. 3593–3598, 2008.

[288] D. Ross and F. Ebner, "Increased excitability of thalamic relay neurons in the ventrobasal complex following ablation of the si cortex in the adult rat," in *Soc. Neurosci. Abstr.*, vol. 12, p. 983, 1986.

[289] A. Angel and K. Clarke, "An analysis of the representation of the forelimb in the ventrobasal thalamic complex of the albino rat.," *The Journal of physiology*, vol. 249, no. 2, pp. 399–423, 1975.

[290] M. J. Hosko and F. C. Helm, "Augmentation of the somatosensory thalamic response by "local" cerebral ischemia," *Life sciences*, vol. 8, no. 5, pp. 301–306, 1969.

[291] H. Fujioka, H. Kaneko, S. S. Suzuki, and K. Mabuchi, "Hyperexcitability-associated rapid plasticity after a focal cerebral ischemia," *Stroke*, vol. 35, no. 7, pp. e346–e348, 2004.

[292] A. Destexhe, "Spike-and-wave oscillations based on the properties of gabab receptors," *Journal of Neuroscience*, vol. 18, no. 21, pp. 9099–9111, 1998.

[293] E. Alonso-Calvino, I. Martinez-Camero, E. Fernandez-Lopez, D. Humanes-Valera, G. Foffani, and J. Aguilar, "Increased responses in the somatosensory thalamus immediately after spinal cord injury," *Neurobiology of disease*, vol. 87, pp. 39–49, 2016.

[294] S. Temereanca and D. J. Simons, "Local field potentials and the encoding of whisker deflections by population firing synchrony in thalamic barreloids," *Journal of neurophysiology*, vol. 89, no. 4, pp. 2137–2145, 2003.

[295] S. Temereanca and D. J. Simons, "Functional topography of corticothalamic feedback enhances thalamic spatial response tuning in the somatosensory whisker/barrel system," *Neuron*, vol. 41, no. 4, pp. 639–651, 2004.

[296] R. J. Nudo, "Mechanisms for recovery of motor function following cortical damage," *Current opinion in neurobiology*, vol. 16, no. 6, pp. 638–644, 2006.

[297] S. T. Carmichael, "Plasticity of cortical projections after stroke," *The Neuroscientist*, vol. 9, no. 1, pp. 64–75, 2003.

[298] S. T. Carmichael, I. Archibeque, L. Luke, T. Nolan, J. Momiy, and S. Li, "Growth-associated gene expression after stroke: evidence for a growth-promoting region in peri-infarct cortex," *Experimental neurology*, vol. 193, no. 2, pp. 291–311, 2005.

[299] S. T. Carmichael, "Cellular and molecular mechanisms of neural repair after stroke: making waves," *Annals of Neurology: Official Journal of the American Neurological Association and the Child Neurology Society*, vol. 59, no. 5, pp. 735–742, 2006.

[300] J. A. Williams, J. Comisarow, J. Day, H. C. Fibiger, and P. B. Reiner, "State-dependent release of acetylcholine in rat thalamus measured by in vivo microdialysis," *Journal of Neuroscience*, vol. 14, no. 9, pp. 5236–5242, 1994.

[301] G. Aston-Jones, C. Chiang, and T. Alexinsky, "Discharge of noradrenergic locus coeruleus neurons in behaving rats and monkeys suggests a role in vigilance," *Progress in brain research*, vol. 88, pp. 501–520, 1991.

[302] M. A. Castro-Alamancos and E. Oldford, "Cortical sensory suppression during arousal is due to the activity-dependent depression of thalamocortical synapses," *The Journal of physiology*, vol. 541, no. 1, pp. 319–331, 2002.

[303] M. A. Castro-Alamancos, "Different temporal processing of sensory inputs in the rat thalamus during quiescent and information processing states in vivo," *The Journal of physiology*, vol. 539, no. 2, pp. 567–578, 2002.

[304] A. Destexhe, Z. F. Mainen, and T. J. Sejnowski, "Synthesis of models for excitable membranes, synaptic transmission and neuromodulation using a common kinetic formalism," *Journal of computational neuroscience*, vol. 1, no. 3, pp. 195–230, 1994.

[305] M. A. Castro-Alamancos and M. E. Calcagnotto, "High-pass filtering of corticothalamic activity by neuromodulators released in the thalamus during arousal: in vitro and in vivo," *Journal of Neurophysiology*, vol. 85, no. 4, pp. 1489–1497, 2001.

[306] M. A. Castro-Alamancos, "Properties of primary sensory (lemniscal) synapses in the ventrobasal thalamus and the relay of high-frequency sensory inputs," *Journal of Neurophysiology*, vol. 87, no. 2, pp. 946–953, 2002.

[307] T. Markman, C. Liu, J. Zhang, K. Kobayashi, J. Kim, and F. Lenz, "Thalamic burst firing in response to experimental pain stimuli and in patients with chronic neuropathic pain may be a carrier for pain-related signals," in *Chronic Pain and Brain Abnormalities*, pp. 41–60, Elsevier, 2014.

[308] A. Groh, R. Mease, and P. Krieger, "Pain processing in the thalamocortical system," *e-Neuroforum*, vol. 23, no. 3, pp. 117–122, 2017.

[309] R. A. Harrison and T. S. Field, "Post stroke pain: identification, assessment, and therapy," *Cerebrovascular diseases*, vol. 39, no. 3-4, pp. 190–201, 2015.

[310] K. Takami, W. Fujita-Hamabe, S. Harada, and S. Tokuyama, "Aβ and aδ but not c-fibres are involved in stroke related pain and allodynia: an experimental study in mice," *Journal of Pharmacy and Pharmacology*, vol. 63, no. 3, pp. 452–456, 2011.

[311] M. J. O'Donnell, H.-C. Diener, R. L. Sacco, A. A. Panju, R. Vinisko, and S. Yusuf, "Chronic pain syndromes after ischemic stroke: Profess trial," *Stroke*, vol. 44, no. 5, pp. 1238–1243, 2013.

[312] G. Wang and S. M. Thompson, "Maladaptive homeostatic plasticity in a rodent model of central pain syndrome: thalamic hyperexcitability after spinothalamic tract lesions," *Journal of Neuroscience*, vol. 28, no. 46, pp. 11959–11969, 2008.

[313] R. Caton, "The electric currents of the brain," *Br Med J*, vol. 2, p. 278, 1875.

[314] S. Finger, *Origins of neuroscience: a history of explorations into brain function*. Oxford University Press, USA, 2001.

[315] A. Kuruvilla and R. Flink, "Intraoperative electrocorticography in epilepsy surgery: useful or not?," *Seizure*, vol. 12, no. 8, pp. 577–584, 2003.

[316] V. Malinova, A. Pinter, C. Dragaescu, V. Rohde, C. Trenkwalder, F. Sixel-Döring, and K. L. von Eckardstein, "The role of intraoperative microelectrode recording and stimulation in subthalamic lead placement for parkinson's disease," *Plos one*, vol. 15, no. 11, p. e0241752, 2020.

[317] G. Buzsáki, C. A. Anastassiou, and C. Koch, "The origin of extracellular fields and currents: Eeg, ecog, lfp and spikes," *Nature reviews neuroscience*, vol. 13, no. 6, p. 407, 2012.

[318] S. Katzner, I. Nauhaus, A. Benucci, V. Bonin, D. L. Ringach, and M. Carandini, "Local origin of field potentials in visual cortex," *Neuron*, vol. 61, no. 1, pp. 35–41, 2009.

[319] B. Pesaran, M. Vinck, G. T. Einevoll, A. Sirota, P. Fries, M. Siegel, W. Truccolo, C. E. Schroeder, and R. Srinivasan, "Investigating large-scale brain dynamics using field potential recordings: analysis and interpretation," *Nature neuroscience*, vol. 21, no. 7, pp. 903–919, 2018.

[320] H. Lindén, T. Tetzlaff, T. C. Potjans, K. H. Pettersen, S. Grün, M. Diesmann, and G. T. Einevoll, "Modeling the spatial reach of the lfp," *Neuron*, vol. 72, no. 5, pp. 859–872, 2011.

[321] P. Tzvetanov, R. Rousseff, and I. Milanov, "Lower limb ssep changes in stroke - predictive values regarding functional recovery," *Clinical neurology and neurosurgery*, vol. 105, no. 2, pp. 121–127, 2003.

[322] P. Tzvetanov and R. T. Rousseff, "Predictive value of median-ssep in early phase of stroke: a comparison in supratentorial infarction and hemorrhage," *Clinical neurology and neurosurgery*, vol. 107, no. 6, pp. 475–481, 2005.

[323] A. Hirata and M. A. Castro-Alamancos, "Neocortex network activation and deactivation states controlled by the thalamus," *Journal of neurophysiology*, vol. 103, no. 3, pp. 1147–1157, 2010.

[324] T. Jellema, C. Brunia, and W. Wadman, "Sequential activation of microcircuits underlying somatosensory-evoked potentials in rat neocortex," *Neuroscience*, vol. 129, no. 2, pp. 283–295, 2004.

[325] J. A. Barios, L. Pisarchyk, L. Fernandez-Garcia, L. C. Barrio, M. Ramos, R. Martinez-Murillo, and D. Gonzalez-Nieto, "Long-term dynamics of somatosensory activity in a stroke model of distal middle cerebral artery oclussion," *Journal of Cerebral Blood Flow & Metabolism*, vol. 36, no. 3, pp. 606–620, 2016.

[326] G. Steinberg, A. Gelb, A. Lam, P. Manninen, S. Peerless, A. Rassi Neto, and P. Floyd, "Correlation between somatosensory evoked potentials and neuronal ischemic changes following middle cerebral artery occlusion.," *Stroke*, vol. 17, no. 6, pp. 1193–1197, 1986.

[327] P. Coyer, J. Lesnick, J. Michele, and F. Simeone, "Failure of the somatosensory evoked potential following middle cerebral artery occlusion and high-grade ischemia in the cat–effects of hemodilution.," *Stroke*, vol. 17, no. 1, pp. 37–43, 1986.

[328] K. Iwayama, K. Mori, K. Yamashiro, S. Sakai, and K. Iwamoto, "Influence of the ipsilateral hemisphere upon somatosensory evoked potential in cats," *Neurological research*, vol. 10, no. 2, pp. 115–119, 1988.

[329] K. Mishima, "Facilitatory and inhibitory processes in the thalamic ventrobasal nucleus of the rat," *The Japanese journal of physiology*, vol. 42, no. 2, pp. 193–210, 1992.

[330] J. Arezzo, A. D. Legatt, and V. Vaughan Jr, "Topography and intracranial sources of somatosensory evoked potentials in the monkey. i. early components," *Electroencephalography and clinical neurophysiology*, vol. 46, no. 2, pp. 155–172, 1979.

[331] M. Kirzon and A. Y. Kaplan, "Depression of evoked potentials in rat thalamic ventro-basal complex and somatosensory cortex after reticular stimulation," *Neurophysiology*, vol. 8, no. 5, pp. 355–362, 1976.

[332] P. Andersen, C. M. Brooks, J. Eccles, and T. Sears, "The ventro-basal nucleus of the thalamus: potential fields, synaptic transmission and excitability of both presnyaptic and post-synaptic components," *The Journal of physiology*, vol. 174, no. 3, pp. 348–369, 1964.

[333] V. Fokin and R. Veskov, "Spatiotemporal characteristics of evoked potentials in the posterior ventrolateral nucleus of the cat thalamus," *Neurophysiology*, vol. 4, no. 4, pp. 336–342, 1972.

[334] M. Miyata, H. Kashiwadani, M. Fukaya, T. Hayashi, D. Wu, T. Suzuki, M. Watanabe, and Y. Kawakami, "Role of thalamic phospholipase cβ4 mediated by metabotropic glutamate receptor type 1 in inflammatory pain," *Journal of Neuroscience*, vol. 23, no. 22, pp. 8098–8108, 2003.

[335] B. Yuan, T. Morrow, and K. Casey, "Responsiveness of ventrobasal thalamic neurons after suppression of s1 cortex in the anesthetized rat," *Journal of Neuroscience*, vol. 5, no. 11, pp. 2971–2978, 1985.

[336] T. Tokuno, K. Kataoka, T. Asai, S. Chichibu, R. Kuroda, M. Ioku, K. Yamada, and T. Hayakawa, "Functional changes in thalamic relay neurons after focal cerebral infarct: a study of unit recordings from vpl neurons after mca occlusion in rats," *Journal of Cerebral Blood Flow & Metabolism*, vol. 12, no. 6, pp. 954–961, 1992.

[337] J. L. Burchfiel and F. H. Duffy, "Corticofugal influence upon cat thalamic ventrobasal complex," *Brain research*, vol. 70, no. 3, pp. 395–411, 1974.

[338] P. M. Anderson, N. C. Jones, T. J. O'Brien, and D. Pinault, "The n-methyl d-aspartate glutamate receptor antagonist ketamine disrupts the functional state of the corticothalamic pathway," *Cerebral Cortex*, vol. 27, no. 6, pp. 3172–3185, 2017.

[339] M. E. Diamond, M. Armstrong-James, M. J. Budway, and F. F. Ebner, "Somatic sensory responses in the rostral sector of the posterior group (pom) and in the ventral posterior medial nucleus (vpm) of the rat thalamus: dependence on the barrel field cortex," *Journal of Comparative Neurology*, vol. 319, no. 1, pp. 66–84, 1992.

[340] A. B. Uzdensky, "Photothrombotic stroke as a model of ischemic stroke," *Translational stroke research*, vol. 9, no. 5, pp. 437–451, 2018.

[341] L. T. Watts, W. Zheng, R. J. Garling, V. C. Frohlich, and J. D. Lechleiter, "Rose bengal photothrombosis by confocal optical imaging in vivo: a model of single vessel stroke," *JoVE (Journal of Visualized Experiments)*, no. 100, p. e52794, 2015.

[342] S. Kang, Y. Hayashi, M. Bruyns-Haylett, E. Delivopoulos, and Y. Zheng, "Model-predicted balance between neural excitation and inhibition was maintained despite of age-related decline in sensory evoked local field potential in rat barrel cortex," *Frontiers in Systems Neuroscience*, vol. 14, p. 24, 2020.

[343] G. Paxinos *et al.*, *Paxinos and Franklin's the mouse brain in stereotaxic coordinates*. Elsevier/Academic Press Boston, 2013.

[344] R. J. Mullen, C. R. Buck, and A. M. Smith, "Neun, a neuronal specific nuclear protein in vertebrates," *Development*, vol. 116, no. 1, pp. 201–211, 1992.

[345] H. K. Wolf, R. Buslei, R. Schmidt-Kastner, P. K. Schmidt-Kastner, T. Pietsch, O. D. Wiestler, and I. Blümcke, "Neun: a useful neuronal marker for diagnostic histopathology.," *Journal of Histochemistry & Cytochemistry*, vol. 44, no. 10, pp. 1167–1171, 1996.

[346] P. Welch, "The use of fast fourier transform for the estimation of power spectra: a method based on time averaging over short, modified periodograms," *IEEE Transactions on audio and electroacoustics*, vol. 15, no. 2, pp. 70–73, 1967.

[347] C. A. Schneider, W. S. Rasband, and K. W. Eliceiri, "Nih image to imagej: 25 years of image analysis," *Nature methods*, vol. 9, no. 7, pp. 671–675, 2012.

[348] T. Ridler, S. Calvard, *et al.*, "Picture thresholding using an iterative selection method," *IEEE trans syst Man Cybern*, vol. 8, no. 8, pp. 630–632, 1978.

[349] P. Barthó, A. Slézia, F. Mátyás, L. Faradzs-Zade, I. Ulbert, K. D. Harris, and L. Acsády, "Ongoing network state controls the length of sleep spindles via inhibitory activity," *Neuron*, vol. 82, no. 6, pp. 1367–1379, 2014.

[350] L. Q. Uddin, "Bring the noise: reconceptualizing spontaneous neural activity," *Trends in Cognitive Sciences*, 2020.

[351] I. Ünal-Çevik, M. Kılınç, Y. Gürsoy-Özdemir, G. Gurer, and T. Dalkara, "Loss of neun immunoreactivity after cerebral ischemia does not indicate neuronal cell loss: a cautionary note," *Brain research*, vol. 1015, no. 1-2, pp. 169–174, 2004.

[352] A. Sobolewski, E. Kublik, D. A. Swiejkowski, J. Kamiński, and A. Wróbel, "Alertness opens the effective flow of sensory information through rat thalamic posterior nucleus," *European Journal of Neuroscience*, vol. 41, no. 10, pp. 1321–1331, 2015.

[353] Y. Son, "Molecular mechanisms of general anesthesia," *Korean journal of anesthesiology*, vol. 59, no. 1, pp. 3–8, 2010.

[354] P. Arhem, G. Klement, and J. Nilsson, "Mechanisms of anesthesia: towards integrating network, cellular, and molecular level modeling," *Neuropsychopharmacology*, vol. 28, no. 1, p. S40, 2003.

[355] A. Li, L. Zhang, M. Liu, L. Gong, Q. Liu, and F. Xu, "Effects of different anesthetics on oscillations in the rat olfactory bulb," *Journal of the American Association for Laboratory Animal Science*, vol. 51, no. 4, pp. 458–463, 2012.

[356] C. J. Lobb, A. K. Zaheer, Y. Smith, and D. Jaeger, "In vivo electrophysiology of nigral and thalamic neurons in alpha-synuclein-overexpressing mice highlights differences from toxin-based models of parkinsonism," *Journal of neurophysiology*, vol. 110, no. 12, pp. 2792–2805, 2013.

[357] C. De Kock, R. M. Bruno, H. Spors, and B. Sakmann, "Layer-and cell-type-specific suprathreshold stimulus representation in rat primary somatosensory cortex," *The Journal of physiology*, vol. 581, no. 1, pp. 139–154, 2007.

[358] J. MacDonald, Z. Miljkovic, and P. Pennefather, "Use-dependent block of excitatory amino acid currents in cultured neurons by ketamine," *Journal of neurophysiology*, vol. 58, no. 2, pp. 251–266, 1987.

[359] N. Anis, S. Berry, N. Burton, and D. Lodge, "The dissociative anaesthetics, ketamine and phencyclidine, selectively reduce excitation of central mammalian neurones by n-methyl-aspartate," *British journal of pharmacology*, vol. 79, no. 2, pp. 565–575, 1983.

[360] Z. Xiong, L. Chang, Y. Qu, Y. Pu, S. Wang, Y. Fujita, T. Ishima, J. Chen, and K. Hashimoto, "Neuronal brain injury after cerebral ischemic stroke is ameliorated after subsequent administration of (r)-ketamine, but not (s)-ketamine," *Pharmacology Biochemistry and Behavior*, vol. 191, p. 172904, 2020.

[361] J. D. Bell, "In vogue: ketamine for neuroprotection in acute neurologic injury," *Anesthesia & Analgesia*, vol. 124, no. 4, pp. 1237–1243, 2017.

[362] M. Gerke, A. Duggan, L. Xu, and P. Siddall, "Thalamic neuronal activity in rats with mechanical allodynia following contusive spinal cord injury," *Neuroscience*, vol. 117, no. 3, pp. 715–722, 2003.

[363] L. Liang and L. M. Mendell, "Bilateral transient changes in thalamic nucleus ventroposterior lateralis after thoracic hemisection in the rat," *Journal of neurophysiology*, vol. 110, no. 4, pp. 942–951, 2013.

[364] R. Patel and A. H. Dickenson, "Neuronal hyperexcitability in the ventral posterior thalamus of neuropathic rats: modality selective effects of pregabalin," *Journal of neurophysiology*, vol. 116, no. 1, pp. 159–170, 2016.

[365] L. K. Ong, Z. Zhao, M. Kluge, F. R. Walker, and M. Nilsson, "Chronic stress exposure following photothrombotic stroke is associated with increased levels of amyloid beta accumulation and altered oligomerisation at sites of thalamic secondary neurodegeneration in mice," *Journal of Cerebral Blood Flow & Metabolism*, vol. 37, no. 4, pp. 1338–1348, 2017.

[366] L. T. McPhail, C. B. McBride, J. McGraw, J. D. Steeves, and W. Tetzlaff, "Axotomy abolishes neun expression in facial but not rubrospinal neurons," *Experimental neurology*, vol. 185, no. 1, pp. 182–190, 2004.

[367] L. D. F. Moon, "Chromatolysis: Do injured axons regenerate poorly when ribonucleases attack rough endoplasmic reticulum, ribosomes and rna?," *Developmental neurobiology*, vol. 78, no. 10, pp. 1011–1024, 2018.

[368] S. Sanchez-Bezanilla, N. D. Åberg, P. Crock, F. R. Walker, M. Nilsson, J. Isgaard, and L. K. Ong, "Growth hormone promotes motor function after experimental stroke and enhances recovery-promoting mechanisms within the peri-infarct area," *International journal of molecular sciences*, vol. 21, no. 2, p. 606, 2020.

[369] S. Sanchez-Bezanilla, N. D. Åberg, P. Crock, F. R. Walker, M. Nilsson, J. Isgaard, and L. K. Ong, "Growth hormone treatment promotes remote hippocampal plasticity after experimental cortical stroke," *International journal of molecular sciences*, vol. 21, no. 12, p. 4563, 2020.

[370] Y. Sakurai and S. Takahashi, "Dynamic synchrony of firing in the monkey prefrontal cortex during working-memory tasks," vol. 26, no. 40, pp. 10141–10153.

[371] R. Q. Quiroga, Z. Nadasdy, and Y. Ben-Shaul, "Unsupervised spike detection and sorting with wavelets and superparamagnetic clustering," vol. 16, no. 8, pp. 1661–1687.

[372] U. Rutishauser, E. M. Schuman, and A. N. Mamelak, "Online detection and sorting of extracellularly recorded action potentials in human medial temporal lobe recordings, in vivo," vol. 154, no. 1-2, pp. 204–224.

[373] J. H. Choi, H. K. Jung, and T. Kim, "A new action potential detector using the mteo and its effects on spike sorting systems at low signal-to-noise ratios," vol. 53, no. 4, pp. 738–746.

[374] S. Mukhopadhyay and G. Ray, "A new interpretation of nonlinear energy operator and its efficacy in spike detection," vol. 45, no. 2, pp. 180–187.

[375] S. N. Gozani and J. P. Miller, "Optimal discrimination and classification of neuronal action potential waveforms from multiunit, multichannel recordings using software-based linear filters," vol. 41, no. 4, pp. 358–372.

[376] S. Kim and J. McNames, "Automatic spike detection based on adaptive template matching for extracellular neural recordings," vol. 165, no. 2, pp. 165–174.

[377] F. Franke, M. Natora, C. Boucsein, M. H. J. Munk, and K. Obermayer, "An online spike detection and spike classification algorithm capable of instantaneous resolution of overlapping spikes," vol. 29, no. 1-2, pp. 127–148.

[378] F. Franke, R. Q. Quiroga, A. Hierlemann, and K. Obermayer, "Bayes optimal template matching for spike sorting–combining fisher discriminant analysis with optimal filtering," vol. 38, no. 3, pp. 439–459.

[379] N. Mtetwa and L. S. Smith, "Smoothing and thresholding in neuronal spike detection," vol. 69, no. 10-12, pp. 1366–1370.

[380] G. Turin, "An introduction to matched filters," vol. 6, no. 3, pp. 311–329.

[381] A. F. Atiya, "Recognition of multiunit neural signals," vol. 39, no. 7, pp. 723–729.

[382] M. S. Lewicki, "Bayesian modeling and classification of neural signals," in *Advances in Neural Information Processing Systems 6* (J. D. Cowan, G. Tesauro, and J. Alspector, eds.), pp. 590–597, Morgan-Kaufmann.

[383] C. Ekanadham, D. Tranchina, and E. P. Simoncelli, "A unified framework and method for automatic neural spike identification," vol. 222, pp. 47–55.

[384] J. S. Prentice, J. Homann, K. D. Simmons, G. Tkačik, V. Balasubramanian, and P. C. Nelson, "Fast, scalable, bayesian spike identification for multi-electrode arrays," vol. 6, no. 7.

[385] J. W. Pillow, J. Shlens, E. Chichilnisky, and E. P. Simoncelli, "A model-based spike sorting algorithm for removing correlation artifacts in multi-neuron recordings," vol. 8, no. 5.

[386] Y. Mokri, R. F. Salazar, B. Goodell, J. Baker, C. M. Gray, and S.-C. Yen, "Sorting overlapping spike waveforms from electrode and tetrode recordings," vol. 11, p. 53.

[387] M. S. Lewicki, "A review of methods for spike sorting: the detection and classification of neural action potentials," vol. 9, no. 4, pp. R53–R78.

[388] P.-M. Zhang, J.-Y. Wu, Y. Zhou, P.-J. Liang, and J.-Q. Yuan, "Spike sorting based on automatic template reconstruction with a partial solution to the overlapping problem," vol. 135, no. 1-2, pp. 55–65.

[389] D. Donoho, M. Elad, and V. Temlyakov, "Stable recovery of sparse overcomplete representations in the presence of noise," vol. 52, no. 1, pp. 6–18.

[390] C. Herzet, A. Dremeau, and C. Soussen, "Relaxed recovery conditions for OMP/OLS by exploiting both coherence and decay," vol. 62, no. 1, pp. 459–470.

[391] K. Schnass, "Average performance of orthogonal matching pursuit (OMP) for sparse approximation," vol. 25, no. 12, pp. 1865–1869.

[392] Y. C. Pati, R. Rezaiifar, and P. S. Krishnaprasad, "Orthogonal matching pursuit: recursive function approximation with applications to wavelet decomposition," in *Proceedings of 27th Asilomar Conference on Signals, Systems and Computers*, IEEE Comput. Soc. Press.

[393] S. Chen, S. A. Billings, and W. Luo, "Orthogonal least squares methods and their application to non-linear system identification," vol. 50, no. 5, pp. 1873–1896.

[394] R. A. Delgado and R. H. Middleton, "Sparse representation using stepwise Tikhonov regularization with offline computations," vol. 26, no. 6, pp. 873–877.

[395] B. L. Sturm and M. G. Christensen, "Comparison of orthogonal matching pursuit implementations," in *2012 Proceedings of the 20th European Signal Processing Conference (EUSIPCO)*, pp. 220–224.

[396] I. Obeid and P. D. Wolf, "Evaluation of spike-detection algorithms fora brain-machine interface application," vol. 51, no. 6, pp. 905–911.

[397] J. Martinez, C. Pedreira, M. J. Ison, and R. Q. Quiroga, "Realistic simulation of extracellular recordings," vol. 184, no. 2, pp. 285–293.

[398] L. A. Camuñas-Mesa and R. Q. Quiroga, "A detailed and fast model of extracellular recordings," vol. 25, no. 5, pp. 1191–1212.

[399] D. Heeger, "Poisson model of spike generation," vol. 5, pp. 1–13.

[400] M. Falk, "A simple approach to the generation of uniformly distributed random variables with prescribed correlations," vol. 28, no. 3, pp. 785–791.

[401] M. K. Hosain, A. Kouzani, and S. Tye, "Closed loop deep brain stimulation: an evolving technology," *Australasian physical & engineering sciences in medicine*, vol. 37, no. 4, pp. 619–634, 2014.

[402] M. Parastarfeizabadi and A. Z. Kouzani, "Advances in closed-loop deep brain stimulation devices," *Journal of neuroengineering and rehabilitation*, vol. 14, no. 1, p. 79, 2017.

[403] G. Buzsáki, "Large-scale recording of neuronal ensembles," vol. 7, no. 5, pp. 446–451.

[404] J.-O. Muthmann, H. Amin, E. Sernagor, A. Maccione, D. Panas, L. Berdondini, U. S. Bhalla, and M. H. Hennig, "Spike detection for large neural populations using high density multielectrode arrays," vol. 9, p. 28.

[405] V. R. Muddapu, A. Mandali, V. S. Chakravarthy, and S. Ramaswamy, "A computational model of loss of dopaminergic cells in parkinson's disease due to glutamate-induced excitotoxicity," *Frontiers in neural circuits*, vol. 13, p. 11, 2019.

[406] V. R. Muddapu and V. S. Chakravarthy, "A multi-scale computational model of excitotoxic loss of dopaminergic cells in parkinson's disease," *Frontiers in Neuroinformatics*, vol. 14, 2020.

[407] S. Sahai, E. T. Effendi, E. C. Mahoney, H. R. Tucker, B. J. Moolick, G. Mamone, S. Mikkilineni, M. Gupta, A. Nicholson, F. Y. Chua, *et al.*, "Effects of subthalamic nucleus deep brain stimulation on neuronal spiking activity in the substantia nigra pars compacta in a rat model of parkinson's disease," *Neuroscience Letters*, vol. 739, p. 135443, 2020.

[408] J. K. Muir, D. Lobner, H. Monyer, and D. W. Choi, "Gabaa receptor activation attenuates excitotoxicity but exacerbates oxygen-glucose deprivation-induced neuronal injury in vitro," *Journal of Cerebral Blood Flow & Metabolism*, vol. 16, no. 6, pp. 1211–1218, 1996.

[409] M. D. Ginsberg, "Neuroprotection for ischemic stroke: past, present and future," *Neuropharmacology*, vol. 55, no. 3, pp. 363–389, 2008.

[410] C.-M. Gerardo and M.-M. V. Manuel, "The thalamic reticular nucleus: A common nucleus of neuropsychiatric diseases and deep brain stimulation," *Journal of Clinical Neuroscience*, vol. 73, pp. 1–7, 2020.

[411] V. M. Magdaleno-Madrigal, G. Contreras-Murillo, I. Camacho-Abrego, J. V. Negrete-Díaz, A. Valdés-Cruz, R. Fernández-Mas, S. Almazán-Alvarado, and G. Flores, "Short-term deep brain stimulation of the thalamic reticular nucleus modifies aberrant oscillatory activity in a neurodevelopment model of schizophrenia," *Neuroscience*, vol. 357, pp. 99–109, 2017.

[412] S. Thankachan, F. Katsuki, J. T. McKenna, C. Yang, C. Shukla, K. Deisseroth, D. S. Uygun, R. E. Strecker, R. E. Brown, J. M. McNally, *et al.*, "Thalamic reticular nucleus parvalbumin neurons regulate sleep spindles and electrophysiological aspects of schizophrenia in mice," *Scientific reports*, vol. 9, no. 1, pp. 1–16, 2019.

[413] L. D. Lewis, J. Voigts, F. J. Flores, L. I. Schmitt, M. A. Wilson, M. M. Halassa, and E. N. Brown, "Thalamic reticular nucleus induces fast and local modulation of arousal state," *elife*, vol. 4, p. e08760, 2015.

[414] K.-M. Ni, X.-J. Hou, C.-H. Yang, P. Dong, Y. Li, Y. Zhang, P. Jiang, D. K. Berg, S. Duan, and X.-M. Li, "Selectively driving cholinergic fibers optically in the thalamic reticular nucleus promotes sleep," *elife*, vol. 5, p. e10382, 2016.

[415] Z. I. Nanobashvili, A. G. Surmava, I. G. Bilanishvili, M. G. Barbaqadze, M. D. Mariamidze, and N. A. Khizanishvili, "Significance of the thalamic reticular nucleus gabaergic neurons in normal and pathological activity of the brain," *J Behav Brain Sci*, vol. 2, pp. 436–444, 2012.

[416] A. N. Clarkson, B. S. Huang, S. E. MacIsaac, I. Mody, and S. T. Carmichael, "Reducing excessive gaba-mediated tonic inhibition promotes functional recovery after stroke," *Nature*, vol. 468, no. 7321, pp. 305–309, 2010.

[417] M. Ghorbani, P. Shahabi, P. Karimi, H. Soltani-Zangbar, M. Morshedi, S. Bani, M. Jafarzadehgharehziaaddin, B. Sadeghzadeh-Oskouei, and A. Ahmadalipour, "Impacts of epidural electrical stimulation on wnt signaling, faah, and bdnf following thoracic spinal cord injury in rat," *Journal of Cellular Physiology*, vol. 235, no. 12, pp. 9795–9805, 2020.

[418] K. Faust, P. Vajkoczy, B. Xi, and D. Harnack, "The effects of deep brain stimulation of the subthalamic nucleus on vascular endothelial growth factor, brain-derived neurotrophic factor, and glial cell line-derived neurotrophic factor in a rat model of parkinson's disease," *Stereotactic and Functional Neurosurgery*, vol. 99, no. 3, pp. 256–266, 2021.

[419] T. Morimoto, H. Kanda, M. Kondo, H. Terasaki, K. Nishida, and T. Fujikado, "Transcorneal electrical stimulation promotes survival of photoreceptors and improves retinal function in rhodopsin p347l transgenic rabbits," *Investigative ophthalmology & visual science*, vol. 53, no. 7, pp. 4254–4261, 2012.

[420] A. A. Al-Majed, C. M. Neumann, T. M. Brushart, and T. Gordon, "Brief electrical stimulation promotes the speed and accuracy of motor axonal regeneration," *Journal of Neuroscience*, vol. 20, no. 7, pp. 2602–2608, 2000.

[421] C. C. McIntyre and W. M. Grill, "Extracellular stimulation of central neurons: Influence of stimulus waveform and frequency on neuronal output," *Journal of Neurophysiology*, vol. 88, no. 4, pp. 1592–1604, 2002.

[422] K. L. Schaar, M. M. Brenneman, and S. I. Savitz, "Functional assessments in the rodent stroke model," *Experimental & translational stroke medicine*, vol. 2, no. 1, pp. 1–11, 2010.

[423] J. W. Salatino, K. A. Ludwig, T. D. Kozai, and E. K. Purcell, "Glial responses to implanted electrodes in the brain," *Nature biomedical engineering*, vol. 1, no. 11, pp. 862–877, 2017.

[424] V. Sankar, E. Patrick, R. Dieme, J. C. Sanchez, A. Prasad, and T. Nishida, "Electrode impedance analysis of chronic tungsten microwire neural implants: understanding abiotic vs. biotic contributions," *Frontiers in neuroengineering*, vol. 7, p. 13, 2014.

[425] R. Cubo and A. Medvedev, "Accuracy of the finite element method in deep brain stimulation modelling," in *Control Applications (CCA), 2014 IEEE Conference on*, pp. 1479–1484, IEEE, 2014.

[426] A.-K. Gellner, J. Reis, and B. Fritsch, "Glia: a neglected player in non-invasive direct current brain stimulation," *Frontiers in cellular neuroscience*, vol. 10, p. 188, 2016.

[427] A. Roitbak and V. Fanardjian, "Depolarization of cortical glial cells in response to electrical stimulation of the cortical surface," *Neuroscience*, vol. 6, no. 12, pp. 2529–2537, 1981.

[428] P. T. Doughty, I. Hossain, C. Gong, K. A. Ponder, S. Pati, P. U. Arumugam, and T. A. Murray, "Novel microwire-based biosensor probe for simultaneous real-time measurement of glutamate and gaba dynamics in vitro and in vivo," *Scientific reports*, vol. 10, no. 1, pp. 1–19, 2020.

[429] F. Francis, *Pacemaking Neurons in the study of Parkinson's Disease*. PhD thesis, National University of Ireland Maynooth, 2012.

[430] A. L. Wright and B. Vissel, "The essential role of ampa receptor glur2 subunit rna editing in the normal and diseased brain," *Frontiers in molecular neuroscience*, vol. 5, p. 34, 2012.

[431] R. Spreafico, C. Frassoni, P. Arcelli, G. Battaglia, R. Wenthold, and S. De Biasi, "Distribution of ampa selective glutamate receptors in the thalamus of adult rats and during postnatal development. a light and ultrastructural immunocytochemical study," *Developmental brain research*, vol. 82, no. 1-2, pp. 231–244, 1994.

[432] E. Mineff and R. Weinberg, "Differential synaptic distribution of ampa receptor subunits in the ventral posterior and reticular thalamic nuclei of the rat," *Neuroscience*, vol. 101, no. 4, pp. 969–982, 2000.

[433] M. Marhl, T. Haberichter, M. Brumen, and R. Heinrich, "Complex calcium oscillations and the role of mitochondria and cytosolic proteins," *Biosystems*, vol. 57, no. 2, pp. 75–86, 2000.

[434] A. Z. Harris and D. L. Pettit, "Extrasynaptic and synaptic nmda receptors form stable and uniform pools in rat hippocampal slices," *The Journal of physiology*, vol. 584, no. 2, pp. 509–519, 2007.

[435] O. Warr, M. Takahashi, and D. Attwell, "Modulation of extracellular glutamate concentration in rat brain slices by cystine-glutamate exchange," *The Journal of physiology*, vol. 514, no. 3, pp. 783–793, 1999.

[436] S. Pendyam, A. Mohan, P. Kalivas, and S. Nair, "Computational model of extracellular glutamate in the nucleus accumbens incorporates neuroadaptations by chronic cocaine," *Neuroscience*, vol. 158, no. 4, pp. 1266–1276, 2009.

[437] V. Parpura and P. G. Haydon, "Physiological astrocytic calcium levels stimulate glutamate release to modulate adjacent neurons," *Proceedings of the National Academy of Sciences*, vol. 97, no. 15, pp. 8629–8634, 2000.

[438] N. B. Hamilton and D. Attwell, "Do astrocytes really exocytose neurotransmitters?," *Nature Reviews Neuroscience*, vol. 11, no. 4, pp. 227–238, 2010.

[439] B. Flanagan, L. McDaid, J. Wade, K. Wong-Lin, and J. Harkin, "A computational study of astrocytic glutamate influence on post-synaptic neuronal excitability," *PLoS computational biology*, vol. 14, no. 4, p. e1006040, 2018.

[440] J. Li, J. Tang, J. Ma, M. Du, R. Wang, and Y. Wu, "Dynamic transition of neuronal firing induced by abnormal astrocytic glutamate oscillation," *Scientific reports*, vol. 6, no. 1, pp. 1–10, 2016.

[441] A. N. Silchenko and P. A. Tass, "Computational modeling of paroxysmal depolarization shifts in neurons induced by the glutamate release from astrocytes," *Biological Cybernetics*, vol. 98, no. 1, pp. 61–74, 2008.

[442] Q.-p. Dong, J.-q. He, and Z. Chai, "Astrocytic ca2+ waves mediate activation of extrasynaptic nmda receptors in hippocampal neurons to aggravate brain damage during ischemia," *Neurobiology of Disease*, vol. 58, pp. 68–75, 2013.

[443] M. Rowan, S. Neymotin, and W. Lytton, "Electrostimulation to reduce synaptic scaling driven progression of alzheimer's disease," *Frontiers in computational neuroscience*, vol. 8, p. 39, 2014.

[444] J. Iglesias and A. E. Villa, "Emergence of preferred firing sequences in large spiking neural networks during simulated neuronal development," *International Journal of Neural Systems*, vol. 18, no. 04, pp. 267–277, 2008.

[445] V. R. Muddapu and V. S. Chakravarthy, "Influence of energy deficiency on the subcellular processes of substantia nigra pars compacta cell for understanding parkinsonian neurodegeneration," *Scientific reports*, vol. 11, no. 1, pp. 1–36, 2021.

[446] L. M. Biga, S. Dawson, A. Harwell, R. Hopkins, J. Kaufmann, M. LeMaster, P. Matern, K. Morrison-Graham, D. Quick, and J. Runyeon, "Anatomy & physiology," 2020.

[447] B. G. Sanganahalli, P. Herman, D. L. Rothman, H. Blumenfeld, and F. Hyder, "Metabolic demands of neural-hemodynamic associated and disassociated areas in brain," *Journal of Cerebral Blood Flow & Metabolism*, vol. 36, no. 10, pp. 1695–1707, 2016.

[448] M. Faulkner, S. Hannan, K. Aristovich, J. Avery, and D. Holder, "Feasibility of imaging evoked activity throughout the rat brain using electrical impedance tomography," *Neuroimage*, vol. 178, pp. 1–10, 2018.

[449] Y. Uemura, T. Haque, F. Sato, Y. Tsutsumi, H. Ohara, A. Oka, T. Furuta, Y. C. Bae, T. Yamashiro, Y. Tachibana, *et al.*, "Proprioceptive thalamus receiving forelimb and neck muscle spindle inputs via the external cuneate nucleus in the rat," *Brain Structure and Function*, vol. 225, no. 7, pp. 2177–2192, 2020.

[450] K. Alloway, M. Johnson, and M. Wallace, "Thalamocortical interactions in the somatosensory system: interpretations of latency and cross-correlation analyses," *Journal of neurophysiology*, vol. 70, no. 3, pp. 892–908, 1993.

[451] L. Li and F. F. Ebner, "Cortical modulation of spatial and angular tuning maps in the rat thalamus," *Journal of Neuroscience*, vol. 27, no. 1, pp. 167–179, 2007.

[452] H. A. Swadlow and A. G. Gusev, "The influence of single vb thalamocortical impulses on barrel columns of rabbit somatosensory cortex," *Journal of Neurophysiology*, vol. 83, no. 5, pp. 2802–2813, 2000.

[453] F. Harris, "Functional subsets of neurons in somatosensory thalamus of the cat," *Experimental neurology*, vol. 58, no. 2, pp. 149–170, 1978.

[454] T. Allison and A. L. Hume, "A comparative analysis of short-latency somatosensory evoked potentials in man, monkey, cat, and rat," *Experimental neurology*, vol. 72, no. 3, pp. 592–611, 1981.

[455] N. M. Branston, A. Ladds, L. Symon, and A. D. Wang, "Comparison of the effects of ischaemia on early components of the somatosensory evoked potential in brainstem, thalamus, and cerebral cortex," *Journal of Cerebral Blood Flow & Metabolism*, vol. 4, no. 1, pp. 68–81, 1984.

[456] A. Ladds, N. Branston, J. Vajda, J. E. McGillicuddy, and L. Symon, "Changes in somatosensory evoked potentials following an experimental focal ischaemic lesion in thalamus," *Electroencephalography and Clinical Neurophysiology/Evoked Potentials Section*, vol. 71, no. 3, pp. 233–240, 1988.

[457] Y. Temel, V. Visser-Vandewalle, M. van der Wolf, G. H. Spincemaille, L. Desbonnet, G. Hoogland, and H. W. Steinbusch, "Monopolar versus bipolar high frequency stimulation in the rat subthalamic nucleus: differences in histological damage," *Neuroscience letters*, vol. 367, no. 1, pp. 92–96, 2004.

[458] C. H. Halpern, M. A. Attiah, A. Tekriwal, and G. H. Baltuch, "A step-wise approach to deep brain stimulation in mice," *Acta neurochirurgica*, vol. 156, no. 8, pp. 1515–1521, 2014.

[459] L. Desbonnet, Y. Temel, V. Visser-Vandewalle, A. Blokland, V. Hornikx, and H. W. Steinbusch, "Premature responding following bilateral stimulation of the rat subthalamic nucleus is amplitude and frequency dependent," *Brain research*, vol. 1008, no. 2, pp. 198–204, 2004.

[460] Y. Temel, V. Visser-Vandewalle, B. Aendekerk, B. Rutten, S. Tan, B. Scholtissen, C. Schmitz, A. Blokland, and H. W. Steinbusch, "Acute and separate modulation of motor and cognitive performance in parkinsonian rats by bilateral stimulation of the subthalamic nucleus," *Experimental neurology*, vol. 193, no. 1, pp. 43–52, 2005.

[461] R. Vlamings, V. Visser-Vandewalle, G. Koopmans, E. Joosten, R. Kozan, S. Kaplan, H. Steinbusch, and Y. Temel, "High frequency stimulation of the subthalamic nucleus improves speed of locomotion but impairs forelimb movement in parkinsonian rats," *Neuroscience*, vol. 148, no. 3, pp. 815–823, 2007.

[462] I. Arrieta-Cruz, C. Pavlides, and G. M. Pasinetti, "Deep brain stimulation facilitates memory in a model of alzheimer's disease," *Translational Neuroscience*, vol. 1, no. 2, pp. 170–176, 2010.

[463] S. K. Tan, R. Vlamings, L. Lim, T. Sesia, M. L. Janssen, H. W. Steinbusch, V. Visser-Vandewalle, and Y. Temel, "Experimental deep brain stimulation in animal models," *Neurosurgery*, vol. 67, no. 4, pp. 1073–1080, 2010.

[464] C. H. Halpern, A. Tekriwal, J. Santollo, J. G. Keating, J. A. Wolf, D. Daniels, and T. L. Bale, "Amelioration of binge eating by nucleus accumbens shell deep brain stimulation in mice involves d2 receptor modulation," *Journal of Neuroscience*, vol. 33, no. 17, pp. 7122–7129, 2013.

[465] W. Doucette, J. Khokhar, and A. Green, "Nucleus accumbens deep brain stimulation in a rat model of binge eating," *Translational psychiatry*, vol. 5, no. 12, pp. e695–e695, 2015.

[466] S. Hao, B. Tang, Z. Wu, K. Ure, Y. Sun, H. Tao, Y. Gao, A. J. Patel, D. J. Curry, R. C. Samaco, *et al.*, "Forniceal deep brain stimulation rescues hippocampal memory in rett syndrome mice," *Nature*, vol. 526, no. 7573, pp. 430–434, 2015.

[467] D. M. Keenan, A. W. Quinkert, and D. W. Pfaff, "Stochastic modeling of mouse motor activity under deep brain stimulation: the extraction of arousal information," *PLoS computational biology*, vol. 11, no. 2, p. e1003883, 2015.

[468] I. Kamali Sarvestani, N. P. Visanji, M. C. Creed, Z. Shams Shoaei, J. Nobrega, C. Hamani, and L.-N. Hazrati, "Deep brain stimulation of the subthalamic nucleus preferentially alters the translational profile of striatopallidal neurons in an animal model of parkinson's disease," *Frontiers in cellular neuroscience*, vol. 9, p. 221, 2015.

[469] J. S. Schor, A. B. Nelson, *et al.*, "Multiple stimulation parameters influence efficacy of deep brain stimulation in parkinsonian mice," *The Journal of clinical investigation*, vol. 129, no. 9, pp. 3833–3838, 2019.

[470] A. M. Brown, J. J. White, M. E. van der Heijden, J. Zhou, T. Lin, and R. V. Sillitoe, "Purkinje cell misfiring generates high-amplitude action tremors that are corrected by cerebellar deep brain stimulation," *Elife*, vol. 9, p. e51928, 2020.

[471] A. A. Rogers, L. M. Aiani, L. T. Blanpain, S. Yuxian, R. Moore, and J. T. Willie, "Deep brain stimulation of hypothalamus for narcolepsy-cataplexy in mice," *Brain stimulation*, vol. 13, no. 5, pp. 1305–1316, 2020.

[472] F. Xia, A. Yiu, S. S. Stone, S. Oh, A. M. Lozano, S. A. Josselyn, and P. W. Frankland, "Entorhinal cortical deep brain stimulation rescues memory deficits in both young and old mice genetically engineered to model alzheimer's disease," *Neuropsychopharmacology*, vol. 42, no. 13, pp. 2493–2503, 2017.

[473] A. Mann, E. Gondard, D. Tampellini, J. A. Milsted, D. Marillac, C. Hamani, S. K. Kalia, and A. M. Lozano, "Chronic deep brain stimulation in an alzheimer's disease mouse model enhances memory and reduces pathological hallmarks," *Brain stimulation*, vol. 11, no. 2, pp. 435–444, 2018.

[474] A. E. Pohodich, H. Yalamanchili, A. T. Raman, Y.-W. Wan, M. Gundry, S. Hao, H. Jin, J. Tang, Z. Liu, and H. Y. Zoghbi, "Forniceal deep brain stimulation induces gene expression and splicing changes that promote neurogenesis and plasticity," *Elife*, vol. 7, p. e34031, 2018.

[475] M. Jeffrey, M. Lang, J. Gane, C. Wu, W. M. Burnham, and L. Zhang, "A reliable method for intracranial electrode implantation and chronic electrical stimulation in the mouse brain," *BMC neuroscience*, vol. 14, no. 1, pp. 1–8, 2013.

[476] Y. Wang, J. Liang, C. Xu, Y. Wang, Y. Kuang, Z. Xu, Y. Guo, S. Wang, F. Gao, and Z. Chen, "Low-frequency stimulation in anterior nucleus of thalamus alleviates kainate-induced chronic

epilepsy and modulates the hippocampal eeg rhythm," *Experimental neurology*, vol. 276, pp. 22–30, 2016.

[477] H. Miyamoto, T. Tatsukawa, A. Shimohata, T. Yamagata, T. Suzuki, K. Amano, E. Mazaki, M. Raveau, I. Ogiwara, A. Oba-Asaka, *et al.*, "Impaired cortico-striatal excitatory transmission triggers epilepsy," *Nature communications*, vol. 10, no. 1, pp. 1–13, 2019.

[478] A. Berényi, M. Belluscio, D. Mao, and G. Buzsáki, "Closed-loop control of epilepsy by transcranial electrical stimulation," *Science*, vol. 337, no. 6095, pp. 735–737, 2012.

[479] S. Little and P. Brown, "What brain signals are suitable for feedback control of deep brain stimulation in parkinson's disease?," *Annals of the New York Academy of Sciences*, vol. 1265, no. 1, pp. 9–24, 2012.

[480] A. A. Kühn, F. Kempf, C. Brücke, L. G. Doyle, I. Martinez-Torres, A. Pogosyan, T. Trottenberg, A. Kupsch, G.-H. Schneider, M. I. Hariz, *et al.*, "High-frequency stimulation of the subthalamic nucleus suppresses oscillatory β activity in patients with parkinson's disease in parallel with improvement in motor performance," *Journal of Neuroscience*, vol. 28, no. 24, pp. 6165–6173, 2008.

[481] S. Little, A. Pogosyan, S. Neal, B. Zavala, L. Zrinzo, M. Hariz, T. Foltynie, P. Limousin, K. Ashkan, J. FitzGerald, *et al.*, "Adaptive deep brain stimulation in advanced parkinson disease," *Annals of neurology*, vol. 74, no. 3, pp. 449–457, 2013.

[482] B. Rosin, M. Slovik, R. Mitelman, M. Rivlin-Etzion, S. N. Haber, Z. Israel, E. Vaadia, and H. Bergman, "Closed-loop deep brain stimulation is superior in ameliorating parkinsonism," *Neuron*, vol. 72, no. 2, pp. 370–384, 2011.

[483] M. Rosa, M. Arlotti, G. Ardolino, F. Cogiamanian, S. Marceglia, A. Di Fonzo, F. Cortese, P. M. Rampini, and A. Priori, "Adaptive deep brain stimulation in a freely moving parkinsonian patient," *Movement Disorders*, vol. 30, no. 7, pp. 1003–1005, 2015.

[484] I. Osorio, M. G. Frei, S. Sunderam, J. Giftakis, N. C. Bhavaraju, S. F. Schaffner, and S. B. Wilkinson, "Automated seizure abatement in humans using electrical stimulation," *Annals of neurology*, vol. 57, no. 2, pp. 258–268, 2005.

[485] E. H. Kossoff, E. K. Ritzl, J. M. Politsky, A. M. Murro, J. R. Smith, R. B. Duckrow, D. D. Spencer, and G. K. Bergey, "Effect of an external responsive neurostimulator on seizures and electrographic discharges during subdural electrode monitoring," *Epilepsia*, vol. 45, no. 12, pp. 1560–1567, 2004.

[486] L. B. Good, S. Sabesan, S. T. Marsh, K. Tsakalis, D. Treiman, and L. Iasemidis, "Control of synchronization of brain dynamics leads to control of epileptic seizures in rodents," *International journal of neural systems*, vol. 19, no. 03, pp. 173–196, 2009.

[487] P. Andersen, J. Eccles, R. Schmidt, and T. Yokota, "Slow potential waves produced in the cuneate nucleus by cutaneous volleys and by cortical stimulation," *Journal of neurophysiology*, vol. 27, no. 1, pp. 78–91, 1964.

[488] P. Andersen, J. Eccles, R. Schmidt, and T. Yokota, "Depolarization of presynaptic fibers in the cuneate nucleus," *Journal of neurophysiology*, vol. 27, no. 1, pp. 92–106, 1964.

[489] F. Bengtsson, R. Brasselet, R. S. Johansson, A. Arleo, and H. Jörntell, "Integration of sensory quanta in cuneate nucleus neurons in vivo," *PloS one*, vol. 8, no. 2, p. e56630, 2013.

Appendix A

Additional Background

A.1 EEG Frequency Bands

Frequency bands from EEG recordings are classified as having particular physiological significance [28], described in Table A.1. Slight discrepancies in the frequency ranges and combining of bands is common in literature, therefore this thesis uses the definitions given below.

Table A.1: Frequency Band Classifications of Brain Activity

Name	**Frequency (Hz)**	**Description**
Delta (δ)	< 4	Slow-Wave Sleep (non-REM)
Theta (θ)	4 - 8	Idling, Arousal/Drowsiness
Alpha (α)	8 - 12	Awake - Resting State Activity
Beta (β)	12 - 32	Active Thinking & Motor Function
Gamma (γ)	32+	Somatosensory & Higher-Order Cognitive Function

A.2 Somatosensory Pathway

The somatosensory pathway relays sensory signals, transduced from receptors in the peripheral nervous system, to the corresponding area of the cortex. Neurons in this pathway are classified based on their order in the transmission sequence. First-order neurons are the sensory neurons located in the peripheries with cell bodies in the dorsal root ganglion. Second-order neurons relay the signal from the first-order (sensory) neurons to the thalamus and finally the third order neurons are the thalamocortical neurons that relay the signal to the cortex.

There exist two distinct routes that transmit touch and proprioceptive or nociceptive signals. The first is known as the medial lemniscal path whose first-order sensory neurons travel up the spinal cord and synapse in the dorsal column nuclei, and in particular the cuneate or gracile nucleus for forelimb and hindlimb signals respectively. The second order neurons decussate accross the spinal cord and project to the thalamus, and are known as the medial lemniscal fibres. The second path is via the spinothalamic tract. First order neurons in this pathway synapse directly at the spinal cord to second order neurons that decussate and project directly to the thalamus. A depiction of these pathways are shown in Figure A.1.

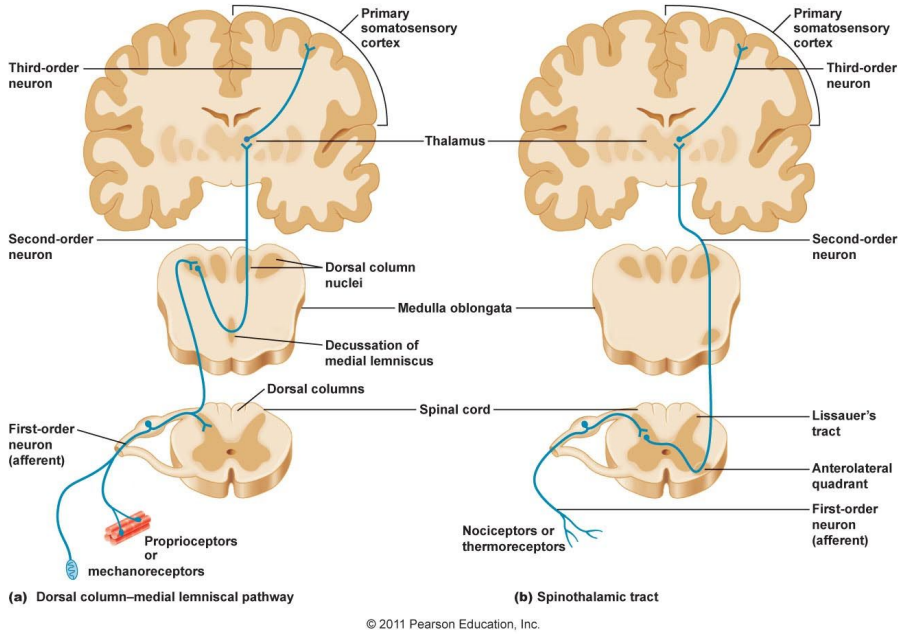

Figure A.1: A depiction of the somatosensory pathway showing the two distinct systems: medial lemniscal pathway for touch receptors and the spinothalamic tract for nociceptors. (Image from Biga *et al.* [446] - available under CC BY-SA 4.0)

A.3 Tabulated Thalamic SSEP Latencies

Table A.2: Latencies of SSEPs recorded in the VB Thalamus

Species	Nuclei	Stim Location	Latency [ms]	Signal Type	Anaesthesia	Note	Author
Rat	VB (VPL)	Wrist - Elec Wrist - Mech	4.5 6.6	Unit	Urethane	-	Angel *et al.* 1975 [289]
Rat	VPL	Forepaw - Elec	7.1	Unit	Choral Hydrate	-	Tokuno *et al.* 1992 [336]
Rat	VPL VPM	Forepaw - Mech Hindpaw - Mech Whisker - Mech	6.8 11.2 4.5	Unit	Pentobarbital or Urethane	-	Aguilar *et al.* 2008 [36]
Rat	VPL	Forepaw - Elec	3.8 (Onset)	MUA	α-Cholarose	-	Sanganahalli *et al.* 2016 [447]
Rat	VPL	Forepaw - Elec	7.3	LFP	α-Cholarose	Positive LFP Peak	Faulkner *et al.* 2018 [448]
Rat	VPL	Forepaw - Elec Hindpaw - Elec	$\sim$ 5-7 $\sim$8-9	LFP + MUA	Urethane	Negative LFP Peak + Late Latency Response	Alonso-Calvino *et al.* 2016 [293]
Rat	VPL	Median Nerve	4.1	LFP	Ketamine/Xylazine	Negative LFP Peak	Uemura *et al.* 2020 [449]
Rat	VPL	Hindpaw - Air Puff	12.5	Unit	Halothane	-	Alloway *et al.* 1993 [450]
Rat	VPM	Whisker - Mech	4.3	LFP	Fentanyl (Light)	Negative LFP Peak + Late Latency Response	Temereanca *et al.* 2003 [294]
Rat	VPM	Whisker - Mech	$\sim$ 6-7	LFP	Fentanyl (Light)	Negative LFP Peak + Late Latency Response	Temereanca *et al.* 2004 [295]
Rat	VPM	Whisker - Mech	$\sim$ 6	Unit	Urethane		Li *et al.* 2007 [451]
Rat	VPM POm	Whisker - Mech	6.0 15.3	Unit	Urethane		Diamond *et al.* 1992 [339]
Rat	VPM TRN	Whisker - Mech	5 9-14	Unit	-	+ Late Latency Response	Hirai *et al.* 2017 [115]
Rat	VPM	Whisker - Mech	3-7	Unit	Urethane		Castro-Alamancos *et al.* 2002 [302]
Rabbit	VPM	Whisker - Mech	$\sim$ 6	Unit	-		Swadlow *et al.* 2000 [452]
Cat	VPL	Forepaw - Elec	7.9	Unit	α-Cholarose	-	Harris *et al.* 1978 [453]
Cat	VPL	Median Nerve	7	LFP	Pentobarbital	Negative LFP Peak	Allison *et al.* 1981 [454]

Baboon	VPL	Median Nerve	8.68	LFP	α-Cholarose	Postitive LFP Peak	Branston *et al.* 1984 [455]
Baboon	VPL	Median Nerve	$\sim$10	LFP	α-Cholarose	Postitive LFP Peak	Ladds *et al.* 1988 [456]

A.4 Rodent DBS Applications

Table A.4: DBS use in Rodent Models

Species	Target	Electrode (Contact Size)	Parameters	Application	Note	Author
Rat	STN	Mono+Bipolar (200 µm)	300 µA	Assess Stimulation Damage	Bipolar = significant damage	[457]
Rat	NAc	Bipolar (75 µm)	75-100 µA 60-90 µs 130-160Hz	Obesity		[458]
Rat	STN	Bipolar (50 µm)	3,30,150 µA 60, 120 µs 30-130Hz	PD		[459]
Rat	STN	Bipolar (50 µm)	1,3,30,150 µA 60 µs 130Hz	PD		[460]
Rat	STN	Bipolar (50 µm)	0,3,30,150 µA 60 µs 130Hz	PD		[461]
Mouse	MTN (Thal)	Bipolar (100 µm)	300 µA 25Hz	Alzheimers		[462]
Rat	STN	Concentric Bipolar (50 µm)		PD	≥200µA = damage	[463]
Mouse	NAc	Bipolar	75,150 µA 60 µs 160Hz	Obesity		[464]
Rat	NAc	Bipolar*	150 µA 60 µs 150Hz	Obesity		[465]

Mouse	Fornix	Bipolar (50 µm)	60 µs 130Hz	Memory	1hr/day for 14 days	[466]
Mouse	Central Thalamus	Monopolar (300 µm)	75,100,125 µA 100 µs 50,125,175,225Hz	Motor Activity		[467]
Mouse	STN	Monopolar (125 µm)	100 µA 90 µs 130 Hz	PD	4hrs/day for 5 days	[468]
Mouse	NAc	Custom Array	100 µA 90 µs 130 Hz	Obesity		[59]
Mouse	STN	Bipolar (72.5 µm)	200 µA 60 µs 120 Hz	PD	$>$ 400 µA = occurrence of seizures	[469]
Mouse	Cerebellar	Bipolar* (50 µm)	30 µA 60 µs 125 Hz	ET		[470]
Mouse	Hypothalamus/ZI	Concentric Bipolar	2.5-4V 15-130 Hz	Narcolepsy		[471]
Mouse	Entorhinal Cortex	Concentric Bipolar	90 µs 130 Hz	Alzheimers		[472]
Mouse	Entorhinal Cortex	Concentric Bipolar (100 µm)	50 µA 90 µs 130 Hz	Alzheimers		[473]

Mouse	Fornix	Bipolar	50 µA 60 µs 130 Hz	Neurogenesis (AD)		[474]
Mouse	Hippocampus	Bipolar* (200 µm)	10-150 µA 500 µs	Kindling		[475]
Mouse	ANT (Thal)	Bipolar (125 µm)	300 µA 100 µs 1 Hz	Alleviate Seizures	30min/day for 7 days	[476]
Mouse	CPu	Bipolar (100 µm)	100-200 µA 100-200 µs 0.25 Hz	Induce Seizures		[477]
Rat	LCN	Monopolar (175 µm)	70-130 µA 400 µs 30 Hz	Stroke (Neurogenesis)	8hr/day	[199]
Rat	STN	Monopolar	50 µA 52 µs 130 Hz	PD	+ Increased BDNF	[418]

A.5 Closed Loop DBS

Deep Brain Stimulation has most commonly been used in an open loop configuration, where initial stimulation parameters are set post-operatively and infrequently adjusted by a physician in follow-up consultations [174, 177]. Adjustments include determining the most effective electrode on a multi-unit probe, stimulation amplitude, pulse width and frequency [177].

A number of limitations exist for such an open-loop scheme:

1. Lost efficacy over time, resulting in ineffective treatment for up to months until the next consultation.
2. Time-consuming tuning procedures; requiring a professional clinician that incurs high costs.
3. Potentially inducing side effects through constant stimulation, even when symptoms are not present.

A closed-loop DBS (CLDBS)[1] system uses feedback to determine when stimulation is required and how effective the current treatment is so that parameters can automatically be adjusted and optimised. Closed-looped DBS systems are seeing a rise in popularity [401] as they address many of the limitations of traditionally OL treatment methods:

- Adaptively correct for lost efficacy over time (due to hardware degradation or disease progression) by automatically adjusting stimulation parameters for more effective treatment and reduction of regular consultations.
- Limit potential side-effects by removing stimulation when symptoms are not present.
- Save on battery life[2], reducing the number of battery replacement surgeries that carry the potential to cause complications.
- Individualise and optimise parameters to each patient to most effectively quench the underlying pathology.

The key components required for a closed loop DBS system include: stimulating electrode(s), sensing of physiological biomarker(s) as feedback, a controller and control algorithm [401].

[1] In literature Closed Loop DBS is often referred to as 'Adaptive' DBS (aDBS) and Open Loop as 'Continuous' DBS (cDBS)

[2] Assuming recording & processing power are minimised

A.5.1 Biomarkers

Identifying reliable biomarkers has been one of the greatest obstacles in the progression to closed-loop neuromodulation thus far [402]. It is crucial that a potential biomarker is causal to or a direct result of the underlying pathophysiology of the condition [478, 479].

In terms of neurological disorders, biomarkers are classified as internal i.e. measurements of signals within the brain, or external i.e. measurements from peripheries encompassing detection of symptoms such as movement disorders via accelerometers, EMGs or other wearable sensors [479, 401, 402].

The most commonly used feedback from surgically implanted electrodes are the LFP signals [479, 402], as they provide superior spatiotemporal resolution and are often combined with stimulation from adjacent contacts on the one probe. Alternative internal biomarkers include SUA, surface EEG, ECoG, NIR, fMRI and more recently neurotransmitter microdialysis probes [479, 177, 401, 402]. Biomarkers must be chosen and optimised for each patient as disorders can manifest in different ways [479] and may require multiple biomarkers to sufficiently treat each impairment e.g. in stages of PD, rigidity and tremors show different characteristic activity.

Targeting SND via the underlying pathological activity is imperative as symptoms and degenerative effects take days, weeks or months to present. Pending data collection a robust biomarker will need to be determined from LFP signals. It is hypothesised that the hyperactivity is not as significant as epileptic episodes and therefore a similar but new detection algorithm will be developed. A common trend is shifting towards learning algorithms for biomarker detection [479]

A.5.2 Applications & Control Strategies

Current CLDBS systems are predominately of a simple 'ON/OFF' nature (Reviewed in [402]); detecting pathological activity using various thresholding algorithms and switching on stimulation in response. Recent work has began to adapt an additional parameter, most commonly pulse-amplitude or frequency, linearly with increasing 'error' (Proportional) or observed efficacy throughout the treatment period (Integral) (Reviewed in [402]). A summary of current closed-loop neuromodulation systems is provided in Table A.6.

Epilepsy is the most popular target of recent developments as it is considered a "comparatively simple disorder", characterised by distinct episodes of aberrant brain activity [401] that are easily identified in LFP, EEG and ECoG recordings using Line-Length (LL) or windowed RMS calculations. This allows the trigger for stimulation and effectiveness of treatment to be readily assessed and adapted to by the controller.

Table A.6: Closed Loop DBS System Review

Disorder	Input / Output	Control Strategy	Effectiveness	Author
PD	STN / STN	Trigger HFS on LFP β-band crossing individualised threshold. Stimulus sustained until β-amplitude dropped below threshold	27% improvement of motor scores over cDBS 56% reduction in stimulation time	Little et al. [481]
PD	M1 / GPi	Trigger HFS train (7 pulses @ 130Hz) 80ms after AP detected in M1 cortex	aDBS significantly better than cDBS	Rosin et al. [482]
PD	STN / STN	Stimulation voltage proportional to LFP β-band power (130Hz [0-2V])	aDBS outperformed cDBS	Rosa et al. [483]
Epilepsy	Thal. / Thal.	Optogenetic inhibition of thalamus upon LL-threshold of LFP	Proof of concept	Paz et al. [106]
Epilepsy	ECoG / TES	TES applied on spike threshold of epileptic waveform	Decreased seizure duration by 60% on average Response delay was intensity dependent	Berenyi et al. [478]
Epilepsy	ECoG / TES	TES applied upon threshold of signal power 1 sec. pulse train applied up to 5 times/min	50% decrease in clinical seizures [3]	Osorio et al. [484]
	ECoG / Thal.	TES applied upon threshold of signal power 2.5 - 30 sec pulse train applied **In both cases frequency was incremented after 2 failed stimulations	40% decrease in clinical seizures	
Epilepsy	ECoG / TES	TES applied on seizure detection 200Hz 95ms trains with individualised intensities	n=2 100% effective n=1 unresponsive	Kossoff et al. [485]
	Hippocampi	DBS applied on seizure detection 200Hz 95ms train	n=1 100% effective	
Epilepsy	Cortex & Hipp. / Thal.	Threshold detection of synchronisation at recording sites Triggered 1min HFS to thalamus	Improved performance over cDBS "per energy"	Good et al. [486]

[3] i.e. seizures did not develop into symptoms

PD is also seeing a rise in CLDBS trials. Increased β-band activity has been found to correlate with symptoms of PD [213, 480] and is the predominant biomarker used, although recent suggestions of phase-amplitude coupling of β-γ activity as a target [183].

Early stages of more typical controller designs are starting to appear. A proportional controller has been used in [483] to vary stimulation current based on β-band activity above the 'pathological' threshold. A pseudo-integral controller has been used by [484] to increment frequency of DBS after two instances of failed interruptions.

There are a number of key topics of investigation in the area of CLDBS systems:

- Removal of stimulus artefacts to prevent interference with recordings and biomarkers.
- Optimal Control Algorithms.
- Wireless Telemetry to allow freely moving patients and enhance quality-of-life.
- Low Power Consumption for increased battery life and reduction of periodic surgeries.
- Robust Biomarkers that are effective in different patient states (moving, sleeping, under pharmacological effects).

Appendix B

Additional Results

This appendix contains results that provide additional support to works describe in the thesis, including:

1. An example of a thalamic SSEP recorded after hindlimb stimulation.
2. An example of an SSEP recorded from the brainstem after forelimb stimulation.
3. An example of late-latency oscillations in the thalamic forelimb SSEP.
4. A comparison of reference location on the thalamic forelimb SSEP waveform.
5. Recordings under Isoflurane anaesthesia.
6. Additional simulated thalamic SSEP waveforms.

B.1 Mouse Hindlimb SSEP

We recorded SSEPs elicited from subcutaneous electrical stimulation of the mouse hind-paw, one example is shown in Figure B.1 - recorded from a Naive mouse with monopolar recording configuration. Note the response to hindlimb stimulation occurs $\sim$ 4-5 ms later than that of forelimb evoked responses. Hindlimb evoked SSEPs were not used in the results contained in the thesis due to the lack of reliability in obtaining a response. This is believed to be due to the smaller representation area of the hindlimb within the thalamus.

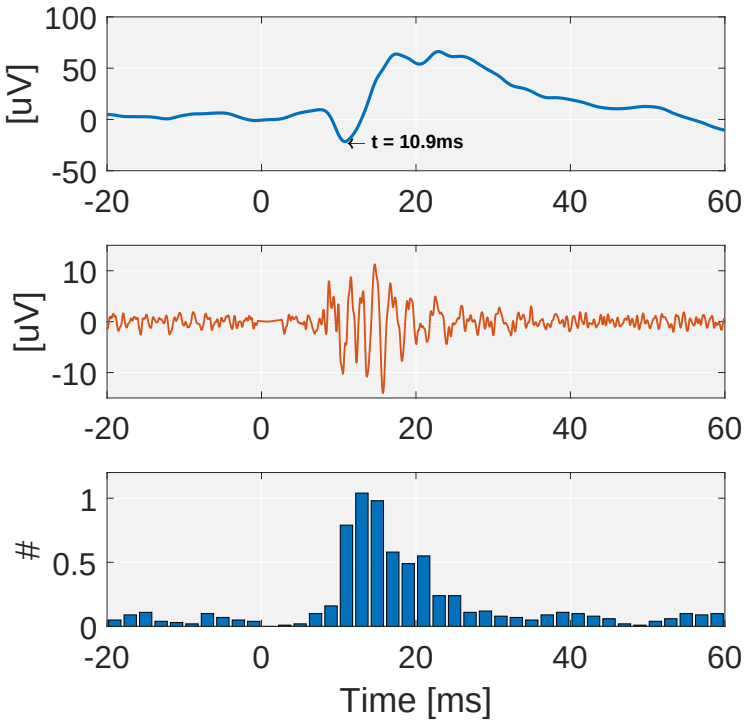

Figure B.1: Hindpaw evoked SSEP recorded in the VPL of a naive mice. (Top) LFP response, (Middle) MUA Response, (Bottom) Spike Histogram.

B.2 Brainstem Recordings

We performed direct recordings from the dorsal column nuclei of a single mouse under Ketamine/Xylazine anaesthesia. We showed the LFP and unit responses to forepaw stimulation occurred at a latency of $\sim$ 4 milliseconds after stimulation, in agreement with that from rats [487, 488, 489]. The surface LFP response had a dominant negative peak which inverted as the electrode was inserted deeper. The recording configuration was using a monopolar PlasticsOne electrode as described previously, referenced to a needle electrode subcutaneously inserted into the neck muscle.

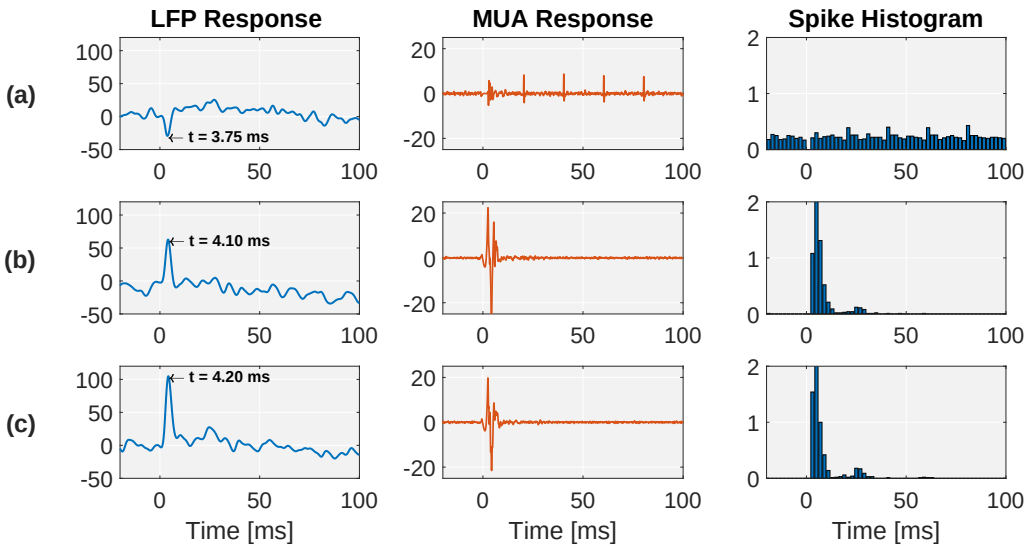

Figure B.2: Evoked potentials recorded from the dorsal column nuclei to forepaw stimulation: (a) surface recording, (b) depth = 0.4mm, (c) depth = 0.6mm. **Note:** Noise artefacts exist in the MUA response from the surface recording.

B.3 Late-Latency Oscillatory SSEP Components

We recorded late-latency oscillations in thalamic SSEP waveforms, similar to Andersen *et al.* [332]. While the initial negative peaks remain relatively constant, the oscillations vary over time with the depth of anaesthesia.

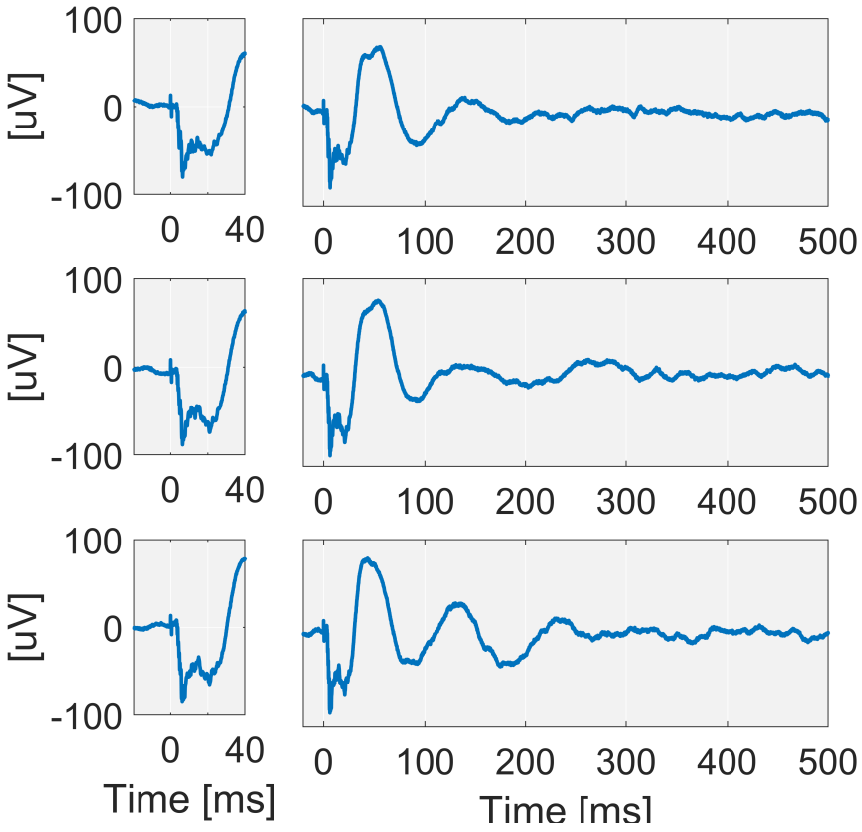

Figure B.3: Presence of oscillations in the thalamic forelimb SSEP. 3 sets of 100 trials were taken 10 minutes apart and shown from top to bottom. The early latency component remains unchanged but a late oscillatory component develops as anaesthesia presumably becomes lighter.

The occurrence of additional negative peaks (at $\approx$ 90, 180 ms post-stimulation) occurred at the same time as unit activity recorded by Andersen *et al.* [332] and 'late-period' firing by Hirai *et al.* [115].

B.4 Effect of Reference Location on Thalamic SSEPs

We compared the effect of the reference electrode location on the thalamic SSEP waveform. Here we used either an ECoG screw, located over the olfactory bulb, or a needle electrode, inserted into the neck muscle of the mouse as the reference and a monopolar recording configuration as described previously. We observed no noticeable differences in the MUA signal, spike histogram or early latency N1 and N2 peaks of the LFP response. A small difference in late latency response was observed that may reflect slight changes in the depth of anaesthesia as was the case in the previous section B.3. A small difference in the P1 peak may just be variability or could be a contribution from the cervical spinal cord near the placement of the neck reference electrode. Nevertheless we conclude that there is no influence of reference location on the early evoked response (N1 & N2 peaks) and therefore they must originate from the extracellular potentials at the electrode inserted in the thalamus.

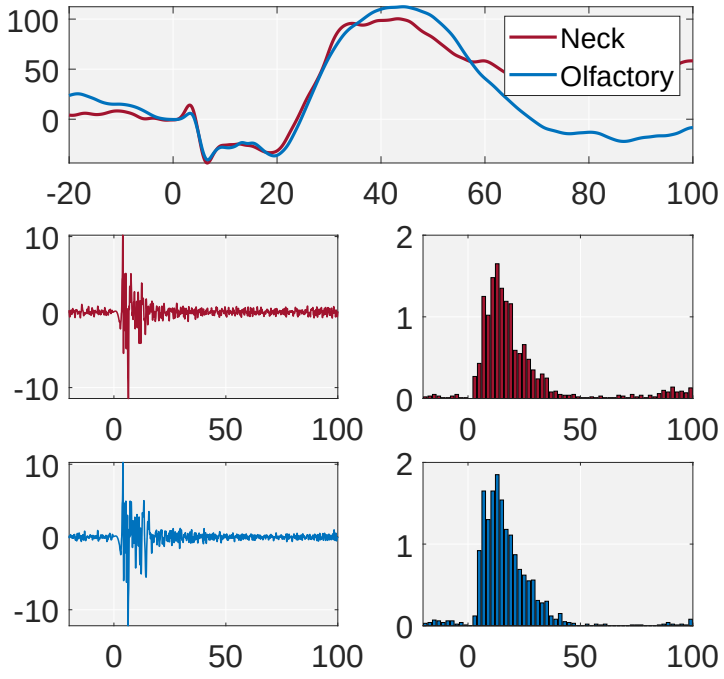

Figure B.4: The effect of reference location on the thalamic SSEP waveform: (top) LFP, (bottom left) MUA, (bottom right) Spike Histogram.

B.5 Recordings under Isoflurane

In this section we show results for electrophysiological recordings taken from the cortex and thalamus of mice under Isoflurane anaesthesia (1.5-2%). The recording configuration was that described in Chapter 5, with an ECoG screw placed over the SSFL region of the cortex and bipolar electrode inserted into the VPL. A reference ECoG screw was placed over the cerebellum. All thalamic signals below represent the differential recording between a single thalamic electrode and the reference.

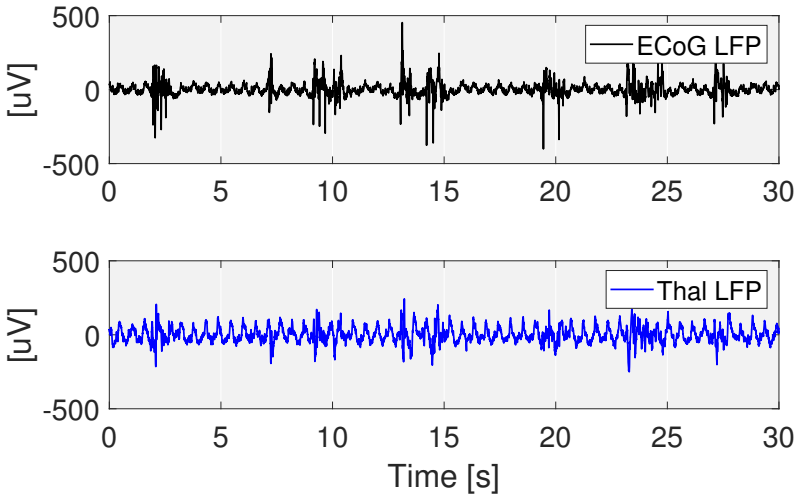

Figure B.5: A comparison of spontaneous activity in the cortex and thalamus from a naive mouse under Isoflurane (1.5-2%) anaesthesia.

Interestingly we obtain a similar thalamic SSEP waveform to that recorded from our stroke mouse, that being an early negative peak corresponding to unit activity. The only difference is the positive peak following the initial response is present in Isoflurane anaesthetised mice, that shows similarity to SSEPs recorded under urethane by others [293]. As mentioned previously, this is likely hyperpolarisation from the TRN. It does not however contain any later negative peaks that would represent corticothalamic feedback, which is expected as from Figure B.6, the cortical response is absent.

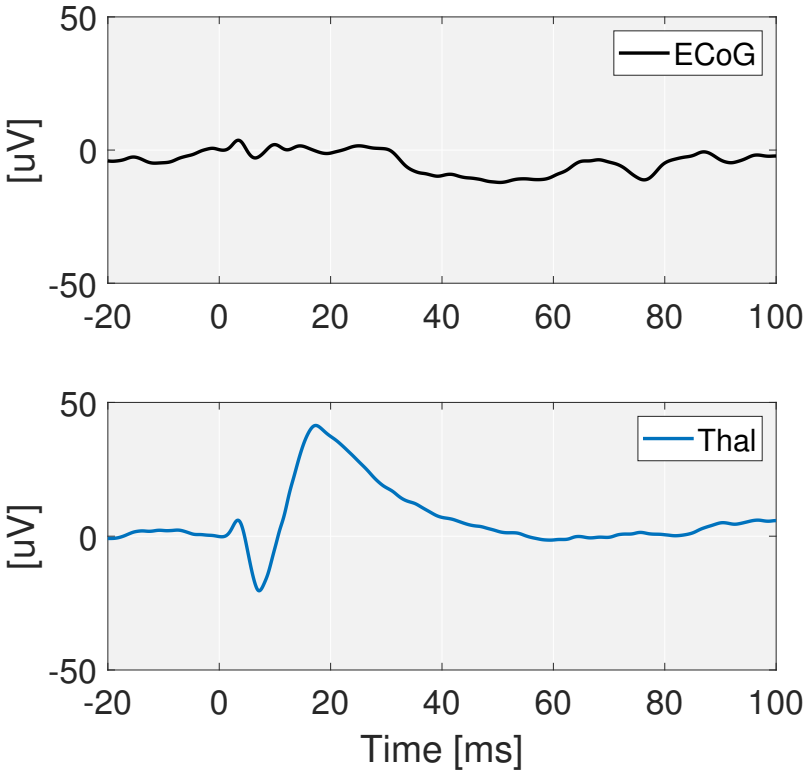

Figure B.6: A comparison of SSEPs evoked in the cortex and thalamus from a naïve mouse under Isoflurane (1.5-2%) anaesthesia. An early response is evident in the thalamus but the cortical SSEP is completely abolished.

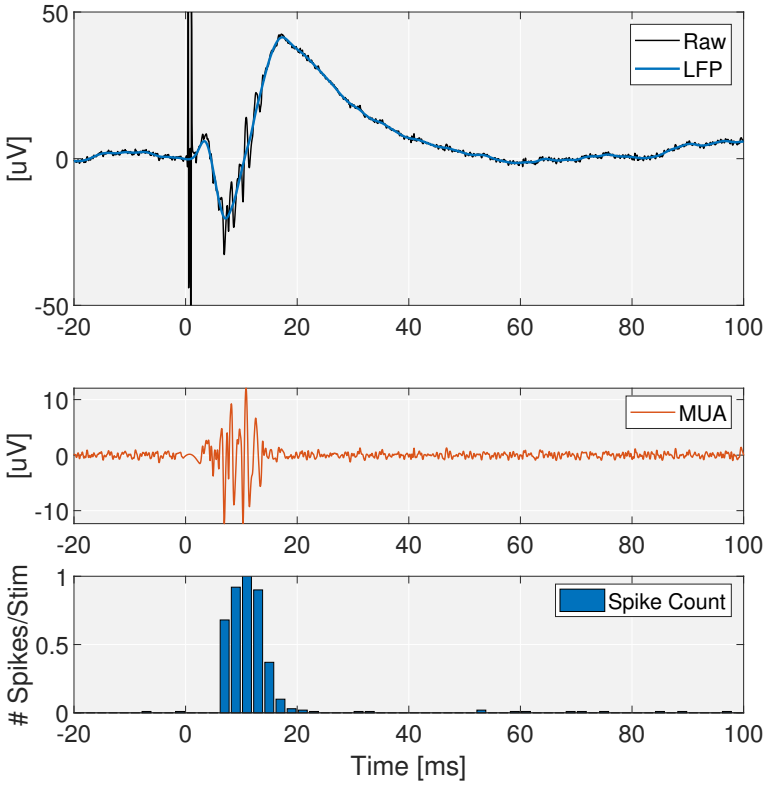

Figure B.7: A closer look at SSEPs evoked in the VPL of a naïve mouse under Isoflurane (1.5-2%) anaesthesia. The waveform consists of an early negative peak at ≈ 7ms, which corresponds with unit activity, followed by a brief positive peak where there is no unit activity.

B.6 Additional Simulated Thalamic SSEPs

Given the hypothesis that the slow positive wave following the first negative deflection in the thalamic SSEP waveform is generated by hyperpolarising currents driven by TRN neurons, we can moderately adjust our simulated SSEP model from Section 2.4 to replicate this phenomena. The activation of GABAaR's is relatively quick and not consistent with the time scale of this positive waveform, although does fit the sharper positive wave generated following initial depolarisation. The synaptic currents generated by GABAbR's however are much slower as it takes time to generate enough G-Protein to open the hyperpolarising K^+channels. Their activation requires significant and prolonged concentrations of synaptic GABA which can develop from LTS bursting of TRN neurons. By doubling the GABAbR conductance, removing the GABAaR conductance and speeding up the time constants we can begin to observe the development of a more prolonged positive wave and in instances the generation of the oscillatory phenomenon mentioned by Andersen *et al.* [332], Mishima *et al.* [329] and in our recordings (Appendix B.3). The simulated waveform is shown in Figure B.8.

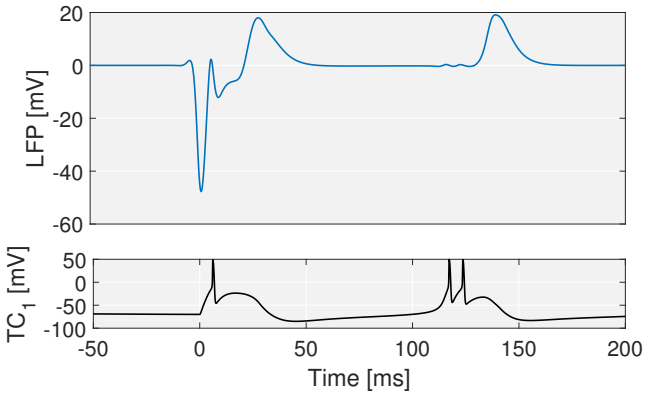

Figure B.8: Simulated thalamic SSEP with large hyperpolarising currents generating a late prolonged positive wave that can trigger oscillatory LTS bursts between TC and TRN populations.

The peak in the thalamic SSEP waveform that is of most speculation is the N2 waveform. We have described that it could be both cortical feedback or a volume-conducted potential from the cortex if the latencies from TC-Ctx and Ctx-TC are short enough. We also suggest that the N2 waveform may be generated within the TRN, which is only 100's of µm from the recording location in the VPL of a mouse. By incorporating the synaptic currents generated in the TRN into Equation 2.70 and using radial distances distributed between 100-250 µm we observe a similar N2 waveform generated by the excitatory synaptic current from thalamocortical collaterals.

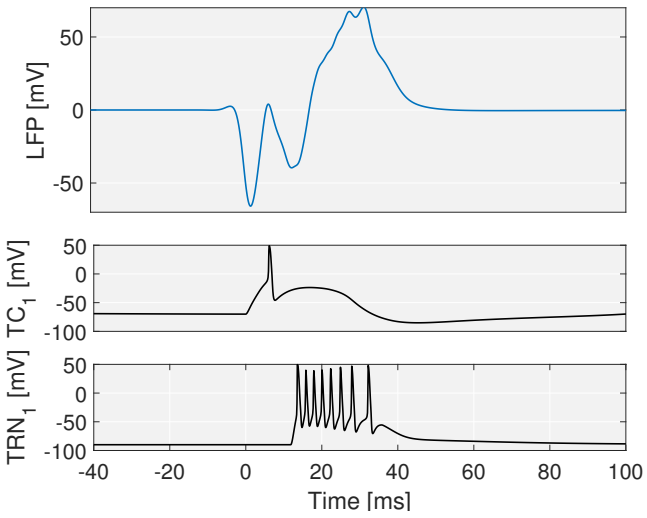

Figure B.9: Simulated Thalamic SSEP with second negative peak originating from the synaptic depolarisation of TRN neurons by TC input.